

INVESTIGATING THE ADVERSE EFFECTS OF NOVEL TUMOUR-SPECIFIC IAP ANTAGONISTS

Thesis submitted for the degree of
Doctor of Philosophy
at the University of Leicester

by

Giles Mortimer Hayward
(BSc Hons; Exeter, MRes DIC; Imperial College London)
MRC Toxicology Unit
University of Leicester

December 2016

Investigating the Adverse Effects of Novel Tumour-Specific IAP Antagonists

By Giles M Hayward

Inhibitor of apoptosis (IAP) proteins are negatively regulated by the mitochondrial pro-apoptotic protein, SMAC, through a tetrapeptide binding-motif. A class of drugs mimicking this motif have been developed as anti-cancer agents and have further highlighted IAP signalling in regulation of cell death. These SMAC mimetics (SMs) activate the non-canonical NF- κ B pathway, induce TNF α secretion and selectively promote cell death in tumour cells; an effect potentiated in a TNF α -rich microenvironment. However, due to this mechanism of action, SMs have the potential to induce toxicity in non-tumour cells residing in this environment. The aim of this thesis was two-fold: to determine the effect of SMs in non-tumour derived cells both *in vitro* and *in vivo*.

I determined a robust methodology in sensitive and resistant tumour cells with SMs as single agents. I found that MDA-MB-231 and MDA-MB-468 cells were sensitive and resistant to SMs as single agents, respectively. Furthermore, the pan caspase inhibitor, zVAD, actually inhibited TNF α secretion in combination with the bivalent SM, BV6. In hepatocyte-like and epithelial non-tumour cells *in vitro*, I found that SMs did not induce cell death, even when co-treated with TNF α . These data suggest that SMs under clinical development do not have significant toxicity in non-tumour derived cells suggesting a large therapeutic window in the clinic.

As liver regeneration is also TNF α -dependent, SMs have the potential to exacerbate liver injury. To determine whether the SM, TL-32711, could induce NF- κ B activation *in vivo*, I used mice expressing an NF- κ B reporter gene (mice^{luc}) allowing for quantification of NF- κ B activity via *in situ* live imaging. Mice^{luc} were dosed with TL-32711, either alone, or in combination with two hepatotoxins. Strikingly, TL-32711 alone induced significant liver-specific NF- κ B activation and protected against liver injury. These data show that SMs could have real clinical relevance for use as a treatment to ameliorate hepatotoxicity.

Acknowledgments

Firstly, I would like to thank my supervisors Prof. Marion MacFarlane, Prof Matthew Wright and Prof. Heather Wallace for giving me the opportunity to undertake this PhD under their tutelage. Thank you for supporting me through all my ups and downs and the input you have provided over the last 4 and a bit years. I'd also like to thank the MRC Integrative Toxicology Training Partnership (ITTP) for funding my project.

I am so grateful to everyone in 416 for their help, fun and support. Without you guys I don't know if I'd have done it! Jo, Michelle, Ian and Sara, you guys were my lifeline and gave me so much input I don't think I'd have enough paper to write it down. I'd also like to thank Dr Tatanya Chernova for always being there for a chat and for helping so much with the Kupffer cell preps and analysis.

Also, I want to thank everyone in Matthew's laboratory in Newcastle for all the help I received when I was there. Without your help, the whole *in vivo* project could not have happened. Thank you for making me feel so welcome when I came up to visit.

I would like to thank my family; Mum, Dad and Holly. I couldn't have done it without you lot.

Finally, I want to thank my God, Jesus. As a scientist, I have the immense privilege of uncovering the world He created. Every time I discovered something new, I always felt Him smile saying, "You think that's cool, wait until you see this!" Whenever it got too much, I just had to look to Him and remember that His goodness restores my dry and weary soul.

Abbreviations

ADR	Adverse Drug Reactions
ANIT	α -Naphthylisothiocyanate
Annexin V	Annexin-V FITC
BIR	Baculovirus IAP repeat
BIRC	Baculovirus IAP repeat Containing
CARD	Caspase Activation and Recruitment Domain
Caspase	Cystein-dependent aspartyl specific protease
CCl ₄	Carbon Tetrachloride
cFLIP _{L/S}	Cellular Flip Long/Short isoforms
cIAP	Cellular Inhibitor of Apoptosis
CYP(XXX)	Cytochrome P(XXX)
DD	Death Domain
DED	Death Effector Domain
ELISA	Enzyme-linked Immunosorbent Assay
FADD	Fas-associated Death Domain protein
IAP	Inhibitor of Apoptosis Protein
IC ₅₀	Half Maximal Inhibitory Concentration
I κ B	Inhibitor of kappa-light-chain-enhancer of activated B cells
IKK	Inhibitor of kappa-light-chain-enhancer of activated B cells Kinase
K_i	Inhibitory Constant
mg	Milligram
mg/kg	Milligrams per Kilogram
NF- κ B	Nuclear Factor kappa-light-chain-enhancer of activated B cells
ng	Nanogram
NSA	Necrosulfonamide
NIK	NF- κ B Inducing Kinase
PBMC	Peripheral Blood Mononuclear Cell
RING	Really Interesting New Gene
RIP	Receptor Interacting Protein
SEM	Standard Error of Mean
SM	SMAC mimetic

Abbreviations

SMAC	Second Mitochondrial-derived Activator of Caspase
TNF α	Tumour Necrosis Factor alpha
TNFR1	Tumour Necrosis Factor Receptor 1
TNFRSF	Tumour Necrosis Factor Receptor Super Family
TRADD	TNF receptor-associated protein with death domain
TRAF	TNF receptor-associated factor
μ g	Microgram
μ l	Microlitre
μ M	Micromolar
WT	Wildtype
XIAP	X-chromosome linked Inhibitor of Apoptosis
zVAD.fmk	Carbobenzoxy-Val-Ala-Asp-(O-methyl)-fluoromethylketone

2. TABLE OF CONTENTS

1. Introduction	13
Types of cell death	13
1.1.1. Apoptosis	13
1.1.2. Necroptosis and Necrosis	15
1.1.3. Caspases	16
Mammalian IAPs	19
1.1.4. Structure and function	19
1.1.5. Ubiquitination	26
SMAC.....	26
TNF α signalling	28
1.1.6. Pro-survival Complex I	28
1.1.7. Pro-death Complex II	29
NF- κ B pathway.....	32
1.1.8. Canonical and non-canonical NF- κ B signalling	34
Development of small molecule inhibitors	35
SMAC mimetics (SMs)	36
1.1.9. SMs used in this project	36
1.1.10. Reported adverse effects of SMs.....	42
Drug-induced liver injury (DILI)	43
1.1.11. Role of Kupffer cells in DILI	46
1.1.12. Hepatotoxins used in this project	47
Project Aims	48
2. Materials and methods	51
Materials	51
Cell culture	52
2.1.1. Cell Lines and Culturing Conditions	52

Table of Contents

2.1.2. Freezing Down and Recovering Cells from Liquid Nitrogen	53
2.1.3. Cell seeding and treatments.....	54
2.1.4. Treatment of cells with zVAD and NSA	54
2.1.5. Kupffer cell isolation, culture and treatment.....	54
SDS-PAGE (Sodium Dodecyl Sulfate Polyacrylamide Gel Electrophoresis)	55
2.1.6. Protein extraction	55
Bradford Assay.....	56
RNA Extraction.....	58
2.1.7. Cell lines	58
2.1.8. Tissue Homogenates	58
2.1.9. Kupffer cells	58
cDNA synthesis.....	59
Quantitative Polymerase Chain Reaction Optimisation	59
ELISA (Enzyme-Linked Immunosorbent Assay).....	59
Caspase-3/7 Activity Assay	60
Flow Cytometry	60
2.1.10. Analysis of cell death	60
2.1.11. Quantification of TNFR1 cell surface expression	63
Cell viability Assays.....	63
2.1.12. MTT Assays.....	63
2.1.13. Nuclei Counting	63
Confocal Microscopy	64
In vivo experiments	64
2.1.14. Pilot Study to determine the appropriate dose of TL-32711	64
2.1.15. TL-32711 in combination with the hepatotoxins ANIT and CCL ₄	65
2.1.16. Luminescent imaging of mice.....	66
Immunohistochemistry	66
2.1.17. Haematoxylin and Eosin Staining	66

Table of Contents

2.1.18. Antigen retrieval method	66
3. Characterising the response of tumour cell lines to SMAC mimetics in vitro	70
Introduction	70
MDA-MB-231 cells, but not MDA-MB-468 cells, are sensitive to SMs at clinically relevant concentrations	71
3.1.1. Method optimisation with the 'tool' compound, LBW242	71
3.1.2. AT-406	76
3.1.3. GDC-0152	80
3.1.4. BV6	84
3.1.5. TL-32711	88
Bivalent SMs induce cell death at nanomolar concentrations as single agents	92
TNF α secretion and cell death induced by SMs in MDA-MB-231 cells is correlated to activation of the non-canonical NF- κ B	97
BV6 induces necrosis at 30 μ M, but apoptosis at lower concentrations	101
Discussion.....	105
3.1.6. Future Work	110
4. Characterising the response of non-tumour cell lines to SMAC mimetics in vitro.....	112
Introduction	112
MCF-10A cells, B-13 and hepatocyte-like B-13/H cells are relatively resistant to SMs as single agents	113
4.1.1. MCF-10A cells.....	113
4.1.2. B-13 cells	117
4.1.3. B-13/H cells.....	121
SMs have similar kinetics in MCF-10A cells compared to tumour cells	124
AT-406 does not induce proliferation in MCF-10A cells.....	126
MCF-10A, but not B-13 and B-13/H cells, are able to form Complex I and undergo Complex II-mediated cell death	128
B-13 and B-13/H have a mutation in the cflar gene	145

Table of Contents

Discussion.....	149
4.1.4. Future work	154
5. Investigating the potential hepatotoxicity induced by TL-32711 in vivo	157
Introduction	157
In vivo pilot to determine optimum TL-32711 dose	157
TL-32711 ameliorates liver damage induced by two classic hepatotoxins.....	169
5.1.1. TL-32771 prevents ANIT and CCL ₄ induced hepatotoxicity.....	169
5.1.2. TL-32771 promotes NF- κ B activity and Kupffer cell recruitment.....	174
5.1.3. TL-32711 promotes proliferation and apoptosis simultaneously	182
TL-32711-induced NF- κ B activation and the resulting TNF α up-regulation is mediated by Kupffer cells	187
Conclusions.....	189
5.1.4. Future Work	195
6. Final discussion	197
Key findings.....	197
6.1.1. Results Chapter 3 - SM structure predicts efficacy in tumour cells	197
6.1.2. Results Chapter 4 - SMs exhibit limited toxicity in non-tumour cells	199
6.1.3. Results Chapter 5 - The SM, TL-32711, prevents liver injury in vivo ...	200
6.1.4. Concluding remarks	202
Future work	203
Appendix.....	206
Appendix 1: List of genes relevant to TNF α signalling in B-13 genome (as detailed in Chapter 4)	206
Appendix 2: Reanalysed data from Chapter 5.....	208
References.....	210

Table of Figures

Table of Figures

CHAPTER 1

FIGURE 1.1 CASPASE STRUCTURE.....	17
FIGURE 1.2 STRUCTURE OF THE MAMMALIAN IAP FAMILY.....	20
FIGURE 1.3 STRUCTURE AND FUNCTION OF SMAC.....	27
FIGURE 1.4 CANONICAL NF- κ B ACTIVATION THROUGH TNFR1	30
FIGURE 1.5 NON-CANONICAL NF- κ B SIGNALLING CAN BE DEPENDENT OR INDEPENDENT OF TNFR1	31
FIGURE 1.6 TRANSCRIPTION FACTORS AND INHIBITORS OF THE NF- κ B PATHWAY.....	33
FIGURE 1.7 DIAGRAMMATIC OVERVIEW OF HEPATOTOXICITY	45

CHAPTER 2

FIGURE 2.1 FLOW CYTOMETRY ANALYSIS OF CELLS	62
---	----

CHAPTER 3

FIGURE 3.1 LBW242 INDUCES APOPTOSIS IN PARALLEL WITH SECRETION OF TNFA.....	73
FIGURE 3.2 LBW242 ACTIVATES CASPASES, AND RESULTS IN A DECREASE IN CELL VIABILITY IN MDA-MB-231 CELLS.....	74
FIGURE 3.3 LBW242 DEGRADES CIAP1 IN BOTH SENSITIVE AND RESISTANT CELLS BUT ONLY ACTIVATES CASPASES IN CELLS WITH AN INDUCIBLE TNFA AUTOCRINE LOOP.....	75
FIGURE 3.4 AT-406 INDUCES APOPTOSIS IN CELLS WITH A TNFA- AUTOCRINE LOOP	77
FIGURE 3.5 AT-406 PROMOTES CASPASE ACTIVITY AND A DECREASE IN CELL VIABILITY IN MDA-MB-231 CELLS.....	78
FIGURE 3.6 AT-406 DEGRADES CIAP1 IN ALL CELL LINES BUT ONLY ACTIVATES CASPASES IN CELLS WITH TNFA AUTOCRINE ACTIVITY	79
FIGURE 3.7 GDC-0152 INDUCES CELL DEATH IN CELLS WITH A TNFA AUTOCRINE LOOP	81
FIGURE 3.8 GDC-1052 INDUCES CASPASE ACTIVITY AND DECREASES CELL VIABILITY IN MDA-MB-231 CELLS.....	82
FIGURE 3.9 GDC-0152 DEGRADES CIAP1 IN BOTH, BUT DOES NOT INDUCE CASPASE PROCESSING IN NON-TUMOUR DERIVED CELLS.....	83
FIGURE 3.10 BV6 INDUCES CELL DEATH EVEN IN CELLS WHERE IT DOES NOT INDUCE SECRETION OF TNFA	85
FIGURE 3.11 BV6 INDUCES CASPASE ACTIVITY AND DECREASES CELL VIABILITY IN BOTH MDA-MB-231 AND MDA-MB-468 CELLS. CELLS WERE TREATED FOR 24 H.....	86
FIGURE 3.12 BV6 DEGRADES CIAP1/2 AND XIAP, AND INDUCES CASPASE ACTIVATION EVEN IN CELLS WHERE IT DOES NOT ACTIVATE A TNFA AUTOCRINE LOOP	87
FIGURE 3.13 TL-32711 INDUCES SIGNIFICANT APOPTOSIS IN CELLS WITH A TNFA AUTOCRINE LOOP. MDA-MB-231 AND MDA-MB-468 CELLS WERE TREATED FOR 24 H.....	89
FIGURE 3.14 TL-32771 INDUCES CASPASE ACTIVITY AND DECREASES CELL VIABILITY IN BOTH MDA-MB-231 CELLS, BUT NOT MDA-MB-468 CELLS	90
FIGURE 3.15 TL-32711 INDUCES CIAP1 DEPLETION AND NON-CANONICAL NF- κ B ACTIVATION.....	91

Table of Figures

FIGURE 3.16 BIVALENT SMS INDUCE CELL DEATH AT NANOMOLAR CONCENTRATIONS IN MDA-MB-231 CELLS.....	94
FIGURE 3.17 BIVALENT SMS INDUCE PHOSPHATIDYLSERINE EXPOSURE IN SENSITIVE MDA-MB-231 CELLS, BUT NOT THE RESISTANT MDA-MB-468 CELLS.....	95
FIGURE 3.18 BIVALENT SMS DEplete CIAP1 AND INDUCE CELL DEATH AT LOWER NANOMOLAR CONCENTRATIONS IN SENSITIVE MDA-MB-231 CELLS	96
FIGURE 3.19 CELL DEATH AND TNFA SECRETION ARE INITIATED WITH SIMILAR KINETICS BY MONOVALENT AND BIVALENT SMS.....	99
FIGURE 3.20 SMS RAPIDLY DEplete CIAP1 AND ACTIVATE THE NON-CANONICAL NF-kB PATHWAY WITHIN HOURS. MDA-MB-231 CELLS WERE LYSED IN RIPA BUFFER AND PROTEIN CONCENTRATION WAS DETERMINED BY BRADFORD ASSAY	100
FIGURE 3.21 BV6 INDUCES NECROSIS AT HIGH CONCENTRATIONS.....	103
FIGURE 3.22 ZVAD PROTECTS AGAINST BV6-INDUCED CELL DEATH AT LOWER CONCENTRATIONS.....	104

CHAPTER 4

FIGURE 4.1 CLINICALLY RELEVANT SMS DO NOT INDUCE CELL DEATH OR TNFA SECRETION IN MCF-10A CELLS.....	114
FIGURE 4.2 BV6 INDUCES PRIMARILY APOPTOSIS IN MCF-10A CELLS	115
FIGURE 4.3 SMS DEplete CIAP1, INDUCE NON-CANONICAL NF-kB ACTIVATION, BUT DO NOT PROMOTE CASPASE CLEAVAGE IN MCF-10A CELLS.....	116
FIGURE 4.4 B-13 CELLS ARE RESISTANT TO MONOVALENT SMS BUT ARE SENSITIVE TO BIVALENT SMS. B-13 CELLS WERE TREATED FOR 24 H WITH THE FOUR SM COMPOUNDS	118
FIGURE 4.5 B-13 CELL ARE MORE SENSITIVE TO BIVALENT SMS	119
FIGURE 4.6 SMS ACTIVATE THE NON-CANONICAL NF-kB PATHWAY IN B-13 CELLS	120
FIGURE 4.7 B-13/H CELLS ARE RESISTANT TO SMS IN CLINICAL TRIALS	122
FIGURE 4.8 CLINICALLY RELEVANT SMS ACTIVATE THE NON-CANONICAL NF-kB PATHWAY IN B-13/H CELLS.....	123
FIGURE 4.9 SMS DEplete CIAP1 AND ACTIVATE THE NON-CANONICAL NF-kB PATHWAY WITH SIMILAR KINETICS IN MCF-10A CELLS COMPARED TO TUMOUR CELLS	125
FIGURE 4.10 SMS DO NOT INDUCE PROLIFERATION IN MCF-10A CELLS	127
FIGURE 4.11 CLINICALLY RELEVANT SMS DO NOT INDUCE CELL DEATH IN COMBINATION WITH TNFA IN MCF-10A CELLS	129
FIGURE 4.12 CLINICALLY RELEVANT SMS ACTIVATE THE NON-CANONICAL NF-kB PATHWAY, BUT DO NOT INDUCE CELL DEATH IN COMBINATION WITH TNFA IN MCF-10A CELLS	130
FIGURE 4.13 CLINICALLY RELEVANT SMS DO NOT INDUCE CELL DEATH IN COMBINATION WITH TNFA (BIOVISION) IN B-13 CELLS.....	131
FIGURE 4.14 CLINICALLY RELEVANT SMS ACTIVATE THE NON-CANONICAL NF-kB PATHWAY, BUT DO NOT ACTIVATE CASPASE-3 IN COMBINATION WITH TNFA (BIOVISION) IN B-13 CELLS	132
FIGURE 4.15 CLINICALLY RELEVANT SMS DO NOT INDUCE CELL DEATH IN COMBINATION WITH BIOVISION TNFA IN B-13/H CELLS	133

Table of Figures

FIGURE 4.16 CLINICALLY RELEVANT SMS ACTIVATE THE NON-CANONICAL NF- κ B PATHWAY, BUT DO NOT ACTIVATE CASPASE-3 IN COMBINATION WITH TNFA (BIOVISION) IN B-13/H CELLS.....	134
FIGURE 4.17 MCF-10A CELLS UNDERGO P65-MEDIATED TRANSLOCATION	136
FIGURE 4.18 B-13 CELLS DO NOT UNDERGO TNFA-MEDIATED P65 TRANSLOCATION	137
FIGURE 4.19 B-13/H CELLS DO NOT UNDERGO TNFA-MEDIATED P65 TRANSLOCATION.....	138
FIGURE 4.20 MCF-10A CELLS HAVE THE ABILITY TO UNDERGO COMPLEX II-MEDIATED CELL DEATH....	139
FIGURE 4.21 B-13 CELLS ARE UNABLE TO UNDERGO TNFA-INDUCED COMPLEX II-MEDIATED CELL DEATH	140
FIGURE 4.22 B-13 AND B-13/H CELLS ARE UNABLE TO UNDERGO HIGH LEVELS OF TNFA-INDUCED COMPLEX II-MEDIATED CELL DEATH	141
FIGURE 4.23 MCF-10A AND B-13 CELLS EXPRESS TNFR1	142
FIGURE 4.24 THE COMMERCIALLY AVAILABLE TNFA FROM R&D IS FUNCTIONALLY ACTIVATE AS EVIDENCED BY P65 TRANSLOCATION	144
FIGURE 4.25 THE <i>CFLAR</i> GENE IS MUTATED IN B-13 CELLS	146
FIGURE 4.26 B-13 AND B-13/H CELLS DO NOT EXPRESS CFLIP _L OR CFLIP _S	148

CHAPTER 5

FIGURE 5.1 TL-32711 DOES NOT INDUCE INCREASES IN ALT OR ALP	159
FIGURE 5.2 TL-32711 INDUCES SINUSOIDAL ENLARGEMENT, SCATTERED APOPTOSIS AND PROLIFERATION	161
FIGURE 5.3 TL-32711 INDUCES SINUSOIDAL ENLARGEMENT, SCATTERED APOPTOSIS AND PROLIFERATION	162
FIGURE 5.4 TL-32711 INDUCES INFILTRATION OF KUPFFER CELLS.....	163
FIGURE 5.5 TL-32711 INDUCES INFILTRATION OF KUPFFER CELLS.....	164
FIGURE 5.6 TL-32711 INDUCES SCATTERED STAINING OF CLEAVED C3, INDICATIVE OF APOPTOSIS.....	165
FIGURE 5.7 TL-32711 INDUCES SCATTERED STAINING OF CLEAVED C3, INDICATIVE OF APOPTOSIS.....	166
FIGURE 5.8 TL-32711 INDUCES AN INCREASE IN CLEAVED PARP.	167
FIGURE 5.9 TL-32711 INDUCES AN INCREASE IN CLEAVED PARP	168
FIGURE 5.10 TL-32711 PROTECTS AGAINST ANIT AND CCL ₄ INDUCED HEPATOXICITY	170
FIGURE 5.11 TL-32711 AMELIORATES ANIT- AND CCL ₄ -INDUCED INJURY	172
FIGURE 5.12 TL-32711 AMELIORATES ANIT- AND CCL ₄ -INDUCED INJURY	173
FIGURE 5.13 TL-32711-INDUCED NF- κ B ACTIVATION DIFFERENTIALLY CORRELATES WITH ITS HEPATOPROTECTIVE PROPERTIES.....	175
FIGURE 5.14 TL-32711 ACTIVATES THE NF- κ B PATHWAY WITHIN 4-8 H, WHICH IS LOCALISED PREDOMINANTLY TO THE LIVER	176
FIGURE 5.15 TL-32711 RESULTS IN INCREASES IN KUPFFER CELL NUMBER	178
FIGURE 5.16 TL-32711 AMELIORATES ANIT- AND CCL ₄ -INDUCED INJURY	179
FIGURE 5.17 TL-32711 REDUCES ANIT-INDUCED NEUTROPHIL INFILTRATION	180
FIGURE 5.18 TL-32711 REDUCES ANIT-INDUCED NEUTROPHIL INFILTRATION	181
FIGURE 5.19 TL-32711 INDUCES PROLIFERATION AS A SINGLE AGENT	183

Table of Figures

FIGURE 5.20 TL-32711 INDUCES PROLIFERATION AS A SINGLE AGENT	184
FIGURE 5.21 TL-32711 AMELIORATES HEPATOXICITY BY PROMOTING APOPTOSIS	185
FIGURE 5.22 TL-32711 AMELIORATES HEPATOXICITY BY PROMOTING APOPTOSIS	186
FIGURE 5.23 KUPFFER CELLS MEDIATE TL-32711-INDUCED TNFA MRNA UP-REGULATION AND SECRETION	188
FIGURE 5.24 SCHEMATIC REPRESENTATION OF THE MAJOR FINDING OF THE <i>IN VIVO</i> COMBINATION STUDY	194
FIGURE 6.1 SCHEMATIC REPRESENTATION OF THE MAJOR FINDINGS FROM THIS PROJECT	204

APPENDIX

FIGURE APPENDIX 2.1 TL-32711 DOES NOT AMELIORATE HEPATOXICITY BY PROMOTING APOPTOSIS ..	208
---	-----

Table of Tables

Table of Tables

CHAPTER 1

TABLE 1.1 REPORTED INHIBITORY CONSTANTS (K_i IN M) FROM IAP AGAINST HUMAN CASPASES. ADAPTED FROM ³⁵	22
TABLE 1.2 STRUCTURE AND CLINICAL PROGRESS OF SMS USED IN THIS PROJECT.	38
TABLE 1.3 REPORTED INHIBITORY CONSTANTS (K_i) IN NM FOR THE SMS USED IN THIS PROJECT. NOT REPORTED (NR)	39

CHAPTER 2

TABLE 2.1 PRIMARY ANTIBODIES USED FOR IMMUNOBLOTTING	57
--	----

CHAPTER 3

TABLE 3.1 EC_{50} VALUES FOR THE FOUR DIFFERENT SMS IN MDA-MB-231 AND MDA-MB-468 CELLS.	76
--	----

Chapter 1

Introduction

1. INTRODUCTION

Types of cell death

Cell death is essential for survival. It maintains tissue homeostasis, is involved in embryogenesis and can resolve inflammation and disease. There are many types of cell death, including apoptosis, necroptosis and necrosis. These all have unique functions and occur in specific biological situations. For example, when caspases (cysteine-dependent aspartate-specific proteases) are inhibited, or their function blocked, cell death modes independent of caspases occur, such as necroptosis and autophagy.

1.1.1. Apoptosis

Apoptosis is type of programmed cell death mediated by caspases. Apoptosis is the preferred mode of cell death as its execution does not result in extensive inflammation. There are two major pathways by which apoptosis is initiated: the extrinsic and the intrinsic pathway. The extrinsic pathway is tightly regulated by a subset of the tumour necrosis factor receptor superfamily (TNFRSF), known as death-receptors (DRs), whereas the intrinsic pathway is regulated by the integrity of the mitochondrial outer membrane and the BCL-2 protein family^{1,2}.

1.1.1.1. *Intrinsic Apoptotic Pathway*

The intrinsic pathway is regulated *via* intracellular signals, namely growth factor withdrawal, DNA damage, U.V. irradiation, and reactive oxygen species (ROS) perturbation of the surrounding milieu. Activation of the intrinsic pathway is tightly regulated by a group of proteins called the BCL-2 family, which are characterised by the presence of one or more BH3 motifs. Due to their divergent nature, the members of the BCL-2 family have been grouped into three classes: anti-apoptotic - BCL-2, BCL-XL and MCL-1; effector - BAX, BAK and BOK; and pro-apoptotic BH3-only proteins, which contain only one BH3 motif - NOXA, BIM, and (t-)BID². The conserved BH3-domain in BH3-only proteins can bind to and regulate other family members, promoting apoptosis. These proteins work in concert to block or cause mitochondrial outer membrane permeabilization (MOMP), which releases

Introduction

apoptogenic proteins. MOMP is dependent on BAX and BAK which form mitochondrial pores releasing cytochrome *c*, SMAC/DIABLO (Second Mitochondrial-derived Activator of Caspase/Direct IAP binding protein with low pI – referred hitherto as SMAC) and Omi/HrtA2 from the mitochondria. Cytochrome *c* forms the Apoptosome with the initiator caspase, caspase-9, and APAF-1 (apoptosis associated factor-1), activating caspase-9, and subsequently caspase-3 and -7 inducing apoptosis³. Two models have been proposed for the role of the BCL-2 family; the direct activation model, in which pro-apoptotic BCL-2 members activate BAX and BAK, or the indirect activation model, in which pro-apoptotic BCL-2 proteins inhibit anti-apoptotic proteins. However, recently a unified model has been proposed where BCL-2-like proteins are sequestered by BH3-only proteins, after which BAX/BAK are then activated, allowing apoptosis induction⁴.

1.1.1.2. *Extrinsic Apoptotic Pathway*

Fas/CD95 and TRAIL

The extrinsic apoptotic pathway is initiated by binding of specific extracellular ligands to receptors on the cell surface, known as DRs. The TNFSF comprises eight DRs, including TNF (Tumour Necrosis Factor) -R1 (DR1) Fas/CD95 (DR2) and TNF-related apoptosis inducing ligand (TRAIL)-R1/R2 (DR4/DR5). While these DRs have structural homology, i.e. an extracellular ligand binding domain and an intracellular death domain (DD), there are differences in signalling between CD95 and TRAIL, and TNF. Upon ligation of Fas/CD95 and TRAIL-R1/R2 with the cognate ligand, the intracellular DD recruits the adaptor protein FADD (Fas-associated protein with DD) *via* homotypic interaction *via* the C-terminal DD of FADD. FADD also contains an N-terminal death effector domain (DED), by which the initiator caspases (8 and 10), are recruited through homotypic interaction of the DEDs. While the traditional model had proposed a 1:1 stoichiometry of TRAIL-R1, FADD and caspase-8, recent data demonstrated a 3:1 ratio of receptor:FADD⁵. Furthermore, the ratio of FADD:caspase-8 was ~1:9, which lead to the proposal of a caspase-8 chaining model, in which an initial caspase-8 molecule recruits additional caspase-8 molecules to the death inducing signalling complex (DISC)

Introduction

through an phenylalanine-leucine-motif in DED2⁵. This caspase-8 chain can be regulated through cellular FLICE-like inhibitory protein (cFLIP). cFLIP is a caspase-8 homologue with tandem DED repeats and occurs predominantly in two isoforms; cFLIP long (cFLIP_L), and cFLIP short (cFLIP_S). Former models maintained that cFLIP is a direct competitor of caspase-8 for binding FADD to the DISC. However, recently it was shown that the presence of cFLIP_L is essential for efficient DISC formation⁶. In this model, caspase-8 recruits cFLIP_L or cFLIP_S through a hierarchical binding mechanism. The subsequent ratio of caspase-8 to cFLIP_{L/S} determines the amount of cell death. However, unlike cFLIP_L, the short isoform of cFLIP actually inhibits caspase-8 chain assembly, as it lacks enzymatic activity. DISC-associated active caspase-8 is then released from the DISC allowing caspase-8 to cleave and activate the effector caspases, caspase-3 and -7⁶. Once activated, caspases-3 and -7 begin cleaving their vast repertoire of intracellular substrates, including poly (ADP-ribose) polymerase (PARP), structural proteins and nuclear lamins. While there is evidence DR4 and DR5 can signal for survival⁷, it appears their primary purpose is to initiate apoptosis.

In addition, there is interplay between the extrinsic and intrinsic pathway. This cross-talk is achieved through caspase-8-mediated cleavage of Bid⁸. This acts to amplify the apoptotic signal through mitochondrial release of cytochrome *c* and SMAC. Cells can therefore be classified into two subsets in response to extrinsic signals; type I cells effectively induce apoptosis *via* the extrinsic pathway, without the need for the intrinsic pathway assistance; type II cells, however, require activation of the intrinsic pathway to induce effective apoptosis.

1.1.2. Necroptosis and Necrosis

Necroptosis, or programmed necrosis, is a caspase independent cell death that occurs in situations of caspase and inhibitor of apoptosis (IAP) inhibition. In these conditions, RIP1 binds to RIP3 through the RIP homotypic interaction motif⁹. Once activated by phosphorylation, RIP1/3 stabilises to form an amyloid-like filamentous structure, called the necrosome¹⁰. The necrosome then recruits its substrate, mixed lineage kinase domain-like (MLKL), through RIP3¹¹. Upon phosphorylation, MLKL form oligomers that translocate to the inner membrane which induce

Introduction

membrane rupture^{12,13}. While it has no unique biochemical markers, necroptosis can be confirmed by plasma rupture and a lack of apoptotic signatures such as caspase cleavage¹⁴. While necrostatin-1 has been used to inhibit RIP1-mediated necroptosis, recently an MLKL inhibitor, necrosulfonamide (NSA), has been developed that allows for a more robust, specific inhibition of necroptosis.

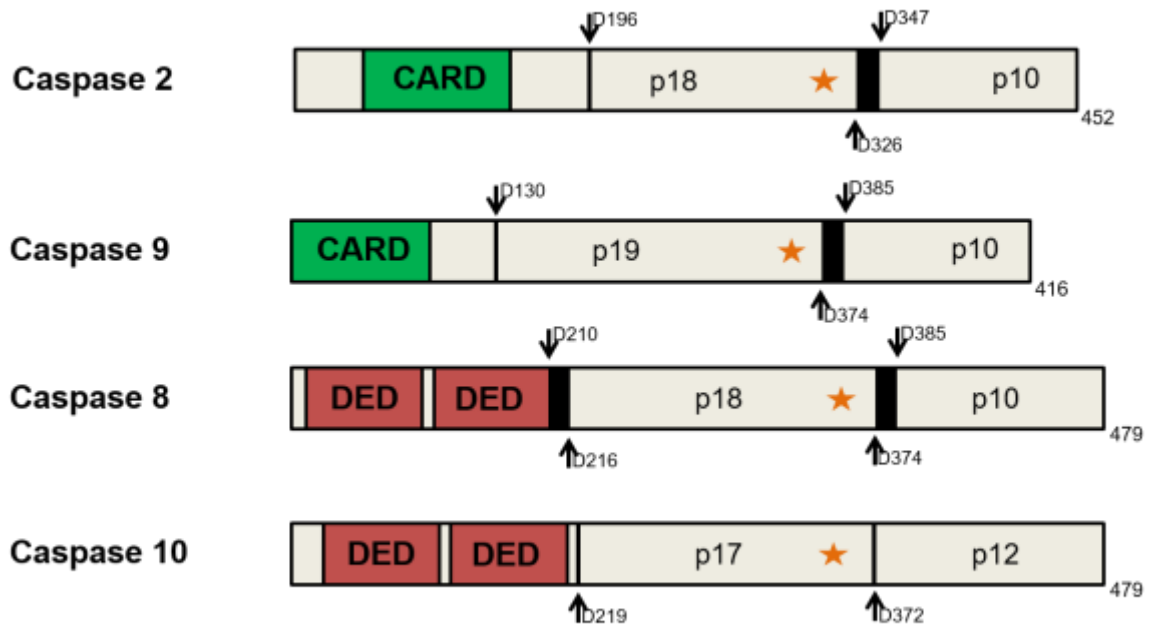
Unlike, apoptosis, necroptosis results in significant inflammation and damage-associated molecular patterns' (DAMPs)¹⁴. DAMPs are intracellular molecules that can be divided into two categories; 1) non-inflammatory molecules that acquire immunomodulatory properties upon release, and 2) alarmins that possess cytokine-like functions and promote inflammation^{14–16}. While the precise mode of cell death induced by necroptosis is under discussion, it is generally accepted this pathway results in ROS production and MLKL-induced membrane rupture.

Necrosis, however is an unregulated form of cell death in which a cell undergoes autolysis resulting in loss of cell membrane integrity. Consequently, the intracellular components are released into the extracellular space. This results in similar outcomes to necroptosis. The only difference between necrosis and necroptosis is that necrosis is uncontrolled cell death, whereas necroptosis is programmed and can be inhibited.

1.1.3. Caspases

Caspases are a group of proteases that effect apoptotic signals through cleavage of a specific repertoire of proteins. As the name suggests, they target aspartate residues in substrates, using a cysteine side chain to catalyse peptide cleavage¹⁷. Caspases, with the exception of caspase-14, are expressed ubiquitously, and have been traditionally categorised as apoptotic vs. non-apoptotic. While this is broadly correct, most apoptotic proteins have at least one non-apoptotic role¹⁸. Within apoptosis, caspases may be further subdivided into initiator/apical caspases and executioner/effector caspases (**Figure 1.1**).

Initiator Caspases



Executioner Caspases

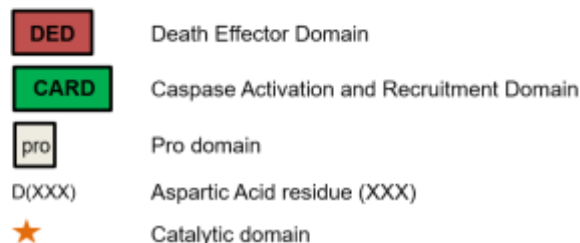
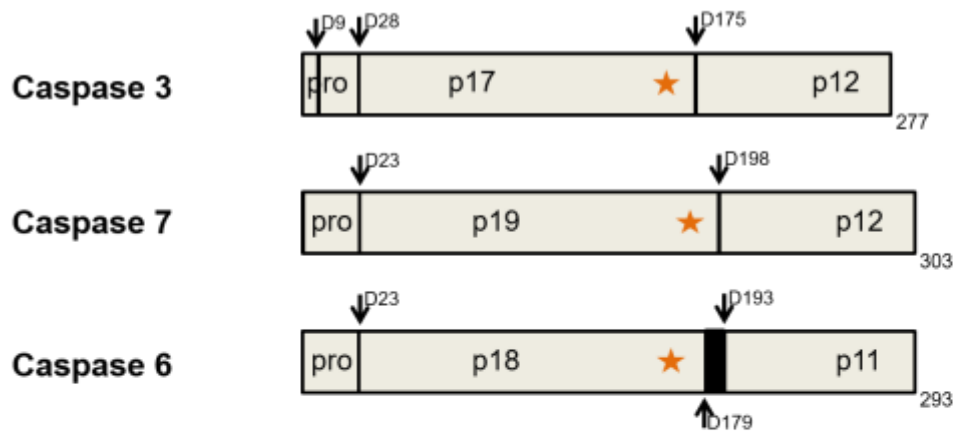


Figure 1.1 | Caspase Structure. Caspases are divided into initiator/apical and executioner/effector. Caspases-8 and -10 are recruited via their DEDs, whereas caspases-2 and -9 via their CARDS to their relevant activation complexes. The executioner caspases are activated through cleavage by the initiator caspases.

Introduction

Caspases result in the induction of both intrinsic and extrinsic apoptosis. All caspases are expressed as inactive zymogens, which require activation through dimerization or cleavage. Initiator caspases require dimerization by oligomerization through homotypic domain interactions and subsequent cleavage to gain full functionality^{7,19}. This activation only occurs when the initiator caspases are recruited by adaptor proteins into the membrane bound DISC (in the case of caspase-8 and -10) or the intracellular Apoptosome (in the case of caspase-9)¹⁷. In the case of executioner caspases, i.e. caspase-3, -6 and -7, they are activated through cleavage by the initiator caspases. Interestingly, while all executioner caspases induce apoptosis, caspase-6 has unique target substrates compared to caspases-3 and -7¹⁷.

Caspases induce cell death through cleavage and inactivation of a vast repertoire of proteins. *In vivo*, targeted proteomics demonstrated that approximately 400 proteins are caspase substrates^{20,21}. While this may give an overestimation of the true caspase substrate set, it still demonstrates the significance that caspases play in cellular and whole organism homeostasis¹⁷. Many of the target substrates are pro-survival proteins that are inactivated upon cleavage by caspases²², including PARP, which is involved in DNA repair²³, and inhibitor of caspase-activated DNase, that inhibits apoptosis-induced DNA fragmentation²⁴. Paradoxically, there are also proteins that undergo a gain of function upon caspase cleavage²², including the executioner caspases and Bid, mentioned above. While this project is mainly focused on the caspases outlined above, other caspases, i.e. caspase-2 and caspase-6, also have important physiological roles in the induction of apoptosis. One such example is caspase-2, which is activated by the PIDDosome in response to genotoxic stress²⁵.

Mammalian IAPs

1.1.4. Structure and function

The first baculovirus *iap* gene was discovered in 1993 in virally infected *Spodoptera frugiperda* insect cells²⁶. It was reported these proteins were involved in suppressing the host cell's induction of apoptosis. Since then *iap* homologs have been found in yeast, nematodes, flies, and higher vertebrates, highlighting their importance in cellular processes^{27–30}. IAPs are a conserved family of proteins, characterised by the presence of one to three repeats of the BIR (baculovirus IAP-repeat) domains. These BIR domains are ~70-residue-large zinc binding domains that contain the signature sequence CX₂CX₁₆HX₆C (C, cysteine; H, histidine; and X, any amino acid). These sheets fold as three-stranded β sheets surrounded by four α helices that mediate protein-protein interaction. The RING (really interesting new gene) domain in IAPs has received much attention due to its ability for autoubiquitylation and transubiquitylation of their binding partners³¹. This ubiquitination results in signalling for complex formation or degradation. In addition to promoting ubiquitylation, certain IAP proteins can also bind to other ubiquitin (K11, K48 or K63) linkages through their Ubiquitin Binding Association (UBA) domains^{32–34}. In mammals, there are 8 known IAP proteins – NAIP (neuronal apoptosis inhibitory protein; BIRC1), cIAP1 (cellular inhibitor of apoptosis 1; BIRC2), cIAP2 (cellular inhibitor of apoptosis 2; BIRC3), XIAP (X-chromosome-linked inhibitor of apoptosis; BIRC4), Survivin (BIRC5), Apollon/Bruce (BIRC6), ML-IAP (melanoma IAP; BIRC7) and ILP-2 (BIRC8)³⁵ (**Figure 1.2**). Of the mammalian IAPs, the most studied are cIAP1, cIAP2 and XIAP. Originally, it was thought all three were *bona fide* caspase inhibitors. However, more recently, it has come to light that only XIAP can directly inhibit caspases, whereas cIAP1/2 function to regulate TNF α signalling outcome^{36–39}. It is clear that, despite differing functions, all three proteins are predominantly upregulated in many cancers⁴⁰.

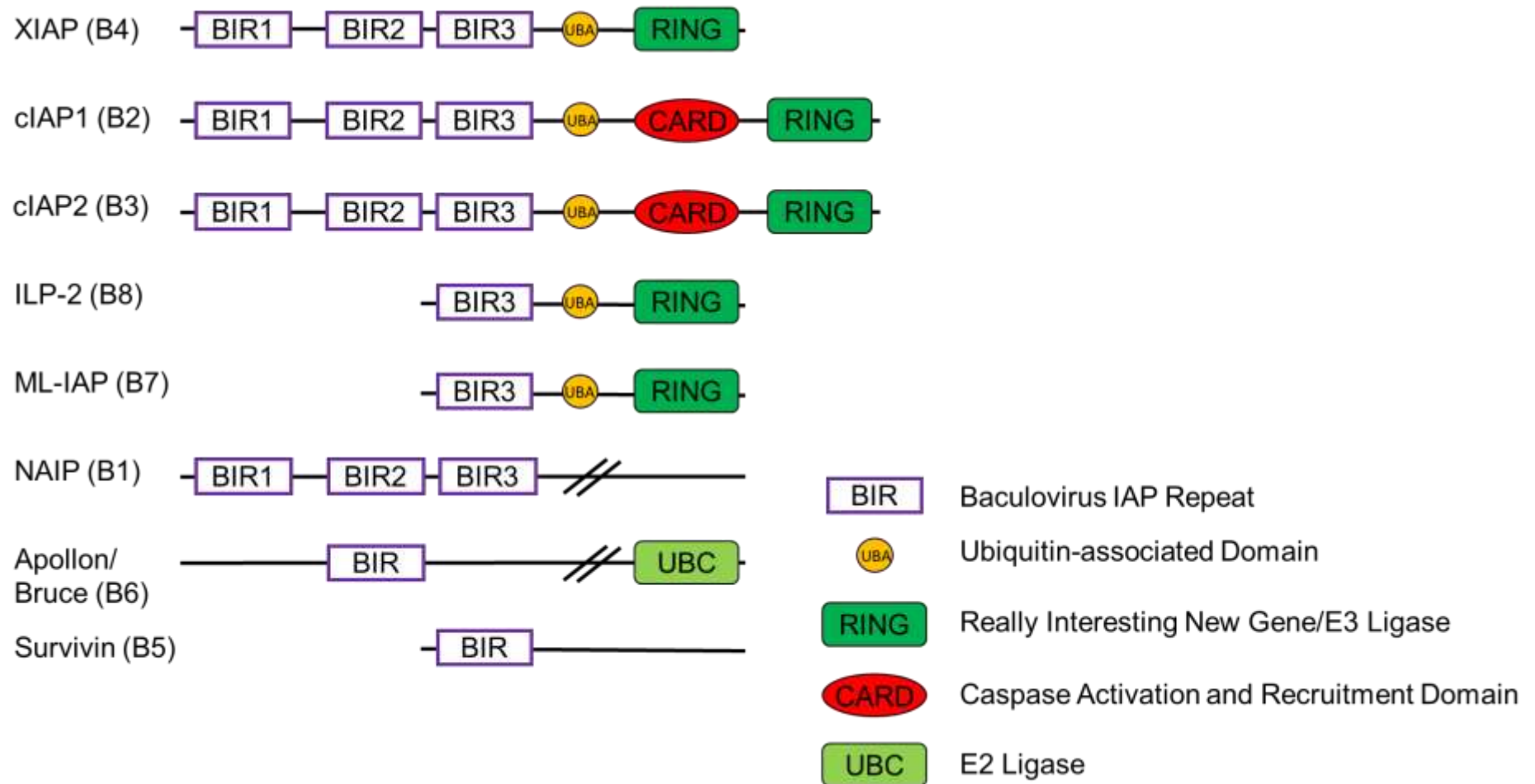


Figure 1.2 | Structure of the mammalian IAP family. IAP proteins are characterised by the presence of one or more BIR domains. It was originally thought these proteins inhibited cell death through directly binding to and inhibiting caspases. However, recently, there has been recognised there is a subset of these proteins may inhibit cell death through ubiquitination and, in some cases, degradation of their target proteins.

1.1.4.1. *clAP1 and clAP2*

clAP1/2 are functionally redundant, likely resulting from a recent evolutionary gene duplication event, as zebrafish only have clAP1⁴¹. It was originally thought that clAP1/2 also functioned as distinct caspase inhibitors due to similar homology to XIAP. It was not until 2007, however, when three groups independently published that clAPs function primarily to regulate TNF α signalling that the true function of clAPs was discovered^{36–38}. These groups found that genetic deletion or pharmacological ablation of clAPs resulted in cell death when TNF α was present. The proposed mechanism was that this death was dependent on the presence of an inducible TNF α autocrine loop. In this model, clAP1/2 is depleted, resulting in activation of the nuclear factor kappa-light-chain-enhancer of activated B cells (NF- κ B) pathway and TNF α secretion. When TNFR1 is activated by TNF α , it forms the pro-survival complex, Complex I (see **Section 1.1.6**). However, in the absence of clAP1/2, RIP is deubiquitinated, forming the pro-death complex, Complex II. Furthermore, regulation of the outcome of TNF α signalling by clAP1/2 was not the only novel finding of these studies. Two groups also uncovered a mechanism by which clAP1/2 regulates the non-canonical NF- κ B pathway through regulation of NF- κ B-inducing kinase (NIK; see **Section 1.1.8**)^{36,38}.

Despite this functional redundancy, clAP1 and clAP2 still have specialised roles. For example, clAP1 targets clAP2 for proteasomal degradation, but not *vice versa*⁴². Indeed, despite both proteins possessing a RING domain, clAP2 is unable to promote autoubiquitylation, thus requiring clAP1 for its ubiquitination and degradation⁴³. However, the RING domain of clAP2 is still fully functional, and is able to ubiquitinate RIP1 and NIK, thereby suppressing apoptosis. As clAP1 is the predominant clAP, its depletion relieves non-canonical NF- κ B suppression, which induces clAP2 expression^{36,38}. This has the ability to promote resistance to TNF α killing as clAP2 can inhibit the apoptotic signalling pathways⁴⁴. As clAP2 depletion is dependent on its RING domain, cancers that express mutant clAP2, i.e. clAP2-MALT1 oncogene in lymphomas⁴⁵, are likely to be resistant to TNF α -mediated cell death. This is because the clAP2-MALT1 fusion protein lacks the clAP2 RING domain which allows for constitutive NF- κ B activity mediated by MALT⁴⁵. This has implications for cancers, as in the absence of clAP1, clAP2 is not degraded,

Introduction

meaning it can continue signalling for survival. Furthermore, cIAP2 is known to be critical for the innate inflammatory response to lipopolysaccharide (LPS)⁴⁶. Indeed, in cIAP2 null mice, macrophage inflammatory action was severely limited, resulting in resistance to sepsis, but increased susceptibility to LPS-induced cell death. cIAP1 also has specialised roles in nitric oxide production and release as, in cIAP1 null mice, inducible nitric oxide synthase expression was impaired, limiting macrophage mediated inflammation⁴². This again demonstrates the importance of cIAPs in inflammation. Due to their regulation of the NF-κB pathway, cIAPs are now recognised as critical determinants at the crossroads between immunity and cell death⁴⁷.

Table 1.1 | Reported inhibitory constants (K_i in M) from IAP against human caspases. Adapted from³⁵

Caspase	cIAP1	cIAP2	XIAP
3	1.08×10^{-7}	3.5×10^{-8}	7×10^{-10}
7	4.2×10^{-8}	2.9×10^{-8}	2×10^{-10}
8			$>10^{-5}$
9			1×10^{-9}

cIAP (cellular IAP), XIAP (X-linked inhibitor of apoptosis)

1.1.4.1. XIAP

XIAP is the most potent caspase inhibitor of the mammalian IAP family. In fact, despite significant homology between many members of this family, only XIAP inhibits caspases at physiologically relevant levels³⁹ (**Table 1.1**). Due to these properties, XIAP is perhaps one of the most studied IAPs. Interestingly, there are two distinct regions by which XIAP binds to caspases⁴⁸. Structural studies have shown that XIAP binds to the small C-terminal subunit of caspase-9 *via* its BIR3 domain, which is only exposed upon caspase-9 cleavage⁴⁹. Conversely, XIAP binds to caspases-3 and-7 through its BIR2 domain and the preceding linker region^{50,51}. Functionally, XIAP upregulation results in resistance to TRAIL-induced cell death due to its ability to inhibit caspases⁵². Conversely, genetic loss of XIAP re-sensitises mouse-derived *Bid*^{-/-} hepatocytes to Fas-induced apoptosis⁵³. This demonstrates that XIAP can discriminate between type I and type II cell death.

Introduction

Outside of its role as a caspase inhibitor, there is evidence that XIAP can function to promote survival through its RING domain³⁵. AKT is a potent signalling for cell survival and is activated by PI3K-induced phosphorylation⁵⁴. PTEN (phosphatase and tensin homolog deleted on chromosome ten) is a tumour suppressor gene known to inhibit AKT phosphorylation and signalling⁵⁵. It was reported that upon XIAP knockdown, there was a reduction in the ubiquitination of PTEN. This resulted in elevated PTEN at the protein level and increased activation of AKT⁵⁶. There are also reports showing XIAP can bind to type-I transforming growth factor- β (TGF- β) and type-I bone morphogenetic (BMP) superfamily members and augment their activity by acting as a stabilising protein^{57,58}. Like cIAPs, XIAP possesses a RING domain, which is reported to ubiquitinate caspase-3 for proteasomal degradation, consequently sensitising cells to Fas agonistic antibodies⁵⁹. Interestingly, unrelated to its RING domain, XIAP has also been implicated in NOD signalling⁶⁰. Through binding to RIP2 *via* its BIR2 domain, XIAP was shown to promote NOD signalosome-mediated NF- κ B activation. This binding pocket is also where the endogenous IAP inhibitor, SMAC, binds⁶¹.

1.1.4.2. NAIP

NAIP was the first of the mammalian IAP proteins to be discovered, where it was found to be partially deleted in the chromosomal region 5q13.3 in patients with spinal muscular atrophy²⁸. As the name suggests, NAIP is expressed in neurons, but also in macrophages⁶². The role of this protein in macrophages was shown to be essential in resistance to *Legionella pneumophila* both *in vitro* and *in vivo*^{62,63}. Using mice sensitive to *Legionella pneumophila*, it was shown that only full length NAIP resulted in inhibition of bacterial growth⁶³. It was hypothesised that this was due to inhibition of caspase-3, thereby prolonging the lifespan and antimicrobial effects of the macrophages⁶². However, it was not until 2003 that it was discovered NAIP directly inhibits caspase-3 and -7 primarily through its BIR2 domain and, to a lesser extent, its BIR3 domain⁶⁴. This caspase inhibition is also demonstrated through its ability to prevent apoptosis after treatment with TNF α and the translation inhibitor, cycloheximide (CHX)⁶⁵.

Introduction

1.1.4.3. *Survivin*

The IAP protein, Survivin, contains just a single BIR domain and, unlike other IAPs which are found in both foetal and adult tissues, is expressed solely in embryonic tissues, including the lung, kidney, brain and liver⁶⁶. Survivin promotes survival through binding to the processed forms of caspase-3 and -7⁶⁷. However, Survivin has also been shown to have roles in mitosis, particularly in cytokinesis³⁵. Indeed, it was found that loss of Survivin *in vivo* resulted in microtubule bundling and impaired cytokinesis⁶⁸. It was thought that this effect was mediated through the Aurora1 kinase, which plays an essential role in mitosis. Due to this role in mitosis, it was recently demonstrated that Survivin has a role in liver regeneration. Indeed, knockdown of Survivin resulted in impaired liver regeneration after a partial hepatectomy in mice⁶⁹. Interestingly, in this study loss of Survivin had no effect on apoptosis. While compounds have been developed that inhibit Survivin expression, most of these act indirectly and do not physically interact with the protein itself⁷⁰. One compound that selectively inhibits *survivin* gene transcription and protein expression has completed phase I and is currently undergoing phase II testing⁷⁰.

1.1.4.4. *Apollon*

Apollon is the largest of the IAP family and is the only member to be membrane bound⁷¹. Apollon primarily inhibits apoptosis through regulation of the pro-apoptotic protein, SMAC, but also through modulation of caspase-3¹⁵. Apollon regulates apoptosis by targeting SMAC and caspase-3 for ubiquitination and degradation *via* its UBC (ubiquitin conjugating) domain, thus relieving SMAC and caspase-3 of their pro-apoptotic effect⁷³. Targeted disruption of Apollon *in vivo* resulted in embryonic and neonatal lethality and, in embryos at E18.5, a body weight reduction of 10-20%. This reduction in body weight was not due to an increase in apoptosis, suggesting an effect on proliferation. Further investigation found that more than half of the mutant embryos had defective angiogenesis, often coinciding with severe oedema⁷³. As such, Apollon is not considered a drug-able target.

Introduction

1.1.4.5. *ML-IAP*

ML-IAP was originally identified in human melanoma cells where it was found to be over-expressed⁷⁴. ML-IAP inhibits apoptosis by directly inhibiting both caspase-3 and caspase-9, which is mediated by ML-IAP's only BIR domain⁷⁴. However, it has also been found to be preferentially expressed in the eye in both humans and mice, particularly in the ciliary body epithelium and retinal pigment epithelium⁷⁵. Interestingly, ML-IAP null mice appeared to have no ocular defects suggesting ML-IAP does not have a role in ocular development. It was hypothesised that as cancer cells are constantly on the verge of death, the protein plays a more prevalent role in their physiology and, in the eye, its role is redundant due to expression of other IAPs⁷⁵.

1.1.4.6. *ILP-2*

ILP-2 is expressed solely in primate species, where, in normal tissues, it is reported to be expressed only in the testis and lymphoblastoid cells⁷⁶. While ILP-2 was found to bind to and inhibit caspase-9, it is unlikely to be a *bona fide* caspase inhibitor like XIAP. This is due to a lack of a linker segment N-terminal to the inhibitory BIR domain. There is currently very little published research on ILP-2, but as the native protein is so unstable, the BIR-dependent functions are thought to be lost³⁵.

1.1.5. Ubiquitination

Ubiquitination is a tri-step post-translational modification (PTM) involved in cell signalling in which ubiquitin-chains are attached to proteins. Depending on the type of ubiquitin-chain attached, this PTM can promote complex assembly, act as a binding protein, or signal for proteasomal degradation. Ubiquitin is a 76-amino acid covalently attached *via* its C-terminus to a lysine residue on the target protein. Briefly, a ubiquitin molecule is transferred to one of two E1 enzymes in an ATP-dependent manner. Once activated, the E1 enzyme transfers the ubiquitin to one of several E2 enzymes in the conjugation step. In the final ligation step, the ubiquitin chain is transferred to one of hundreds of E3 ligases, also known as ubiquitin ligases, which attach the ubiquitin molecule(s) to the target substrate^{77,78}.

There are two types of ubiquitin attachment, mono-ubiquitin, involving just one ubiquitin molecule, and poly-ubiquitin⁷⁹. Poly-ubiquitin can be further divided into linear – where ubiquitins are attached head-to-tail, and lysine (K)-linked chains, where each of the ubiquitin molecules are attached by the K-residue number indicated, i.e. K63-linked chains are joined through the 63rd K-residue in the ubiquitin molecule. Within the K-linked chains, there are three well characterised linkages, K11, K48 and the aforementioned K63-linked ubiquitin-chains. Each of these K-linked chains has a different role - K11-linked chains are involved in complex formation and proteasomal degradation, K63-linked chains in complex assembly and K48-linked chains in proteasomal degradation. cIAP1/2 have the ability to attach all three of these poly-ubiquitin chains to themselves and their target proteins^{32,80}.

SMAC

SMAC/DIABLO is a pro-apoptotic protein released from the mitochondria during apoptosis. SMAC functions by directly binding to and inhibiting or degrading IAPs. SMAC is synthesised as a precursor protein of 239 amino acids and is shuttled into the mitochondria due to its 55 amino acid N-terminal mitochondrial transport sequence (**Figure 1.3**)⁶¹.

Introduction

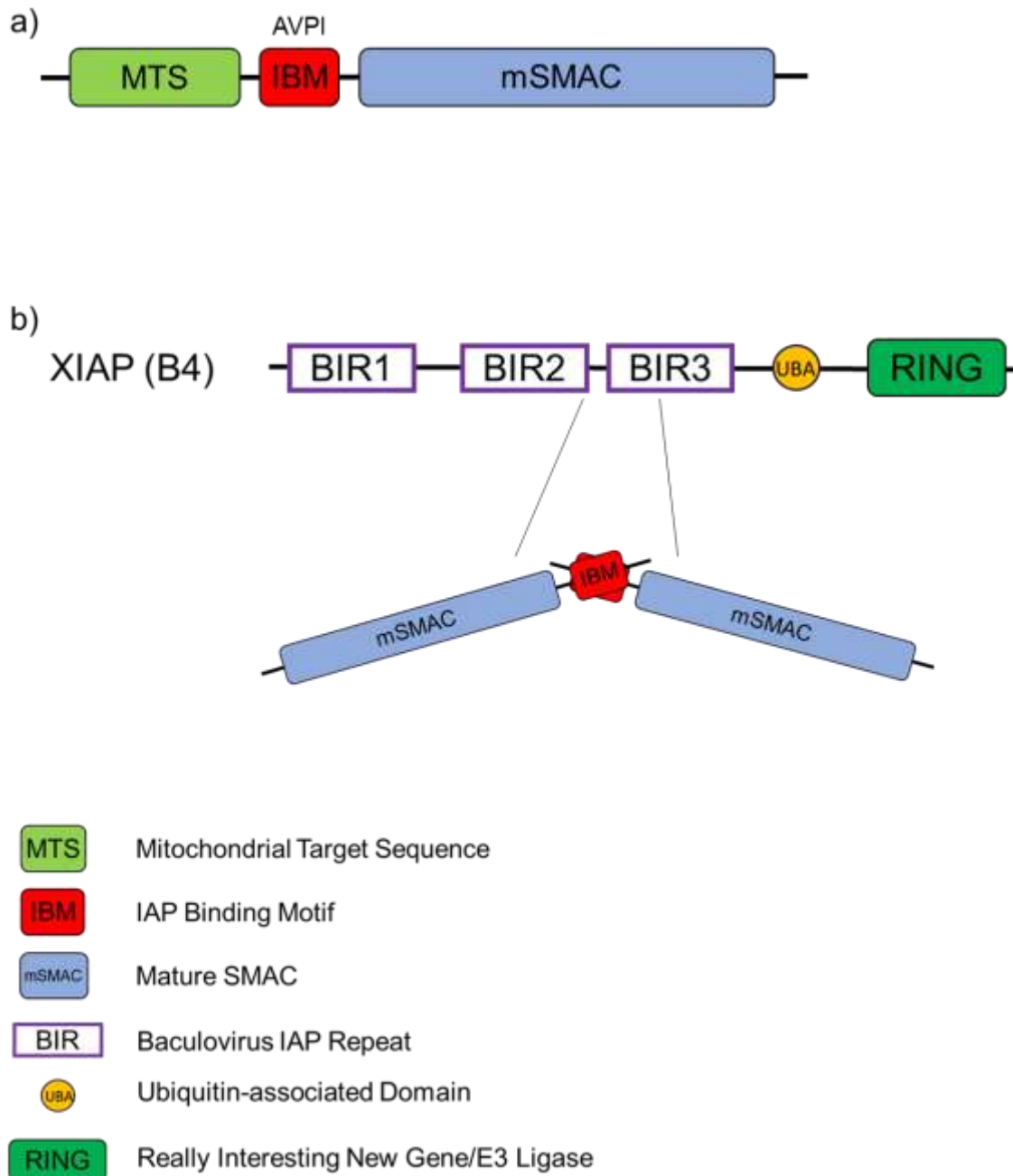


Figure 1.3 | Structure and function of SMAC. a) SMAC is comprised of a mitochondrial targeting sequence which must be removed before it is released from the mitochondria. The IAP binding motif (IBM) interacts with IAP proteins. b) Once dimerised, SMAC inhibits IAP proteins through IBM binding to the BIR3 domain and the preceding linker region.

Introduction

Once translocated to the mitochondria, this target sequence is then removed. During apoptosis, SMAC is released from the mitochondria into the cytosol where it can bind to IAPs, including XIAP and cIAP1/2⁶¹. In solution, SMAC forms a dimer, which is essential for its function as mutations in the dimeric interface completely abolish binding to both BIR2 and BIR3 of XIAP and a total loss of SMAC function⁸¹. The same research also showed that, for the first time, a short, seven residue peptide that mimicked the N-terminal sequence of SMAC, resulted in caspase-3 activation in a cell free assay⁸¹. In the same year, structural studies showed that SMAC binds to the BIR domains of XIAP through the tetrapeptide sequence AVPI (Alanine, Valine, Proline and Isoleucine) which is mediated by hydrogen bonds and van der Waals contacts⁸². As SMAC functions as such a potent pro-apoptotic protein, its role in cancer is very important. However, while there are a small number of reports showing SMAC is up-regulated in cancer, most cancers demonstrated a down-regulation of SMAC⁸³.

TNF α signalling

TNF α is a pleiotropic cytokine involved in processes ranging from cell proliferation, inflammation, immunity, cell survival and, paradoxically, cell death. TNFR1, along with other immune receptors, can activate the NF- κ B pathway, which promotes the expression of a plethora of genes involved in survival, inflammation, proliferation and migration.

1.1.6. Pro-survival Complex I

The canonical pathway is receptor-mediated through ligation of the TNF ligand to TNFR1. TNFR1 is a transmembrane receptor that, upon ligation, trimerises and recruits a pro-survival protein complex, Complex I. Complex I is a membrane bound complex that consists of TRADD (TNFR-adaptor protein with DD), TRAF2 (TNFR-associated factor 2) and cIAP1/2^{84,85}. TRADD binds to TNFR1 *via* homotypic interaction of its DD, which is essential for TRAF2/3 recruitment. TRAF2/3 are E3 ligases that initially were thought to inhibit cell death through recruitment of cIAPs, which were assumed to directly inhibit caspases⁸⁶. Later, in

Introduction

2004, it was discovered that RIP1 was not ubiquitinated in the absence of TRAF2, leading to the hypothesis that TRAF2 was the E3 ligase for RIP1⁸⁷. However, it was not until 2007 that it was discovered that cIAPs ubiquitinated RIP1 and that TRAF2/3 was likely an adaptor protein that facilitated this function^{36–38}. In this model, cIAP1/2 ubiquitinate RIP1, allowing for recruitment of the NF- κ B-activating, IKK (inhibitor of κ B kinase) complex (IKK α , IKK β and NEMO [NF- κ B essential modulator]/IKK γ). Once recruited, this complex phosphorylates I κ B (inhibitor of κ B), inducing its degradation allowing for transcription factor entry into the nucleus. This translocation then induces transcription of a plethora of NF- κ B related genes (**Figure 1.4 and 1.5**).

1.1.7. Pro-death Complex II

While TNF α primarily signals for survival, there are conditions in which it can signal for cell death. It does this through formation of a complex known as Complex II. Formation of Complex II is only possible when RIP1 is deubiquitinated, which occurs in the absence of cIAP1/2. When it was discovered that cIAP1/2 ubiquitinate RIP1, the molecular switch that controlled Complex II formation was finally deciphered. RIP1 is ubiquitinated on the lysine residue K377, and this prevents Complex II formation by sterically inhibiting binding of RIP1 to FADD⁸⁸. However, in cases of genetic or pharmacological depletion of cIAPs, RIP1 is not ubiquitinated. This results in internalisation of the receptor and complex, forming an often cytosolic complex, Complex II, which can be further sub-divided into Complex IIa or IIb⁸⁹ (**Figure 1.4 and 1.5**). Once RIP1 is deubiquitinated, it dissociates from the internalised receptor while still bound to TRADD, allowing FADD recruitment through DD interaction. FADD then recruits caspase-8 through DED homotypic binding. Caspase-8 is then activated, inducing apoptosis⁸⁹. Complex IIb is a secondary pro-death complex that is dependent on RIP3 to induce necroptosis and is found in situations of caspase inhibition^{90,91}.

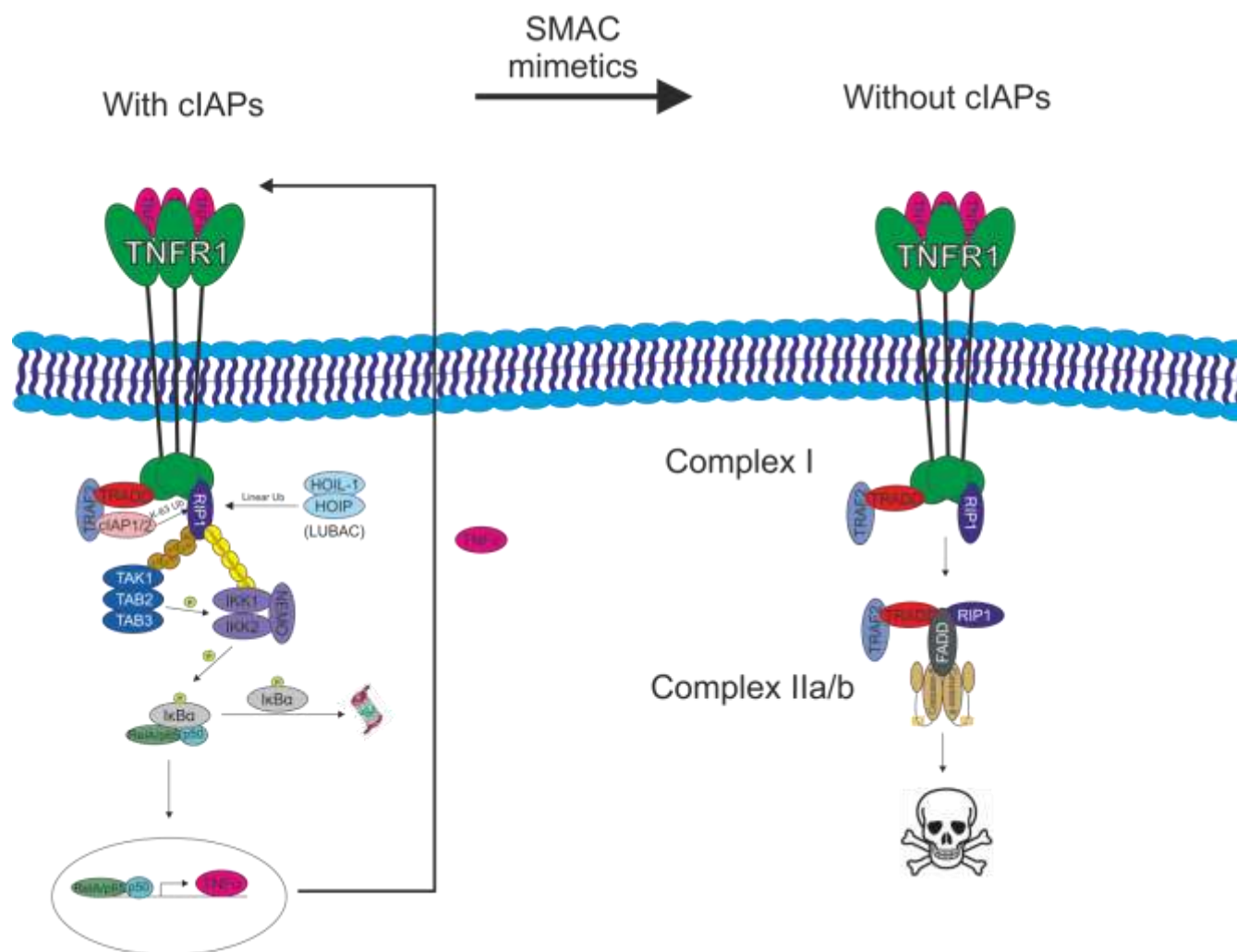


Figure 1.4 | Canonical NF-κB activation through TNFR1. Upon ligation of the receptor with TNFα, Complex I forms, allowing cIAP1/2 to ubiquitinate RIP1, inducing NF-κB signalling. Without cIAPs, RIP1 is not ubiquitinated resulting in formation of the pro-apoptotic, Complex II.

Introduction

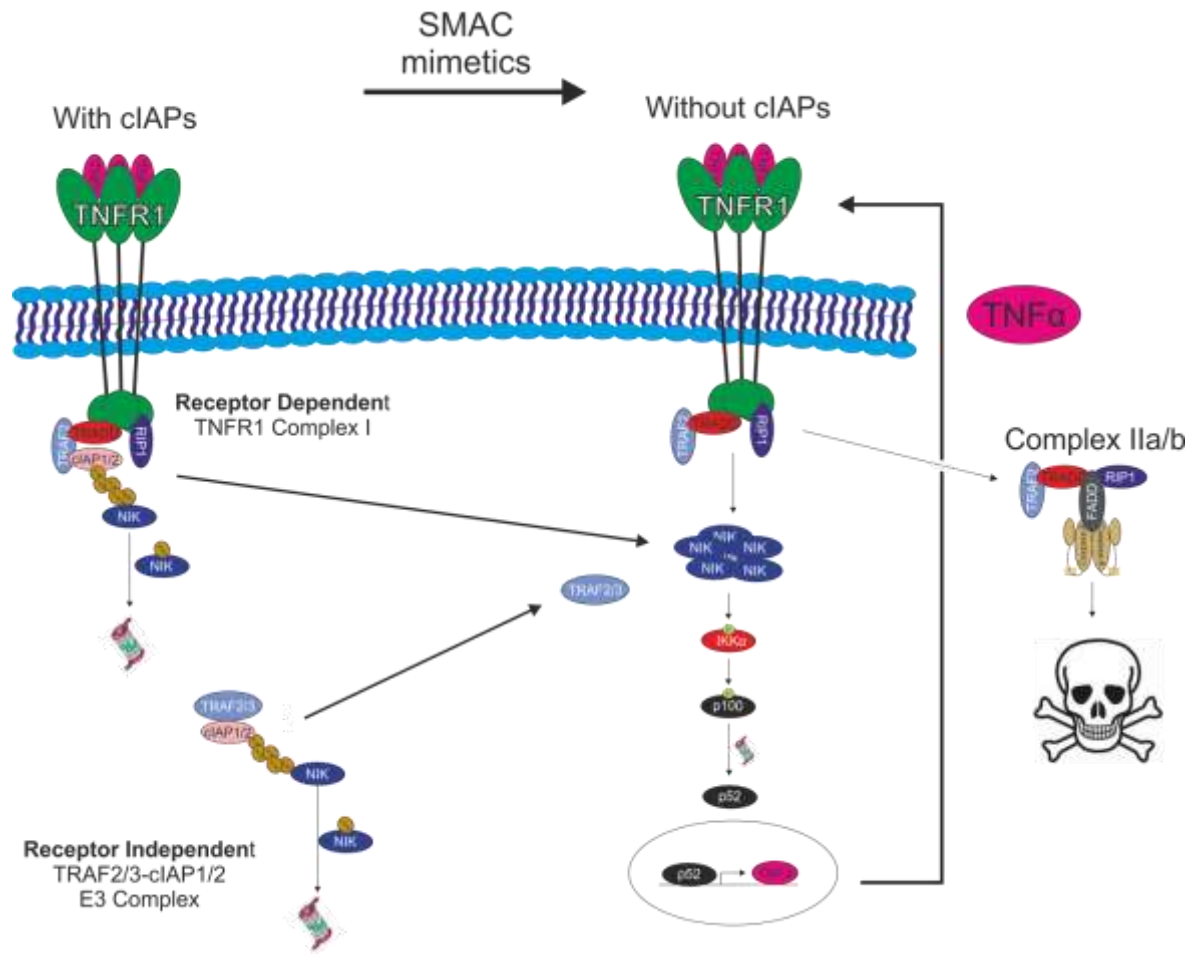


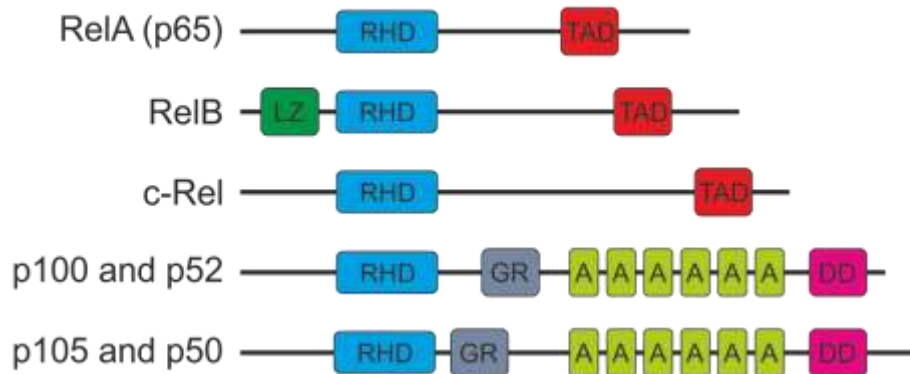
Figure 1.5 | Non-canonical NF-κB signalling can be dependent or independent of TNFR1. Complex I inhibits the non-canonical NF-κB pathway through NIK ubiquitination and degradation, which is mediated by cIAPs. cIAP1/2 can also inhibit this pathway through a cytosolic complex with TRAF2, which also ubiquitinates and degrades NIK.

NF- κ B pathway

The NF- κ B pathway is perhaps one of the most studied inflammatory pathways. NF- κ B is a pro-inflammatory transcription factor family that induces the expression of various cytokines, chemokines and genes⁹². NF- κ B can be activated either canonically, *via*, TNFR1 (**Figure 1.4**), Toll-like receptors, B-cell receptors or T-cell receptors, or non-canonically, through B-cell activating factor belonging to TNF family receptor, CD40, receptor activator for NF- κ B, lymphotoxin β -receptor or TNFR1 via NIK (**Figure 1.5**)⁹³. While its primary role is an inflammatory response, the genes induced by NF- κ B influence cell survival, proliferation and differentiation⁹⁴. As NF- κ B is such a powerful survival pathway, it has many layers of regulation and negative feedback loops. For example, activation of the pathway results in synthesis of its own inhibitory proteins, I κ B α , I κ B β and I κ B ϵ . The NF- κ B protein family consists of five transcription factors, p50, p52, p65/RelA, c-Rel and RelB (**Figure 1.6**). All five proteins share a Rel homology domain (RHD) for homo- and heterodimerisation and DNA binding⁹⁴. The transcription activation domain (TAD), however, which is required for positive gene-regulation, is only present in p65, c-Rel and RelB, meaning TAD deficient proteins cannot induce transcription unless bound to a TAD-containing protein⁹⁴ (**Figure 1.6**). Once bound to the promoter, the NF- κ B pathway regulates transcription of over 150 genes. The vast majority of these are prosurvival proteins, including p53, TNF α , interleukins and tumour suppressors. However, the NF- κ B pathway also transcribes for inhibitors of its own pathway and pro-apoptotic molecules such as CD95 and CD95L⁹⁵.

It was previously thought that under basal conditions, NF- κ B dimers are sequestered in the cytosol by one of three I κ B proteins, or one of two precursor proteins, p100 and p105, thereby preventing nuclear translocation and DNA binding. However, structural studies have shown only the nuclear localisation sequence of p65 is masked, whereas the p50 remains exposed⁹⁶. This, with the nuclear export sequences in I κ B α and p65, results in constant shuttling between the nucleus and cytoplasm. Thus, when I κ B α is degraded, this favours nuclear translocation and binding of the transcription factor to promoter regions containing the κ B sequence, initiating gene transcription⁹⁴. However, it is as yet unknown which combination of the dimers, whether hetero- or homodimers, results in transduction of which genes.

Transcription Factors



NF-κB Inhibitors

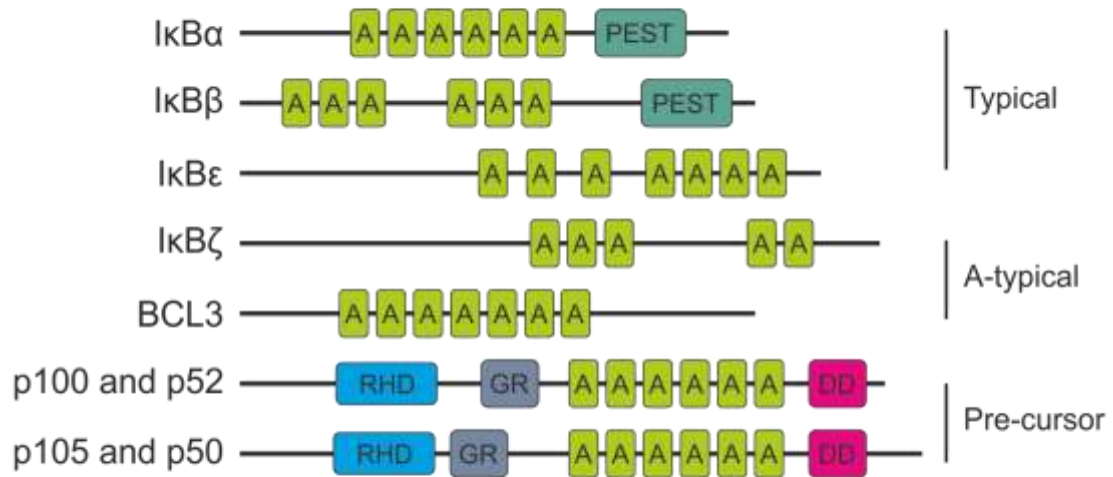


Figure 1.6 | Transcription factors and inhibitors of the NF-κB pathway. There are 5 transcription factors in the NF-κB family, which are characterised by the presence of a RHD. The inhibitors of the NF-κB pathway are divided into typical, a-typical and pre-cursor types (adapted from²⁸³).

1.1.8. Canonical and non-canonical NF- κ B signalling

In the context of the TNF α /NF- κ B pathway, there are two known activation models; the canonical and the non-canonical. Canonically, NF- κ B signalling can be mediated *via* immune receptors; non-canonically, there are two mechanisms, receptor-dependent, or receptor-independent.

1.1.8.1. *Canonical NF- κ B signalling mediated through TNFR1*

TNF α -mediated NF- κ B activation is canonical as the signal transduction is executed through TNFR1 Complex I and is initiated by phosphorylation of I κ B by the IKK complex, which consists of IKK α /IKK1, IKK β /IKK2 and the regulatory subunit NEMO/IKK γ ⁹⁷ (**Figure 1.4**). Once phosphorylated, the I κ B proteins are K48-linked poly-ubiquitinated by the E3 ligase complex, SCF ^{β TrCP}, and degraded by the 26S proteasome⁹⁸. This allows for nuclear translocation and binding of the NF- κ B dimers to promoter and enhancer regions containing the κ B sequence 5' GGRXWYYCC 3' (X - any base, W adenine or thymine, R - purine and Y - pyrimidine)⁹⁹.

1.1.8.2. *Non-canonical NF- κ B signalling*

The non-canonical NF- κ B signalling is both receptor-dependent and receptor-independent. At rest, is NIK negatively regulated by cIAPs in the membrane bound, Complex I, or cytosolic cIAP/TRAF complex (**Figure 1.5**). In the presence of cIAPs, NIK is K48-linked ubiquitinated and degraded, whereas upon cIAP ablation, NIK is up-regulated^{36,38}. Once up-regulated, NIK phosphorylates the IKK α of the IKK complex⁹⁷, which in turn phosphorylates the I κ B domain of p100, resulting in processing to p52 and nuclear localisation (**Figure 1.5**). Alternatively, binding of the TNF superfamily member TWEAK to its receptor promotes degradation of TRAF2 and cIAPs, allowing NIK stabilisation and activation of the non-canonical NF- κ B pathway¹⁰⁰.

Development of small molecule inhibitors

Tumour cells have evolved to become resistant to the plethora of pro-apoptotic signals found in normally functioning cells. Indeed, evasion of apoptosis is one of the hallmarks of cancer¹⁰¹. In an attempt to induce cell death, cytotoxic chemotherapeutics have been developed. Many of the early compounds to treat cancer were DNA damaging agents that simply targeted rapidly proliferating cells, which resulted in significant side-effects such as nausea, hair loss, vomiting and diarrhoea^{102,103}. Additionally, due to the rapidly proliferating and chromosomally unstable nature of tumour cells, many patients relapsed due to the development of resistance to these agents¹⁰².

As such, these drugs resulted in a 'one-size-fits' all approach that emphasised cytotoxic chemotherapy. However, with the development of small molecule inhibitors, there was the ability to agonise or antagonise specific molecules in cells, be they receptors or proteins in a signalling cascade. In pre-clinical studies, these compounds were efficacious in the nanomolar concentrations and very specific to their intended target(s). One of the trail-blazer drugs that validated the drive for small molecule inhibitor development was the discovery of Imatinib, which was used to treat Chronic Myeloid Leukaemia^{104–106}. Imatinib is an inhibitor that targets tyrosine kinase proteins, most notably BCR-ABL, inhibiting their prosurvival signals. Due to the specificity of Imatinib, the side-effects of this drug are relatively benign¹⁰⁷. Imatinib also demonstrated significant clinical efficacy, improving the 5-year survival rate for chronic myeloid leukaemia from 31% 1990 to 63% for patients diagnosed between 2005 and 2011. Furthermore, it was reported that patients on Imatinib had a 5-year survival rate of 89%¹⁰⁸. After the success of this compound, many other drugs were developed that target proteins upregulated in cancer, including epidermal growth factor receptors and oestrogen receptor (ER) inhibitors. Perhaps one of the most well-known of these is Tamoxifen, an ER antagonist used in breast cancer. Tamoxifen is used primarily for treatment of breast cancers where it inhibits ER-induced tumorigenesis. Clinically, Tamoxifen substantially improves 10-year survival rates for ER positive and unknown ER-status women¹⁰⁹. However, problems arose with other small molecule inhibitors

because they had little efficacy in the clinic and the tumours evolved resistance to these targeted molecules. One way to overcome this is to use combination therapies where a small molecule inhibitor would be administered in conjunction with a DNA damaging agent in an effort to 'sensitise' cells, thereby reducing the dose and limiting toxicity to non-tumour cells.

SMAC mimetics (SMs)

In light of the role of SMAC in inhibiting IAPs, there have been several synthetic compounds designed to mimic the AVPI sequence. A seven residue peptide compound showed the N-terminal sequence was essential in mediating SMAC's effect on IAPs⁸¹. However, the first reported case of a synthetic compound based on the AVPI motif was in 2004¹¹⁰. This compound sensitised HeLa cells to both TNF α and TRAIL-induced apoptosis¹¹⁰. The proposed mechanism was that the compound, which bound to cIAP1/2 and XIAP, relieved IAP-mediated caspase inhibition. However, it wasn't until 2007 that the precise mode of action of SMs was determined³⁶⁻³⁸. Using SMs, it was found that cIAP1 indirectly regulates apoptosis through determining the outcome of TNF α signalling. Indeed, it was found that SMs are not required to bind XIAP to induce anti-tumour activity¹¹¹. Since then many SMs have been developed based on this AVPI sequence. SMs induce cIAP1/2 depletion through autoubiquitylation, which signals for proteasomal degradation³⁸. In the absence of SMAC or SMs, cIAP1 sequesters its RING domain within a compact monomeric structure, thus preventing dimerization and subsequent degradation¹¹². There are many reasons why SMs are popular clinical candidates; they are specific to IAPs³⁷, they inhibit cell death through multiple pathways¹¹³ and they do not provoke mutations in surviving cells¹¹⁴.

1.1.9. SMs used in this project

While there are many SMs in development, they all fall into two classes; monovalent and bivalent. Monovalent SMs only contain a single AVPI sequence, limiting them to engaging a single IAP molecule. Bivalent compounds, however, contain two AVPI sequences, allowing them to engage multiple BIR domains. This has significant advantages as SMAC, along with many other anti-apoptotic

Introduction

proteins, is a dimer *in situ*⁸¹. In this study, I wanted to use SMs from both classes to investigate any structural-related difference in activity. I therefore chose four compounds, two monovalent and two bivalent, which are outlined below.

1.1.9.1. AT-406 (SM-406/Debio 1143)

Discovery of AT-406 was first reported in the Journal of Medicinal Chemistry in 2011¹¹⁵. It is a monovalent compound based on the crystal structure of SMAC interacting with the XIAP BIR3 domain^{81,115} (**Table 1.2**). In cell-free assays, AT-406 is reported to target cIAP1, cIAP2 and XIAP BIR3 with K_i of 1.9, 5.1 and 66.4 nM, respectively (**Table 1.3**). In MDA-MB-231 cells, the IC_{50} was 144 nM as determined by the water-soluble tetrazolium cell proliferation assay¹¹⁵. Using murine xenograft models, the same study found that AT-406 was well-tolerated at 100 mg/kg and showed tumour growth inhibition at a dose as low as 30 mg/kg¹¹⁵. Since then, there has been much pre-clinical and clinical data published using AT-406. *In vitro* studies have shown effective anti-tumour activity in a variety of solid tumours, including breast, head and neck squamous cell, and lung cancers, and also that AT-406-induced cytotoxicity is TNF α -dependent^{116–119}. *In vivo*, AT-406 demonstrated tumour growth inhibition in murine xenografts, which was mediated by cIAP1 degradation, and resulted in limited systemic toxicity¹²⁰.

Interestingly, there is published clinical data on AT-406 in 'first-in-man' and a phase I study^{121,122}. The first-in-man study treated patients with doses of AT-406 from 5 mg/kg to 900 mg/kg. Only one dose limiting toxicity (DLT) was reported at 180 mg/kg, which was increase in biomarkers of liver injury¹²¹. While the maximal tolerated dose was not reached in this study, cIAP1 depletion was observed in peripheral blood mononucleocytes (PBMC) at all doses. Most adverse drug reactions (ADRs) were gastrointestinal and just under 60% of patients were reported to have experienced some form of ADR, irrelevant of concentration. While there was no evidence of disease regression with AT-406 as a single agent, disease stabilisation was described in 16% of patients at doses of 120-900 mg. The phase I trial investigated AT-406 in combination with Daunorubicin and Cytarabine in patients with acute myeloid leukaemia¹²². With this treatment regime, it was reported that 38% of patients achieved complete remission, with 8% relapsing within the study period of March 2011 until January 2013.

Introduction

Table 1.2 | Structure and clinical progress of SMs used in this project.

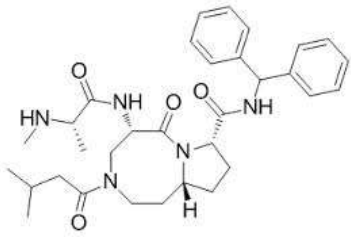
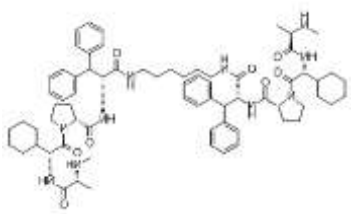
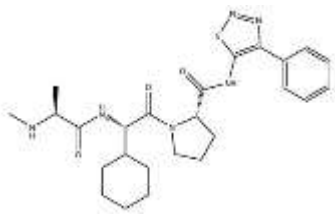
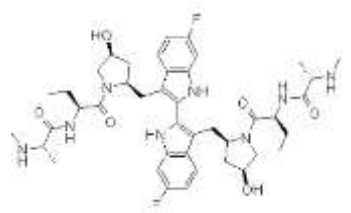
<u>Name</u>	<u>Type</u>	<u>Manufacturer</u>	<u>Structure</u>
AT-406 (SM-406/ Debio 1143)	Monovalent	Ascenta Therapeutics	
		Phase I/II Clinical Trials	
BV6	Bivalent	Genentech	
		Pre-Clinical	
GDC-0152	Monovalent	Genentech	
		Phase I Clinical Trial	
TL-32711 (Birinapant)	Bivalent	Tetralogic Pharmaceuticals	
		Phase I/II Clinical Trials	

Table 1.3 | Reported inhibitory constants (K_i) in nM for the SMs used in this project. Not reported (NR)

Compound	clAP1 BIR3	clAP2 BIR3	XIAP BIR3	ML-IAP
AT-406	1.9	5.1	66.4	N/R
GDC-0152	17	43	28	14
BV6	169	234	486	N/R
TL-32711	1	36	50	1

In the responsive patients, it was found that increases in plasma TNF α and IL-8 after the first dose of AT-406 predicted a better response. These data support the idea that SMs function best in combination with other chemotherapeutic agents.

1.1.9.1. GDC-0152

GDC-0152 is a monovalent compound that is actually based on structural studies of AVP'2,2'-diphenethylamine bound to the BIR domain of ML-IAP (**Table 1.2**)^{123,124}. Modification of the original structure resulted in a pan IAP inhibitor that targeted clAP1, clAP2, XIAP and ML-IAP. GDC-0152 was designed primarily to interact with the BIR3 domains of these proteins; as such the K_i for the BIR3 of clAP1, clAP2, XIAP and ML-IAP is reported to be 17, 43, 28 and 14 nM. For the BIR2 domains of clAP1 and clAP2, however, the K_i is 14.5 and 9.6 μ M, respectively. For the BIR3 of clAP1, clAP2, XIAP and ML-IAP however, the K_i is reported to be 17, 43, 28 and 14 nM, respectively (**Table 1.3**). The same study also investigated the effects of GDC-0152 *in vitro* and *in vivo*. Using MDA-MB-231 cells, the IC₅₀ killing was ~1.2 μ M after three days as determined by the CellTiter Glo cell viability assay. In normal mammary epithelial cells, GDC-0152 was reported to induce no killing¹²⁴. *In vivo*, GDC-0152 was administered weekly for five weeks at 10, 50 and 100 mg/kg of GDC-0152 in a MDA-MB-231 murine xenograft model. All doses demonstrated significant tumour activity and this effect was still seen when mice were dosed at 10 mg/kg daily or every third day for three weeks¹²⁴. Interestingly, while 100 mg/kg showed the quickest tumour regression when administered once weekly, all three doses resulted in 85-95% tumour

Introduction

reduction at day 21. The pharmacokinetics of GDC-0152 was then evaluated in healthy humans. Importantly, GDC-0152 showed linear pharmacokinetics over a wide range of doses in humans without significant toxicity¹²⁴.

There have also been independent investigations into GDC-0152 anti-tumour activity^{125–128}. *In vitro*, GDC-0152 was shown to prevent tumour cell growth in osteosarcoma cells¹²⁵. This effect was mediated by inhibiting the pro-inflammatory protein, ANGPTL2, which abrogated proliferation induced *via* the PI3K/AKT, but not the p38/MAPK pathway. GDC-0152 was also shown to impede glioblastoma cell growth both *in vitro* and *in vivo*, which was mediated through ML-IAP inhibition¹²⁷. At the time of writing there are no published clinical results of GDC-0152 as 'Adis Insight' states GDC-1052 has recently been discontinued as a treatment for cancer¹²⁹. Despite this, a study was published investigating GDC-0152 stability in humans¹³⁰. It was found GDC-0152 was stable in human plasma for one or two years if stored at -20°C or -70°C, respectively. Furthermore, it was stable in plasma for up to 25 h and through three freeze-thaw cycles. In whole blood, GDC-0152 was stable for 12 h if stored at 4°C.

1.1.9.2. BV6

BV6 was developed as a bivalent SM (**Table 1.2**), and was described in the seminal 2007 paper from Varfolomeev *et al.*, which co-discovered the regulation of cIAP1/2 by SMs³⁸. The K_i for BV6 against cIAP1, cIAP2 and XIAP BIR3 was reported as 169, 234 and 486 nM, respectively (**Table 1.3**)³⁸. These values are significantly higher than the other SMs used in this project. However, the potency of BV6 is mediated by its relatively low K_i for XIAP. As BV6 was one of the earlier SMs, it has been used extensively in publications investigating cIAPs signalling^{113,131–144}. Interestingly, BV6 is often used in studies where adverse effects have been found^{145–148}. However, most of these reports demonstrated that toxicity arose from BV6-induced NF- κ B activation. As such, this may be a phenomenon associated with all SMs, not specifically BV6. Despite this, as BV6 targets cIAPs and XIAP, there is also potential for inflammation. Other bivalent SMs induce bone marrow-derived macrophage cell death¹⁴⁹. As such, there is the

Introduction

possibility for BV6 to promote cell death in these cell types because of its affinity for cIAPs and XIAP, which is likely the reason it did not proceed to clinical trials.

1.1.9.3. TL-32711 (*Birinapant*)

TL-32711 is a 'second generation' bivalent SM and one of the most clinically advanced, having undergone extensive testing both in a pre-clinical and clinical setting^{143,144,150–159}. TL-32711 was first reported in 2009 at the 21st EORTC-NCI-AACR Meeting¹⁵⁹. Subsequently, in 2013, TL-32711 was reported to induce TNF α -independent cell death in human breast-tumour cells *in vitro*¹⁴³. While toxicity was not present in non-tumour cells *in vitro*, it was reported that this compound was not well tolerated *in vivo*¹⁵¹. As such, TL-32711 was redesigned to target only cIAP1 and ML-IAP and not inhibit XIAP-mediated NOD signalling (**Table 1.2**)¹⁵¹. This was achieved through removal of a β -branch at the P2' position and replacing it with a non-branched α -aminobutyric acid residue. This resulted in a reduced affinity for cIAP2 and XIAP and reduced cytokine secretion, consequently improving tolerability *in vivo*¹⁵¹. From this study, the reported K_i of TL-32711 for cIAP1, cIAP2, XIAP and ML-IAP are 1, 36, 50 and 1 nM, respectively (**Table 1.3**). *In vivo*, TL-32711 had no adverse effects in a MDA-MB-231 murine xenograft model, compared to the 'first generation' SM, where there were four treatment-related deaths in treated mice¹⁵¹. However, it should be noted that these mice were immunocompromised, and so do not faithfully reflect any immune response induced or modulated by TL-32711 that may be seen in humans.

Independently, TL-32711 has also been reported to be active in xenograft models of patient-derived ovarian, colorectal and melanoma cancers¹⁵⁶. Furthermore, in cell lines treated with TL-32711 in combination with chemotherapeutic drugs, TL-32711 significantly reduced cell viability as assessed by MTT assays. Interestingly, in one cell line, addition of a TNF α blocking antibody had no effect on TL-32711 induced cell death, suggesting both TNF-independent and TNF-dependent killing mechanisms¹⁵⁶. A similar synergistic effect was also shown in head and neck squamous cell carcinoma both *in vitro* and *in vivo*¹⁵⁴. *In vitro*, TL-32711 cytotoxicity was potentiated by the addition of TNF α or TRAIL. This potentiation of cell death is also observed when docetaxel resistant cell lines were sensitised to this drug when treated in combination with TL-32711. *In vivo*, however, despite a marked

Introduction

increase in survival when TL-32711 was administered synergistically with docetaxel, TL-32711 as a single agent actually showed the greatest increase in survival overall¹⁵⁴. This synergistic effect has also been reported in the clinical setting where, in patients, TL-32711 had efficacy both as a single agent and in combination with other chemotherapeutics^{150,155}. While TL-32711 as a single agent demonstrated limited disease stabilisation in patients¹⁵⁵, there is unpublished evidence that TL-32711 can sensitise tumours previously resistant to irinotecan¹⁵⁰. Furthermore, the combination therapy did not increase irinotecan-related toxicity, suggesting a future treatment regime for metastatic colorectal cancer.

1.1.10. **Reported adverse effects of SMs**

Drug-induced toxicity may be defined as the physicochemical characteristics of a compound and its subsequent effects on cellular organelles, membranes, and/or metabolic pathways. This can be further subdivided into two categories: on-target toxicity and off-target toxicity. On-target toxicity is the adverse and exaggerated effects of the compound at the target of interest in the model used. Off-target toxicity results from modulation of other targets which may be either related or unrelated to the target of interest¹⁶⁰. As SMs were designed to be very highly specific for their intended targets³⁷, much of the reported toxicity from these compounds has resulted from on-target toxicity. Adverse effects SMs by have been reported both pre-clinically *in vitro* and *in vivo* and in early phase clinical trials^{148,155,161}. The most widely reported adverse effect is induction of a 'cytokine storm'^{161,162}. Indeed, administration of the clinically-relevant SM, LCL-161, actually reduced survival in MYC-driven lymphoma in mice¹⁶². This was due to LCL-161-induction of a plethora of cytokines, which also resulted in increased susceptibility to endotoxic shock. As SMs de-repress the non-canonical NF- κ B pathway, there are several reports of an increased migration and invasion profile of tumour cells treated with SMs both *in vitro* and *in vivo*^{135,147,163–165}. These studies all indicate that activation of the NF- κ B pathway results in increased expression of a plethora of genes that promote this migratory phenotype.

Interestingly, SMs are also reported to promote bone cancer metastases through activation of the non-canonical NF- κ B pathway¹⁴⁸. This is due to the fundamental

Introduction

role of this pathway in osteoclast differentiation and function¹⁶⁶. Despite a reduction in soft tissue tumours, paradoxically, SMs actually increased the tumour burden in bone¹⁴⁸. Furthermore, in the same study, it was reported that SMs caused osteoporosis, increased osteoclastogenesis, and enhanced tumour-associated osteolysis. Co-treatment with zoledronic acid, a potent osteoclast inhibitor, was able to inhibit the SM-induced bone tumour increase. However, there are currently very little published studies directly investigating any potential adverse effects of SMs in non-tumour cells. To my knowledge, the effect of SMs in combination with TNF α has only been investigated in one non-tumour-derived cell line (HUVECs) and was shown to have no effect³⁶. There is evidence, however, that SMs have the ability to induce cell death in monocytes, PBMC and can have an inhibitory effect on immune cell function^{145,146}.

Adverse drug reactions (ADRs) from SMs are also reported from first-in-man studies and phase I clinical trials^{121,122,150,155}. Despite many SMs being in clinical trials, only trials with AT-406 and TL-32711 have reported findings in man. Overall, these compounds were well tolerated and many side effects were related to gastrointestinal issues or fatigue. More serious side effects included reversible Bell's palsy, elevated serum markers of liver injury and haematological issues, including lymphopenia and febrile neutropenia. While there was no mechanistic insight as to the causes of these, it is likely they result from activation of the NF- κ B pathway, which resulted in elevation of cytokines.

Drug-induced liver injury (DILI)

ADRs are undesirable reactions to drugs and fall into six categories: dose-related, non-dose-related, dose-related and time-related, time-related, withdrawal, and failure of therapy¹⁶⁷. Many drugs fail to make it into the clinic due to these effects, which is why pre-clinical investigation into these reactions is so important. Yet, despite this, ADRs are one of the leading cause of death in the Western world^{168,169}. DILI due to paracetamol and idiosyncratic drug reactions is the primary cause of acute liver failure, with 1 in 100 patients presenting symptoms resulting in up to 0.3% of all inpatient deaths^{168,170,171}. It is also the leading cause

Introduction

of drug withdrawal from the clinic¹⁷²; indeed, between 1975 and 1999, 548 drugs were removed from the market due to hepatotoxicity¹⁷³. The reason the liver is such a significant target for toxicity is that it contains cytochrome (CY)P450 enzymes which are responsible for xenobiotic metabolism, i.e. metabolism of any foreign compound. As such, it is often not the parent compound but its metabolites that induce toxicity, as is the case with paracetamol. In this model, paracetamol is metabolised by CYP2E1 to the reactive metabolite N-acetyl-p-benzoquinone imine (NAPQI)¹⁷⁴. NAPQI depletes glutathione and covalently binds to proteins, impairing their function¹⁷⁵.

However, hepatotoxicity is not solely the result of active metabolites, the complex interplay of the liver microenvironment also plays a significant role. While hepatocytes constitute the bulk of the liver, approximately 35% of liver cells represent non-parenchymal cells, i.e. hepatic stellate cells (HSCs), epithelial cells and, predominantly, Kupffer cells¹⁷⁶. Kupffer cells are the resident liver macrophages and play a vital role in the liver's response to xenobiotics¹⁷⁷. As macrophages, they secrete a range of pro-inflammatory cytokines. While the role of Kupffer cells will be discussed in depth below, it is worth briefly mentioning their mechanism of action (**Figure 1.7**). Upon exposure to a hepatotoxin, hepatocytes undergo necrosis, which activates the Kupffer cells. Kupffer cells then secrete pro-inflammatory cytokines which induces apoptosis, proliferation and inflammation. This inflammation then promotes infiltration of PBMC and accumulation of these and resident monocytes through upregulation of the chemoattractants, MIP-2 and MCP-1. This infiltration then produces reactive oxygen species and nitric oxide, resulting in generalised liver damage¹⁷⁶. Due to the complex interplay of the variety of cell populations in the liver, it is very technically challenging to replicate this *in vitro*. As such, currently the most faithful way to replicate this environment is through the use of *in vivo* murine models. While *in vitro* primary liver models which include Kupffer cells and hepatocytes are available, they are often confined to signal transduction between Kupffer cells and hepatocytes¹⁷⁸. As mentioned earlier, Kupffer cells play an instrumental role in the liver's response to toxic insult. However, whether they function to ameliorate or exacerbate hepatotoxicity is under debate.

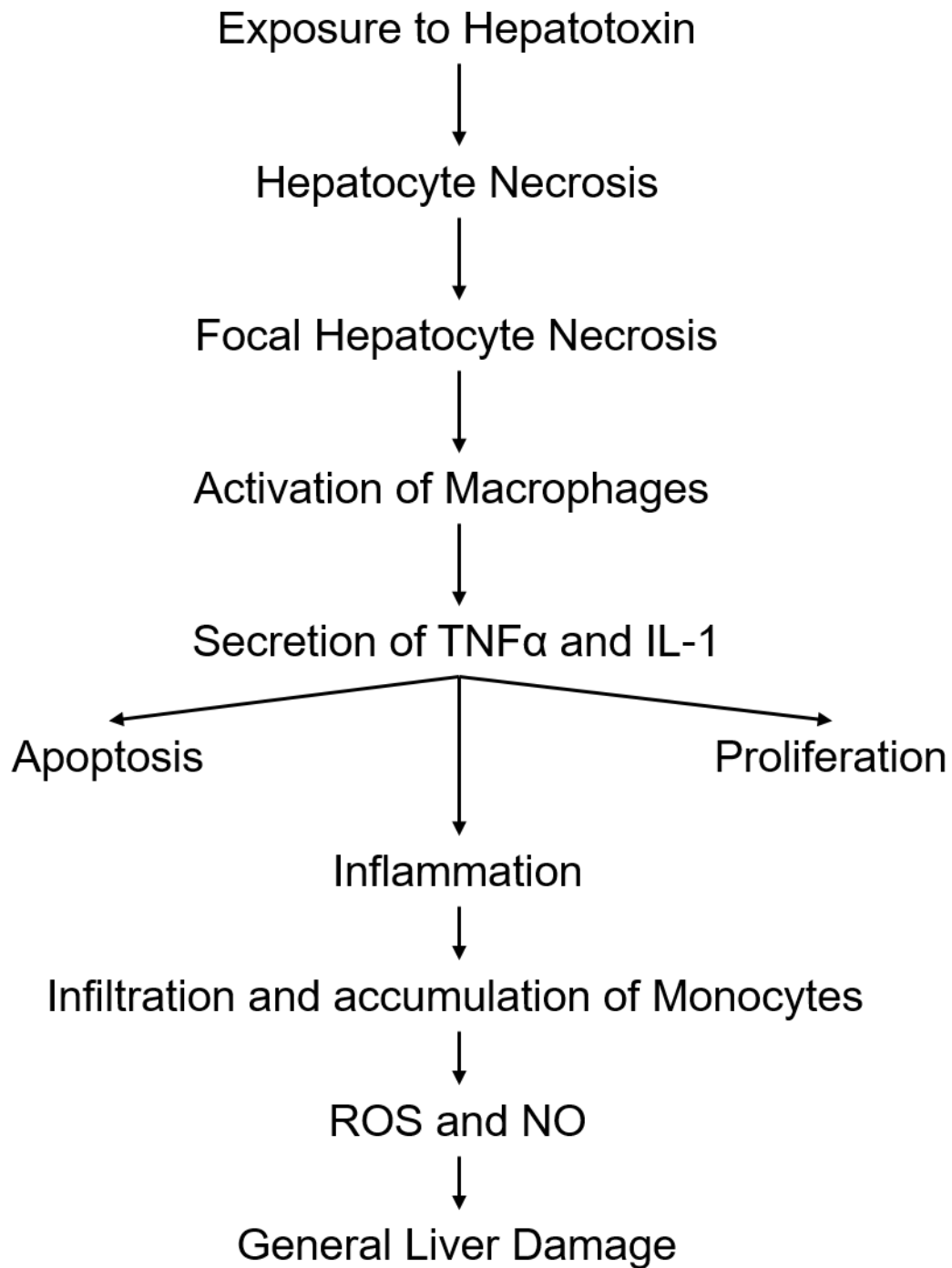


Figure 1.7 | Diagrammatic Overview of Hepatotoxicity. Upon induction of necrosis by hepatotoxins, macrophages are signalled to secrete pro-inflammatory cytokines. This results in inflammation, proliferation and invasion of monocytes. These cells increase reactive oxygen species (ROS) and nitric oxide (NO), leading to liver injury. Adapted from²⁰⁶

1.1.11. **Role of Kupffer cells in DILI**

Kupffer cells constitute 80-90% of the tissue macrophages present in the human body¹⁷⁹. They play a particularly significant role in liver regeneration; indeed, depletion of Kupffer cells is known to impede liver regeneration^{180–182}. These cells exert their effect through secretion of a plethora of cytokines. However, there is also research demonstrating that Kupffer cells can actually exacerbate hepatotoxicity^{183–186}. Upon induction of liver injury, the resident liver macrophages are activated. However, it is an oversimplification to describe all liver macrophages as Kupffer cells. While Kupffer cells are indeed a subpopulation of macrophage, macrophages are known to differentiate from two lineages. A central dogma in immunology was that all macrophages were recruited from blood monocytes¹⁸⁷. However, recent work has shown macrophages, including Kupffer cells, are also derived from the yolk sac and/or foetal liver and maintain themselves through self-renewal, independent from blood-derived monocytes^{188–190}. These infiltrating PBMC can either promote healing or induce inflammation depending on the insult and surrounding milieu^{191–193}.

However, it was unknown whether there was heterogeneity in the response of these two differentially-derived macrophage lineages. As such Zigmond *et al.*, investigated the gene expression profiles of these two cell populations after acute paracetamol-induced liver injury¹⁹⁴. For the first time, it was demonstrated that macrophages from different lineages express a distinct subset of 603 genes. They found that upon injury, liver derived-Kupffer cells numbers were reduced and that infiltrating PBMC promoted early phase restoration. Interestingly, Ly6C^{hi} PBMC were shown to reduce neutrophil recruitment, which is known to exacerbate hepatotoxicity¹⁹⁵. After liver derived-Kupffer cells were replenished through self-proliferation, these cells became the primary acting macrophages in the resolution of liver injury¹⁹⁴.

1.1.12. **Hepatotoxins used in this project**

1.1.12.1. *ANIT*

ANIT (α -Naphthylisothiocyanate) is a biliary toxin which induces acute biliary injury, cholangiolitic hepatitis and intrahepatic cholestasis^{180,196,197}. While ANIT does target periportal hepatocytes, it primarily affects bile duct epithelial cells, promoting invasion of neutrophils¹⁹⁸. After bile duct injury, ANIT treatment results in cessation of bile flow within 24 h¹⁹⁷. This further promotes liver injury through recycling repeated rounds of glutathione conjugation and biliary excretion¹⁹⁹. The infiltration of neutrophils has been reported as critical in ANIT mediated toxicity, as depletion of these cells markedly prevents hepatocellular injury^{195,197,200}. Interestingly, while neutrophil infiltration is independent of CD18, ANIT-induced neutrophil-mediated toxicity is dependent on CD18¹⁹⁵. When neutrophils are activated through this receptor, they promote hepatotoxicity through induction of ROS and proteinases^{201,202}. While Kupffer cells do have a protective effect in liver damage, depletion of Kupffer cells is reported to reduce ANIT toxicity¹⁸⁰.

1.1.12.2. *CCl₄*

CCl₄ is a halogenated alkane which induces severe damage to hepatocytes. CCl₄ is metabolised by CYP2E1, CYP2B1 or CYP2B2 into the trichloromethyl radical, CCl₃²⁰³. This radical can bind to protein and lipids, thereby impairing crucial cellular functions such as lipid metabolism, which induces steatosis²⁰⁴. This radical can also react with oxygen to form the trichloromethylperoxy radical CCl₃OO, a highly active reactive radical²⁰⁵. CCl₃OO initiates lipid peroxidation, which attacks and destroys lipids, especially those associated with phospholipids. Not only does CCl₃ affect lipids but many other cellular organelles, including the mitochondria, endoplasmic reticulum, and plasma membranes, resulting in disruption of calcium homeostasis and severe hepatocyte damage^{206,207}. CCl₄ is also implicated in hypomethylation of proteins and enzyme inhibition leading to inhibition of protein synthesis, and of lipoprotein secretion^{208,209}. Furthermore, CCl₄ promotes TNF α , nitric oxide, interleukin and TGF- α and - β secretion^{210,211}. All of these are powerful

Introduction

inflammatory molecules that promote proliferation, survival and fibrosis. However, as protein synthesis is inhibited with CCl₄, TNF α can actually function to induce apoptosis, rather than inflammation^{206,212}. Rather than a single event, it is the cumulative effects of all these biological processes that ultimately results in CCl₄-mediated hepatotoxicity²⁰⁶. Conversely, while Kupffer cells can ameliorate ANIT toxicity, they are reported to exacerbate CCl₄ induced toxicity^{184,185}.

Project Aims

Chapter 3:

- Compare monovalent and bivalent SMs in two tumour cell lines known to be sensitive and resistant to SMs as single agents
- Examine at what concentration cIAP1 is depleted and whether this correlates with cell death induction
- Investigate temporal aspects of SM activity through a time-course
- Determine the modality of cell death induced by SMs in the sensitive tumour cell line

Chapter 4:

- Compare monovalent and bivalent SMs as single agents in non-tumour derived cell lines
- Replicate the tumour microenvironment through addition of TNF α and SMs in non-tumour derived cell lines
- Examine if SMs have similar kinetics in non-tumour cell lines compared to tumour cell lines
- If no cell death is seen, determine whether these non-tumour cells have the capability to undergo TNF α -mediated signalling and cell death

Chapter 5:

- Investigate the effect of SMs on the outcome of liver regeneration post injury *in vivo*
- Determine the mechanisms of the observed effect

Introduction

We hypothesised that bivalent SMs would induce more cell death compared to the monovalent SMs in sensitive tumour cells. In non-tumour cells, we hypothesised that SMs would not induce cell death, even in combination with TNF α . Lastly, we hypothesised that SMs would exacerbate liver injury when administered in combination with two known hepatotoxins, ANIT and CCl₄.

The different models and lines of investigation will enable us to directly compare SMs in well characterised tumour cells against non-tumour cells *in vitro* and *in vivo*. The data obtained will give new insights into any adverse effect of SMs in a variety of biological systems.

Chapter 2

Materials and Methods

2. MATERIALS AND METHODS

Materials

Unless otherwise stated, all materials were purchased from Fisher Scientific Ltd (Loughborough, UK). BSA (Bovine Serum Albumin), β -mercaptoethanol, bromophenol blue, ammonium persulfate, DMSO, paraformaldehyde, glycine, HEPES, glycerol, imidazole, Kodak biomax XAR Film, magnesium chloride, ponceau S, TEMED, propidium iodide, goat serum, cholera toxin, insulin, DNase 1, OptiPrep, Sodium Dodecyl Sulphate (SDS), hydrocortisone, triton X-100, tween 20, Nalgene® Mr. Frosty cell freezer, HBSS (Hanks Buffered Saline Solution), Thiazolyl Blue Tetrazolium Bromide (MTT; 3-(4,5-dimethylthiazol-2-yl)-2,5-diphenyltetrazolium bromide), BrdU (5-bromo-2'-deoxyuridine) and NuncImmuno™ MicroWell™ 96-well plates were all obtained from Sigma-Aldrich (Poole, UK). Protein assay reagent and precision plus protein standard were both purchased from Bio-Rad (Hertfordshire, UK). Acrylamide was obtained from Geneflow (Staffordshire, UK). ECL was obtained from GE Healthcare (Buckinghamshire, UK). Nitrocellulose membrane (Hybond C) was purchased from Amersham (Buckinghamshire, UK) and PVDF and necrosulfonamide (NSA), an MLKL inhibitor, was obtained from Merk Millipore (Darmstadt, Germany). RPMI 1640, DMEM, DMEM/F12, high glucose DMEM with pyruvate, penicillin/streptomycin, fetal calf serum (FCS), glutaMAX, horse serum, Trizol®, sodium pyruvate, goat anti-mouse Alexa-Fluor 488® antibody, hoescht, epithelial growth factor (EGF) and horse sera were obtained from Invitrogen (Paisley, UK). Collagenase B, pronase, complete™ protease Inhibitor with/without EDTA and PhosSTOP™ phosphatase inhibitor cocktail tablets were obtained from Roche (Sussex, UK). The pan-caspase inhibitor zVAD.fmk and caspase-3/7 substrate afc-DEVD.fmk was obtained from MP Biomedicals (Illkirch, France). Fluoromount-G™ was obtained from eBioscience (San Diego, USA). Vector ABC staining reagents were purchased from Vector Laboratories (CA, USA). DAKO EnVision FLEX+ kit was purchased from Agilent Technologies (CA, USA). Cell strainers were purchased from Falcon (Durham, USA). All ELISA kits were purchased from R&D Systems (Minneapolis,

Materials and Methods

Minnesota, USA). LBW242 was a gift from Novartis (Switzerland). AT-406 was purchased from Active Biochem, and TL-32711 from Active Biochem or Selleckchem. BV6 and GDC-0152 were custom synthesised by Syngene International (India; collaboration with Dr Rajalingam). DRAQ5 was purchased from Abcam (Cambridge, UK). Phalloidin CruzFluor™ was obtained from Santa Cruz Biotechnology, Inc. (Dallas, USA). Novolink™ polymer detection system was obtained from Leica Biosystems (Newcastle, UK). QuickPick™ SML mRNA extraction kit was purchased from Bio-Nobile™ (Finland). FITC conjugated annexin V was made in house.

Cell culture

2.1.1. Cell Lines and Culturing Conditions

Breast epithelial adenocarcinoma cell lines, MDA-MB-231 and MDA-MB-468, were purchased from ATCC (HTB-26 and HTB-132, respectively) and cultured in RPMI 1640, supplemented with 10% FCS and 2 mM GlutaMAX.

B-13 cells (rat pancreatic - kind gift from Prof. Matthew Wright, Newcastle University) were cultured in low glucose DMEM media supplemented with 10% FCS and 2 mM GlutaMAX.

B-13/H cells were obtained by differentiating B-13 cells in the above conditions with the addition of 20 nM Dexamethasone for ≥ 14 days.

MCF-10A cells were obtained from ATCC (CRL-10317™) and cultured in DMEM/F12, supplemented with 5% horse serum (Life Technologies, UK), 20 ng/mL EGF, 0.5 mg/mL hydrocortisone, 1 ng/mL cholera toxin and 10 μ g/mL insulin.

All cell lines were passaged up to 40 times by detachment using trypsin, spun at 200 g for 3 min and then split 1:3 for two days, or 1:6 for four days. Flasks were incubated with humidity at 37°C in 5% CO₂. All cell lines were tested and

Materials and Methods

declared negative for mycoplasma (Mycoplasma Experience, UK) and were authenticated by ATCC upon purchase.

Kupffer cells were cultured in RPMI 1640 supplemented with 2 mM GlutaMAX and penicillin/streptomycin *ex vivo*.

Hepatic Stellate Cells (HSCs) were cultured in high glucose DMEM (4.5g/L) with pyruvate supplemented with 16% FCS and penicillin/streptomycin *ex vivo*.

MEFs were a kind gift from Dr Lia Panman and were cultured in high glucose DMEM (4.5g/L) supplemented with 10% FCS and 2 mM GlutaMAX, 1% penicillin/streptomycin, non-essential amino acids sodium pyruvate, and 0.1 μ M B-Mercaptoethanol.

Cultures were maintained with humidity at 37°C in 5% CO₂ *ex vivo*.

Ex vivo mouse embryonic fibroblasts were a kind gift from Dr Lia Panman and were cultured in high glucose DMEM (4.5g/L), 2 mM GlutaMAX, sodium pyruvate, and pyridoxine hydrochloride, 10% FCS, MEM nonessential amino acids, 0.1 mM 2-mercaptoethanol, 20 mM HEPES, penicillin/streptomycin.

2.1.2. Freezing Down and Recovering Cells from Liquid Nitrogen

Cells were detached and counted using a CASEY Cell Counter (Roche, UK) and resuspended in 100% FCS. An equal volume of 20% DMSO in FCS was added to give $3\text{--}9 \times 10^6$ cells/mL, 1 mL of which was aliquoted into each cryovial. Cells were then frozen at $-1^\circ\text{C}/\text{min}^{-1}$ in a Nalgene Mr Frosty at -80°C and transferred after >24 h to liquid nitrogen. Upon recovery from liquid nitrogen, cryovials were kept on dry ice until ready to be thawed. Vials were allowed to stand for ~1 min at RT before being thawed in a water bath heated to 37°C. Cells were then added to 9 mL of pre-warmed media and spun at 200 g for 3 min. The media was discarded and the pellet was re-suspended in 10 mL fresh pre-warmed media and added to a T-75 or T-25 flask.

2.1.3. Cell seeding and treatments

For experiments, cells were seeded in 6-well plates, 24-well plates (for confocal microscopy) and 96-well plates (for MTT, caspase-3/7 activation assays and Cellomics assays) at the appropriate densities and allowed to adhere for 24-48 h before treatments. Before treating, the original medium was removed and replaced with the appropriate amount of fresh, warmed, drug containing media.

2.1.4. Treatment of cells with zVAD and NSA

MDA-MB-231 cells were seeded at the appropriate density and allowed to adhere for 48 h. Where necessary, cells were pre-treated for 30 min with zVAD at 100 μ M before an equal volume of media was added resulting in a final concentration of 50 μ M. Both BV6 and NSA (1 μ M final concentration) were made at 2x concentration and diluted with either fresh media or the zVAD containing media already in the well.

2.1.5. Kupffer cell isolation, culture and treatment

Mice were culled by cervical dislocation; livers were excised and underwent mechanical dissociation through a tea strainer and washed through with 1x HBSS⁻ (Hanks Balanced Salt Solution, 60 μ M HEPES and 1% (w/v) NaHCO₃) in the presence of 2 mg DNase 1 and 140 mg pronase, both dissolved in HBSS⁺ (HBSS⁻ with 1 μ M CaCl₂). Cells were then filtered through a 100 μ m cell strainer with 25 mg collagenase B in HBSS⁺ and 1 mg DNase 1 and incubated at 37°C for 30-60 min. Cell suspensions were then centrifuged at 4°C for 7 min at 700 *g*. After centrifugation, pellets were re-suspended in HBSS⁺ and 1 mg DNase and re-pelleted as above. To separate HSCs, pellets were then re-suspended in 30 mL HBSS⁺ and 1 mg DNase, to which 6.5 mL OptiPrep was added and mixed thoroughly. To ensure HSCs did not dry out, 2 mL of HBSS⁺ was added on top of the OptiPrep. Cells were then centrifuged at 4°C for 20 min at 1400 *g* with the brake set to 0. HSCs were then collected and the OptiPrep was diluted out with HBSS⁺. HSCs were then centrifuged at 4°C for 7 min at 700 *g* and re-suspended in high glucose DMEM with pyruvate, 16% v/v FCS and penicillin and streptomycin. Kupffer cells were re-suspended in HBSS⁺ and

DNase and re-pelleted at 4°C for 7 min at 700 *g* to remove OptiPrep. Pellet was then re-suspended in serum free RPMI 1640 with 2 mM GlutaMAX and penicillin and streptomycin and aliquoted into 6-well plates for supernatant collection and RNA extraction, or 24-well plates for confocal microscopy.

SDS-PAGE (Sodium Dodecyl Sulfate Polyacrylamide Gel Electrophoresis)

2.1.6. Protein extraction

2.1.6.1. Cell lines

After the indicated treatments, cells were harvested and spun at 400 *g* for 3 min at 4°C after washing with ice-cold phosphate buffered saline (PBS) and snap frozen on dry ice. Whole cell pellets were sonicated in 1x SDS sample loading buffer (63 mM Tris 6.8 pH, 15% glycerol v/v, 1% SDS v/v, 0.05% w/v bromophenol blue and 5% v/v β-mercaptoethanol) sonicated and boiled for 5 min at 95°C. To account for cell death, pellets were lysed in RIPA buffer (150 mM NaCl, 1% NP-40 v/v, 0.1% SDS v/v, 0.5% Sodium Deoxycholate (w/v) and 50 mM Tris-HCL 7.2 pH), sonicated, spun down and then made up to equal concentrations, as determined by Bradford assay, in ultra-pure H₂O and 10x sample buffer before being boiled.

2.1.6.2. Mouse tissue samples

Samples were kept on a metal plate on top of dry ice to prevent protein degradation. They were cut into small slices and then homogenised and lysed on ice in RIPA buffer with protease and phosphatase inhibitors. Lysates were then sonicated and spun down at 4°C at 15,000 *g* and were divided into two tubes; one that was without the debris, the other had the unlysed precipitate. Protein concentration of the lysates was determined by Bradford then made up to equal concentrations in ultra-pure H₂O and 10x sample buffer before being boiled.

Materials and Methods

2.1.6.3. SDS-PAGE

All gels were run using the Mini-PROTEAN[®] II electrophoresis cell (BioRad, Hemel Hempstead, UK). Mini gels were made using a 4% stacking gel (125 mM Tris (Roche, Newhaven, UK)-HCl pH 6.8, 0.1 % w/v SDS, 4 % acrylamide (ProtoGel[®], National Diagnostics, Geneflow Ltd, Fradley, UK)), which was cast on top of the resolving gel (375 mM Tris-HCl pH 8.8, 0.1 % w/v SDS, variable acrylamide). The percentage of the gel was dependent on the protein of interest; however, it was normally between 9 and 15%. After samples were loaded, they were electrophoresed at 50-110 V through polyacrylamide gels (7-15%) and transferred onto a nitrocellulose or PVDF membranes overnight at 25V.

2.1.6.4. Immunoblotting

After determining the quality of the transfer using ponceau S solution, membranes were blocked (10% Marvel/TBS-T (Tris buffered saline, 0.5% Tween)), probed with the indicated antibodies (**Table 2.1**) for up to 2 h at RT (room temperature) or 4°C O/N (overnight) and the appropriate HRP-conjugated secondary antibody for 1 h at RT, and developed using ECL (Enhanced Chemiluminescent) and X-ray film.

Bradford Assay

After whole cell pellets were lysed, sonicated, spun down and protein concentration was analysed in one of two ways. 1 µL of lysate was diluted 1:20 in ultra-pure H₂O and 10 µL was loaded onto a 96 plate in duplicate along with a BSA standard curve of 6 – 0.25 µg/mL to determine protein concentration. 190 µL of Bradford Reagent diluted 1:5 with ultra-pure H₂O was added to each well. Plates were mixed and read at 595 nm. The other method was 1 µL of lysate was diluted and mixed with 1 mL of Bradford Reagent diluted 1:5 with ultra-pure H₂O. This was then measured on a spectrophotometer at 595 nm.

Table 2.1 | Primary antibodies used for immunoblotting

Antibody	Weight (kDa)	Source	Dilution	Host	Catalogue/ Reference
ciAP1	66	R&D	1:2000	Goat	AF8181
ciAP2	65	R&D	1:2000	Goat	AF8171
XIAP	57	BD Biosciences	1:2000	Mouse	610716
p-IkBα (Ser32)	40	Cell Signalling	1:1000	Rabbit	2859
IkBα	38	BD Transduction Laboratories	1:2000	Mouse	610690
NF-κB2	100/52	Upstate/Millipore	1:10000	Mouse	05-361
NF-κB2	100/52	Cell Signalling	1:2000	Rabbit	4882
GAPDH	37	Abcam	1:10000	Mouse	ab9484
Caspase-8	55/53, 43/41, 18	AdipoGen	1:500	Mouse	C15
Caspase-8	55/53, 43/41, 18	In house	1:2000	Rabbit	N/A
Caspase-3	32, 20/19/17	In house	1:2000	Rabbit	N/A
Caspase-3	32, 20/19/17	Cell Signalling	1:2000	Rabbit	9662
cCaspase-3 (Asp172)	20/19/17	Cell Signalling	1:2000	Rabbit	9664
PARP	116/89	Alexis	1:2000	Mouse	804210
PARP	116/89	Cell Signalling	1:2000	Rabbit	9542

RNA Extraction

2.1.7. Cell lines

1 mL of Trizol was added either directly to a 6-well plate or lysed from a snap frozen cell pellet and allowed to stand at RT for 5 min. 200 μ L of chloroform was then added, mixed and allowed to stand at RT for 10 min. Tubes were then centrifuged for 10 min at 4°C at 13.3 *g*. The clear aqueous phase was then transferred to a separate tube, with care being taken not to contaminate the sample with the interface and organic phase. 1 mL of isopropanol was added for either 10 min at RT, or 2 h or O/N at -20°C. Samples were then centrifuged and washed twice with 1 mL 70% ethanol. RNA pellet were allowed to dry and then re-suspended in DEPC-treated water and RNA concentration was determined on a NanoDrop 2000 (ThermoScientific, UK).

2.1.8. Tissue Homogenates

Mouse organs were flash frozen in 1 mL Trizol upon excision from mice. RNA extraction from tissues was similar to cell lines. Tissues were homogenised via mechanical dissociation and homogenates subjected to the protocol as above. If RNA was contaminated, it was then re-suspended in 1 mL Trizol and extracted according to the standard protocol. If RNA was still contaminated at this point, the RNA was re-precipitated with 20 μ L of 3 M sodium acetate (pH 5.2) and 600 μ L 70% ethanol and incubated at RT for 10 min. Samples were then spun and washed once with 70% ethanol. The ethanol was allowed to evaporate and samples were resuspended in DEPC-treated H₂O. Concentration was determined using a NanoDrop 2000 (ThermoScientific, UK).

2.1.9. Kupffer cells

Due to the limited material available from the Kupffer cells, a commercial magnetic bead-based kit was used. The principle of the method is the beads are oligo (dT)₃₀ coated which binds poly-A(+) mRNA allowing for very pure extraction in the presence of limited sample. Extraction was carried out according to manufacturer's instructions after the indicated treatment. Briefly,

Materials and Methods

cells were washed in PBS, lysed and scraped in 300 μL of the provided lysis buffer and then incubated and mixed with the coated magnetic beads that bind to poly-A(+) mRNA at RT for 5 min. Beads were then washed using a PickPen® 1-M that has a retractable magnetic insert that, when descended, the beads are attracted to, and when retracted, the beads are released from the PickPen and can be washed in the wash buffer. The beads are washed 3 times and then deposited in the elution buffer, in which the mRNA is eluted into at 70°C for 5 min, after which the beads are removed and discarded and the sample is ready for making cDNA. mRNA was eluted in 15 μL .

cDNA synthesis

cDNA was made using SuperScript® III First-Strand Synthesis System according to manufacturer's protocol. Briefly 10x RT buffer, 25 mM MgCl_2 , 0.1 M DTT, RNaseOUT™ and SuperScript® III RT (200 U/ μL) were mixed together. RNA was added and placed on ice for 30 sec. Samples were then heated for 10 min at 25°C, followed by 50 min at 50°C for 30 cycles. The reaction was then terminated at 85°C for 5 min, before placing on ice. I then added RNase H to each tube and incubate the tubes for 20 min at 37°C before storing at -20°C.

Quantitative Polymerase Chain Reaction Optimisation

IL-6 and β -actin (Sigma, UK) primers were previously optimised in the laboratory. TNF α primers (Sigma, UK) were optimised using concentrations of 300 nM and 900 nM using 1:10 serial dilutions of cDNA in water starting at either 100 or 50 ng/ μL . Samples were mixed with SYBR-green master mix and ultrapure H_2O .

ELISA (Enzyme-Linked Immunosorbent Assay)

ELISAs performed were duoset, sandwich ELISAs specific to the species and were carried out according the manufactures protocol. Briefly, plates were coated with the capture antibody O/N at RT and then washed and incubated

Materials and Methods

with the samples and with known amounts of the protein to give a standard curve for 2 h at RT. Plates are then washed and incubated with the detection antibody for 2 h at RT. After washing, plates were then incubated with streptavidin-HRP for 20 min in the dark, washed and then incubated with the substrate solution. After sufficient colour development, this was stopped using 2 N H₂SO₄. Plates were read at a wavelength of 450 nm with a wavelength correction of 570 nm.

Caspase-3/7 Activity Assay

Cells were treated in triplicate wells for each biological repeat. After indicated treatment in 50 µL, cells were lysed with 2% Triton-X100, 30 mM Tris pH 7.5, 150 mM NaCl and 10% glycerol for 30 min, then 2.5 mM afc-DEVD.fmk was added in 100 µL of DEVDase assay buffer (100 mM HEPES 7 pH, 10% sucrose, 0.1% Chaps), allowed to sit at 37°C for 5 min and fluorescence was measured on a Victor X4 (PerkinElmer, UK). To determine caspase activity (pMol·min⁻¹), a pre-established linear regression equation, validated using recombinant caspase-3/7 and assuming a final volume of 200 µL, was used to determine caspase activation:

$y = m \text{ (all points between 200-1200)} \times + c$ * multiplied by a factor of 0.224918785

The mean of the triplicate wells was then taken to give one biological repeat. This was repeated on three separate days to give three biological repeats.

Flow Cytometry

2.1.10. Analysis of cell death

After the indicated treatment, media, PBS washes and harvested cells were collected and spun at 500 g for 5 min. If supernatant was required for ELISAs, then the supernatant was collected and spun down at 500 g for 5 min, aliquoted and snap frozen. The pellets were then resuspended in 1 mL pre-warmed

Materials and Methods

media, 800 μL was taken for western blotting and the remaining 200 μL were allowed to recover for ≥ 15 min in the incubator. After the recovery period, 200 μL of cells were added to 800 μL annexin binding buffer (10 mM HEPES/NaOH pH 7.4, 150 mM NaCl, 5 mM KCl, 1 mM $\text{MgCl}_2 \cdot 6\text{H}_2\text{O}$ and 1.8 mM $\text{CaCl}_2 \cdot 2\text{H}_2\text{O}$) which contained a batch dependent concentration of Annexin V-Fluorescein isothiocyanate (FITC; AnV) and incubated in the dark for 8 min. Samples were then transferred to ice and 10 μL PI was added, before being analysed on a FACS Calibur (BD Biosciences, UK).

One of the advantages of using flow cytometry is that the technique can give insight into the mechanisms of cell death. Phosphatidylserine (PS) is a phospholipid that normally resides inside the plasma membrane. However, when cells undergo apoptosis, PS is externalised, allowing apoptotic cells to be recognised and removed by phagocytes in vivo. This PS exposure is a relatively early event in apoptosis. Therefore, the exposure of PS can be used (often in combination with propidium iodide (PI), which is a DNA intercalator and cannot enter healthy cells) as a measure of apoptotic cell death. Cells undergoing early apoptosis will externalise and expose PS, binding AnV but will exclude PI, often referred to as early apoptotic. However, at later time points, apoptotic cells lose their membrane integrity and begin to take up PI, known as late apoptotic/early necrotic. Necrotic cells, however, do not externalise PS and stain only with PI (**Figure 2.1**). The ratio between early apoptotic and late apoptotic/early necrotic (early:late ratio) cells can be observed using flow cytometry, giving insight into the mechanisms of cell death.

Materials and Methods

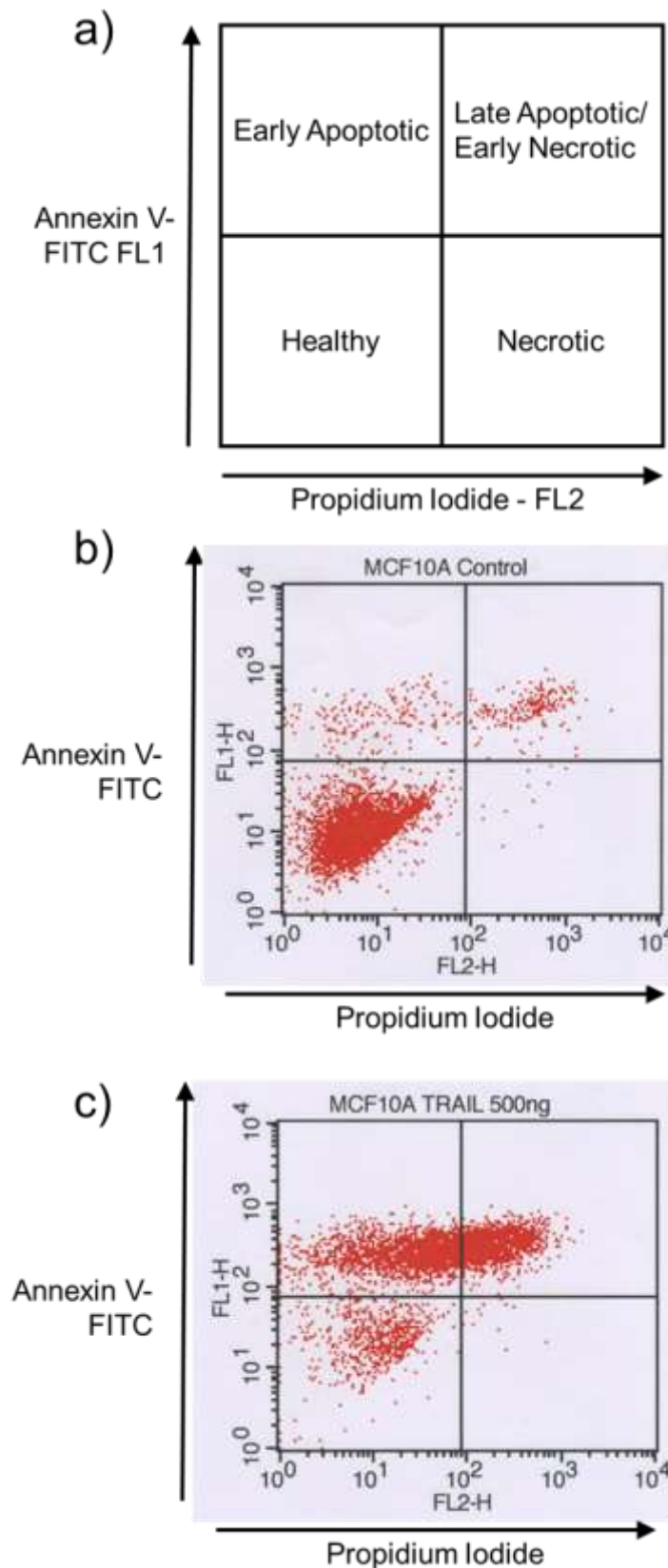


Figure 2.1 | Flow cytometry analysis of cells. a) Diagrammatic representation of the positions of cells undergoing apoptosis as seen by flow cytometry Annexin V-FITC and Propidium Iodide staining. Experimental examples of b) control MCF-10A cells and c) MCF-10A cells treated with TRAIL.

2.1.11. Quantification of TNFR1 cell surface expression

Cells were detached using trypsin and were pelleted at 200 *g* for 3 min at 4 °C, washed in ice cold PBS and resuspended in 10% goat serum. Cells were then labelled with TNFR1 or an IgG isotype control antibody was added 1:50 to relevant aliquots of cells and incubated on ice for 1 h in the dark. Cells were then washed in ice cold PBS, incubated with the corresponding PE-conjugated secondary antibody for 1 h on ice in the dark. Cells were then washed three times in ice cold PBS, resuspended in 500 µl PBS and analysed by flow cytometry using a FACS Canto, with the FL-2 channel (fluorescence on a log scale) measuring antibody binding.

Cell viability Assays

2.1.12. MTT Assays

Cells were treated in triplicate wells for each biological repeat. After the indicated treatment, MTT (5 mg/mL sterile filtered in PBS) was added to each well (1:10) on the 9-well plate. Plates were returned to the incubator for 2.5-4 h upon which the media was aspirated and 100 µL DMSO was added. After ~20 min colour development at RT, absorbance was measured at 570 nm and corrected at 690 nm on a PowerWave HT XS2 Spectrophotometer (BioTek, UK). The mean of the triplicate wells was then taken to give one biological repeat. This was repeated on three separate days to give three biological repeats.

2.1.13. Nuclei Counting

Cells were treated in triplicate wells for each biological repeat. After the indicated treatment, the media was removed and cells were stained with Draq5 at a concentration on 1:1000 for 30 min in culture media. The nuclei of cell were then counted using an automated Cellomics ArrayScan XTI Live Cell Imaging System (ThermoScientific, UK). The mean of the triplicate wells was then taken to give one biological repeat. This was repeated on three separate days to give three biological repeats.

Confocal Microscopy

After the indicated treatments, cells were fixed in 10% NBF (Neutral Buffered Formalin) in H₂O and washed in 0.1% PBS-T. Cells were then permeabilised with 0.5% Triton X-100 in PBS and washed before being blocked in 5% goat serum diluted in PBS. Cover slips were then removed from the plates and stained with the appropriate primary at the optimised concentration O/N at 4°C. Cover clips were then returned to a new 24-well plate, washed and incubated with the appropriate secondary at 1:1000 diluted in 5% goat serum in the dark at RT. Cover slips were then washed and incubated with Hoechst at 1:10,000 diluted in PBS in the dark. Slips were then mounted on glass slides using Fluormount and allowed to dry O/N in the fridge, as the cold room was too humid and did not allow the slides to dry. Cover slips were then fastened to the glass slide using nail varnish.

***In vivo* experiments**

2.1.14. Pilot Study to determine the appropriate dose of TL-32711

All *in vivo* experiments were carried out with Matthew C. Wright from Newcastle University under a UK Home Office license (PPL 60/4534 19b9). For the pilot study, 10-16 week old, male wild type (C57BL/6J genetic background; mice^{WT}) were used. Animals were housed in the Comparative Biology Centre at Newcastle University and kept in accordance with Home Office guidelines. Animals were housed with littermates (no more than 6 to a cage) and *ad libitum* access to food and water. Light was on a 12 h light/dark cycle with regulated humidity (50% ± 10%) and temperature (23°C ± 1°C).

Mice^{WT} were weighed and then dosed daily for five days via intraperitoneal injection (I.P.) by Prof. Wright with either vehicle control (VC; 15% (2-Hydroxypropyl)-β-cyclodextrin, 20 mM succinic acid) or the bivalent SM, TL-32711 at either 5, 10, 20 or 30 mg/kg diluted in VC. There were three mice per group and Schedule 1 was performed by cervical dislocation. The liver was excised and weighed, and, along with the pancreas, was either flash frozen in

Materials and Methods

liquid nitrogen without or with Trizol for either protein or RNA extraction, respectively, or fixed in 10% formalin O/N and transferred to 70% ethanol. Tissues were processed, embedded and cut to 4 microns by the Biobank at Newcastle University or Jenny Edwards (MRC Toxicology Unit). Liver sections were cut and H&E stained (see 2.14.1.) and alanine aminotransferase (ALT) was measured by the Royal Victoria Infirmary Clinical Biochemistry Department in Newcastle. Alkaline phosphatase (ALP) was kindly analysed courtesy of Prof. Wright's group (Dr Philip Probert, Anne Lakey and Stephanie Meyer, Newcastle University) using the Alkaline Phosphatase Assay Kit from Abcam.

2.1.15. TL-32711 in combination with the hepatotoxins ANIT and CCL₄

Mice used for the combination study were transgenic C57BL/6J mice expressed the 3x-κB-luc gene (derived from zygote from Charles River) which, upon activation of the NF-κB pathway, induces a quantifiable, NF-κB-dependent signal (mice^{luc,213}). Mice^{luc} were housed in identical conditions as mice^{WT} and kindly genotyped by Dr Phil Probert and Stephanie Meyer. The combination study consisted of 6 groups; VC (same as the pilot study), TL-32711 (same as the pilot study), ANIT or CCl₄ only, and TL-32711 in combination with ANIT or CCl₄. mice^{luc} being administered TL-32711 were dosed daily with 20 mg/kg TL-32711 (I.P.) for 5 days. Mice^{luc} receiving the hepatotoxins as single agents or in combination with TL-32711 were dosed with a single dose of 50 mg/kg (ANIT in olive oil; oral gavage) on day 3, or 0.5 mL [1:1 v/v with olive oil]/kg (CCl₄; I.P.) on day 4. Post treatment, animals were culled by cervical dislocation. Livers were then excised and weighed and separated into 3 sections, one for protein extraction and one in Trizol for RNA extraction which were flash frozen. The remained section was fixed in 10% formalin along with the pancreas, intestines, spleen, kidneys and intestine/colon O/N. These organs were then transferred to 70% ethanol, processed, embedded and cut to 4-5 μm by The Biobank at Newcastle University or Jenny Edwards (MRC Toxicology Unit). H&E, ALT and ALP were analysed in the same way as the pilot study.

2.1.16. Luminescent imaging of mice

NF- κ B activity was determined using IVIS Xenogen IVIS (*in vivo* imaging system) 200 Spectrum imaging system using the bundled Living Image 4.0 software (Caliper Life Sciences, Hopkinton, USA). Prior to imaging, mice^{luc} were anaesthetised by Dr Probert with isoflurane and had their abdominal fur shaved off. Mice^{luc} were then injected I.P. with 200 μ L D-luciferin (Caliper Life Sciences) at 15 mg/ml in PBS. Analysis was performed using the Living Image software in which regions of interest were highlighted manually, giving total flux values (photons/s)

Immunohistochemistry

2.1.17. Haematoxylin and Eosin Staining

Sections at the MRC Toxicology Unit were H&E stained using a Shandon Varistain 24-4 (ThermoScientific, UK). Briefly, sections were de-paraffinised in xylene and rehydrated through graded alcohol, washed, and incubated with Harris's haematoxylin for 15 min. Sections were then washed, incubated with acetic acid for 25 sec, washed and incubated with eosin for 3 min. Sections were then washed and dehydrated through graded alcohols and mounted using DPX. At The group in Newcastle, sections were dewaxed, and rehydrated through graded ethanol. Sections were incubated with haematoxylin for 1 min and then developed in Scott's tap water (2% (w/v) NaHCO₃ and 0.35% (w/v) MgSO₄ in distilled water) for 10 s. Sections were then washed and stained in eosin for 15 s, before being washed again and dehydrated in increasing gradients of ethanol. Sections were then incubated with xylene and mounted using DPX.

2.1.18. Antigen retrieval method

Slides were de-paraffinised in xylene for 10 min three times and then gradually re-hydrated in 100 – 70% ethanol for 3 min in each, washed in running tap water for 5 min and then rinsed 3 times in greyline water. Antigen retrieval was performed using the citric acid where, after deparaffinisation and rehydration,

Materials and Methods

slides were incubated in 10 μ M citric acid in greyline water, pH 6 for 15 min at 90°C and then cooled in greyline water. Slides were then stained using one of three kits - Novolink Polymer detection system, the ABC method with reagents from Vector or the DAKO AutostainerLink48.

2.1.18.1. *Novolink™ polymer detection system*

Sections were processed according to manufacturer's instruction. Briefly, sections underwent antigen retrieval using the above methods, after which endogenous hydrogen peroxidase activity was blocked for 5 min. Sections were then washed with PBS, blocked for 5 min, washed and incubated for 16 h at 4°C with an optimised primary antibody diluted in 5% goat serum. Sections were washed and incubated with the rabbit Novolink polymer secondary, washed and then incubated with DAB for 5 min. Sections were then washed in running tap water for 5 mins, counterstained with haematoxylin for 15-20 sec, washed with running tap water and then placed in Acetic Alcohol for 3-5 sec. Sections were then washed in running tap water for 5 min before being dehydrated in graded alcohol and xylene and then mounted using DPX.

2.1.18.2. *ABC method*

After antigen retrieval, endogenous peroxidase activity was blocked in 3% H₂O₂ in methanol for 10 min. After washing 2 x 5 min in PBS, sections underwent endogenous biotin activity blocking with avidin and biotin solutions for 15 min each and then were blocked in 20% FCS for 1 h at RT. Sections were then incubated with primary antibodies O/N at 4°C. Sections were then washed and incubated with a biotin-conjugated secondary antibody for 1 h at RT. Sections were then washed, incubated with the ABC reagent for 45 min at RT, washed and then incubated with DAB for 5 min. Sections were then washed in running tap water for 5 min, counterstained with haematoxylin for 15-20 s, washed with running tap water and then placed in Acetic Alcohol for 3-5 s. Sections were then washed in running tap water for 5 min before being dehydrated in graded alcohol and xylene and then mounted using DPX.

Materials and Methods

2.1.18.3. *DAKO Autostainer*

Sections were kindly processed by Leah Officer using the DAKO EnVision FLEX+ kit. Deparaffinisation and retrieval was performed and sections then underwent endogenous peroxidase blocking. Sections were then washed, blocked for 10 min, washed again and incubated with the primary antibody for 20 min at RT. They were then washed, incubated with a rabbit linker, washed and incubated with an HRP-conjugated rabbit secondary. Sections were then washed and incubated with DAB for 10 min, washed and then haematoxylin for 5 min. Sections were then removed from the machine, dehydrated and mounted using DPX.

Chapter 3

Characterising the response of tumour cell lines to SMAC mimetics *in vitro*

3. CHARACTERISING THE RESPONSE OF TUMOUR CELL LINES TO SMAC MIMETICS *IN VITRO*

Introduction

Before any compound is tested in animals, it must undergo extensive *in vitro* testing. Perhaps the most widely used method is through the use of cell lines, particularly cancer cell lines, where a sample is taken from the patient and immortalised, allowing for, in theory, limitless replication and experimentation. There are currently many commercially available breast cancer cell lines used for the development of drugs against this disease. However, while cell lines are a relatively cheap and easy option, they do not faithfully replicate the microenvironment that these cells reside in *in situ*. In spite of this, they do provide a robust, reproducible experimental set up, allowing us to optimise a robust methodology to be used to characterise the response of non-tumour cell lines to SMAC mimetics (SMs). There has been significant evolution of SMs since they were first reported over a decade ago. One of the earliest compounds developed was LBW242, which is a monovalent ‘tool’ compound from Novartis used in the development of SMs to enter the clinic^{214–216}. As SMs have undergone extensive characterisation, their effects in established cancer cell lines are well known. Indeed, our laboratory has used LBW242 extensively in previous work²¹⁷. This, therefore, afforded us the opportunity to develop a robust set of methods to investigate the effects of SMs using a compound that has been characterised previously in the laboratory. The other four SM compounds used in this project have undergone clinical evaluations in many published studies, allowing us to form strong hypotheses about the effect of the SM compounds in my panel of breast tumour cell lines. Two established cell lines that are frequently tested with SMs are the breast cancer cell lines, MDA-MB-231 and MDA-MB-468 cells. These are reported in the literature to be sensitive and resistant to SMs as single agents, respectively^{38,115,120,218–220}. Furthermore, the mechanism behind the sensitivity of MDA-MB-231 cells to SMs is well documented to be a result of an inducible NF- κ B/TNF α autocrine signalling pathway that renders them sensitive to TNF α -mediated cell

death^{37,38,214}. These cell lines, therefore, provided a well-defined tool for robust technique optimisation. However, to my knowledge, there is currently no work directly comparing the effect of monovalent vs. bivalent SMs in sensitive and resistant tumour cell lines. As such, I treated MDA-MB-231 and MDA-MB-468 cells with four SMs – AT-406, GDC-0152 (both monovalent), BV6 and TL-32711 (both bivalent) and determined outcomes such as the mode of cell death, protein activation and degradation, and the kinetics of these events. I hypothesised that MDA-MB-231 cells would demonstrate increased sensitivity to SMs in terms of cell death and increased secretion of TNF α . I also expected to see depletion of cIAP1 in both cell lines, despite their differing sensitivity to SMs.

MDA-MB-231 cells, but not MDA-MB-468 cells, are sensitive to SMs at clinically relevant concentrations

3.1.1. Method optimisation with the ‘tool’ compound, LBW242

Before I used the four clinically-relevant SM compounds outlined in this project, I sought to begin method optimisation using LBW242, allowing us to develop a robust set of experimental procedures. Cells were treated for 16 h, after which, TNF α secretion significantly increased in MDA-MB-231 cells from 0.4 pg/mL in the control to 13.9 pg/mL at 5 μ M LBW242, but no increase was seen in MDA-MB-468 cells, where TNF α secretion only increased by 1.7 pg/mL. LBW242 induced cell death in MDA-MB-231 cells in a dose-dependent manner with a maximum of 68% cell death at 80 μ M LBW242, but no cell death was observed in MDA-MB-468 cells (**Figure 3.1**). Using flow cytometry, I observed higher numbers of early apoptotic cells compared to late apoptotic cells, with an average early:late ratio of 1:1, suggesting apoptosis was the primary mechanism of cell death, but that cell death is initiated before the 16 h time point (**Figure 3.1**). This hypothesis was further validated as the effector caspases, caspase-3/7, also showed a large increase in activity MDA-MB-231 cells at all concentrations, whereas MDA-MB-468 cells only showed increases in caspase-3/7 activity at the highest concentration of LBW242 (**Figure 3.2**). The increases in caspase-3/7 activity, as determined by DEVD.afc assay,

correlated with a decrease in the MTT cell viability assay, which showed a decrease at concentrations as low as 0.63 μM in MDA-MB-231 cells (**Figure 3.2**). However, the cell viability assay only showed a decrease in cell viability in MDA-MB-468 cells at 80 μM LBW242 (**Figure 3.2**).

Following LBW242 treatment, cIAP1 was depleted in both MDA-MB-231 and MDA-MB-468 cells. cIAP2 showed a transient increase in MDA-MB-231 cells before being depleted at higher concentrations. The cleavage fragments of caspase-3 and -8 were only detectable by western blotting in MDA-MB-231 cells, as was the cleaved form of PARP. XIAP showed a decrease in MDA-MB-231 cells, which was to be expected as XIAP is a known target of caspases⁴⁸ (**Figure 3.3**). In summary, LBW242 degrades cIAP1 in both sensitive and resistant cells, but does not induce cell death in cells without an inducible TNF α autocrine loop.

Using the results from the methodology development with LBW242, I slightly amended the protocol. I retained the concentration range in the cell viability and caspase activation assays, however, I decided to decrease the number of concentrations used for analysis by flow cytometry to enable a higher throughput when analysing the four compounds. To maintain the wide dose range, I started the highest concentration of SM at 90 μM , and chose four other concentrations that were 9-fold dilutions of the previous concentration, i.e. 90, 10, 1.11, and 0.12 μM . I decided to choose 24 h as the standard analysis time point as this is often used in the literature and more closely mimics a clinical chemotherapy dosing regimen. While 24 h is too late to detect canonical NF- κB pathway activation, this time point is able to investigate non-canonical NF- κB pathway activation through partial degradation of p100 to p52. This process can be determined by Western blotting, as so it was decided to add this readout to my panel of western blots.

Characterising the response of tumour cell lines to SMAC mimetics *in vitro*

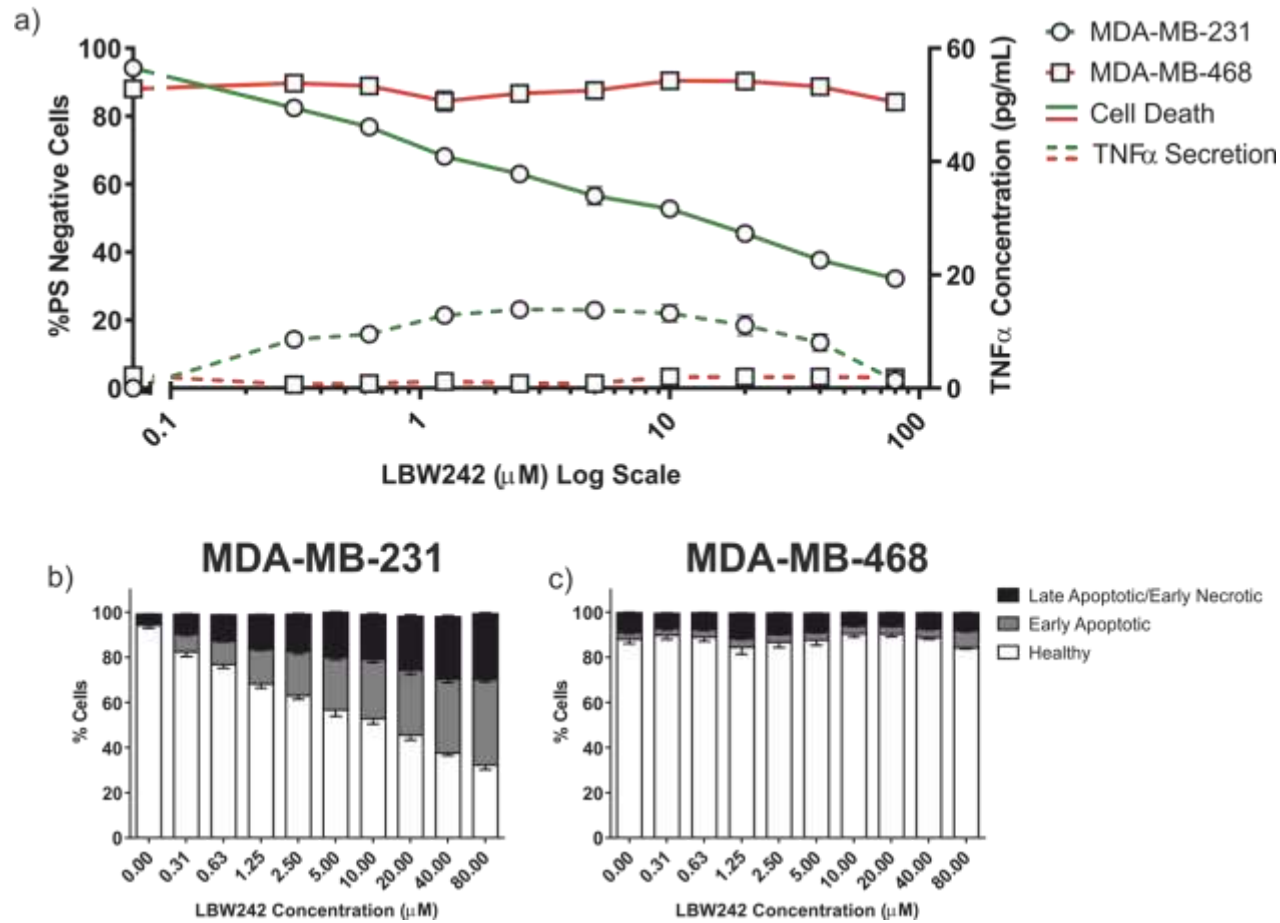


Figure 3.1 | LBW242 induces apoptosis in parallel with secretion of TNF α . **a)** TNF α secretion was measured by ELISA and cell death by flow cytometry at 16 h. **b-c)** Representation of the ratio of healthy, early and late apoptotic/early necrotic cells in MDA-MB-231 and MDA-MB-468 cells, respectively. Values represent mean \pm S.E.M, $n=3$.

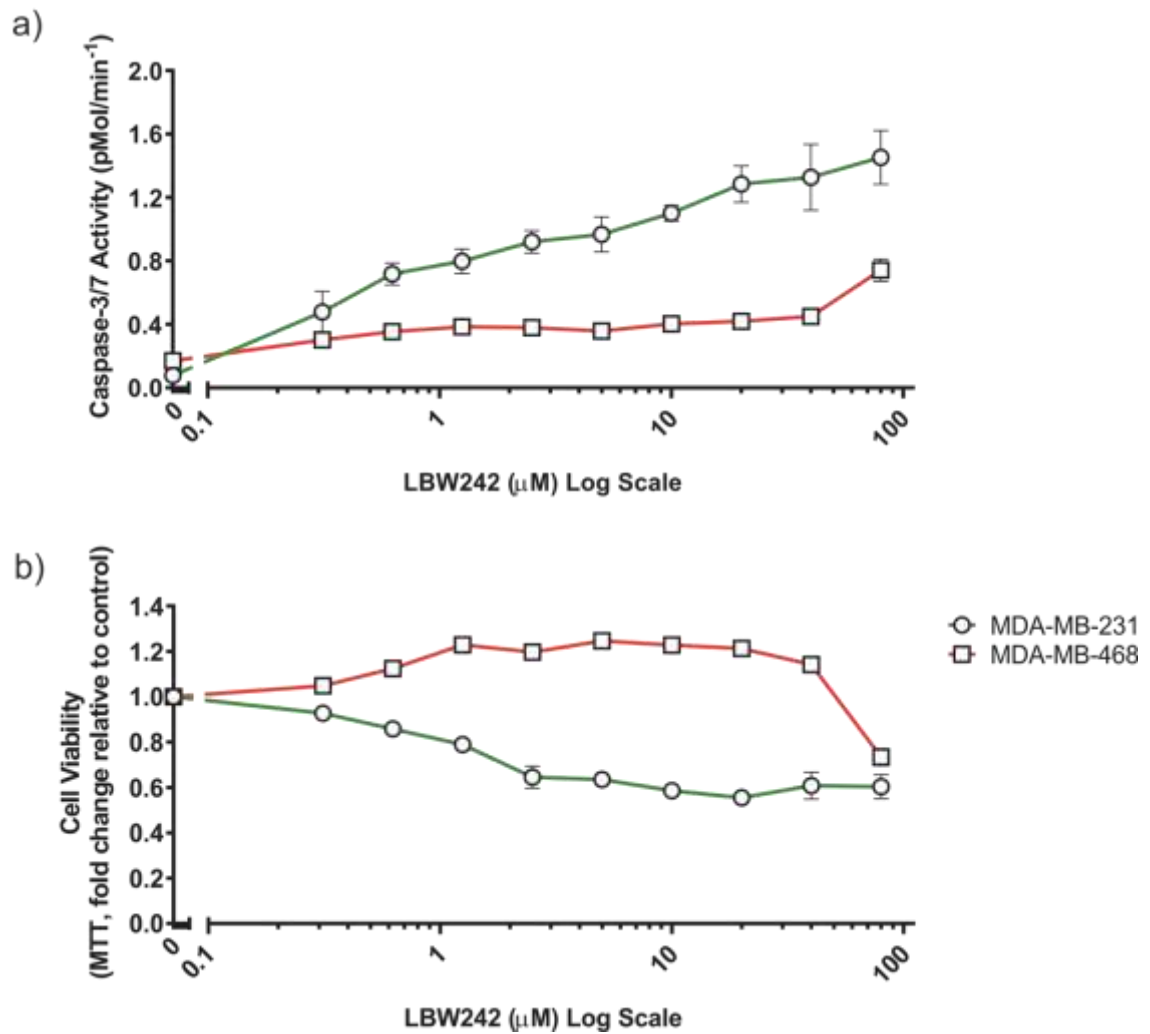


Figure 3.2 | LBW242 activates caspases, and results in a decrease in cell viability in MDA-MB-231 cells. a) Caspase-3/-7 activity was measured via DEVD.afc and **b)** cell viability by MTT assay. Values represent mean \pm S.E.M, $n=3$.

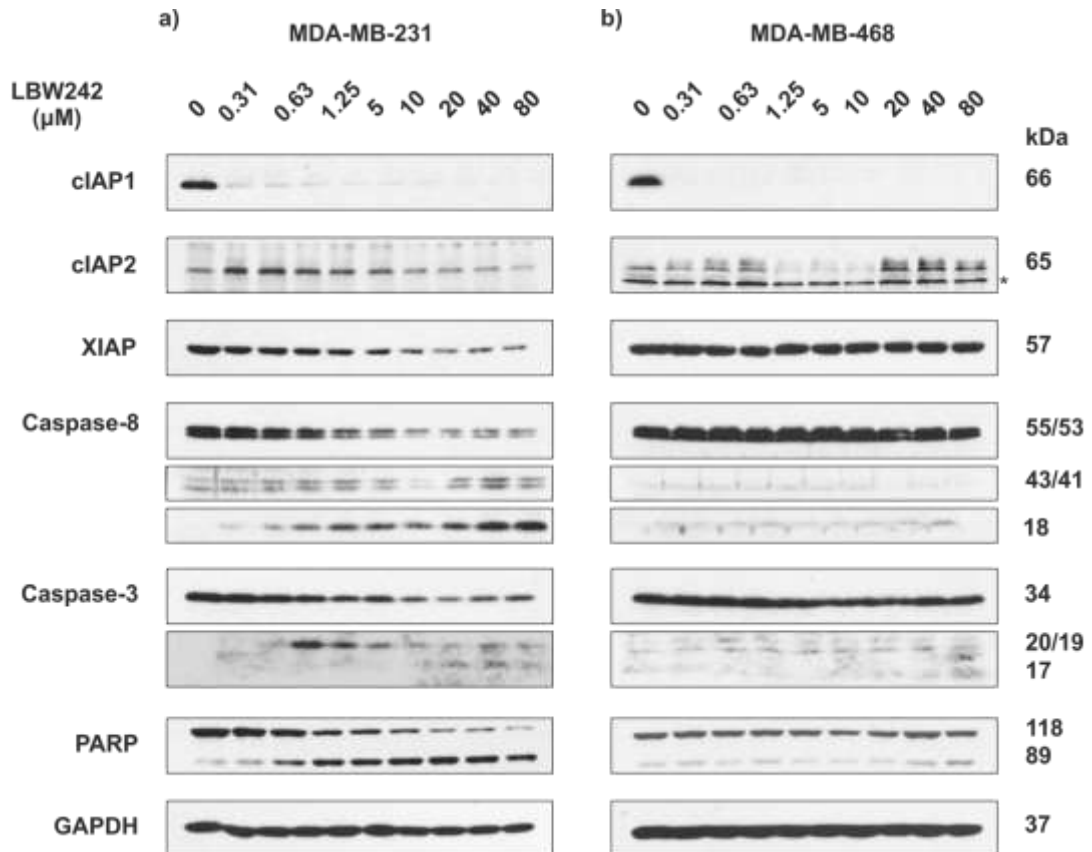


Figure 3.3 | LBW242 degrades cIAP1 in both sensitive and resistant cells but only activates caspases in cells with an inducible TNF α autocrine loop. a) MDA-MB-231 and **b)** MDA-MB-468 cell pellets were lysed directly in 1x sample buffer and loaded according to cell number. Expression levels of proteins targeted by SMs and those relevant to apoptosis were investigated by western blotting. * = non-specific band.

3.1.2. AT-406

AT-406 is a monovalent SM currently in clinical trials for use in advanced solid tumours⁸³. After 24 h, a slight increase of 8% in PS exposure was seen at 0.1 μM in MDA-MB-231 cells, which increased to 30% at 1 μM in these cells. No reduction in the percentage of healthy cells was seen in MDA-MB-468 cells. TNF α secretion was not observed in MDA-MB-468 cells, whereas in MDA-MB-231 cells, TNF α secretion increased to 16.6 ± 2.8 pg/mL at 1.1 μM AT-406. However, with increasing concentrations of AT-406, there was an apparent decrease in TNF α secretion, which is likely due to the observed cell death (**Figure 3.4**). In MDA-MB-231 cells, AT-406 resulted in an equivalent early:late cell ratio, suggesting that the mechanism of cell death was apoptotic. At 90 μM AT-406 there was a slight increase in the late:early ratio compared to other concentrations, suggesting 24 h is a reasonably late time point for this high concentration (**Figure 3.4**). The EC₅₀ of AT-406 was 64 μM , and the caspase-3/7 activation and cell viability assays both demonstrated AT-406 induced cell death at concentrations as low as 0.37 μM (**Table 3.1**; **Figure 3.4**). In MDA-MB-468 cells, AT-406 did not have any effect on caspase activation or cell viability even at the highest concentration of 90 μM (**Figure 3.5**). cIAP1 depletion, however, was seen in both cell lines with AT-406, as was non-canonical NF- κB activation (as shown by p100 degradation to p52; **Figure 3.6**). In MDA-MB-231 cells, activation of caspase-3 and -8 and cleavage of PARP was seen, which, together with the flow cytometry analysis, confirms the role of caspases in AT-406-mediated cell death in MDA-MB-231 cells. As with LBW242, cIAP2 expression levels showed a transient increase, before reducing again to baseline levels in MDA-MB-231 cells. In MDA-MB-468 cells, there was no activation of caspase-3 or caspase-8 or any cleavage of PARP, which is consistent with the lack of cell death observed (**Figure 3.6**).

Table 3.1 | EC₅₀ Values for the four different SMs in MDA-MB-231 and MDA-MB-468 cells.

Cell Line	LBW242	AT-406	GDC-0152	BV6	TL-32711
MDA-MB-231	12.4 μM	65 μM	0.3 μM	N/A	N/A
MDA-MB-468	>80 μM	>90 μM	>90 μM	4.8 μM	>90 μM

EC₅₀ values were determined from %PS negative cells from triplicate experiments. MDA-MB-231 cells were the most sensitive. BV6 was the most potent SM and induced cell death both cell lines, whereas AT-406 induced the least amount of cell death.

Characterising the response of tumour cell lines to SMAC mimetics *in vitro*

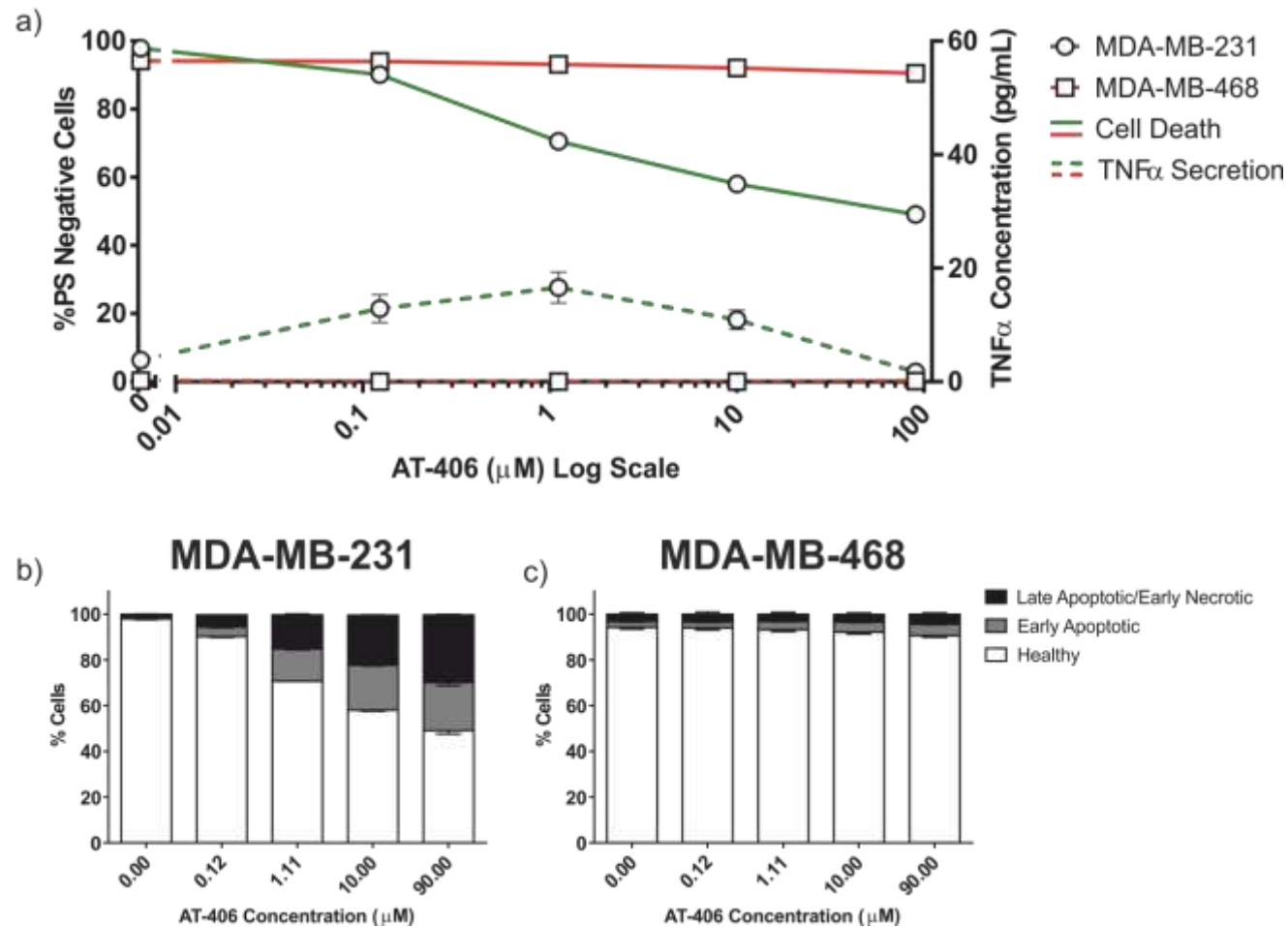


Figure 3.4 | AT-406 induces apoptosis in cells with a TNF α -autocrine loop. MDA-MB-231 and MDA-MB-468 cells were treated with the indicated concentrations of AT-406 for 24 h. **a)** Cell death was determined by flow cytometry and TNF α secretion by ELISA. **b-c)** MDA-MB-231 and MDA-MB-468 cells, respectively, were sorted into healthy, early and late apoptotic/early necrotic cells. Values represent mean \pm S.E.M, $n=3$.

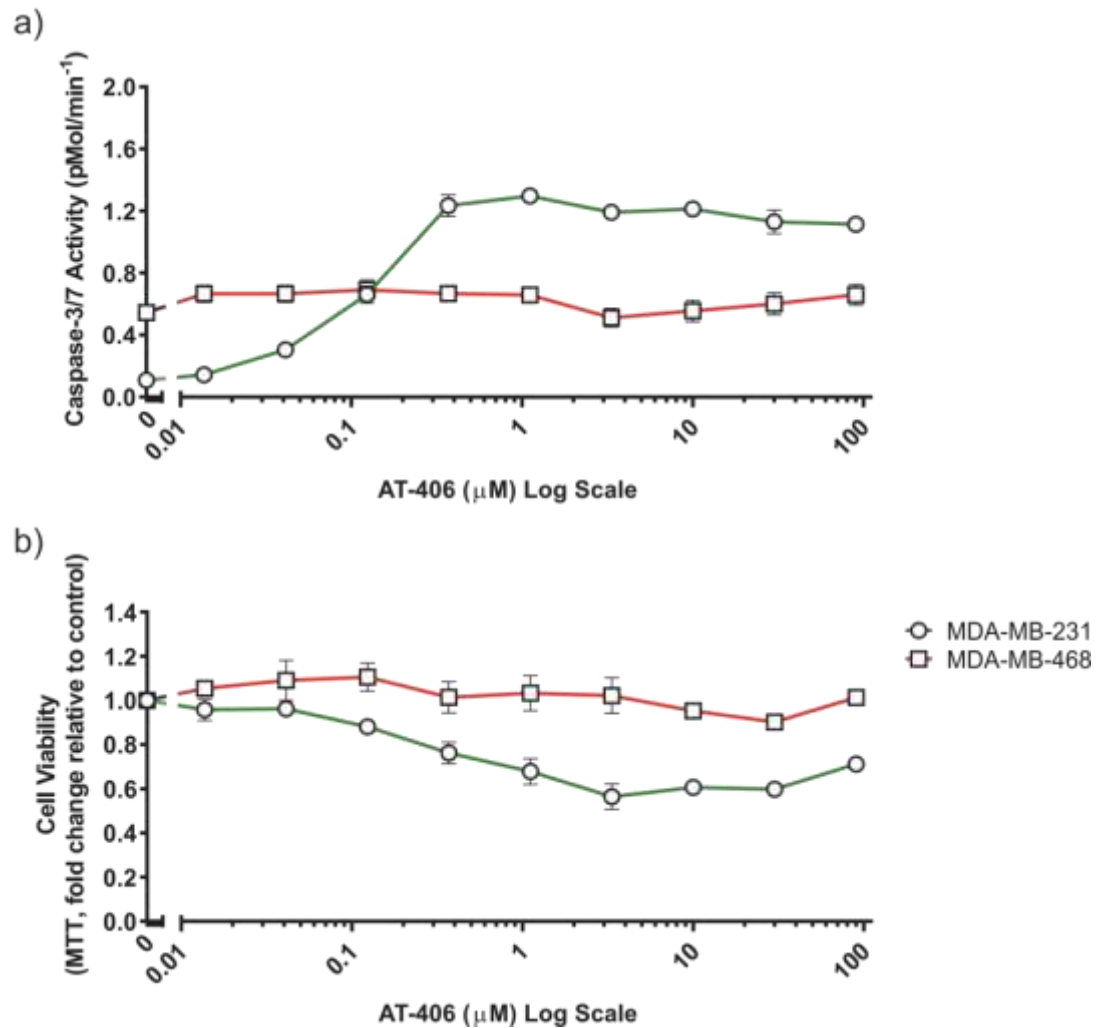


Figure 3.5 | AT-406 promotes caspase activity and a decrease in cell viability in MDA-MB-231 cells. Cells were treated for 24 h. **a)** Caspase-3/-7 activity was measured via DEVD.afc and **b)** cell viability by MTT assay. Values represent mean \pm S.E.M, $n=3$.

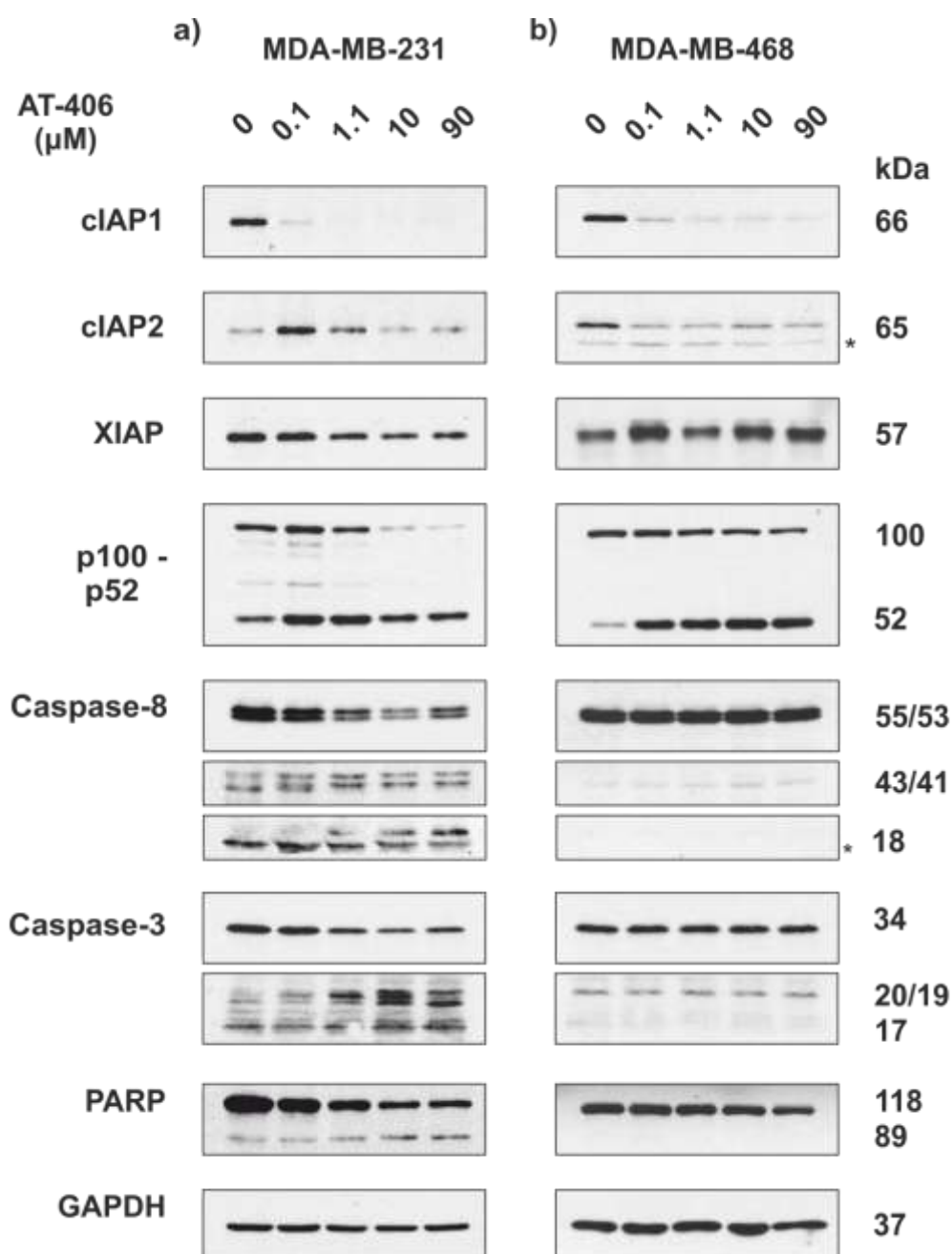


Figure 3.6 | AT-406 degrades cIAP1 in all cell lines but only activates caspases in cells with TNF α autocrine activity. a) MDA-MB-231 and b) MDA-MB-468 cell pellets were directly lysed in 1x sample buffer and loaded based on equal cell numbers. Expression levels of proteins relevant to IAP, non-canonical NF- κ B activation and apoptosis were determined using western blotting. * = non-specific band.

3.1.3. GDC-0152

GDC-0152 is the second monovalent compound under investigation in this study and is currently in clinical trials for solid tumours and Non-Hodgkin's Lymphoma without leukemic phase⁸³. MDA-MB-231 cells showed a significant increase in PS externalisation of 80% after 24 h exposure to GDC-0152, with no change in MDA-MB-468 cells (<10%; **Figure 3.7**). The EC₅₀ for GDC-0152 in MDA-MB-231 and MDA-MB-468 cells was 0.3 µM and >90 µM, respectively (**Table 3.1**). There was no change in TNFα secretion in MDA-MB-468 cells, whereas in MDA-MB-231 cells, there was an increase from 0 pg/mL in the control to a maximum of 23.04 pg/mL at 10 µM (**Figure 3.7**). In MDA-MB-231 cells, there was a similar early:late ratio of apoptotic cells, although, as with AT-406, there was a slight increase in the late:early ratio at 90 µM (**Figure 3.7**). The caspase-3/7 activity assay did not show a difference between the two cell lines, therefore not fully supporting the flow cytometry data and cell viability assays; the MTT assay demonstrated a 68% reduction in MDA-MB-231 cells, compared to less than 15% in MDA-MB-468 cells (**Figure 3.8**). Similar to AT-406, cIAP1 depletion was seen in both cell lines treated with GDC-0152, which resulted in p100 degradation to p52 (**Figure 3.9**). Cleavage of both caspase-8 and caspase-3 was detected by western blotting in MDA-MB-231 cells, but not MDA-MB-468 cells (**Figure 3.9**).

Characterising the response of tumour cell lines to SMAC mimetics *in vitro*

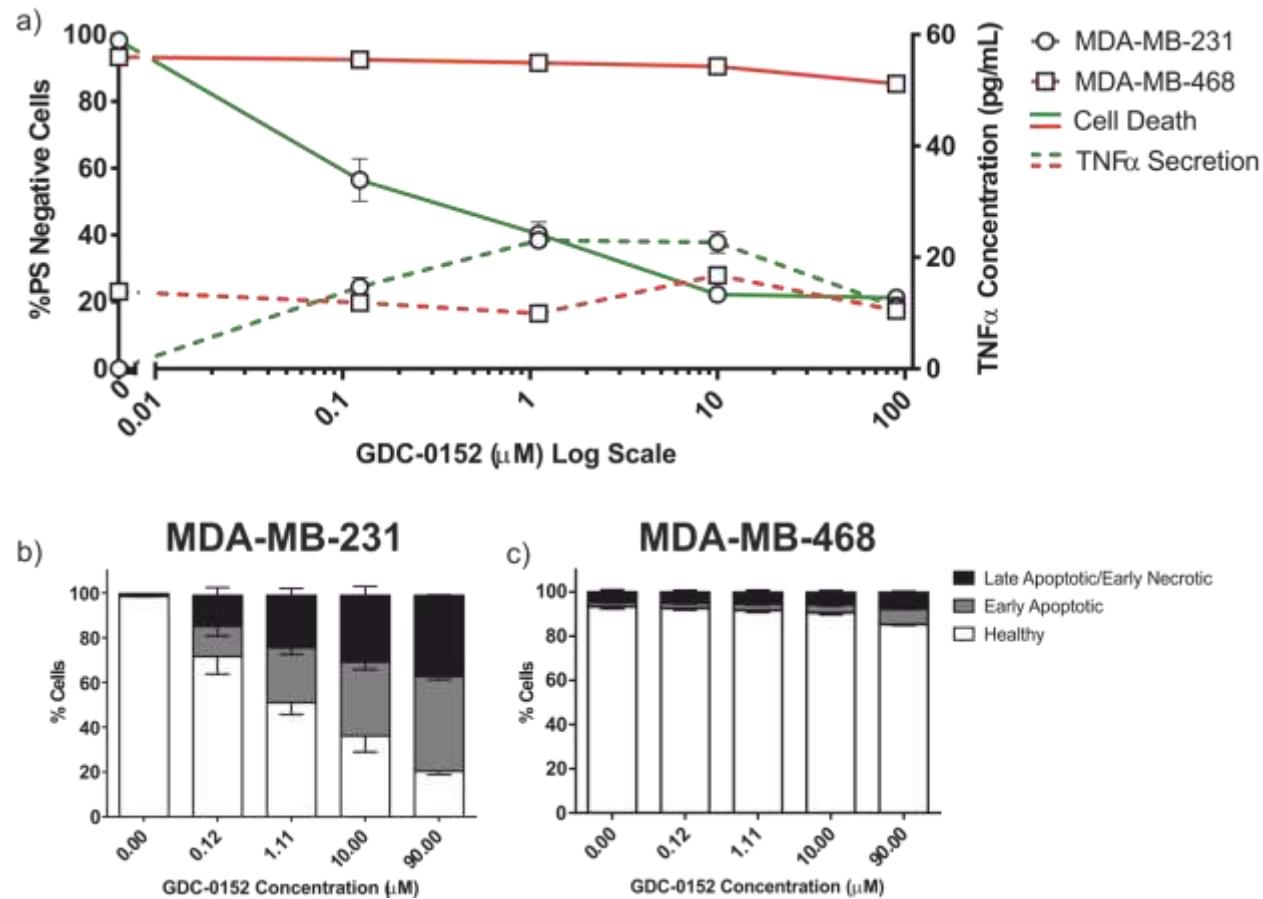


Figure 3.7 | GDC-0152 induces cell death in cells with a TNF α autocrine loop. a) MDA-MB-231 and MDA-MB-468 cells were treated with GDC-0152 for 24 h. **a)** Cell death was determined by flow cytometry and TNF α secretion by ELISA. **b-c)** MDA-MB-231 and MDA-MB-468 cells, respectively, were sorted into healthy cells, early apoptotic and late apoptotic/early necrotic. Values represent mean \pm S.E.M, $n=3$.

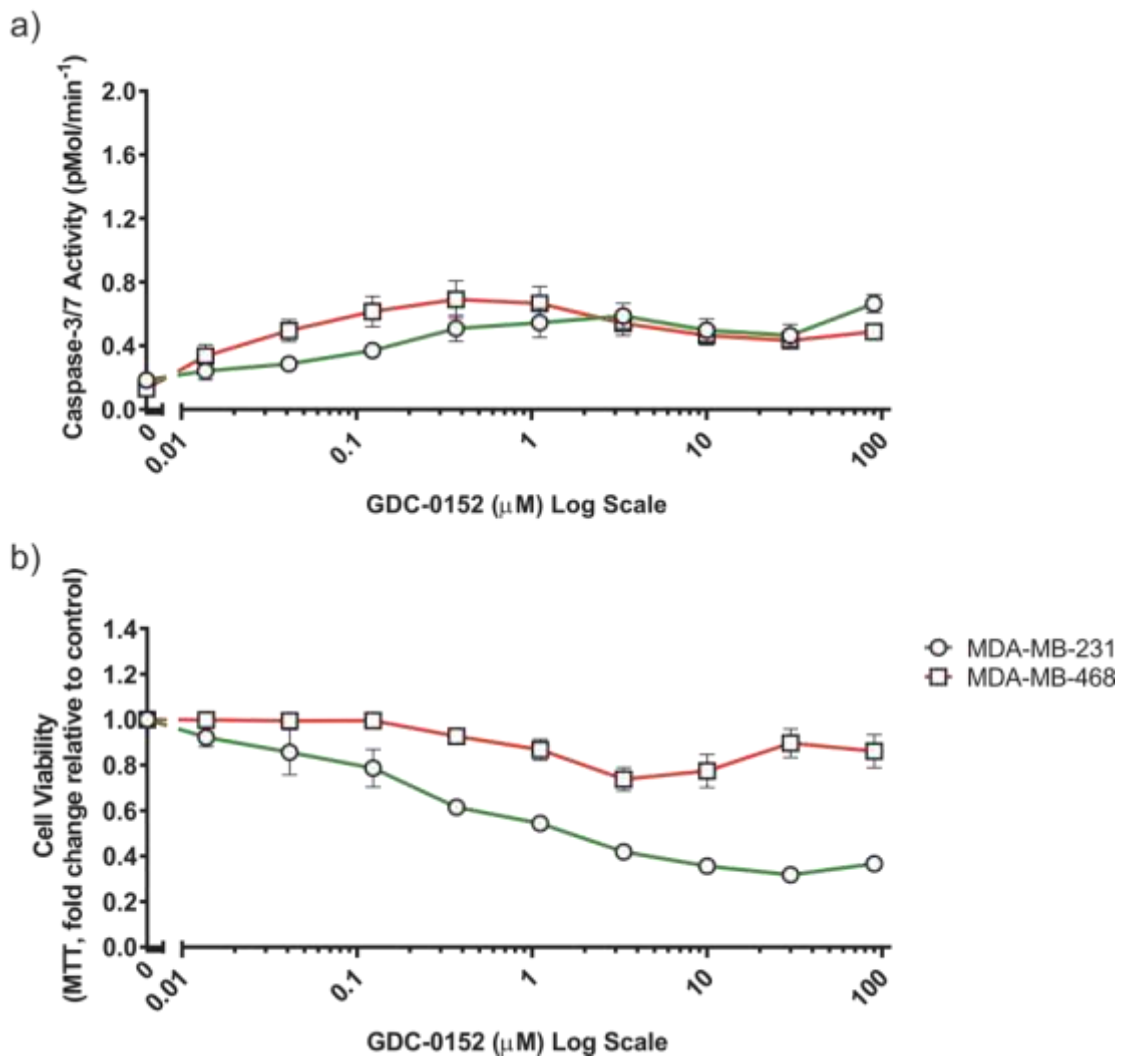


Figure 3.8 | GDC-1052 induces caspase activity and decreases cell viability in MDA-MB-231 cells. Cells were treated for 24 h. **a)** Effector caspase activity was determined by DEVD.afc assays and **b)** cell viability by MTT assay. Values represent mean \pm S.E.M, $n=3$.

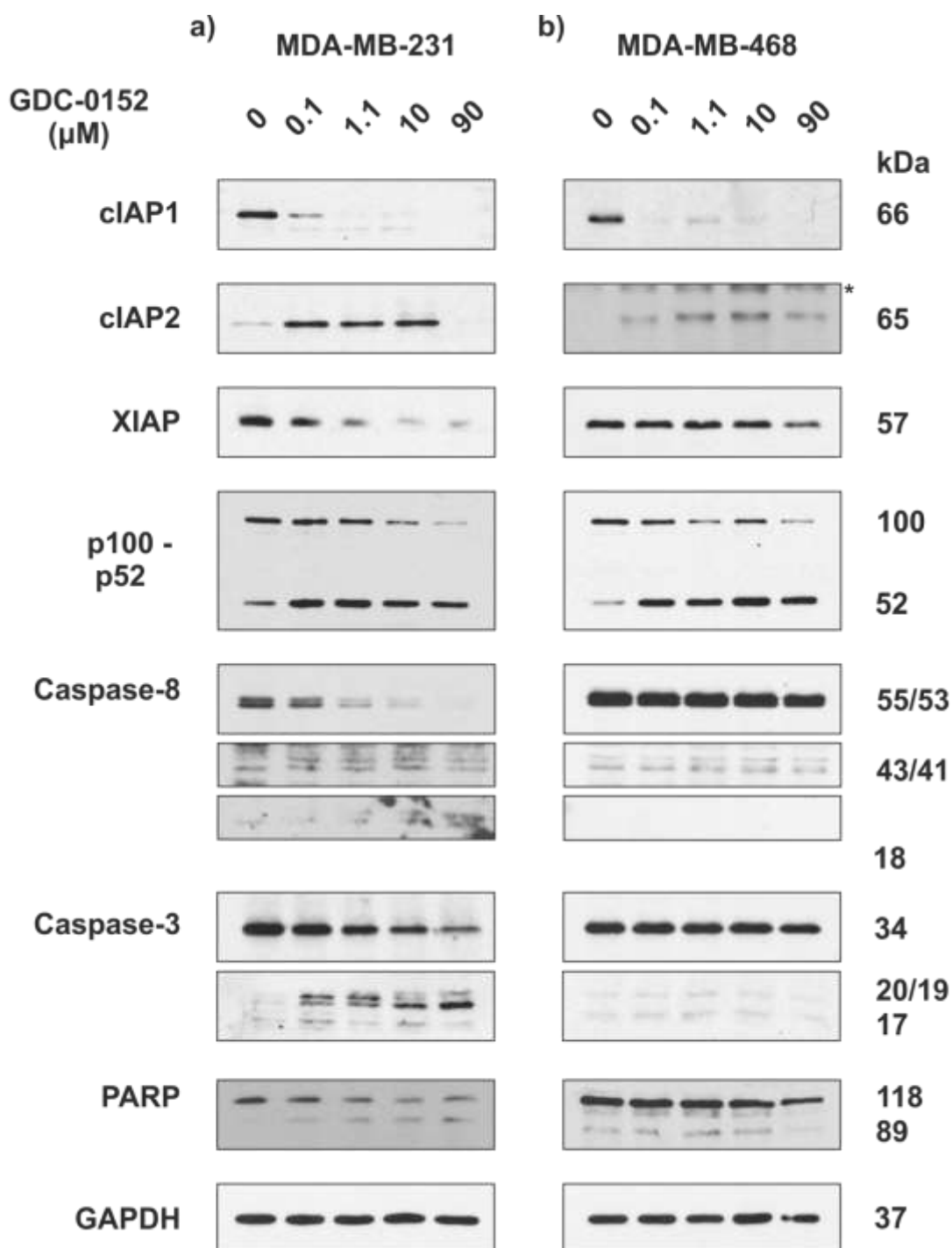


Figure 3.9 | GDC-0152 degrades cIAP1 in both, but does not induce caspase processing in non-tumour derived cells. Cell pellets were lysed in RIPA buffer, after which protein concentration was determined by Bradford assay. Lysates were then loaded according to protein concentration. Expression levels of proteins relevant to IAPs, apoptosis and non-canonical NF- κ B activation were analysed by western blotting.

3.1.4. BV6

BV6 is a bivalent SM, and is therefore expected to be more active than monovalent compounds due to increased XIAP inhibition. In pilot studies (data not shown), I found BV6 to be significantly more active than the two monovalent compounds tested previously, and therefore reduced the highest concentration of BV6 from 90 μ M to 30 μ M. In both MDA-MB-231 and MDA-MB-468 cells, BV6 induced >98% cell death at 30 μ M (**Figure 3.10**). TNF α secretion remained unchanged in MDA-MB-468 cells, but MDA-MB-231 cells saw a 30-fold increase at 41 nM, which decreased as the compound concentration increased (**Figure 3.10**). Upon examination of the early:late apoptotic death ratio, an interesting pattern appeared. In MDA-MB-231 cells, the early:late ratio was ~1:1, except at 30 μ M, where there were slightly more AnV/PI cells (18%). In contrast, in MDA-MB-468 cells, there were 40% more late apoptotic/early necrotic cells compared to early apoptotic cells. This suggests that there is another form of cell death operating at this concentration of BV6 (**Figure 3.10**). The EC₅₀ of BV6 was not determined for MDA-MB-231 cells as the lower concentrations induced such high amounts of cell death, whereas, in MDA-MB-468 cells, the EC₅₀ was 4.8 μ M (**Table 3.1**). The cell viability assay showed a clear difference in the sensitivity of the two cell lines to BV6, supporting the flow cytometry data (**Figure 3.11**). However, caspase activity, as detected by DEVD.afc, was actually higher in MDA-MB-468 cells compared to MDA-MB-231 cells, which is likely due to the significant amount of cell death seen in MDA-MB-231 cells (**Figure 3.11**).

Due to the high cell death, no protein pellet was detectable at 30 μ M of BV6; I therefore only subjected cells treated with the four preceding concentrations to western blot analysis. In these, BV6 degraded cIAP1 in both MDA-MB-231 and MDA-MB-468 cells, although in MDA-MB-231 cells, cell death was so profound it was not possible to load equal protein concentrations for western blotting analysis as seen by the decreasing expression levels of the loading control protein, GAPDH (**Figure 3.12**). The non-canonical NF- κ B pathway was also activated in both cell lines. Caspase-8 and caspase-3 were cleaved in MDA-MB-468 cells and PARP was also cleaved, consistent with the extensive BV6-induced cell death in these cells (**Figure 3.12**).

Characterising the response of tumour cell lines to SMAC mimetics *in vitro*

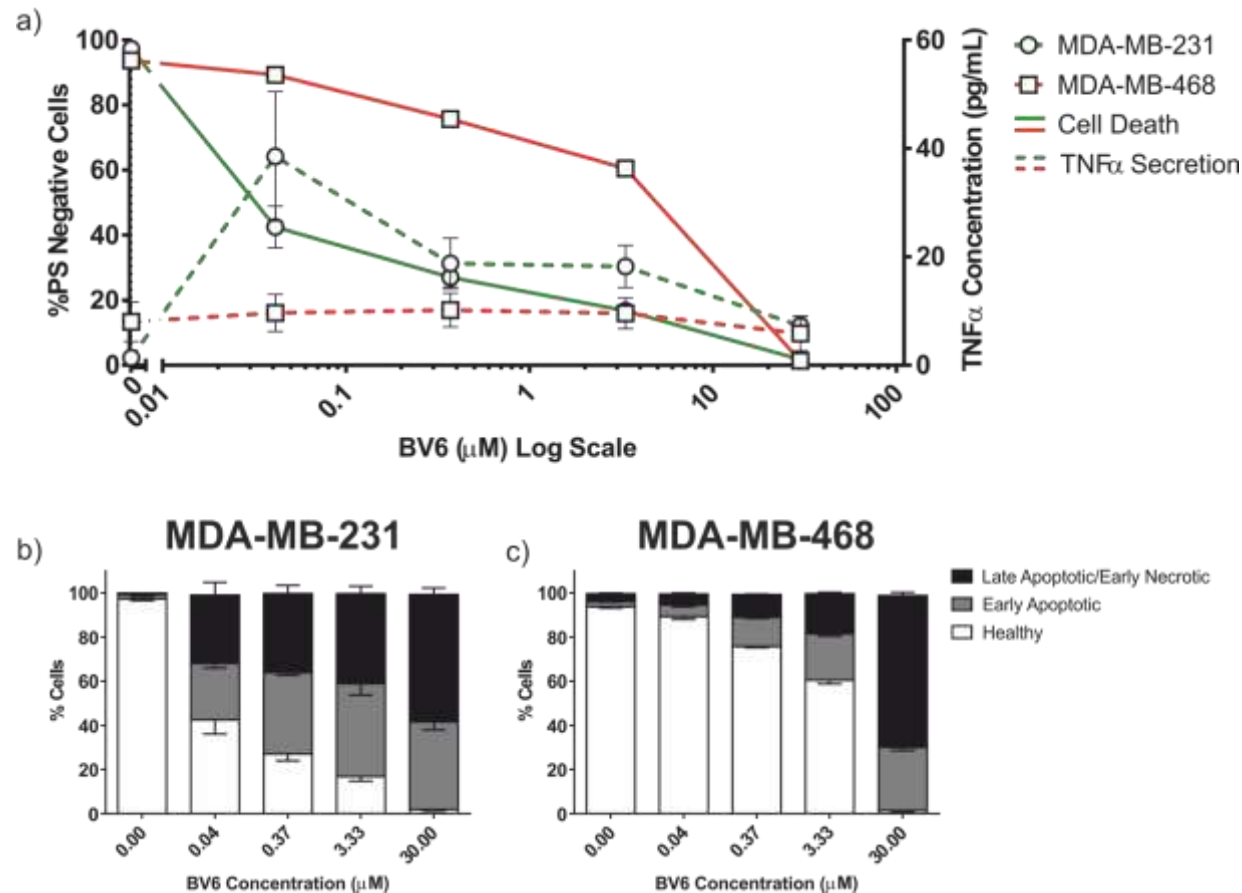


Figure 3.10 | BV6 induces cell death even in cells where it does not induce secretion of TNF α . Cells were treated with BV6 for 24 h. **a)** Cell death was measured by flow cytometry and TNF α secretion was determined by ELISA. **b-c)** MDA-MB-231 and MDA-MB-468 cells were sorted into healthy cells, early apoptotic and late apoptotic/late necrotic cells by flow cytometry, respectively. Values represent mean \pm S.E.M, $n=3$.

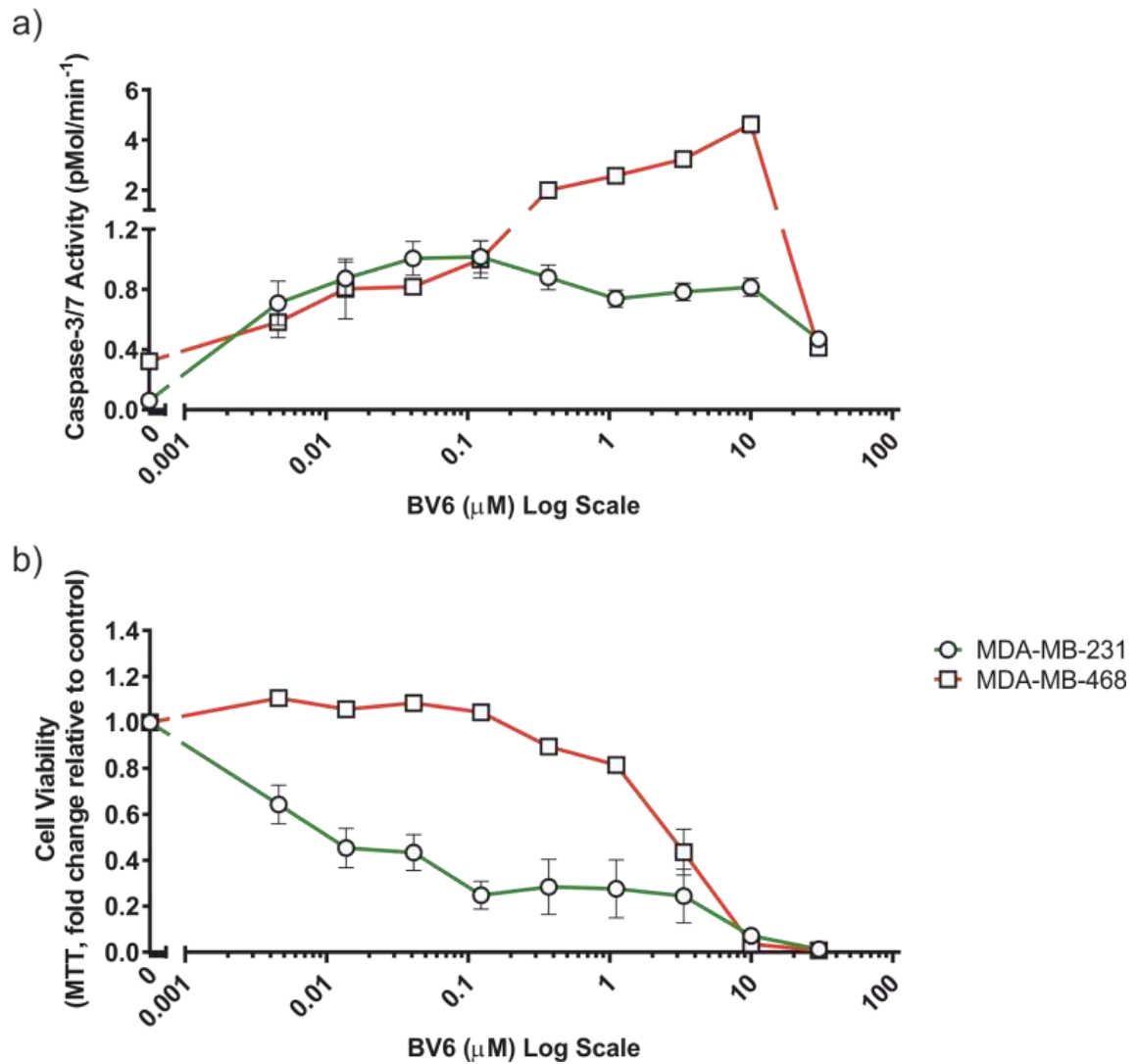


Figure 3.11 | BV6 induces caspase activity and decreases cell viability in both MDA-MB-231 and MDA-MB-468 cells. Cells were treated for 24 h. **a)** Caspase-3/-7 activity was measured by DEVD.afc and **b)** cell viability using MTT assay. Values represent mean \pm S.E.M, $n=3$.

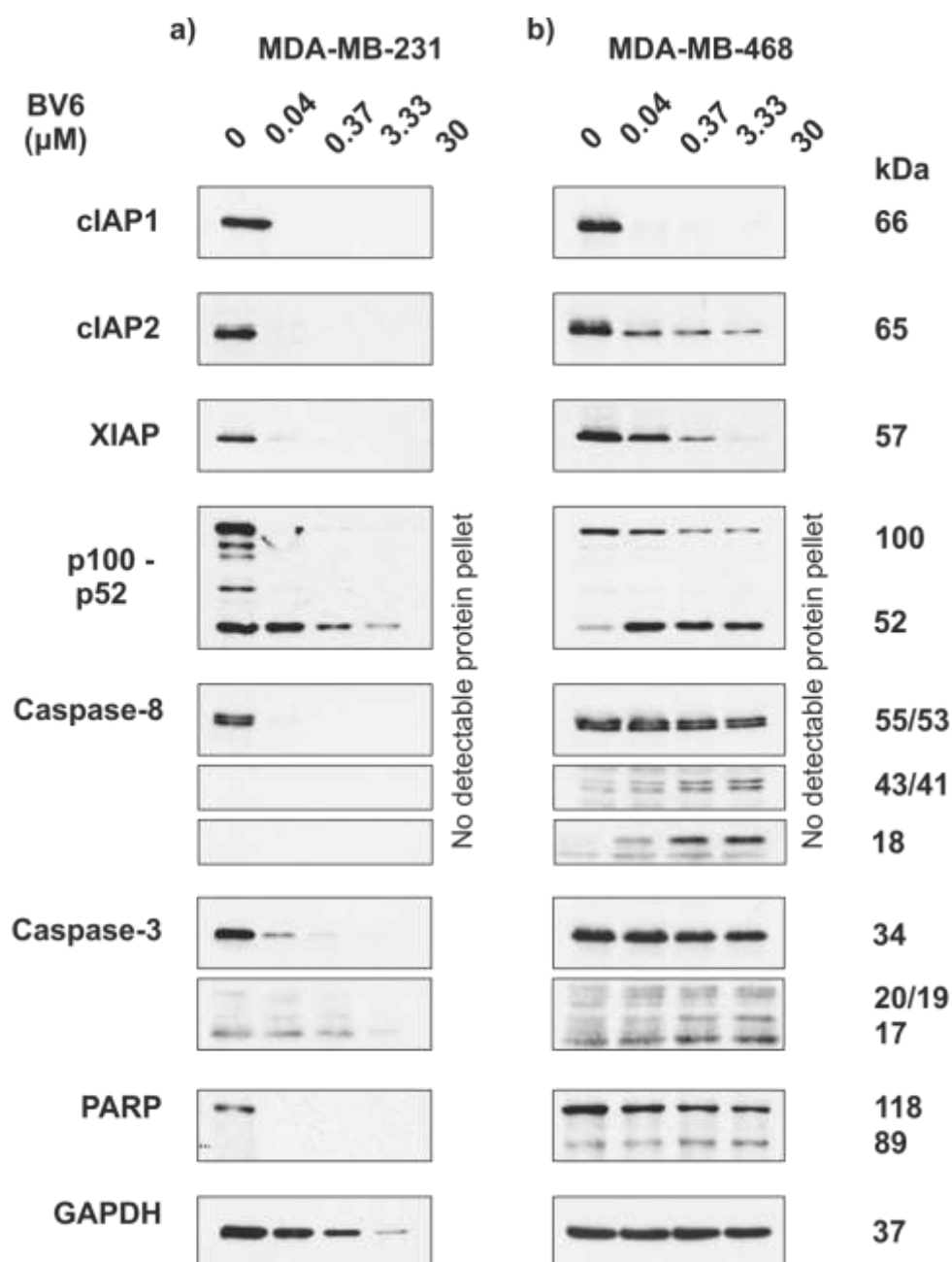


Figure 3.12 | BV6 degrades cIAP1/2 and XIAP, and induces caspase activation even in cells where it does not activate a TNF α autocrine loop. Cells pellets were directly lysed in 1x sample buffer and loaded based on cell number. Expression of IAP proteins, apoptosis and NF- κ B related proteins were analysed via western blotting.

3.1.5. TL-32711

TL-32711 is a bivalent SM in clinical trials⁸³. Interestingly, despite being bivalent, TL-32711 primarily targets cIAP1, and not cIAP2 or XIAP¹⁴⁹. As with BV6, TL-32711 induced significantly more cell death in MDA-MB-231 cells than the monovalent compounds. However, unlike BV6, TL-32711 does not induce high amounts cell death in MDA-MB-468 cells (**Figure 3.13**), which is likely due to a lower affinity for cIAP2 and XIAP. TNF α secretion increased after treatment with TL-32711 from 0 pg/mL to 11.08 pg/mL at 0.12 μ M in MDA-MB-231 cells, whereas in MDA-MB-468 cells, TNF α secretion actually decreased considerably at 1.1 μ M (**Figure 3.13**). It was not possible to determine the EC₅₀ for TL-32711 in either cell line as there was either too much or too little cell death at the concentrations of TL-32711 used (**Table 3.1**). The early:late ratio was similar at all concentrations of TL-32711 in both MDA-MB-231 cells and MDA-MB-468 cells (**Figure 3.13**). As with GDC-0152, there was slightly more caspase-3/-7 activation in MDA-MB-468 cells with TL-32711 (**Figure 3.14**). Cell viability was significantly reduced in both MDA-MB-231 and MDA-MB-468 cells at 90 μ M TL-32711 by 68% and 80%, respectively, although MDA-MB-468 cells remained relatively resistant at concentrations below this (**Figure 3.14**). TL-32711 treatment induced cIAP1 depletion and p100 to p52 degradation in both cell lines and promoted caspase-3 and caspase-8 activation in MDA-MB-231 cells, but not MDA-MB-468 cells (**Figure 3.15**).

Characterising the response of tumour cell lines to SMAC mimetics *in vitro*

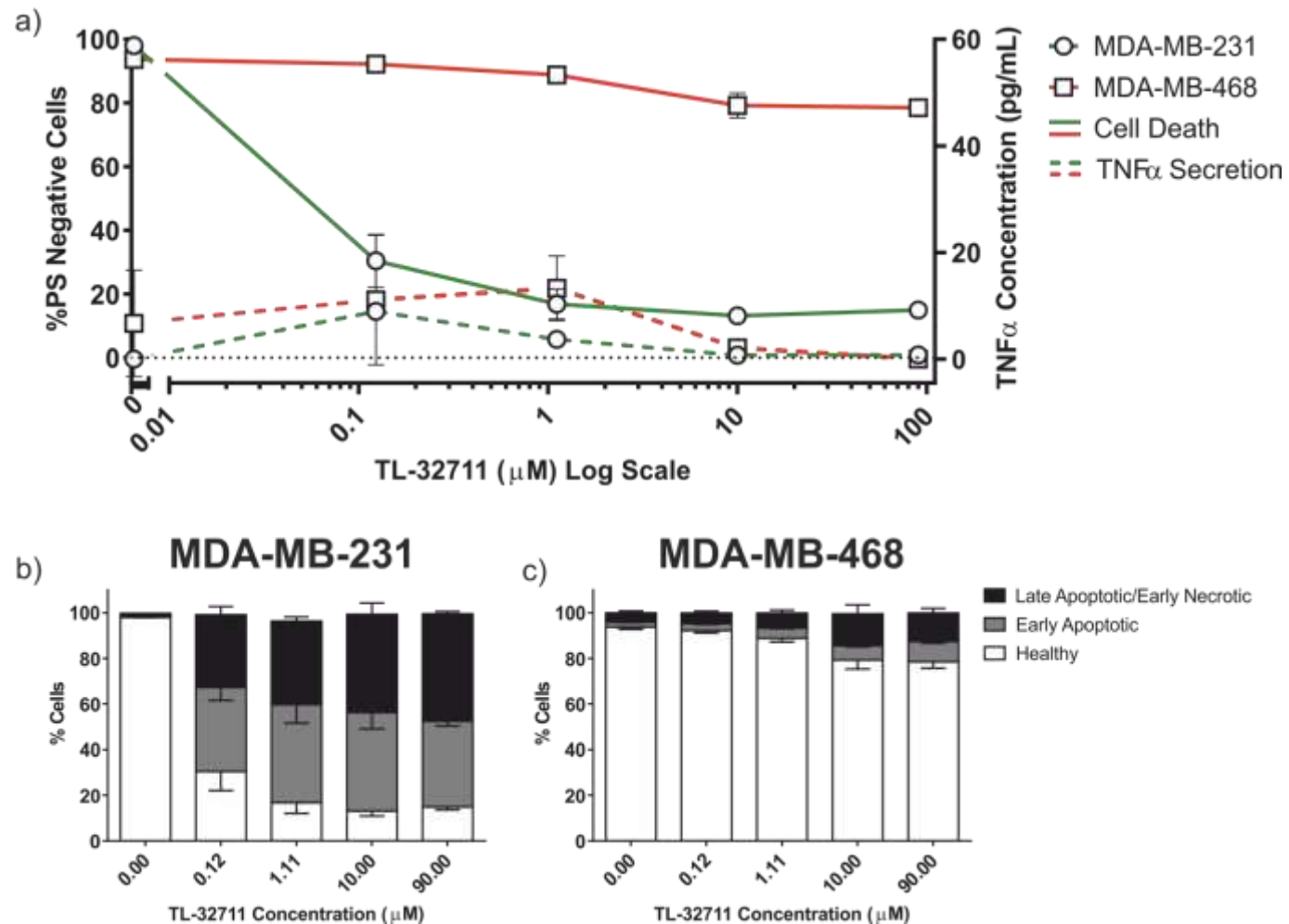


Figure 3.13 | TL-32711 induces significant apoptosis in cells with a TNFα autocrine loop. MDA-MB-231 and MDA-MB-468 cells were treated for 24 h. **a)** Cell death was determined using flow cytometry and TNFα secretion by ELISA. **b-c)** Cells were sorted into healthy, early apoptotic and late apoptotic/early necrotic cells. Values represent mean ± S.E.M, $n=3$.

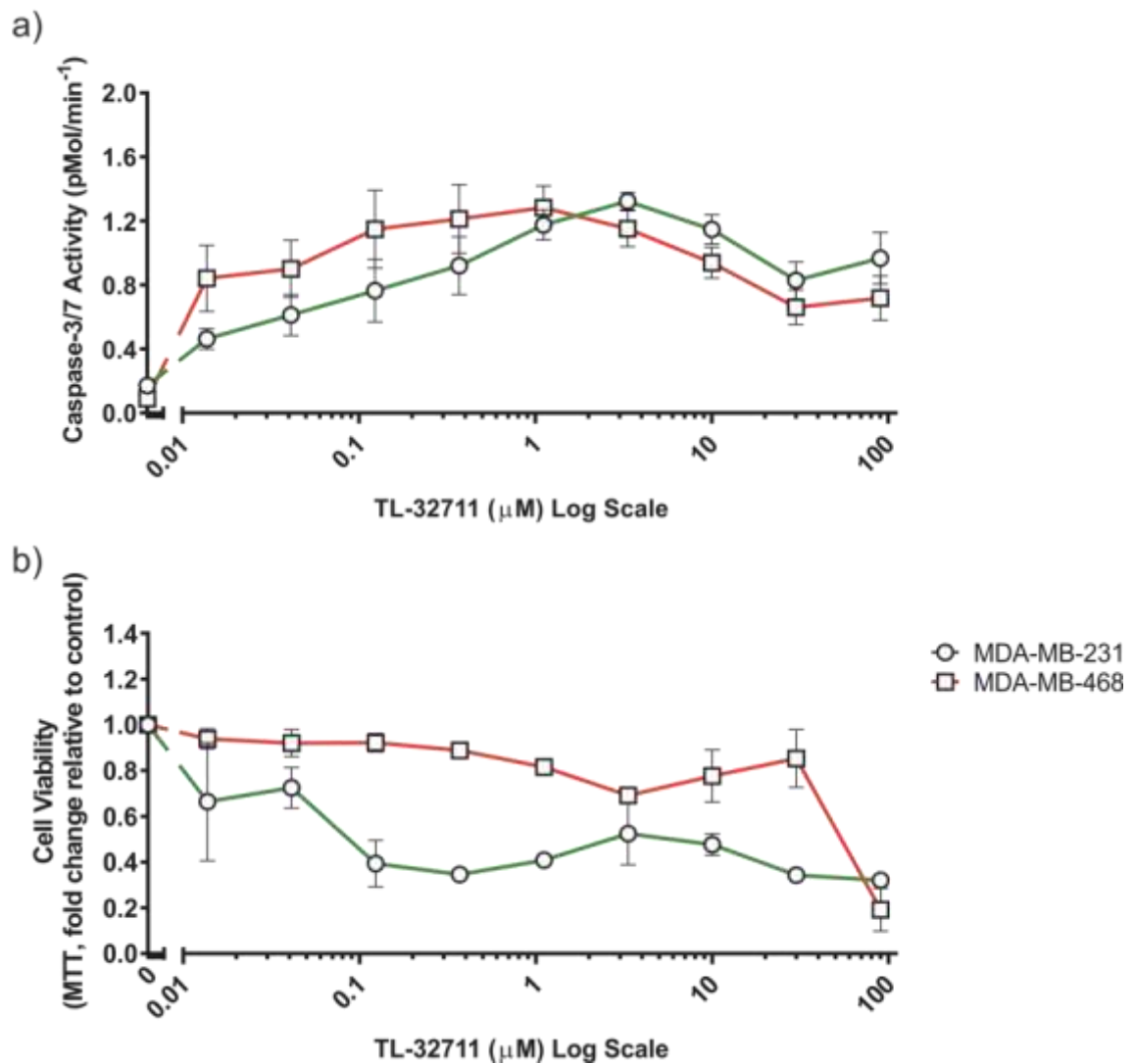


Figure 3.14 | TL-32771 induces caspase activity and decreases cell viability in both MDA-MB-231 cells, but not MDA-MB-468 cells. Cells were treated for 24 h. **a)** Caspase-3/-7 activity was measured by DEVD.afc and **b)** cell viability using MTT assay. Values represent mean \pm S.E.M, $n=3$.

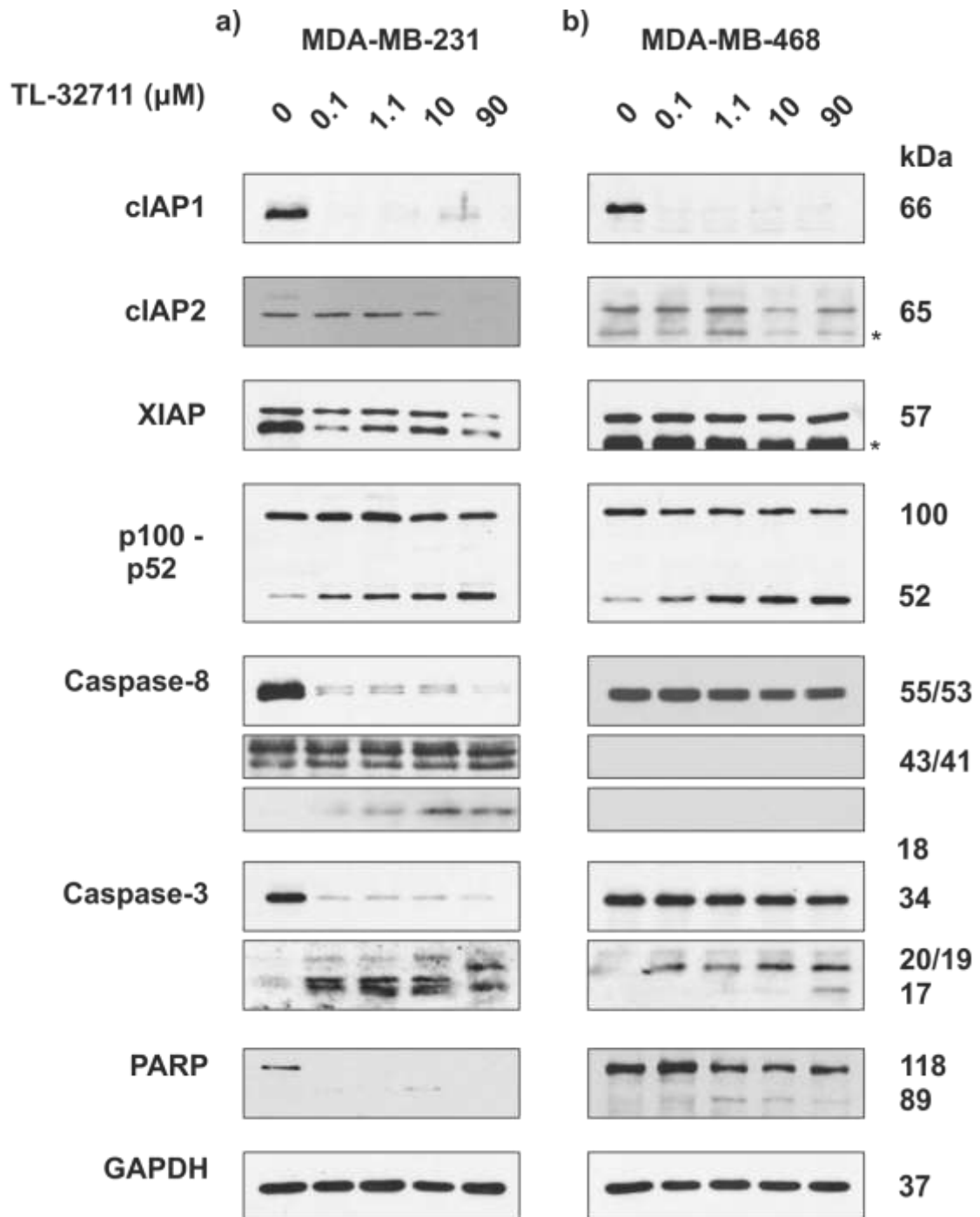


Figure 3.15 | TL-32711 induces cIAP1 depletion and non-canonical NF- κ B activation. Cell pellets were lysed in RIPA buffer, after which protein concentration was determined by Bradford assay. Lysates were then loaded according to protein concentration. Expression profiles of proteins involved in apoptosis and non-canonical NF- κ B activation and IAP proteins were investigated using western blotting. * = non-specific band.

Bivalent SMs induce cell death at nanomolar concentrations as single agents

SMs act in three distinct phases: 1) depletion of cIAP1/2, 2) activation of the non-canonical NF- κ B pathway and, dependent on the presence of TNF α , 3) induction of cell death. From my initial experiments with the two bivalent SMs, BV6 and TL-32711, all these phases had occurred at concentrations lower than the ones used in this study, meaning it was not possible to determine at what concentration of SM cIAP1 was depleted or gain an accurate EC₅₀ for cell death. Thus, to further investigate at what concentrations bivalent SMs began to deplete cIAP1 and activate the non-canonical NF- κ B pathway, I performed an expanded concentration-range in both MDA-MB-231 and MDA-MB-468 cells. I also sought to define at which concentration SMs induce cell death and TNF α secretion in MDA-MB-231 cells. Initially I piloted a 10-fold dilution range of 0.01 nM to 1 μ M (data not shown), however, this was not precise enough to ascertain the answer in MDA-MB-231 cells. I therefore chose two different concentration ranges of BV6 and TL-32711 for MDA-MB-231 cells, and BV6 only for MDA-MB-468 cells.

In MDA-MB-231 cells at 24 h, cIAP1 was completely ablated at 10 nM with both BV6 and TL-32711 (**Figure 3.18**). Cell death induction was seen at concentrations as low as 10 nM for both bivalent SM compounds, with the EC₅₀ being 60 and 25 nM for BV6 and TL-32711, respectively (**Figure 3.16**). It is interesting to note that despite BV6 inducing complete cell death at higher concentrations, the EC₅₀ for TL-32711 was actually more than 2-fold lower than BV6 in MDA-MB-231 cells. The cell death induced by both BV6 and TL-32711 was closely correlated to cIAP1 depletion, non-canonical NF- κ B activation and TNF α secretion. Furthermore, BV6 resulted in much higher TNF α secretion than TL-32711, which may explain why TL-32711 is deemed a more successful and clinically relevant compound as it is less likely to induce a cytokine storm (**Figure 3.16**).

This observation was further corroborated by flow cytometry data which shows, that despite less cell death, the early:late apoptotic cell ratio was higher with BV6, whereas TL-32711, which induces more cell death, actually has a higher early:late ratio, indicative of early apoptosis (**Figure 3.16 and 3.17**). MDA-MB-468 cells, however, were treated with only BV6 at a range of 0.01 nM - 30 μ M as TL-32711 did not induce significant cell death in these cells. In MDA-MB-468 cells, cIAP1 depletion occurred at a much higher concentration compared to MDA-MB-231 cells, but as with the sensitive cells, depletion strongly correlated with cell death, non-canonical NF- κ B activation and a slight increase in TNF α secretion (**Figure 3.16 and 3.18**). It is also interesting to note that the stabilisation of cIAP2 upon SM treatment is only present in MDA-MB-231 cells and not MDA-MB-468 cells.

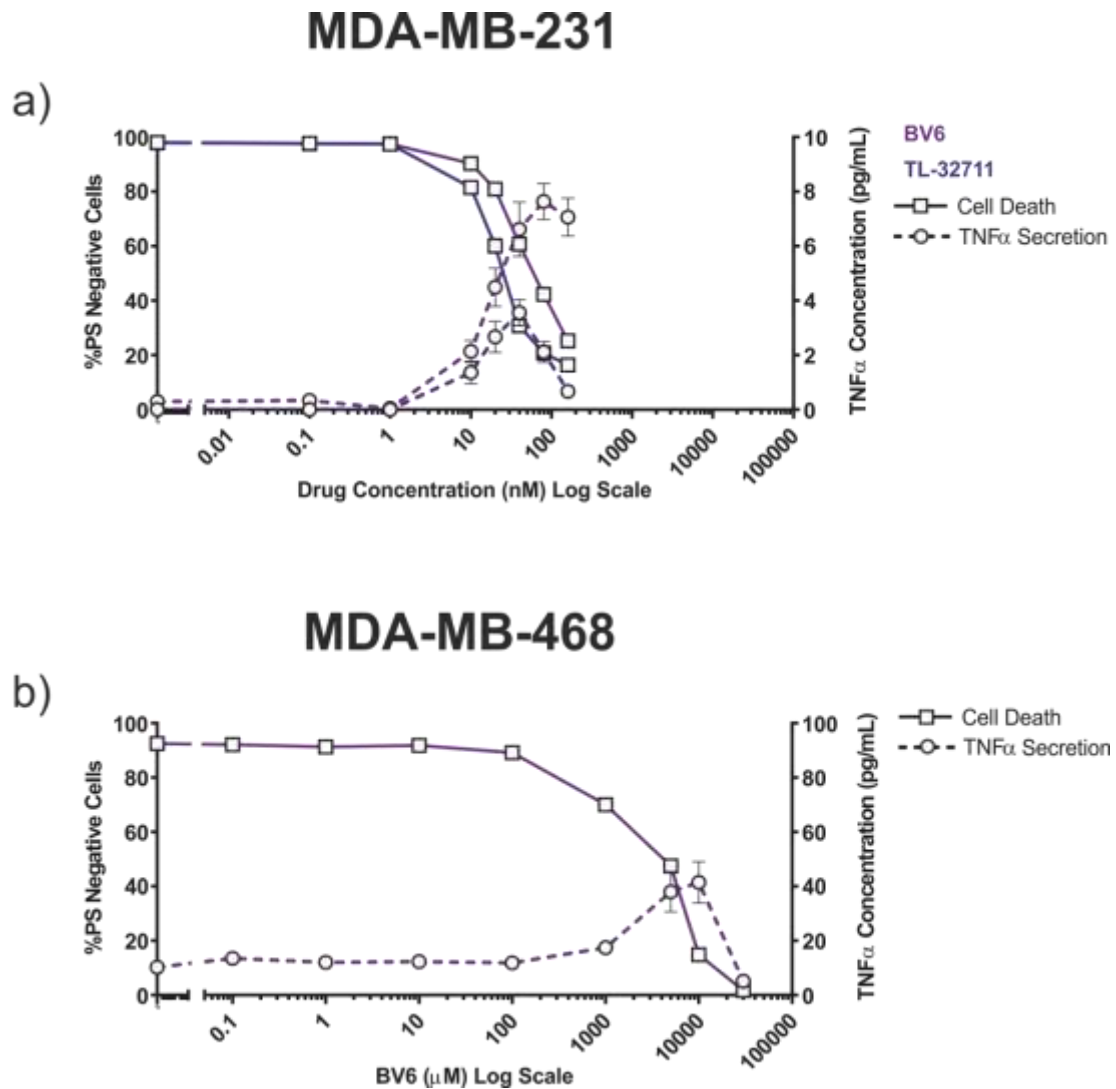


Figure 3.16 | Bivalent SMs induce cell death at nanomolar concentrations in MDA-MB-231 cells. In MDA-MB-468 cells, BV6 induces cell death at micromolar concentrations. MDA-MB-231 and MDA-MB-468 cells were treated with the indicated compounds for 24 h. **a and b)** Cell death was measured using flow cytometry and TNFα secretion was quantified using an ELISA. Values represent mean ± SEM, $n=3$.

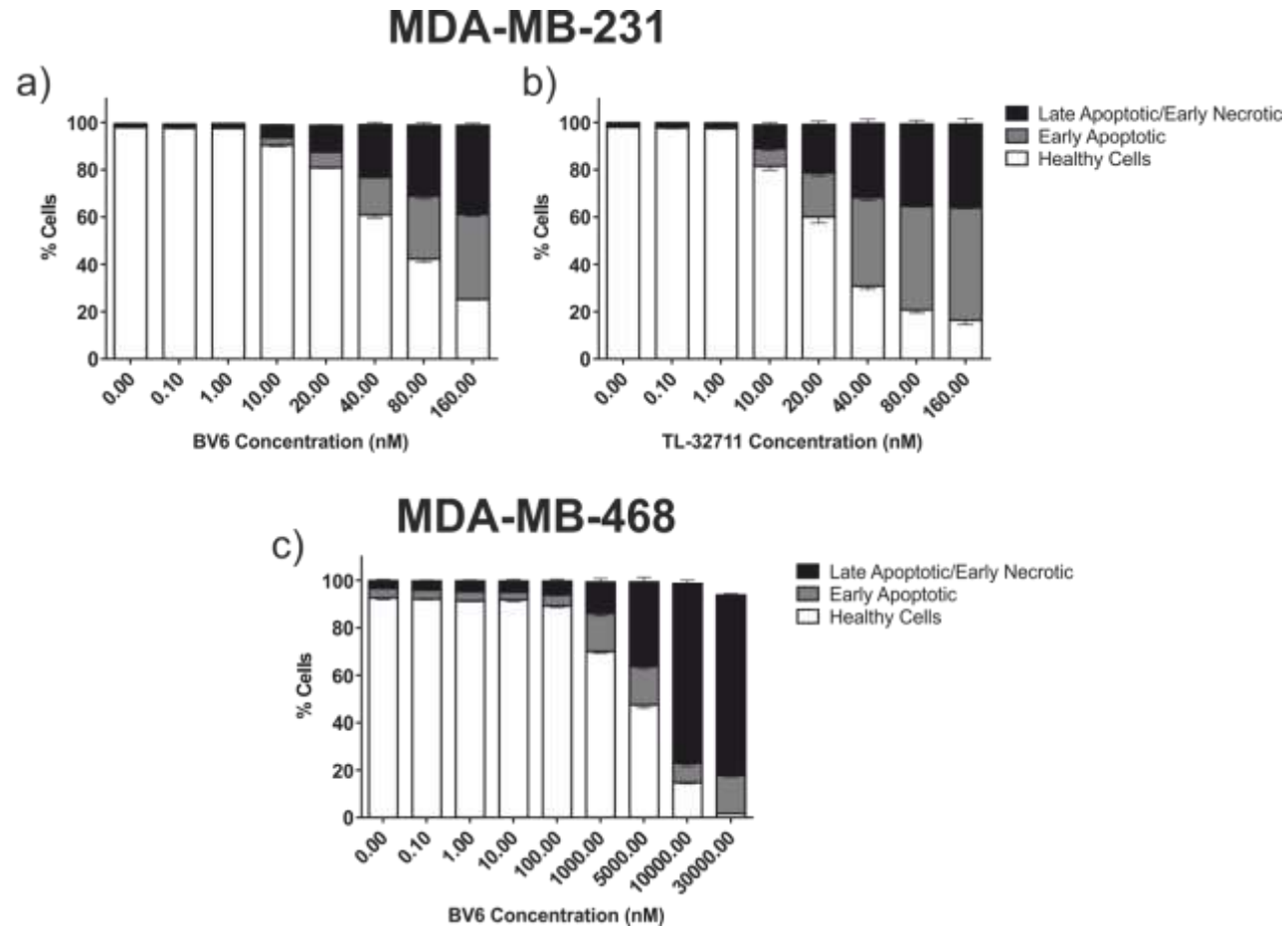


Figure 3.17 | Bivalent SMs induce phosphatidylserine exposure in sensitive MDA-MB-231 cells, but not the resistant MDA-MB-468 cells. a-b) MDA-MB-231 and **c)** MDA-MB-468 cell were treated for 24 h and stained with Annexin V and PI. Cells were sorted into healthy, early apoptotic and late apoptotic/early necrotic cells. Values represent mean \pm SEM, $n=3$.

Characterising the response of tumour cell lines to SMAC mimetics *in vitro*

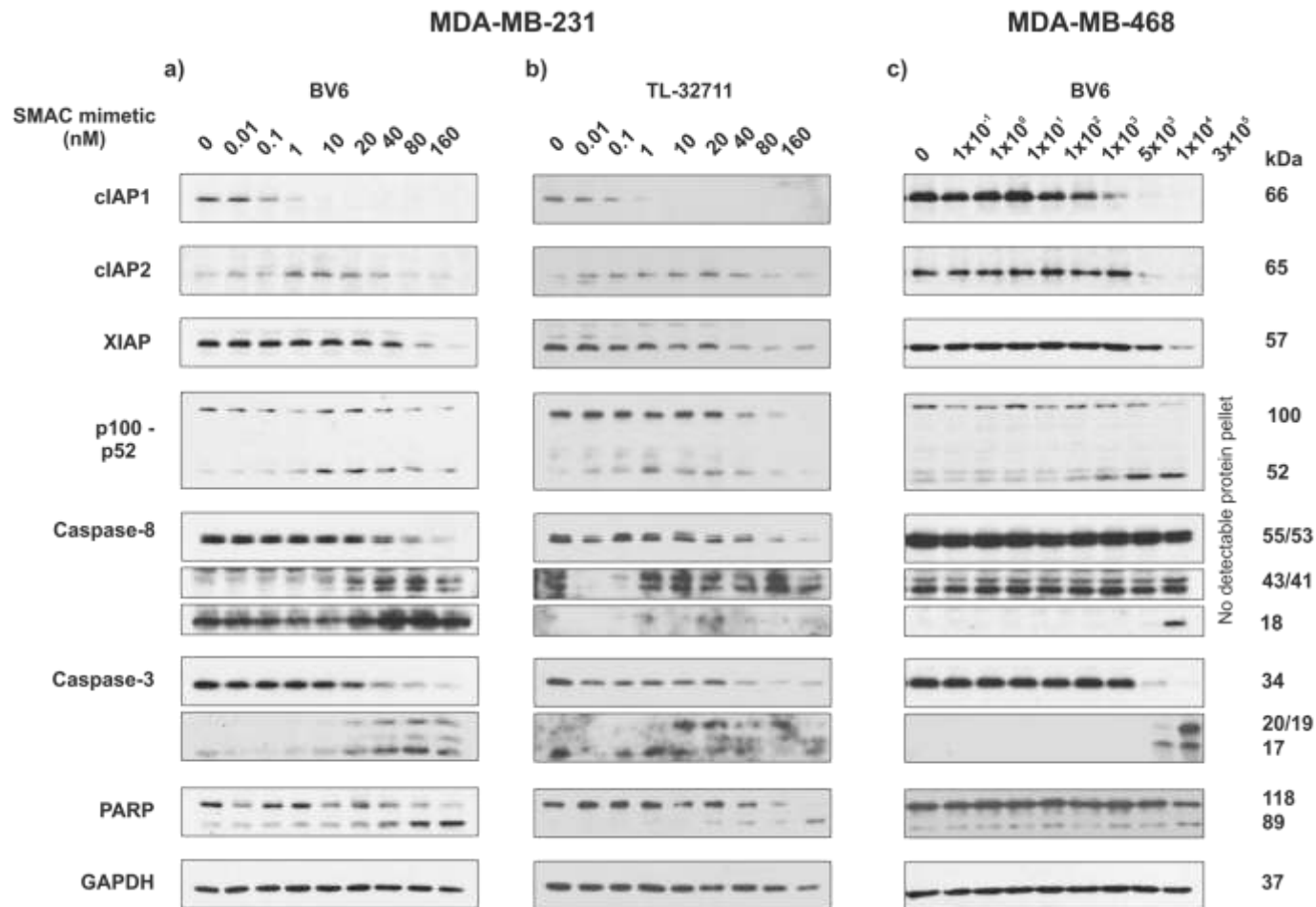


Figure 3.18 | Bivalent SMs deplete cIAP1 and induce cell death at lower nanomolar concentrations in sensitive MDA-MB-231 cells. Cells were lysed in RIPA lysis buffer and loaded based on protein concentration as determined by Bradford assays. Expression of IAP proteins, non-canonical NF- κ B proteins and caspases were determined using western blotting.

TNF α secretion and cell death induced by SMs in MDA-MB-231 cells is correlated to activation of the non-canonical NF- κ B

As mentioned previously, SMs work in three distinct phases. Using the extended concentration range, I have determined at which SM concentration these events occur, however, it was unknown at which time points these occurred. In the initial panel of the four SM compounds, I chose 24 h as the experiment end point as much of the published work with these compounds was performed at this time point. However, this does not give insight to the kinetics of cell death and, as previously mentioned, this late time point resulted in a shift to cells classed as late apoptotic/early necrotic. As shown with the expanded concentration range, while BV6 has a higher EC₅₀ compared to TL-32711, it results in a greater amount of late apoptosis/early necrosis. A time course would, therefore, demonstrate whether this was because of cell death kinetics, or cell death modality. To investigate this, I piloted a time course in the sensitive MDA-MB-231 cells (data not shown). However, after analysis of the data, it was decided that a time point at 12 h should be added. This was because there was a significant increase in cell death between 8 h and 16 h. I choose a concentration of 1 μ M for each compound as I knew each of the three phases was activated at this concentration.

Similarly to previously published work, cIAP1 was depleted within minutes by all compounds^{36–38}, with the non-canonical NF- κ B pathway being activated at around 2-4 h (**Figure 3.20**). TNF α secretion was significantly higher with the two monovalent SM compounds compared to the bivalent SMs and this secretion was first detectable at 8 h (**Figure 3.19**). Interestingly, TNF α secretion appeared to plateau at 16 h and even slightly decreased at 24 h with the monovalent compounds in MDA-MB-231 cells (**Figure 3.19**). As expected, cell death was greater with the two bivalent compounds compared to the monovalent compounds at the same time points, despite both compound types having similar kinetics in terms of the promotion of cell death. In the two monovalent compounds, there was not much difference in the amount of cell death between 16 and 24 h (<6%), whereas with the two bivalent compounds there was 13-

16% difference (**Figure 3.19**). Interestingly, in the case of BV6, the early:late apoptotic cell ratio decreased from 4:1 at 8 h to 1:1 at 24 h, whereas with TL-32711 it decreased from a ratio of 6:1 to 2:1 (**Figure 3.19**). This suggests that, while BV6 initiates cell death with similar kinetics compared to TL-32711, it results in cells passing more rapidly into the late apoptotic/early necrotic phase. The flow cytometry data suggesting that cells were undergoing apoptosis was confirmed through western blotting, which demonstrated PARP cleavage (**Figure 3.19 and 3.20**).

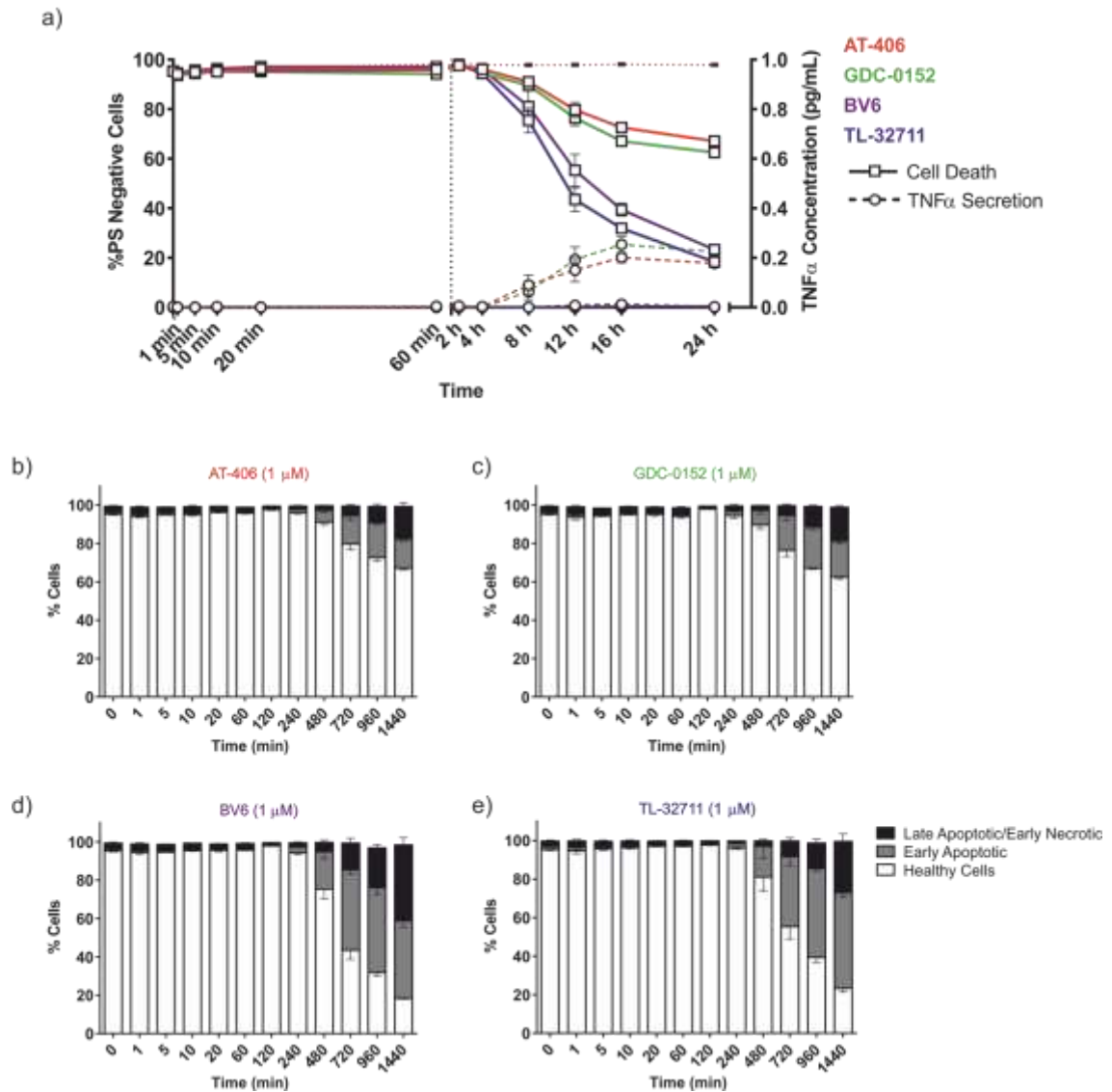


Figure 3.19 | Cell death and TNF α secretion are initiated with similar kinetics by monovalent and bivalent SMs. MDA-MB-231 cells were all treated with SMs at 0 h and then harvested at the indicated time points. **a)** Cell death was measured using flow cytometry and TNF α secretion by ELISA. **b-e)** Cells were divided into healthy, early apoptotic, and early apoptotic/late necrotic using data from flow cytometry experiments. Values represent mean \pm SEM, $n=3$.

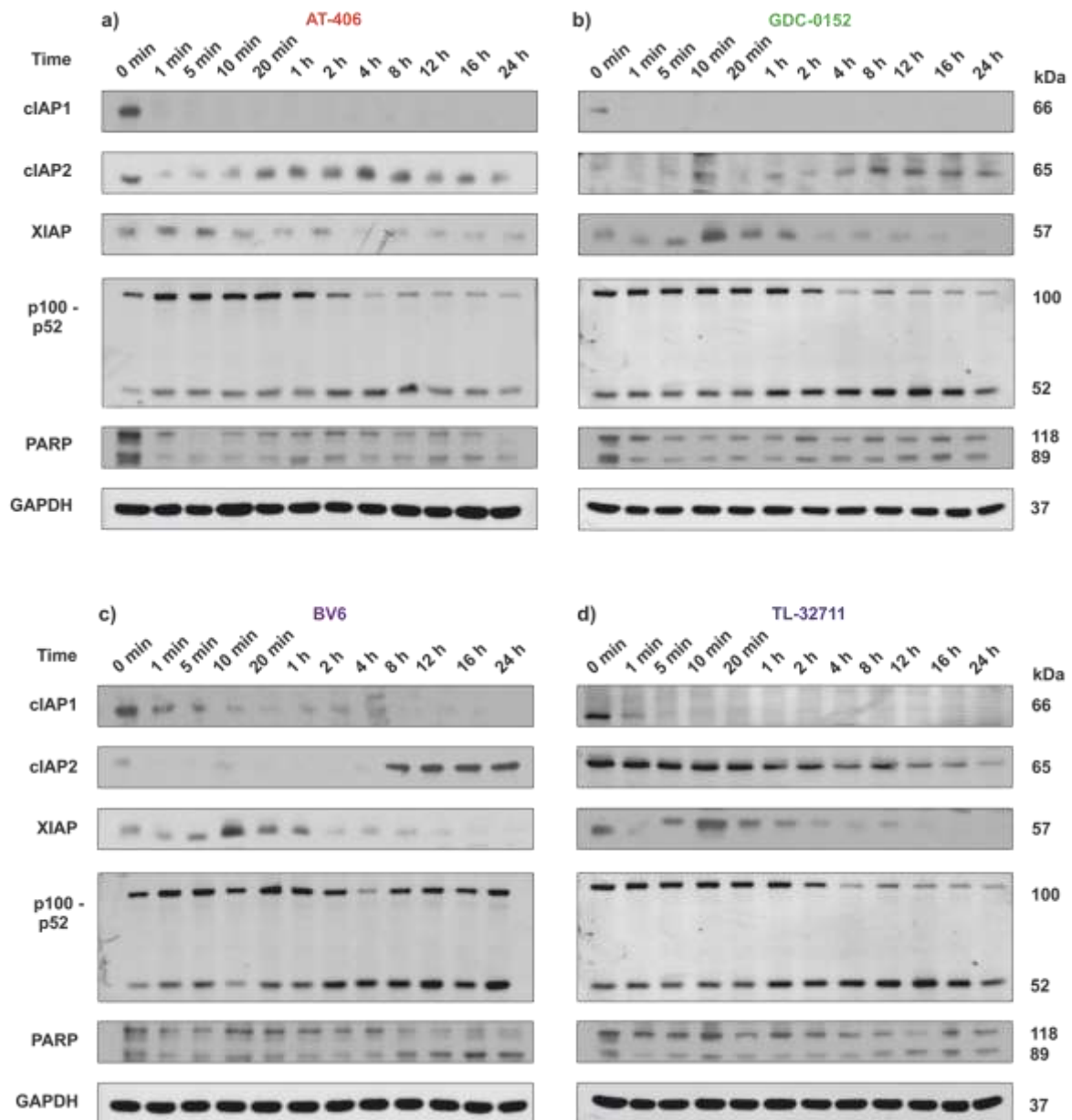


Figure 3.20 | SMs rapidly deplete cIAP1 and activate the non-canonical NF-κB pathway within hours. MDA-MB-231 cells were lysed in RIPA buffer and protein concentration was determined by Bradford assay. Lysates loaded based on protein concentration. Expression of IAP proteins, and NF-κB and apoptosis related proteins were determined using western blotting.

BV6 induces necrosis at 30 μ M, but apoptosis at lower concentrations

One question that is still currently unanswered is the modality of cell death induced by SMs. Much of the previous research has clearly demonstrated that the primary mechanism is apoptosis^{38,139,214,221}, however, to my knowledge, there are no reports of such extensive cell death as I have seen with BV6. This, coupled with the large increase in late apoptotic/early necrotic cells present upon treatment with BV6 after 24 h, led us to hypothesise that BV6 may induce a non-apoptotic form of cell death. The most common forms of cell death are apoptosis, necroptosis, also called programmed necrosis, and necrosis. As such, I sought to determine the modality of cell death through the use of established inhibitors of these cell death types. zVAD is a pan-caspase inhibitor that inhibits apoptosis. While Nec-1 is often used to inhibit necroptosis through RIP1 binding, NSA is more useful as it is an MLKL inhibitor and blocks programmed necrosis further downstream. I hypothesised from the flow cytometry data that, at lower concentrations, zVAD would protect against BV6 induced cell death, whereas at a high concentration of 30 μ M, NSA would be required in combination with zVAD to inhibit apoptosis and necroptosis. I used MDA-MB-231 cells as they are well known to undergo apoptosis with BV6 at lower concentrations^{37,38,146}, and so will serve as a positive control for modality of cell death using zVAD. I used 50 μ M zVAD as this is standard in our laboratory and, after pilot studies, I determined 1 μ M as an appropriate concentration for NSA (data not shown).

Where indicated, MDA-MB-231 cells were pre-treated with zVAD for 30 min before being treated with 0.1, 5 or 30 μ M BV6 and, where appropriate, NSA, for 24 h. zVAD protected against cell death at a concentration of 0.1 and 5 μ M BV6, whereas NSA had no effect on cell death, confirming that at these concentrations, cell death is apoptotic (**Figure 3.21**). At 30 μ M, however, neither zVAD nor NSA had any effect on cell death, suggesting at this concentration, BV6 induces necrosis (**Figure 3.21**). Due to this high cell death, at 30 μ M, no cell pellet was available to interrogate via western blotting. At 0.1 μ M and 5 μ M,

however, zVAD blocked processing of caspase-3 and caspase-8, and PARP confirming the flow cytometry data (**Figure 3.22**). As previously observed, cIAP1 is depleted and non-canonical NF- κ B was activated in the presence of BV6 at all concentrations independent of the addition of zVAD or NSA (**Figure 3.22**). To determine TNF α secretion, I subjected the supernatant to an ELISA. As expected, TNF α secretion was significantly elevated with BV6 as a single agent, but, peculiarly, was actually decreased when cells were co-treated with BV6 and zVAD and, to a lesser extent, BV6 and NSA (**Figure 3.21**).

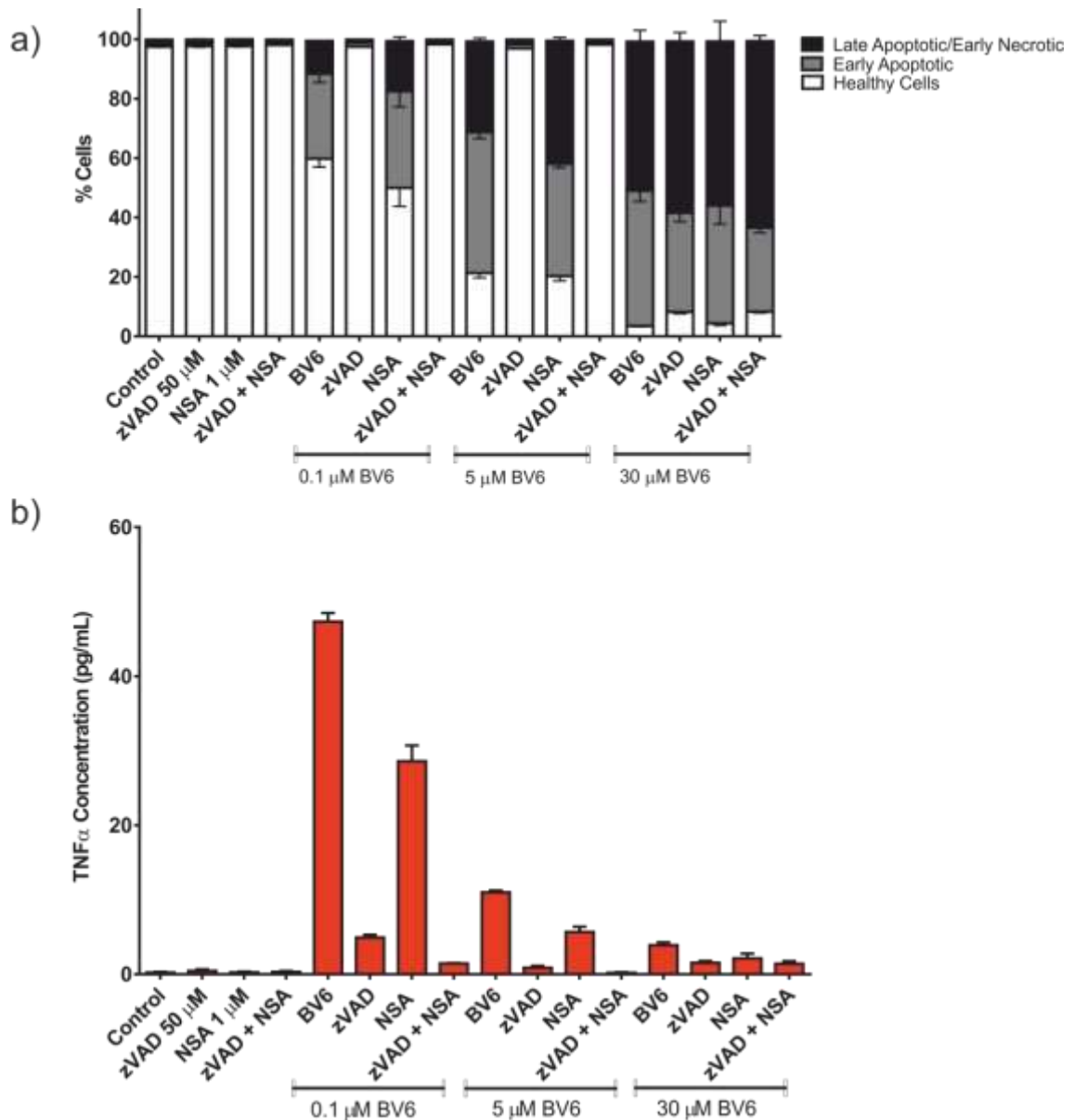


Figure 3.21 | BV6 induces necrosis at high concentrations. MDA-MB-231 cells were pre-treated with 50 μ M zVAD for 30 mins before being treated as indicated with BV6 and NSA at 1 μ M. **a)** Cell death was analysed by flow cytometry. **b)** TNF α secretion was determined by ELISA. Values represent mean \pm SEM, $n=3$.

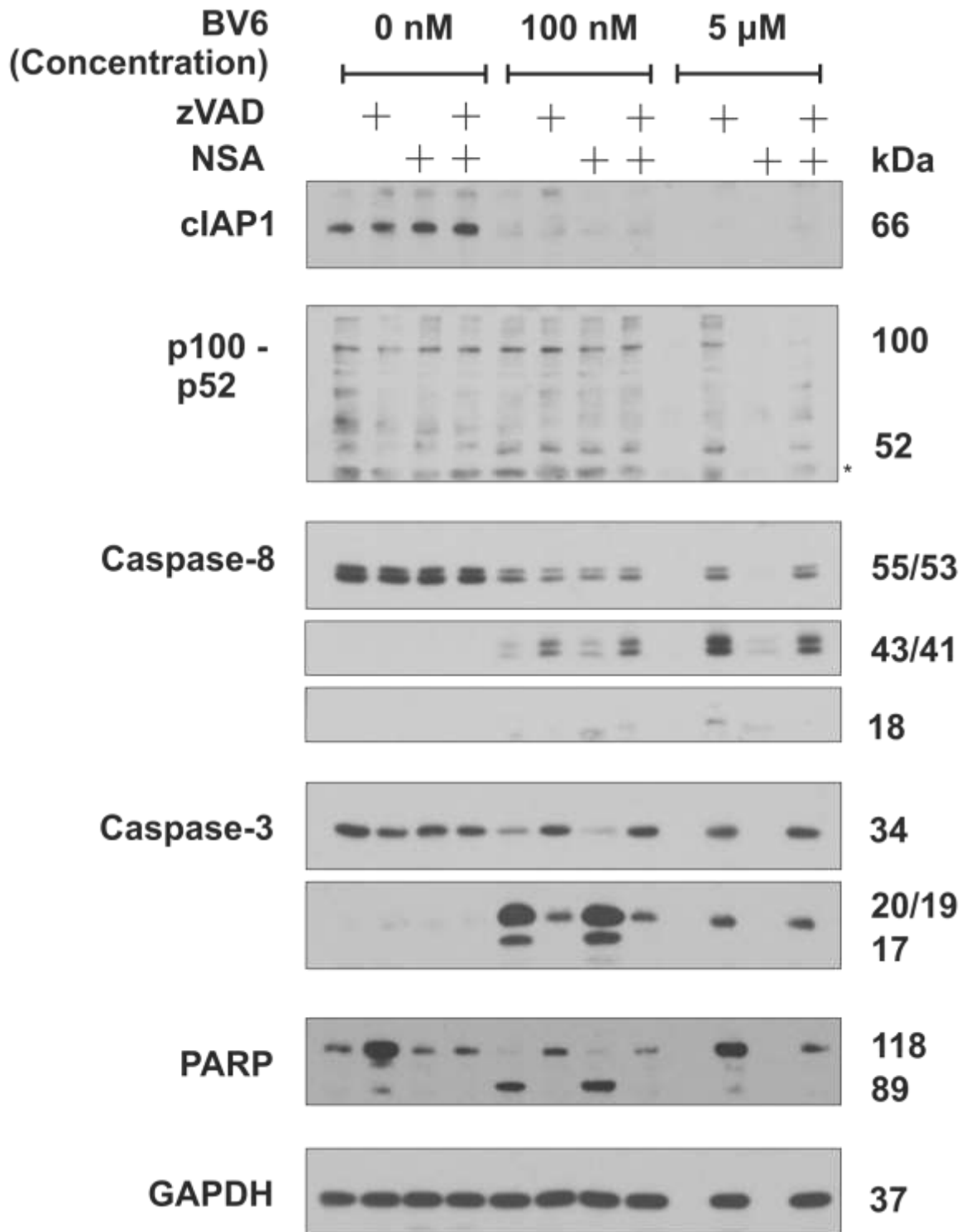


Figure 3.22 | zVAD protects against BV6-induced cell death at lower concentrations. MDA-MB-231 cells were pelleted and snap frozen. They were then lysed in RIPA buffer and loaded according to protein concentration determined by Bradford assay. cIAP1, non-canonical NF- κ B pathway activation and apoptosis related protein expression were determined by Western Blotting. * = non-specific band

Discussion

The aim of this research was to develop a repertoire of robust techniques that could be used to investigate the effect of SMs in non-tumour derived cells. I used the MDA-MB-231 and MDA-MB-468 cells, which are known to be sensitive and resistant to SMs as single agents, respectively^{38,115,120,218–220}. I also sought to directly compare bivalent SMs to monovalent SMs in these cells. My initial experiments were to determine at which concentrations SMs induce cell death and whether they deplete cIAP1 in both sensitive and resistant tumour cells. I used the pre-clinical compound, LBW242, to optimise a methodology before I employed one pre-clinical (BV6) and three clinically-relevant compounds (AT-406, GDC-0152 and TL-32711) used in the rest of this study. From this preliminary work, I found that LBW242 induces cell death in MDA-MB-231 cells, but not MDA-MB-468 cells in line with previously published studies^{38,115,120,218–220}.

I applied the techniques optimised with LBW242 in the context of the four SM compounds: AT-406 and GDC-0152 (monovalent), and BV6 and TL-32711 (bivalent). The two monovalent compounds induced significantly less cell death in the MDA-MB-231 cells compared to the bivalent SMs, but still degraded cIAP1 and promoted non-canonical NF- κ B activation, resulting in TNF α secretion. The ability of SMs to induce cell death is dependent on their ability to deplete cIAP1 but also their ability to inhibit XIAP²²². Monovalent SM compounds are known to be less effective at binding XIAP as they are only able to engage a single BIR domain due to only mimicking one AVPI tetrapeptide sequence^{110,223}. Indeed, it was demonstrated that SMs that do not strongly inhibit XIAP, do not induce high amounts of TNF α -dependent cell death²²⁰. This is because the monovalent compound used in that research (SM-122) has a high affinity for the BIR3 domain, but not BIR2²²⁴. This is crucial as the BIR2 domain and the preceding linker region bind to, and inhibit, caspase-3^{51,225}. This may explain why AT-406 and GDC-0152 did not induce similar amounts of cell death at equimolar concentrations of BV6 and TL-32711. As both AT-406 and GDC-152 were designed to mimic SMAC binding to the BIR3 of XIAP and cIAP1/2^{115,124}. In MDA-MB-486 cells, AT-406 and GDC-0152 do not induce cell

death, despite ablation of cIAP1 and activation of the non-canonical NF- κ B pathway. Interestingly, despite this, TNF α secretion was only observed in MDA-MB-231 cells. It is currently unknown why MDA-MB-468 cell do not have an inducible TNF α autocrine loop, my data suggest the 'blockage' is downstream of the p100 degradation to p52; this may be a potential mechanism of resistance to SMs as a single agent. One factor determining sensitivity of MDA-MB-468 cells to SMs as a single agent was the affinity of the compound for XIAP. Indeed, the two monovalent SM compounds and TL-32711 were designed to preferentially target cIAP1/2 over XIAP and, therefore, displayed very limited cell death in MDA-MB-468 cells, whereas BV6 targets all three proteins.

The two bivalent SMs, BV6 and TL-32711 are far more efficient at depleting cIAP1 because they possess the ability to engage and dimerise two BIR domains in cIAP1 simultaneously⁴⁰, and in the case of BV6, both the BIR2 and BIR3 domain of XIAP²²³. This more closely mimics the function of SMAC, which induces dimerization of targets proteins *in situ*⁸². This explains why the EC₅₀ of AT-406 was over 3000-fold higher than TL-32711. Even in the case of GDC-0152, the EC₅₀ was 64-fold higher than TL-32711 in MDA-MB-231 cells. Indeed, previously published work has shown treatment of MDA-MB-231 with a monovalent compound resulted in a 1000-fold increase in the EC₅₀ compared to the same warhead design but in a bivalent structure³⁸. However, it is interesting that there was more than 2-fold difference in the EC₅₀ between the two bivalent SMs. While these compounds work primarily by switching TNF α signalling from survival to death, it was actually TL-32711 that had the lower EC₅₀, despite inducing lower amounts of TNF α secretion. This is clearly related to the compound structure. Indeed, TL-32711 is a second generation compound that has been specifically designed not to activate the canonical NF- κ B pathway, and is known to have a much reduced toxicity profile^{151,226}. Furthermore, TL-32711 was specifically designed with a reduced affinity for XIAP, and somewhat cIAP2, by removal of a β -branch at the P₂' position and replacing it with a non-branched α -aminobutyric acid residue¹⁵¹. This is important as it reduced the binding affinity for the BIR3 domain of cIAP2 and XIAP 40-fold, but resulted in no difference to its affinity for cIAP1. Interestingly, it has been demonstrated that cIAPs and XIAP restrain RIP1- and RIP3-dependent cytokine production

prior to cell death¹⁴⁹. As TL-32711 does not target cIAP2 or XIAP as strongly as cIAP1, this may explain why there is less TNF α secretion with TL-32711 compared to BV6, which targets cIAP1/2 and XIAP. This is perhaps why BV6 did not progress to clinical trials. It may be that certain structural and target-protein interaction properties result in increased cell death at higher concentrations. One example is that, BV6 has much higher affinity for XIAP compared to TL-32711^{38,151}. As the initial induction of cell death by these two compounds was closely correlated to cIAP1 depletion, it could be argued that the higher cell death observed at the higher concentrations of BV6 is due to its increased ability to bind to XIAP, something TL-32711 lacks. Furthermore, it is known that XIAP is often up-regulated in breast cancers as a survival mechanism, also explaining why MDA-MB-468 cells were sensitive to BV6 at high concentrations^{52,227,228}.

SMs are known to work quickly; I and others have found cIAP1 depletion occurs within minutes, resulting in activation of the canonical NF- κ B pathway within 5-15 minutes^{36,38}. Though not as rapid, SMs induce non-canonical NF- κ B activation within hours³⁸. While it is established at what time points SMs induce cIAP1 depletion and activation of the NF- κ B pathway, there is currently no research comparing the kinetics of both monovalent and bivalent compounds in activation of these pathways and also comparing cell death kinetics. The data here demonstrate that, at equimolar concentrations, there is no difference in kinetics of cIAP1 ablation, non-canonical NF- κ B activation and cell death induction between monovalent and bivalent SM compounds. As expected, there was an increased amount of cell death with the bivalent compounds compared to the monovalent compounds, which occurred between 4-8 h with both structures. Both the canonical and non-canonical NF- κ B pathways result in TNF α mRNA up-regulation and protein secretion^{96,229}. However, despite being one of the most studied signalling pathways, it is currently unknown which combination of the NF- κ B dimers binds to the TNF α promoter region. This, coupled with the fact that there is cross-talk between the canonical and non-canonical NF- κ B pathways²³⁰, means it is very difficult to determine which of these pathways induces the TNF α secretion seen in this work and other published studies^{36,231}. Temporally, TNF α secretion appeared to be more

closely correlated to non-canonical NF- κ B activation, which is also very closely correlated to cell death, but this cannot be confirmed as a causal relationship.

The toxicity of compounds can either be on-target toxicity, where the adverse effects are a result of the agent binding to its target, or off-target toxicity, where the effects result from the molecule binding to an unintended target. SMs are reported to be highly specific to their intended targets; indeed, using a biotinylated SM, Petersen *et al.* reported that only XIAP, cIAP1/2, and their associated proteins - TRAF1/2, were pulled down³⁷. This suggests any adverse effects is very likely to result from on-target toxicity. In light of the extensive cell death observed with BV6 at 30 μ M, I tried to identify which mode of cell death was being induced. Apoptosis is the preferred method of cell death as it does not result in inflammation. This is not to say that other forms of cell death are not useful, particularly in situations of caspase inhibition. SMs can actually promote necroptosis in caspase-null cells²³². However, a form of cell death that does promote serious side-effects is necrosis, where cells undergo autolysis and release their contents into the microenvironment, resulting in significant inflammation. At concentrations of 100 nM and 5 μ M BV6, cell death was apoptotic as cell death was totally inhibited in the presence of the pan-caspase inhibitor, zVAD in MDA-MB-231 cells. However, at 30 μ M, neither the necroptosis inhibitor, NSA, nor zVAD had any effect on survival, showing the mode of cell death to be necrosis. To my knowledge there is only one other report demonstrating SM-mediated necrosis²³³, however this was seen *ex vivo* in suspension cells extracted from ascites and was not properly controlled for using zVAD and either necrostatin-1 or NSA. Therefore, as far as I know, this is the first-time necrosis induced by SMs has been reported using the appropriate controls. This is significant as it could have clinical implications due to dosing. While the mechanism is unknown, it is likely to be a result of the high affinity BV6 has for XIAP as none of the other compounds used in this study targeted XIAP as strongly.

The dual inhibition of cIAP1 and either cIAP2 or XIAP is known to be a lethal combination. Genetic deletion of *clap1* in combination with *Xiap* or *clap2* in mice resulted in embryonic lethality, suggesting that, during development, cIAP1 is

sufficient for embryological development in the absence of cIAP2 and XIAP, but both cIAP2 and XIAP are required if cIAP1 is absent²³⁴. Interestingly, *clap2^{-/-}clap1^{-/-}* (*c2^{-/-}c1^{-/-}*) double mutants were rescued to birth through deletion of the *tnfr1* gene, and deletion of the *Ripk1* gene allowed *Xiap^{-/-}clap1^{-/-}* (*X^{-/-}c1^{-/-}*) double mutants to survive past birth, and prolonged *c2^{-/-}c1^{-/-}* embryonic survival²³⁴. Similarly, using *X^{-/-}c2^{-/-}* mice with myeloid lineage-specific (granulocytes, macrophages, and a minor fraction of dendritic cells) *clap1* gene deletion (*c1^{LC}c2^{-/-}X^{-/-}*), cIAP1 was shown to be essential for normal development in mice¹⁴⁹. *X^{-/-}c2^{-/-}* mice were phenotypically normal, whereas *c1^{LC}c2^{-/-}X^{-/-}* mice were runted, had a splayed gait and hunched posture. This is also demonstrated *in vitro* using bone-marrow derived macrophages (BMDM) as only XIAP-deficient BMDMs underwent cell death with the cIAP1-specific SM, TL-32711¹⁴⁹. As such, it is likely BV6's ability to target cIAP1 and XIAP that results in its toxicity.

Another interesting finding was that zVAD and, to a lesser degree, NSA, actually inhibited TNF α secretion. While it could be argued that TNF α was released as a result of cell death, this is unlikely as there was less TNF α secretion at 5 μ M BV6, despite higher amounts of cell death; if cell death resulted in TNF α secretion, I would expect to see higher amount of TNF α secreted with higher levels of cell death. As SMs are well known to induce TNF α secretion, it should follow that higher concentrations of BV6 combined with lower amounts of cell death should actually result in higher levels of TNF α secretion. That zVAD actually decreased TNF α secretion contradicts this hypothesis. The mechanism behind this is currently unknown, but it should be noted that the ELISA only measures soluble TNF α and TNF α also resides on the cell surface and can also induce TNF signalling²³¹.

In summary, bivalent SMs induce cell death at lower concentrations compared to monovalent compounds and this is likely due to their ability to engage multiple BIR domains at once. Despite the greater ability to promote cell death, both monovalent and bivalent structures have similar kinetics for cIAP1 depletion, non-canonical NF- κ B activation and cell death induction. Using the bivalent compound, BV6, for the first time, I have demonstrated that a SM can

induce necrosis as a form of cell death. This has important implications for the clinical applications of SMs. This toxicity could likely be ameliorated through modification of the structure to reduce its affinity for all three IAPs simultaneously, but retain specificity for cIAP1.

3.1.6. Future Work

While these SMs have already been extensively characterised in the literature, there are still a number of questions still to be answered by the results generated in this project. Firstly, I have shown that cIAP1 depletion correlated with cell death induction by the two bivalent compounds. It would be interesting to see if this was also the case with the two monovalent compounds used, i.e. AT-406 and GDC-0152. Secondly, it appeared that cIAP1 depletion occurred at higher concentrations in the resistant MDA-MB-468 cells, compared to the sensitive MDA-MB-231 cells with BV6. Further trying to elucidate the mechanisms behind this may help with further SMs development and refinement. Lastly, when I treated MDA-MB-231 with BV6 and zVAD, I actually found a complete ablation of TNF α secretion when cell death was inhibited. This was completely unexpected and would be a very exciting avenue of future research.

Chapter 4

Characterising the response of non-tumour cell lines to SMAC mimetics *in vitro*

4. CHARACTERISING THE RESPONSE OF NON-TUMOUR CELL LINES TO SMAC MIMETICS *IN VITRO*

Introduction

Toxicity to non-tumour cells in either the surrounding microenvironment or systemically is a significant drawback to the use of chemotherapeutics. As SMs are known to induce cell death in a TNF α -rich microenvironment, this may result in toxicity to non-tumour cells in the surrounding milieu. While it has been reported that many cell lineages are resistant to SMs, both as single agents, and in an inflammatory setting, there is currently very little mechanistic insight as to the reason behind this. To my knowledge, there is only one paper where non-tumour derived cells (HUVEC cells) are treated with TNF α in the presence of SMs, and no cell death was reported³⁶. Cell death with SMs as single agents was demonstrated in freshly isolated human monocytes, but not monocyte-derived immune cells and T-cells, suggesting lineage dependent effects¹⁴⁶. While multiple murine *in vivo* studies have reported no toxicity with SMs, even with acute doses as high as 100 mg/kg body weight^{115,120,216,220,235–237}, there is some evidence to suggest SMs can induce toxicity as single agents in non-tumour cells^{161,215}. A classic target organ of toxicity is the liver; however, there are currently no cost effective, high-throughput *in vitro* methods for investigating hepatotoxicity in human cells. To overcome this, it has been reported that rat pancreatic cells (B-13 cells) have the ability to transdifferentiate into hepatocyte-like cells (B-13/H cells) *in vitro*²³⁸. This results in the potential for generating a theoretically limitless supply of metabolically functional hepatocyte-like cells^{239–241}. This is achieved through treatment with a low concentration of dexamethasone, a synthetic glucocorticoid, which results in Sgk1 induction, and a transient suppression of WNT signalling and epigenetic changes^{242–244}. This induces expression of liver-specific transcription factors and many members of the CYP450 family at levels similar to hepatocytes. B-13/H cells take on a hepatocyte morphology and enter a replicatively quiescent state²³⁹. Furthermore, these cells are sensitive to paracetamol and methapyrilene whose metabolites, but not parent compounds, are hepatotoxic. In contrast the progenitor cell line (B-13 cells) are not, suggesting B-13/H cells are useful for screening compounds for potential hepatotoxicity²⁴⁰.

The purpose of this study, therefore, was to determine the effects of SMs either as single agents, or in combination with TNF α , in non-tumour derived cell line models and to dissect their apparent resistance to SM-mediated cell death. I used the human breast epithelial cell line, MCF-10A, the rat pancreatic progenitor cells, B-13, and the hepatocyte-like cells, B-13/H, as my *in vitro* non-tumour cell models. I hypothesised that SMs would not induce cell death in these cells either as single agents or in combination with TNF α at clinically relevant concentrations.

MCF-10A cells, B-13 and hepatocyte-like B-13/H cells are relatively resistant to SMs as single agents

4.1.1. MCF-10A cells

I had already established the repertoire of techniques to be used through use of the two tumour cell lines as described in Chapter 3. As such, MCF-10A cells were treated with the same four SM compounds at the same range of concentrations as the tumour cells. There was no cell death at any concentration with any of the clinically relevant compounds in MCF-10A cells. Interestingly, BV6 induced significant cell death at 30 μ M (85%), but not at any other concentration (**Figure 4.1**). The amount of cell death at this concentration in MCF-10A cells was actually slightly less than that seen in the tumour cells at the same concentration of 30 μ M BV6, with an EC_{50} of 12 μ M in MCF-10A cells compared to 60 nM – 4.8 μ M in the tumour cells (**Table 3.1**). Furthermore, there was an increase in caspase-3/7 activity at this concentration in MCF-10A cells not seen in the tumour cells, suggesting induction of apoptosis (**Figure 4.1**). However, this could not be investigated further as there was no detectable cell pellet in MCF-10A cells after treatment with BV6 due to the extensive amount of cell death. Surprisingly, a significant proportion of the dying cells were early apoptotic, as determined by Annexin V/PI staining, further confirming apoptosis as the mode of cell death (**Figure 4.2**). No caspase-3/7 activation was seen with any other of the other SM compounds in MCF-10A cells. This lack of caspase activation was also demonstrated by western blotting, where no cleavage of caspase-8, caspase-3 or PARP was seen (**Figure 4.3**). Despite cIAP1 ablation and p100 degradation to p52, there was no detectable increase in TNF α secretion with any of the four compounds in MCF-10A cells (**Figure 4.1 and 4.3**).

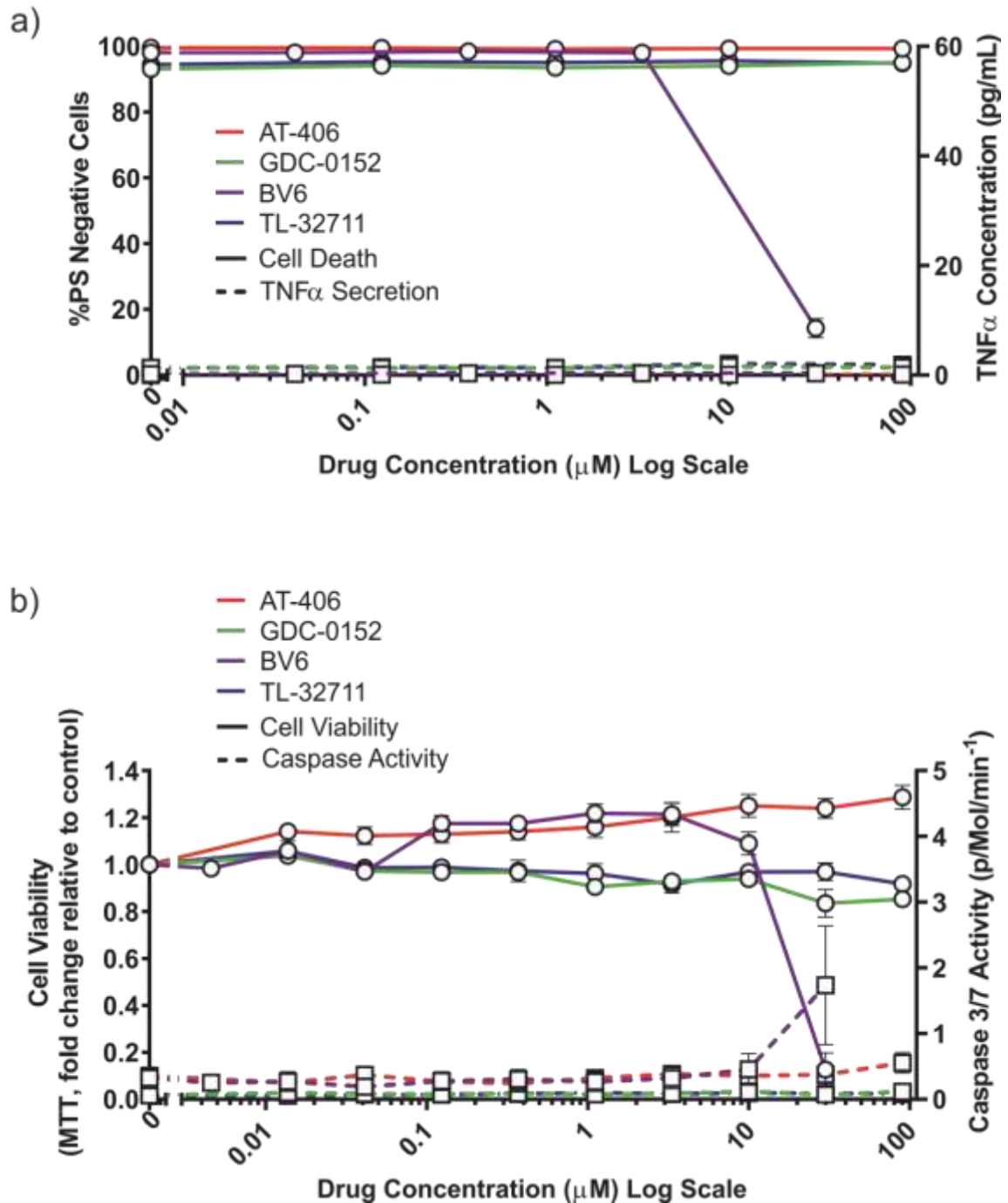


Figure 4.1 | Clinically relevant SMs do not induce cell death or TNF α secretion in MCF-10A cells. MCF-10A cells were treated for 24 h with the four SM compounds indicated before analysis by **a)** flow cytometry, collection of supernatant for ELISA and **b)** determination of caspase activity and cell viability. Values represent mean \pm SEM, $n=3$.

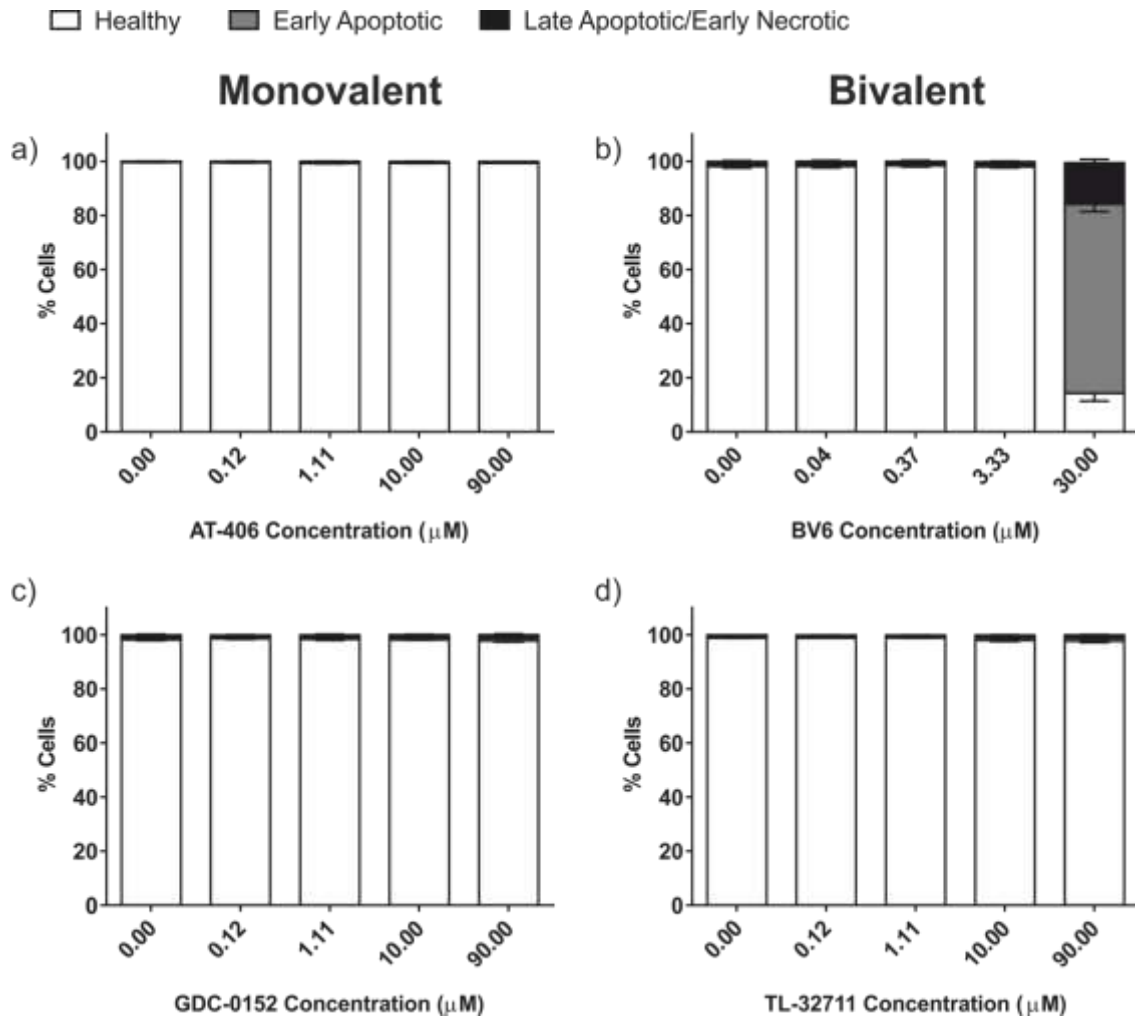


Figure 4.2 | BV6 induces primarily apoptosis in MCF-10A cells. a-d) MCF-10A cells were divided into healthy, early apoptotic and late apoptotic/early necrotic cells based on their staining profile with Annexin V and PI. **a, c-d)** No cell death was detected in MCF-10A cells when challenged with clinically-relevant SMs, whereas **b)** the pre-clinical SM BV6 induced an early apoptotic staining profile in MCF-10A cells. Values represent mean \pm SEM, $n=3$.

4.1.2. B-13 cells

Treating B-13 cells with the monovalent compounds, AT-406 and GDC-0152 resulted in 26% and 20% cell death, respectively, as determined by Annexin V/PI staining. There were similar increases in caspase-3/7 activity with both compounds, and slight decreases in cell viability, but no TNF α secretion (**Figure 4.4**). Flow cytometry demonstrated that most of the dying cells were undergoing apoptosis. As previously observed in Chapter 3, the bivalent compounds induced more cell death in B-13 cells. Indeed, BV6 induced total cell death at 30 μ M and TL-32711 induced 45% cell death at 90 μ M (**Figure 4.4**). Comparable reductions in cell viability were also seen. In the case of BV6, flow cytometry revealed nearly all cells were late apoptotic/early necrotic, whereas with TL-32711, the majority of cells were early apoptotic (**Figure 4.5**). This finding was further ratified as TL-32711 promoted a large increase in caspase-3/7 activity in B-13 cells, whereas no such effect was seen with BV6 (**Figure 4.4**). As the B-13 cells were derived from rats, only a limited number of antigens could be examined by western blot analysis. As such, I was unable to determine cIAP1 depletion, despite using several antibodies from various companies. However, I was able to demonstrate p100 loss in the presence of both monovalent and bivalent SMs. This suggested cIAP1 was indeed degraded, although, this did not result in TNF α secretion for any of the compounds (**Figure 4.4 and 4.6**). Using PARP and caspase-3 antibodies, I also demonstrated that, despite non-canonical NF- κ B activation, the clinically relevant monovalent SMs were unable to induce PARP and caspase-3 cleavage in B-13 cells as single agents at any concentrations tested (**Figure 4.6**). The two bivalent compounds did induce cell death at ≥ 90 μ M, but not at concentrations achievable in the clinic.

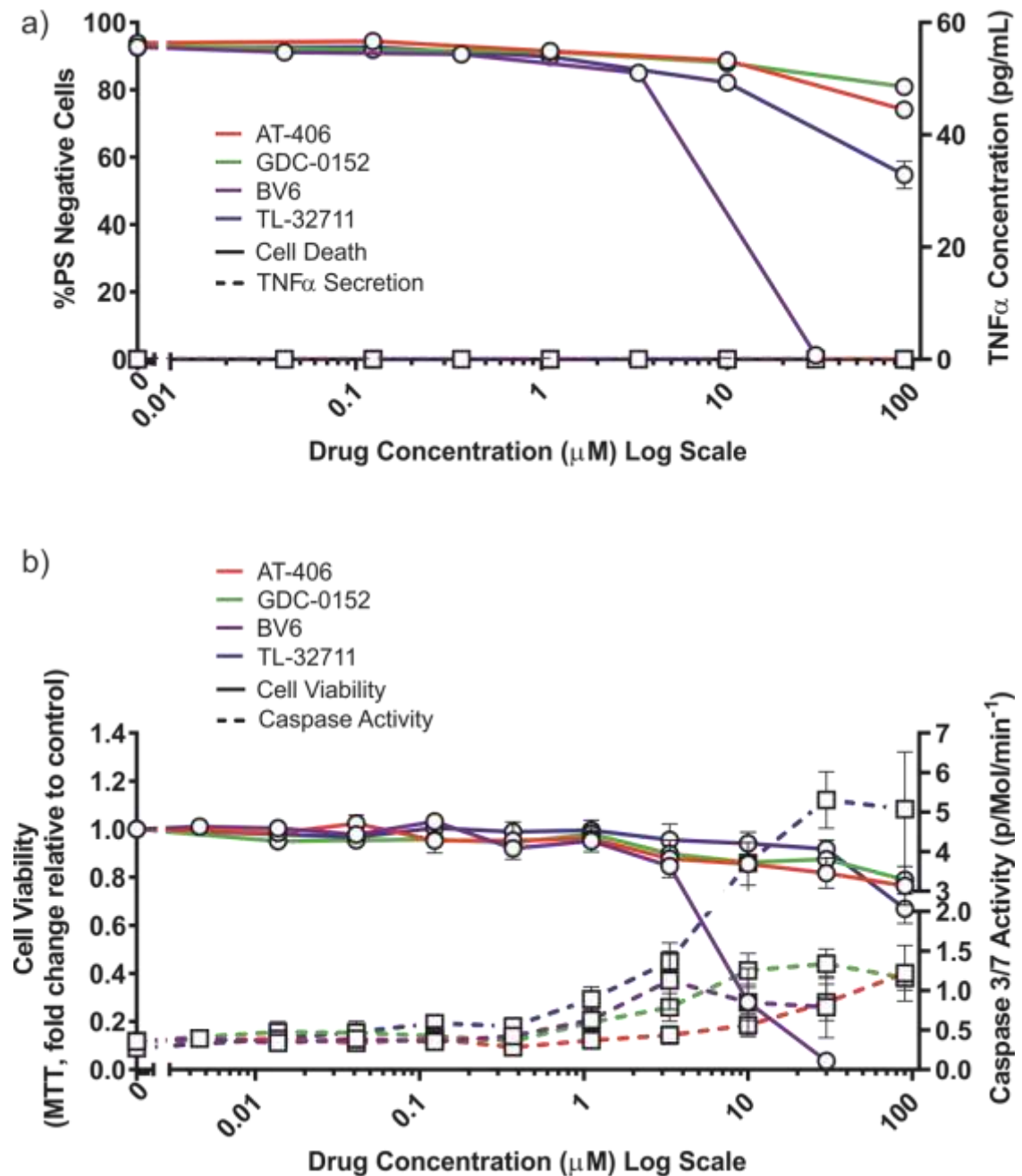


Figure 4.4 | B-13 cells are resistant to monovalent SMs but are sensitive to bivalent SMs. B-13 cells were treated for 24 h with the four SM compounds. **a)** After treatment, B-13 cells were stained with Annexin V and PI and analysed by flow cytometry and the supernatant was collected for analysis of TNF α secretion by rat ELISA. **b)** Cell viability was determined by MTT assays and effector caspase activity by DEVDase.afc assays. Values represent mean \pm S.E.M, n=3.

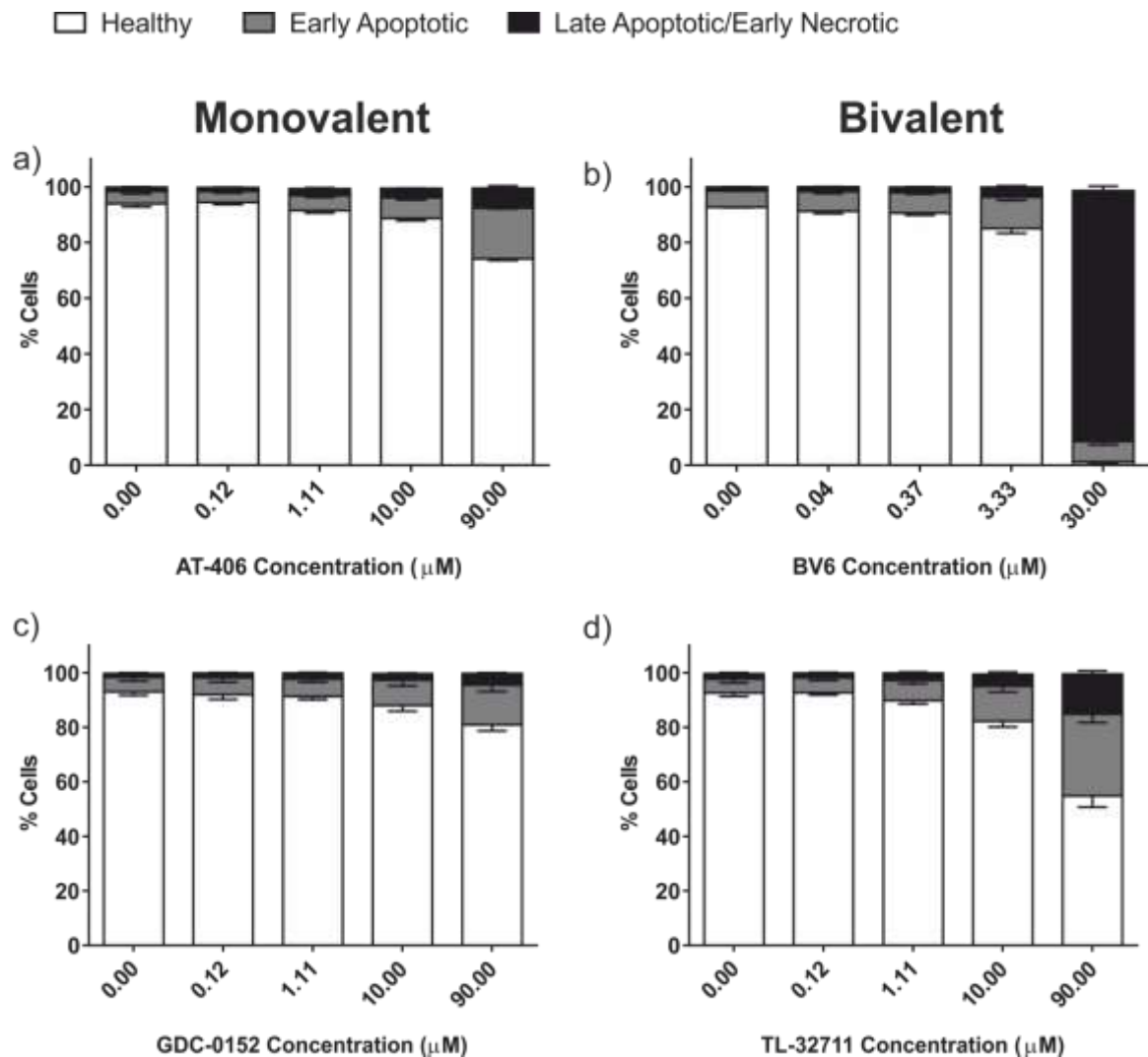


Figure 4.5 | B-13 cell are more sensitive to bivalent SMs. **a-d)** B-13 cells were separated based on their staining profile into healthy, early apoptotic, and late apoptotic/early necrotic subpopulations. **b)** In B-13 cells, BV6 induced a primarily late apoptotic/early necrotic staining profile. **d)** Of the clinically relevant compound, TL-32711 induced the most cell death in B-13 cells, which was primarily an early apoptotic staining profile. Values represent mean \pm S.E.M, n=3.

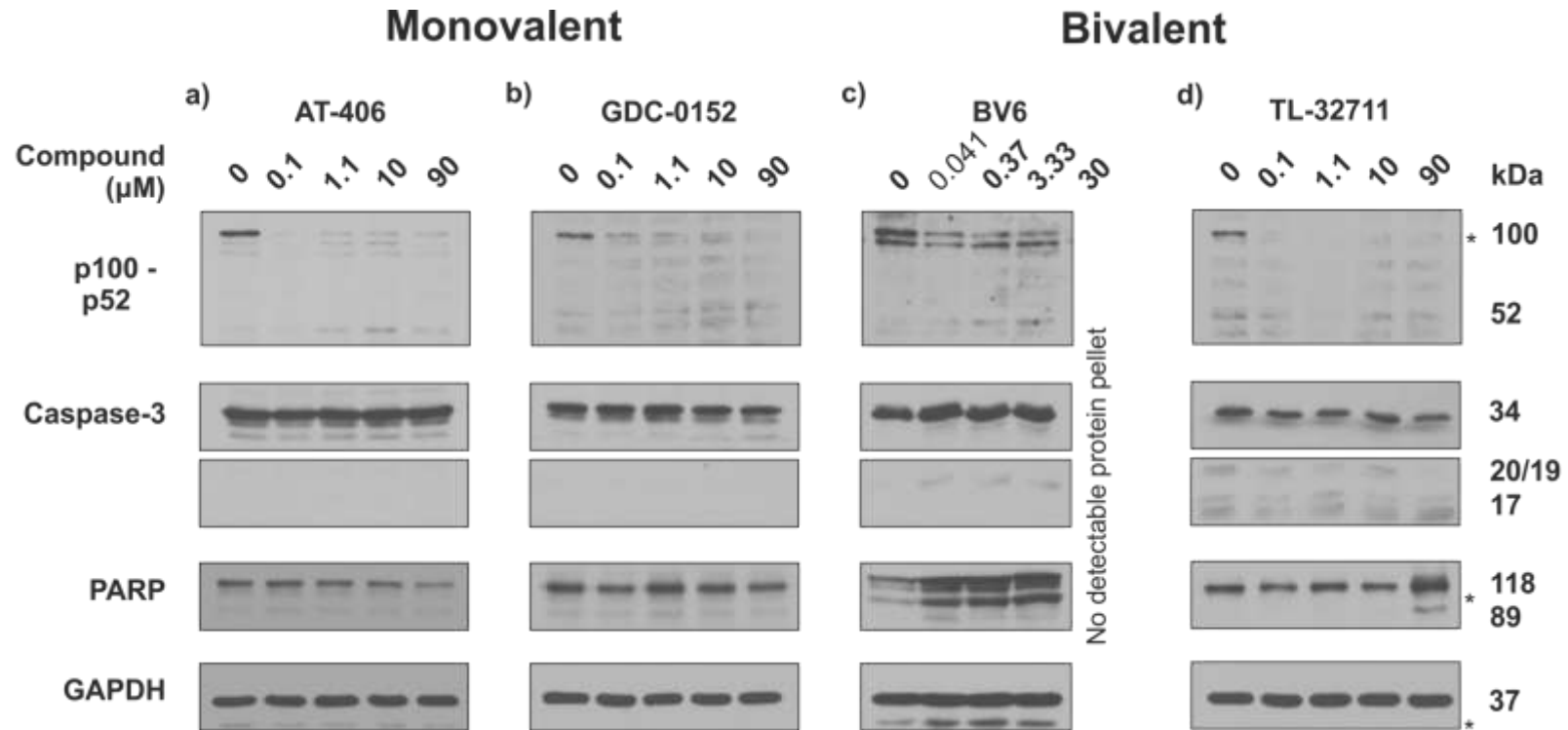


Figure 4.6 | SMs activate the non-canonical NF-κB pathway in B-13 cells. B-13 cells were trypsinised and snap frozen. Pellets were then lysed in RIPA buffer and subjected to a Bradford Assay to determine protein concentration. Lysates were loaded by concentration (20 μg) and analysed by western blotting. * = non-specific band.

4.1.3. B-13/H cells

Once differentiated, B-13/H cells did not stain for Annexin V, although cell death was apparent through morphological examination. While the precise mechanism for this is unknown, it may be that once B-13 cells are transdifferentiated into B-13/H cells, they lose their ability to externalise PS, perhaps through loss of the enzyme flippase. I therefore used cell viability and caspase-3/7 assays to determine the cytotoxic effects of SMs on B-13/H cells. The MTT cell viability assay showed only a slight reduction in viable cells, except with BV6, where there were no viable cells at 30 μ M (**Figure 4.7**). Interestingly, despite being a replicatively quiescent cell type, the cell viability assay actually indicated an increase in the number of viable cells. The caspase activation assays demonstrated no increase in caspase activation, in line with the MTT cell viability assay, except in the case of TL-32711, where there was a 7-fold increase in caspase activity at a concentration of 90 μ M (**Figure 4.7**). This appears to contradict the MTT cell viability assay where TL-32711 resulted in a 21% increase in absorbance, which, theoretically, means there was a 21% increase in the number of viable cells. As with the B-13 cells, there was no SM-induced TNF α secretion in B-13/H cells (**Figure 4.7**). Using the same antibodies as in the B-13 cells, I was able to demonstrate non-canonical NF- κ B activation but no caspase or PARP cleavage (**Figure 4.8**).

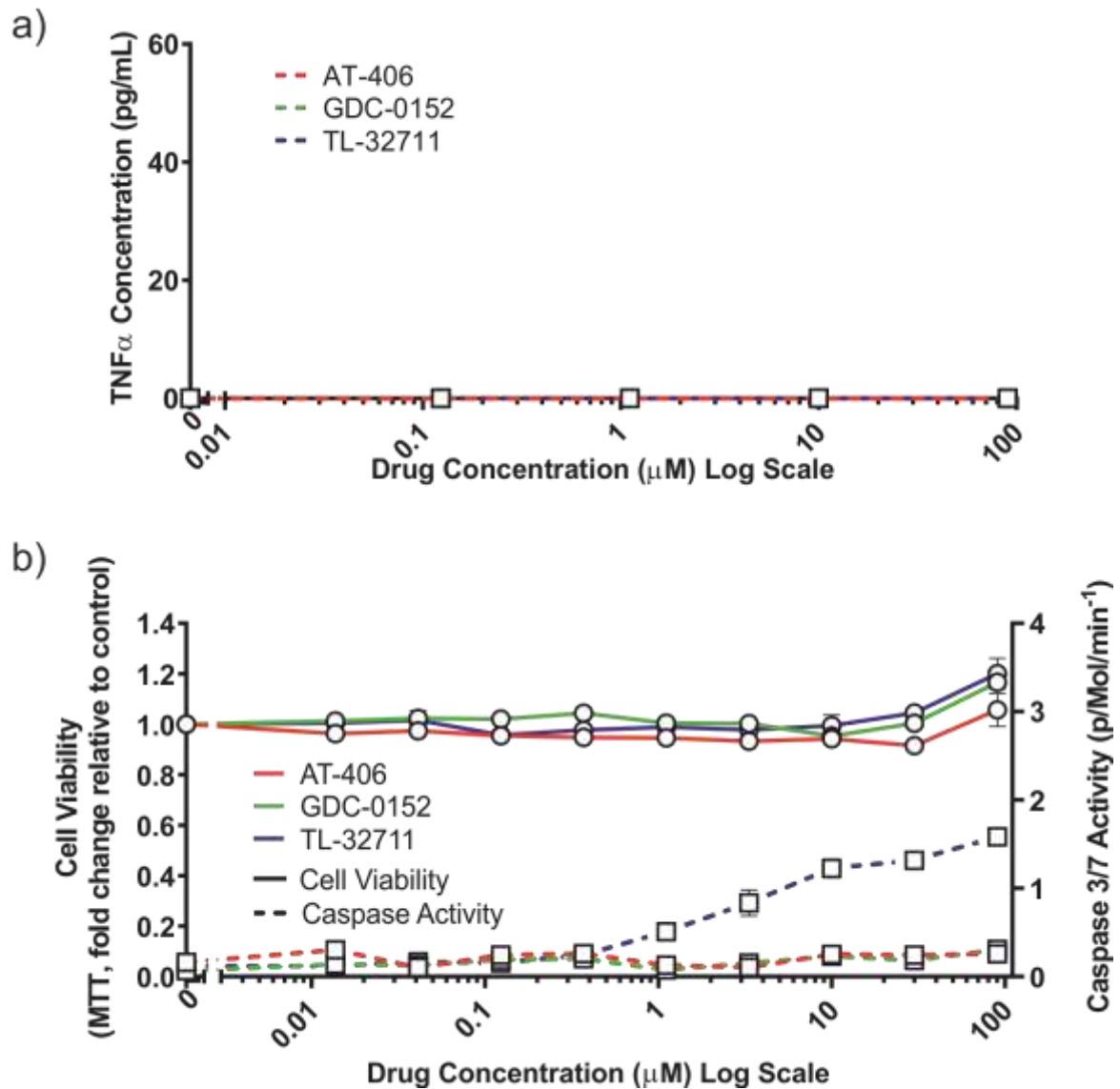


Figure 4.7 | B-13/H cells are resistant to SMs in clinical trials. a) After 24 h treatment with SMs, supernatant was collected from B-13/H cells and TNF α secretion determined by rat ELISA. **b)** Cell viability was investigated by MTT assays and caspase-3/-7 activity by DEVD.afc assays. Values represent mean \pm S.E.M, n=3.

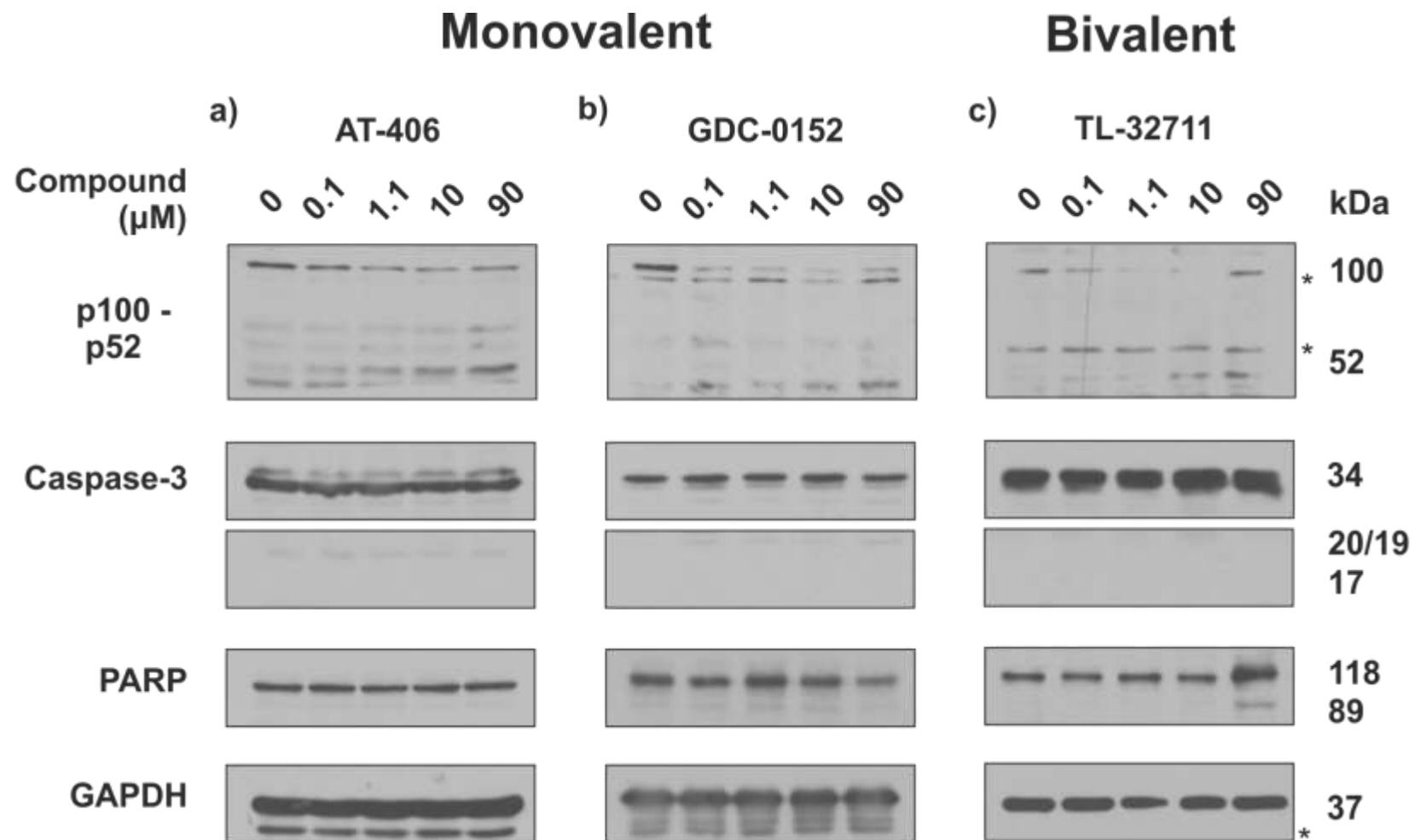


Figure 4.8 | Clinically relevant SMs activate the non-canonical NF-κB pathway in B-13/H cells. B-13/H cells were trypsinised and snap frozen. Pellets were then lysed in RIPA buffer protein and concentration was determined by Bradford assay. Lysates were loaded according to protein concentration (20 μg) and analysed by western blotting. * = non-specific band.

SMs have similar kinetics in MCF-10A cells compared to tumour cells

To determine if SMs had similar kinetics in terms of cIAP1 depletion and non-canonical NF- κ B activation in MCF-10A cells as they did in MDA-MB-231 cells, I performed a time course. However, as these compounds did not induce cell death, it was decided to use reduced time points. Based on pilot studies (data not shown), I decided to use 6 h as the latest time point as p100 processing to p52 was clearly evident (**Figure 4.9**). It was also decided to use one monovalent and one bivalent SM; I therefore chose GDC-0152 and TL-32711 as these were the most structurally advanced SMs. cIAP1 was depleted with similar kinetics in MCF-10A cells compared to the tumour cells used in this project (**Figure 4.9**). cIAP2 protein levels underwent an increase with GDC-0152, but were degraded with TL-32711 (**Figure 4.9**). As canonical NF- κ B activation occurs primarily within the first hour, the use of a time course enabled us to determine activation kinetics of this arm of the NF- κ B pathway. Using phosphorylation of I κ B α as a marker, I found that the monovalent compound GDC-0152 induced canonical NF- κ B activation at 10 min which continued to up to 1 hr post treatment. While not as clear, it appeared TL-32711 also promoted phosphorylation of I κ B α , primarily within the first hour (**Figure 4.9**). Non-canonical NF- κ B was activated at 2 h by both SMs, which is similar to the MDA-MB-231 tumour cells described in Chapter 3. In summary, in the non-tumour MCF-10A cells, cIAP1 was degraded with similar kinetics as the tumour cells used in this project, and the non-canonical NF- κ B pathway was also activated in a similar timeframe. However, these cells were resistant to SM induced cell death.

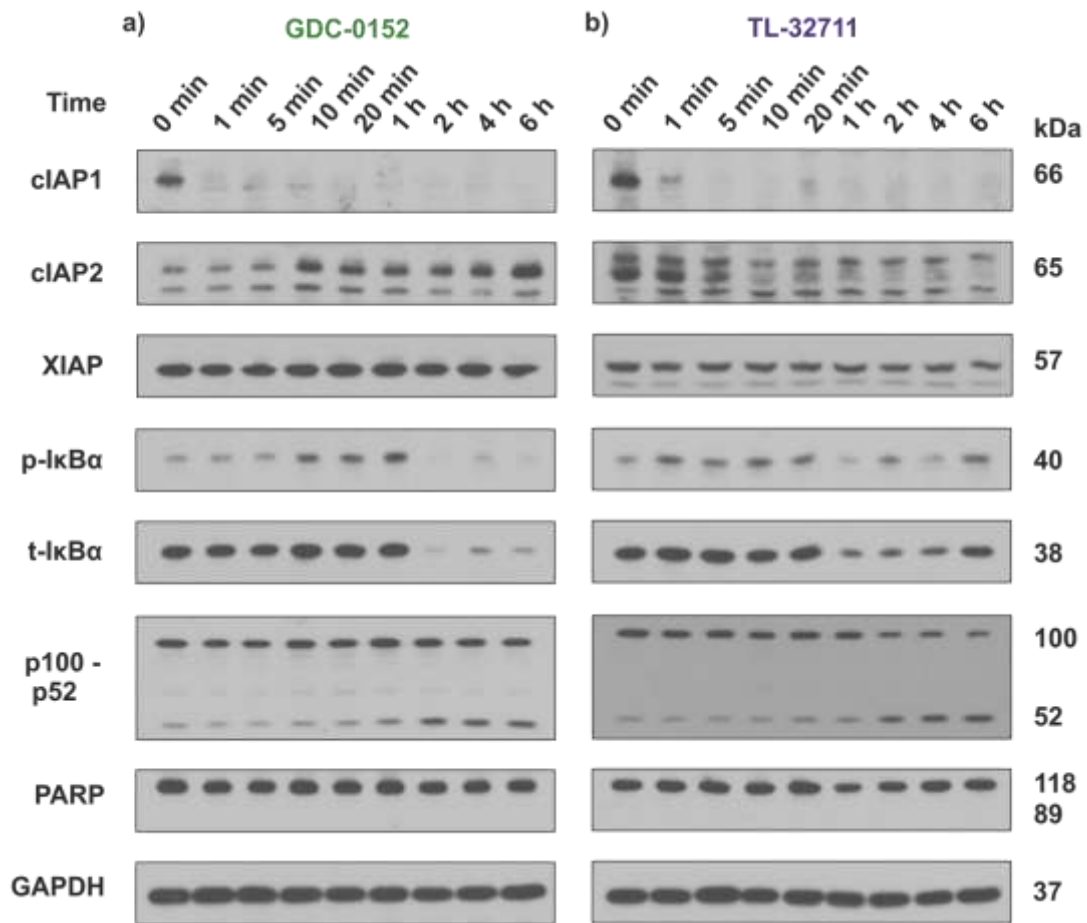


Figure 4.9 | SMs deplete cIAP1 and activate the non-canonical NF-κB pathway with similar kinetics in MCF-10A cells compared to tumour cells. a-b) MCF-10A cells were treated for the indicated time points, trypsinised, snap frozen and then lysed in RIPA buffer. Protein concentration was determined by Bradford Assay and SDS gels were loaded equally based on proteins concentration (20 µg). * = non-specific band.

AT-406 does not induce proliferation in MCF-10A cells

MTT cell viability assays suggested that SMs may increase the number of cells at 24 h. This is important as I had demonstrated activation of the non-canonical NF- κ B and, despite no TNF α secretion, this may have resulted in induction of genes regulating proliferation. If SMs did indeed promote proliferation in non-tumour cells, this is of toxicological importance as there is the potential for tumorigenesis. To further investigate the finding that SMs may increase the number of cells demonstrated by MTT assays, I sought to directly determine the number of cells after treatment with SMs. AT-406 was chosen as this compound resulted in the largest increase in MTT-related absorption. To increase experimental efficiency and remove human error, I used an automated Cellomics ArrayScan XTI Live Cell Imaging System, which counts the nuclei of cells stained with a fluorescent marker. Initially I thought to use a non-toxic dye so that I could directly observe the same cells before and after treatment with SMs. I piloted a new, purportedly non-toxic stain called Draq5 at various concentrations; however, the stain appeared to be toxic (data not shown) and so cell number was compared to an untreated control. Using the Cellomics platform, I found there was not a significant increase in cell number with AT-406 in MCF-10A cells, and there was actually a slight reduction in the number of viable cells (**Figure 4.10**). This contradicts the MTT assays which showed an increase in the number of viable cells, not a decrease. The discrepancy is currently unknown, however there are many limitations to the MTT assay, one being it is technically a metabolic assay as it is dependent on the activity of NADPH-dependent cellular oxidoreductase enzymes. As such, augmented metabolism may explain the observed increase in the MTT viability assay. In conclusion, AT-406 does not induce proliferation in MCF-10A cells.

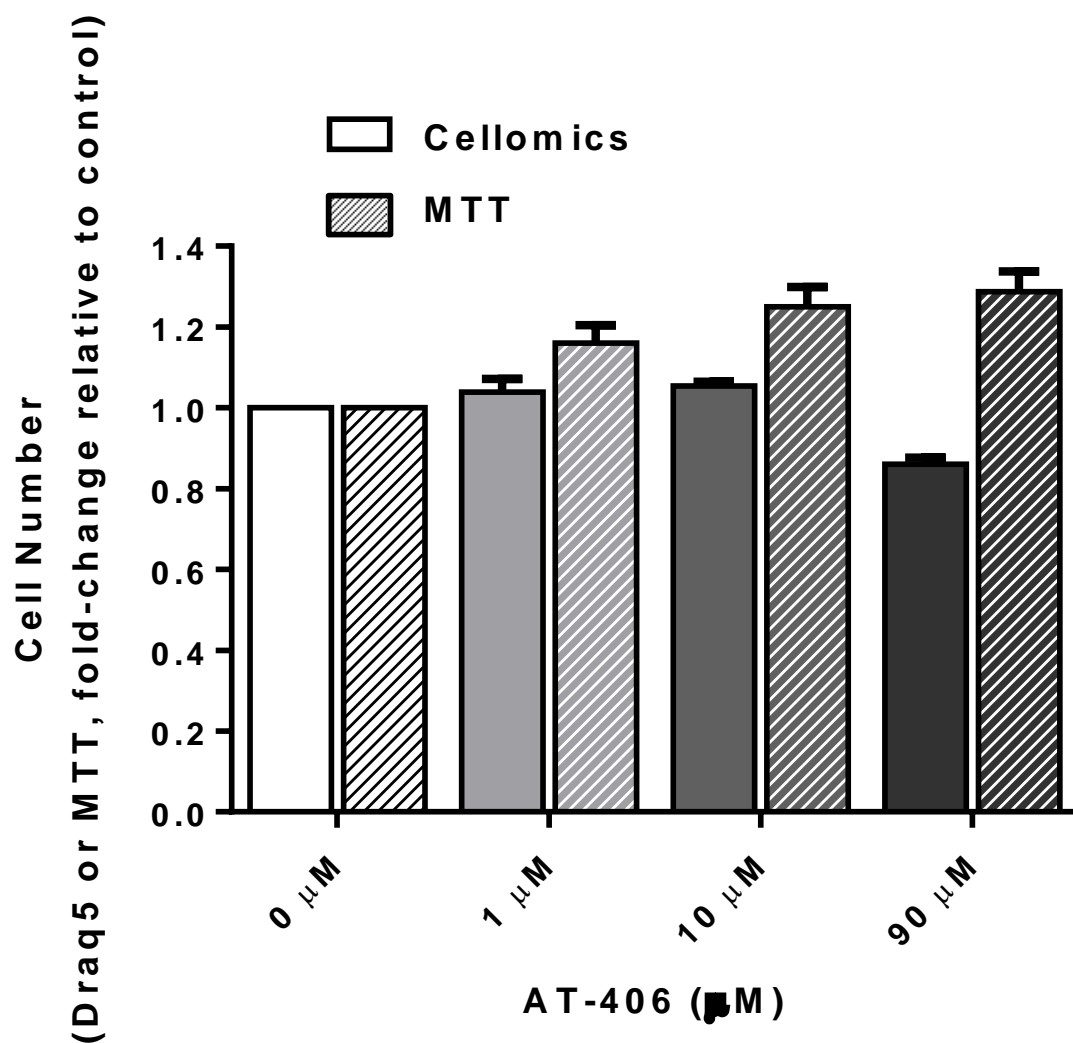


Figure 4.10 | SMs do not induce proliferation in MCF-10A cells. MCF-10A cells were treated with AT-406 for 24 h and then stained with the live cell nuclear dye, Draq5. Cells were then counted using an automated fluorescent microscope. Values represent mean \pm S.E.M, n=3.

MCF-10A, but not B-13 and B-13/H cells, are able to form Complex I and undergo Complex II-mediated cell death

As clinically relevant SMs did not induce high levels of cell death in non-tumour cells as single agents, I sought replicate a TNF α -rich microenvironment. I therefore treated cells with the SMs under investigation and species-specific TNF α at a concentration range to mimic a biologically relevant TNF α -rich microenvironment²⁴⁵. MCF-10A and B-13 cells were analysed by flow cytometry, whereas B-13/H cells were analysed using the Cellomics platform in combination with caspase activation assays. There was no increase in cell death at any concentration of TNF α in combination with SMs in any of the cells tested (**Figure 4.11, 4.13. and 4.15**). Western blotting demonstrated cIAP1 depletion and non-canonical NF- κ B activation in MCF-10A cells. While cIAP1 depletion was unable to be directly observed in the rat cells, p100 processing to p52 strongly suggests cIAP1 was depleted in the B-13 and B-13/H cells as well. While there was PARP cleavage in B-13 cells with TL-32711, this did not result in cell death (**Figure 4.12, 4.14 and 4.16**) In the event that 50 ng/mL TNF α was not sufficient to activate TNFR1-mediated signalling, I used 200 ng/mL TNF α in combination with TL-32711 in MCF-10A cells; this also did not induce cell death (data not shown).

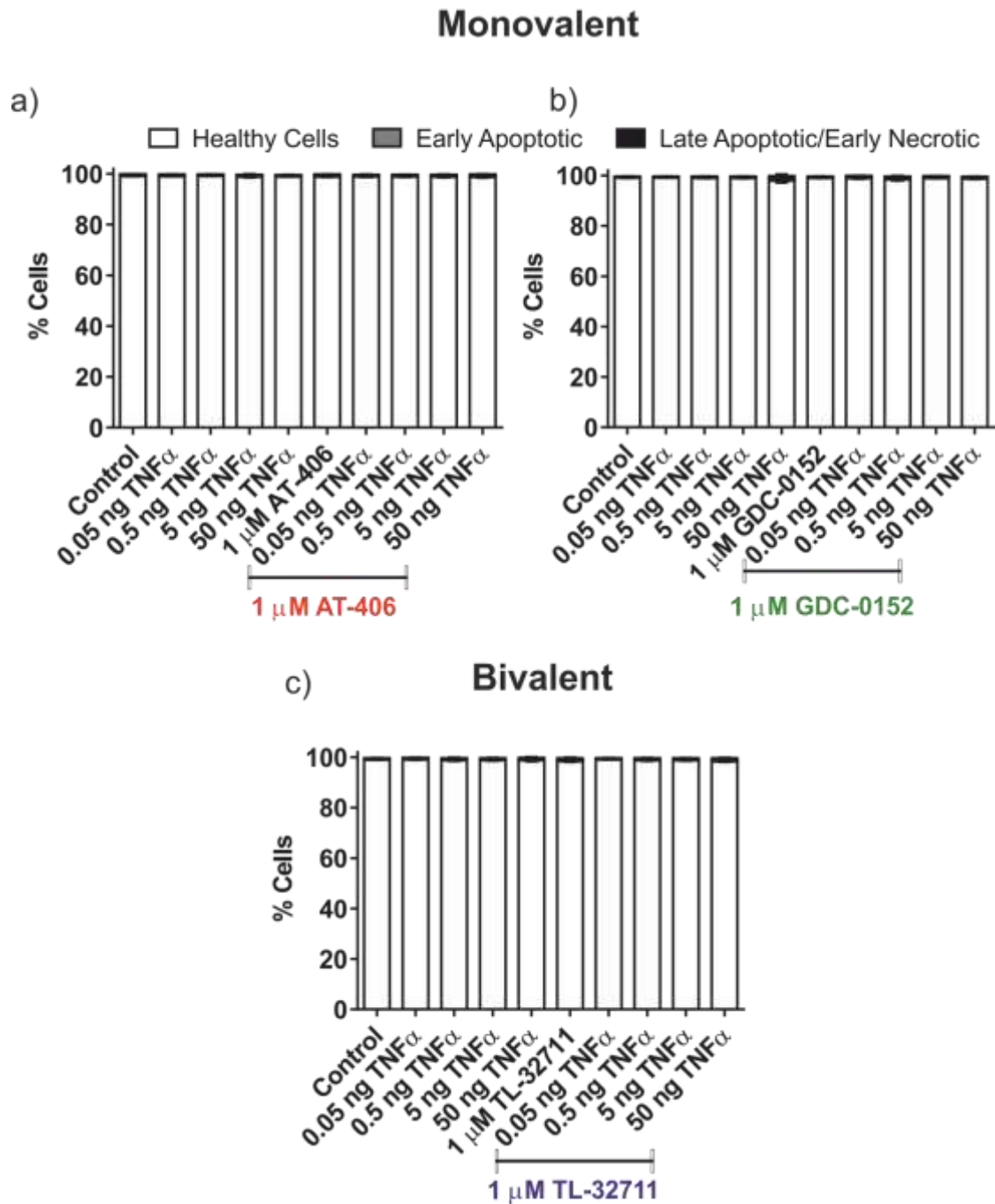


Figure 4.11 | Clinically relevant SMs do not induce cell death in combination with TNF α in MCF-10A cells. a) MCF-10A cells were treated with AT-406, GDC-0152 and TL-32711 at 1 μ M and human TNF α at a range of concentrations. Cell death was determined by flow cytometry after cells were stained with Annexin V and PI. Values represent mean \pm S.E.M, n=3.

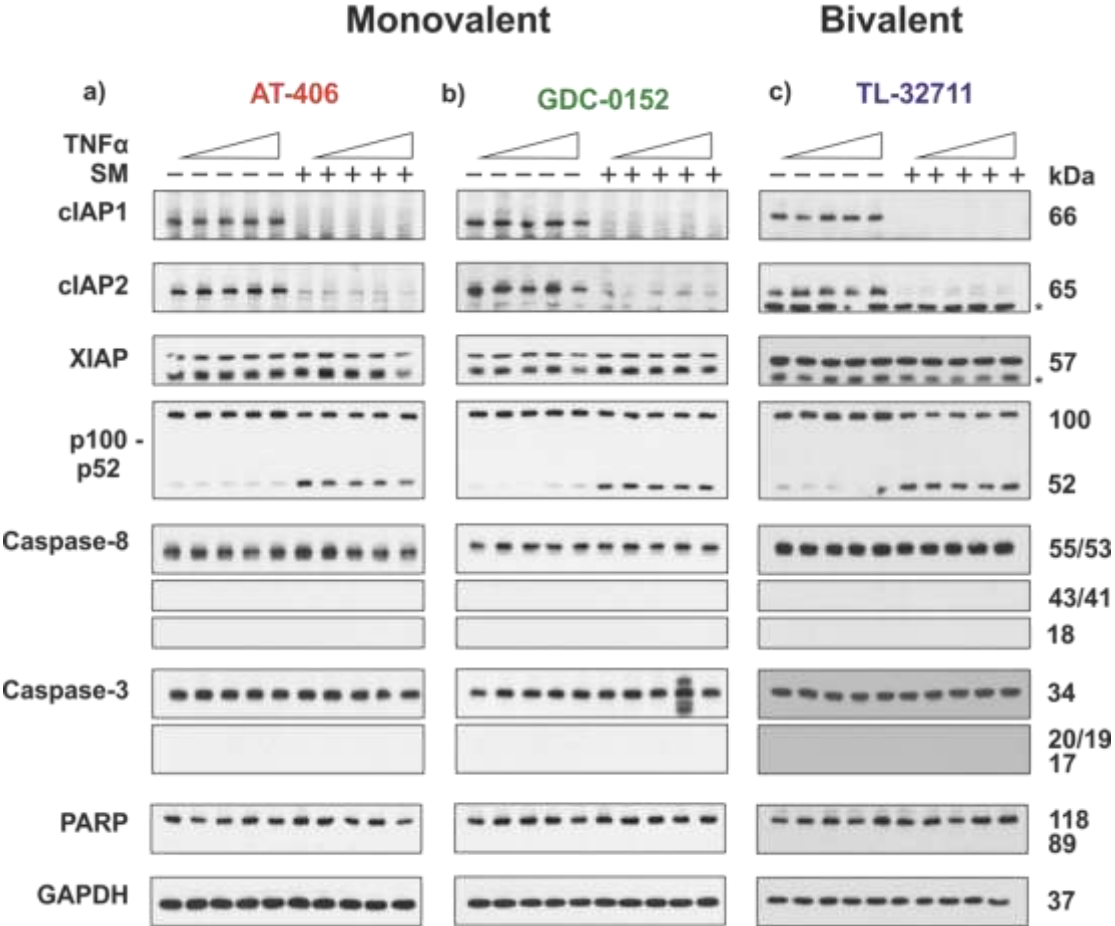


Figure 4.12 | Clinically relevant SMs activate the non-canonical NF-κB pathway, but do not induce cell death in combination with TNFα in MCF-10A cells. After MCF-10A cells were treated as indicated in figure 4.11, they were trypsinised, snap frozen and then lysed in RIPA buffer. Protein concentration was determined by Bradford Assay and SDS gels loaded based on equal protein amounts (20 µg). * = non-specific band.

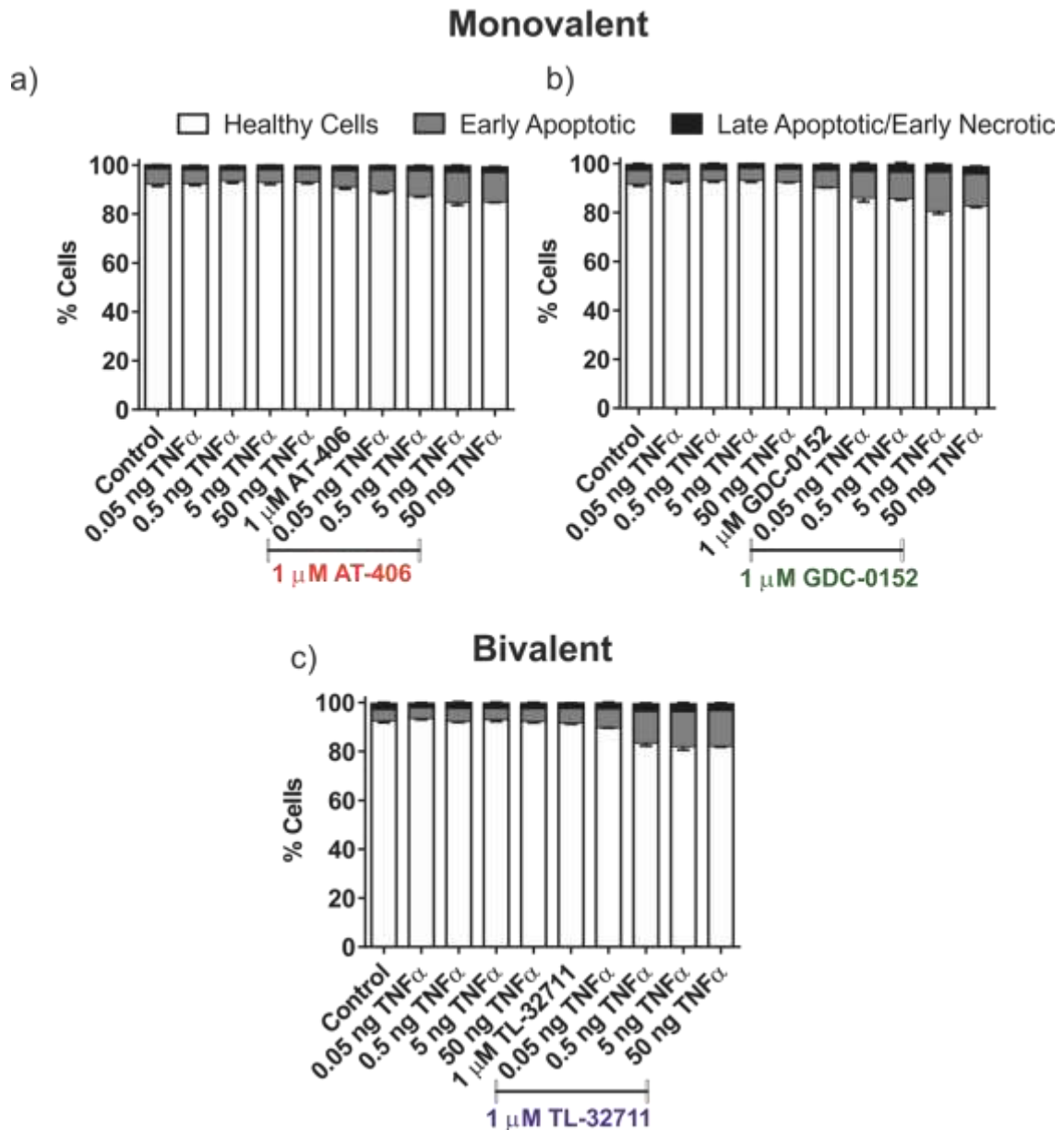


Figure 4.13 | Clinically relevant SMs do not induce cell death in combination with TNFα (Biovision) in B-13 cells. B-13 cells were treated with rat TNFα at a range of physiologically concentrations, and **a)** AT-406, **b)** GDC-0152 and **c)** TL-32711 at 1 μM for 24 h. Cell death was determined by flow cytometry after cells were stained with Annexin V and PI. Values represent mean ± S.E.M, n=3.

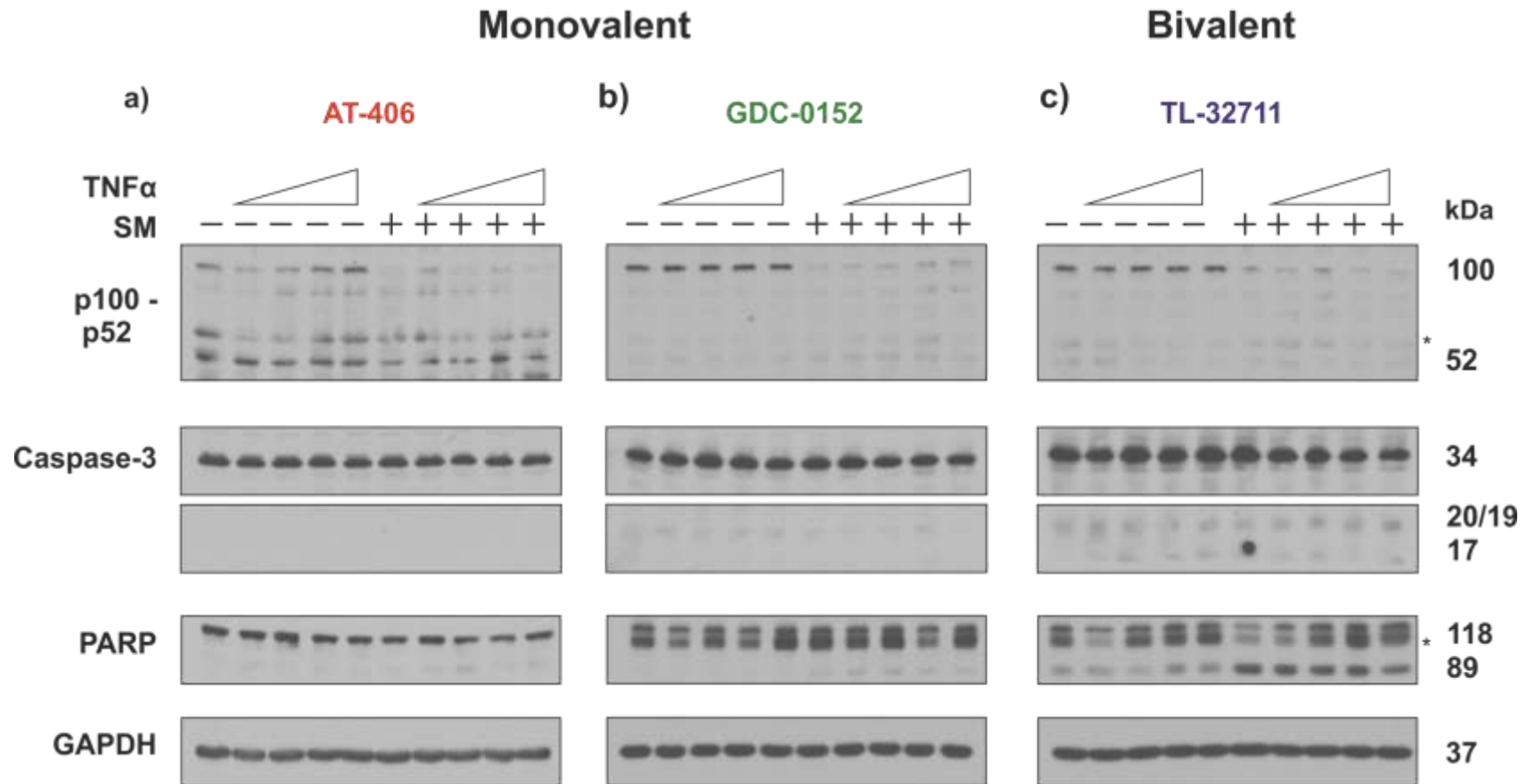


Figure 4.14 | Clinically relevant SMs activate the non-canonical NF-κB pathway, but do not activate caspase-3 in combination with TNFα (Biovision) in B-13 cells. After the indicated treatment, B-13 cells were trypsinised, snap frozen and then lysed in RIPA buffer. Protein concentration was determined by Bradford Assay and SDS gels loaded based on equal protein amounts (20 µg). * = non-specific band.

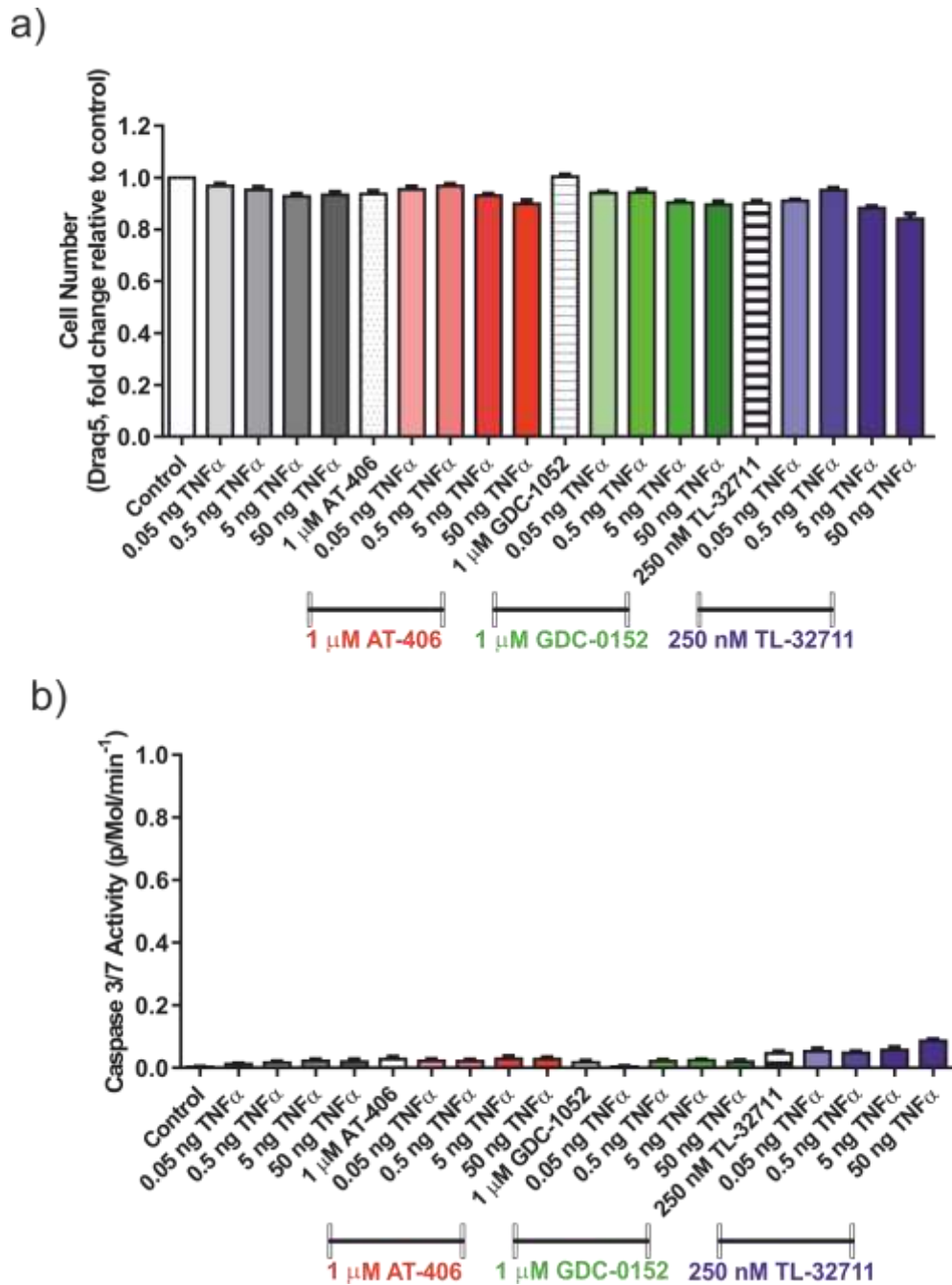


Figure 4.15 | Clinically relevant SMs do not induce cell death in combination with Biovision TNF α in B-13/H cells. B-13/H cells were treated with rat TNF α at a range of concentrations, and with AT-406 and GDC-0152 at 1 μ M and TL-32711 at 250 nM for 24 h. **a)** Cell number was determined by automated counting of Draq5 stained nuclei and **b)** caspase activity by DEVD.afc assays. Values represent mean \pm S.E.M, n=3.

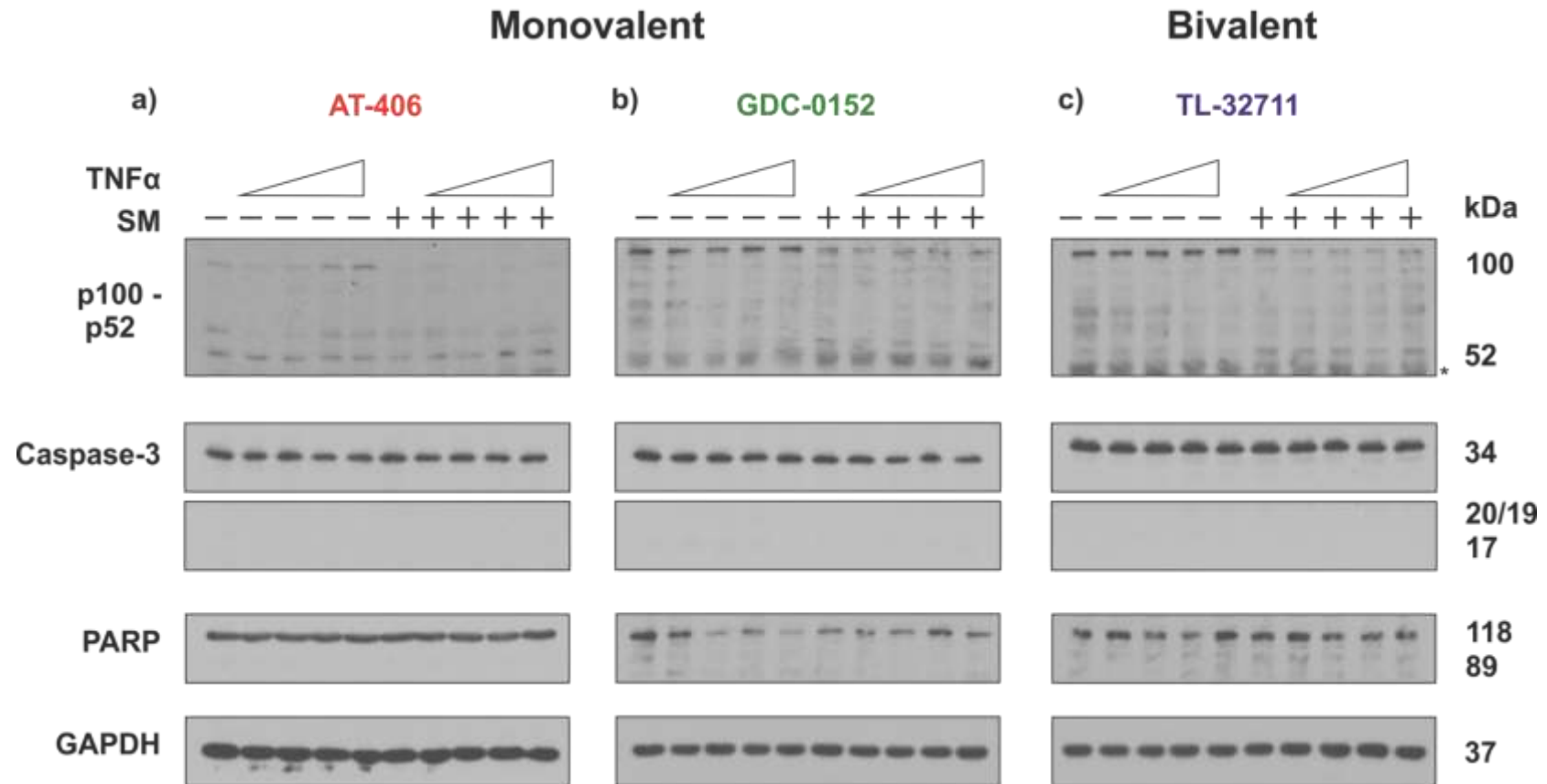


Figure 4.16 | Clinically relevant SMS activate the non-canonical NF- κ B pathway, but do not activate caspase-3 in combination with TNF α (Biovision) in B-13/H cells. After the indicated treatment outlined in figure 4.15, B-13/H cells were trypsinised, snap frozen and then lysed in RIPA buffer. Protein concentration was determined by Bradford Assay and SDS gels loaded based on equal protein amounts (20 μ g).

* = non-specific band.

This led us to question whether the non-tumour cells used were able to form the functional protein complexes associated with TNFR1 engagement, i.e. Complex I and Complex II. To test this, I treated MCF-10A, B-13 and B-13/H cells with species-specific TNF α and then used confocal microscopy to look for p65 translocation. In MCF-10A cells, treatment with 100 ng/mL resulted in p65 translocation, showing that these cells have a functional Complex I (**Figure 4.17**). However, neither the B-13 nor B-13/H cells demonstrated p65 translocation, despite the use of two independently sourced rat specific recombinant TNF α proteins (**Figure 4.18 and 4.19**). To determine whether MCF-10A, B-13 and B-13/H cells actually had the ability to undergo Complex II-mediated cell death, I treated cells with TNF α in combination with the protein translation inhibitor, cycloheximide (CHX). In MCF-10A cells, TNF α in combination with CHX resulted in an increase in cell death of 22-28% as determined by flow cytometry. Western blotting demonstrated cleavage of caspase-8, caspase-3 and PARP, suggesting that the MCF-10A cells do indeed have the ability to undergo Complex II-mediated cell death (**Figure 4.20**). Conversely, however, B-13 and B-13/H cells did not undergo cell death with CHX and TNF α sourced from Biovision, even at a concentration of 200 ng/mL TNF α , as shown by flow cytometry for B-13 cells and Cellomics for B-13/H cells (**Figure 4.21 and 4.22**). To make sure it that the lack of p65 translocation was not due to the commercial TNF α being non-functional, I purchased another rat-specific TNF α from R&D. This TNF α resulted in slight increases in cell death of B-13 and B-13/H cells of 18% and 26%, respectively (**Figure 4.22**). While these data argue the R&D sourced TNF α can induce TNF α -mediated cell death, this appeared to conflict with the apparent lack of p65 translocation. As such, I continued to investigate the potential reason B-13 and B-13/H cells are not able to promote Complex I-mediated p65 nuclear translocation. One hypothesis was that these cells do not possess TNFR1. To test this, I stained for surface level expression of TNFR1 in B-13 cells, using MCF-10A cells as a positive control. Interestingly, I found that B-13 cells express high amounts of TNFR1, despite their apparent inability to form Complex I (**Figure 4.18**).

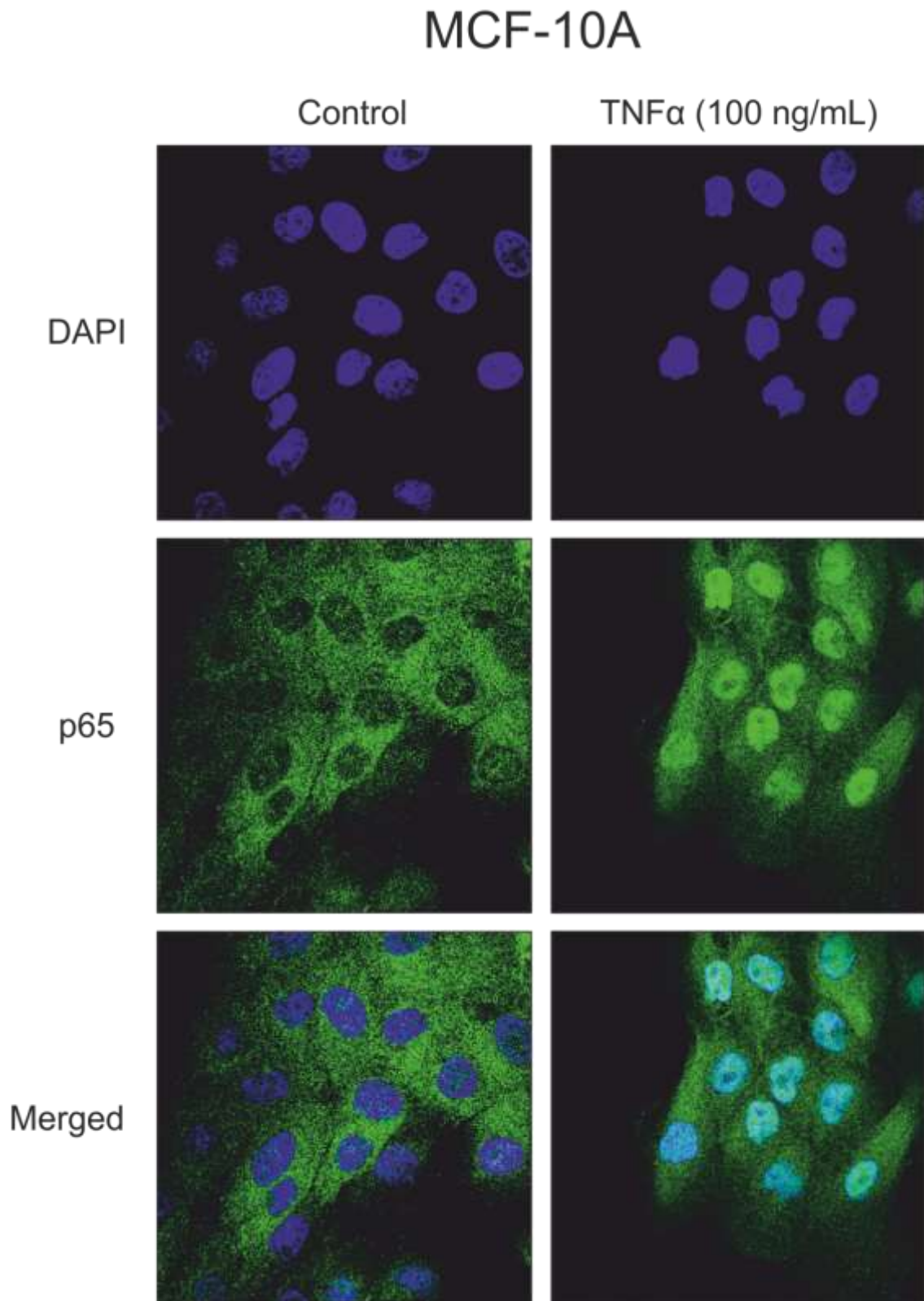


Figure 4.17| MCF-10A cells undergo p65-mediated translocation. MCF-10A cells were treated with human TNF α at a concentration of 100 ng/mL for 30 mins before being fixed. p65 nuclear translocation was visualised by confocal microscopy. Representative image of n=3.

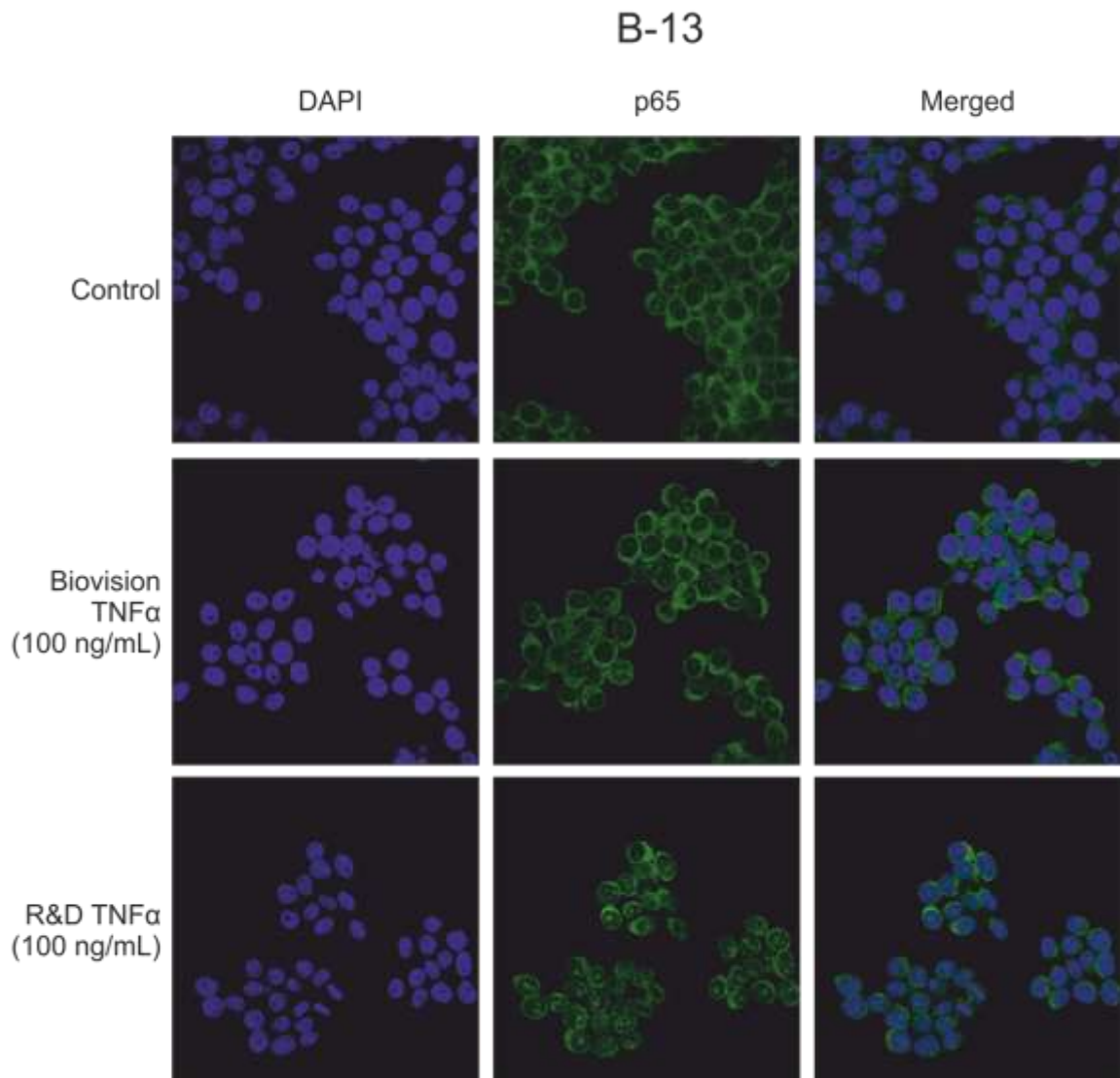


Figure 4.18 | B-13 cells do not undergo TNF α -mediated p65 translocation. B-13 cells were treated with two differently sourced rat TNF α proteins at a concentration of 100 ng/mL for 30 mins before being fixed. p65 nuclear translocation was visualised by confocal microscopy. Representative image of n=3.

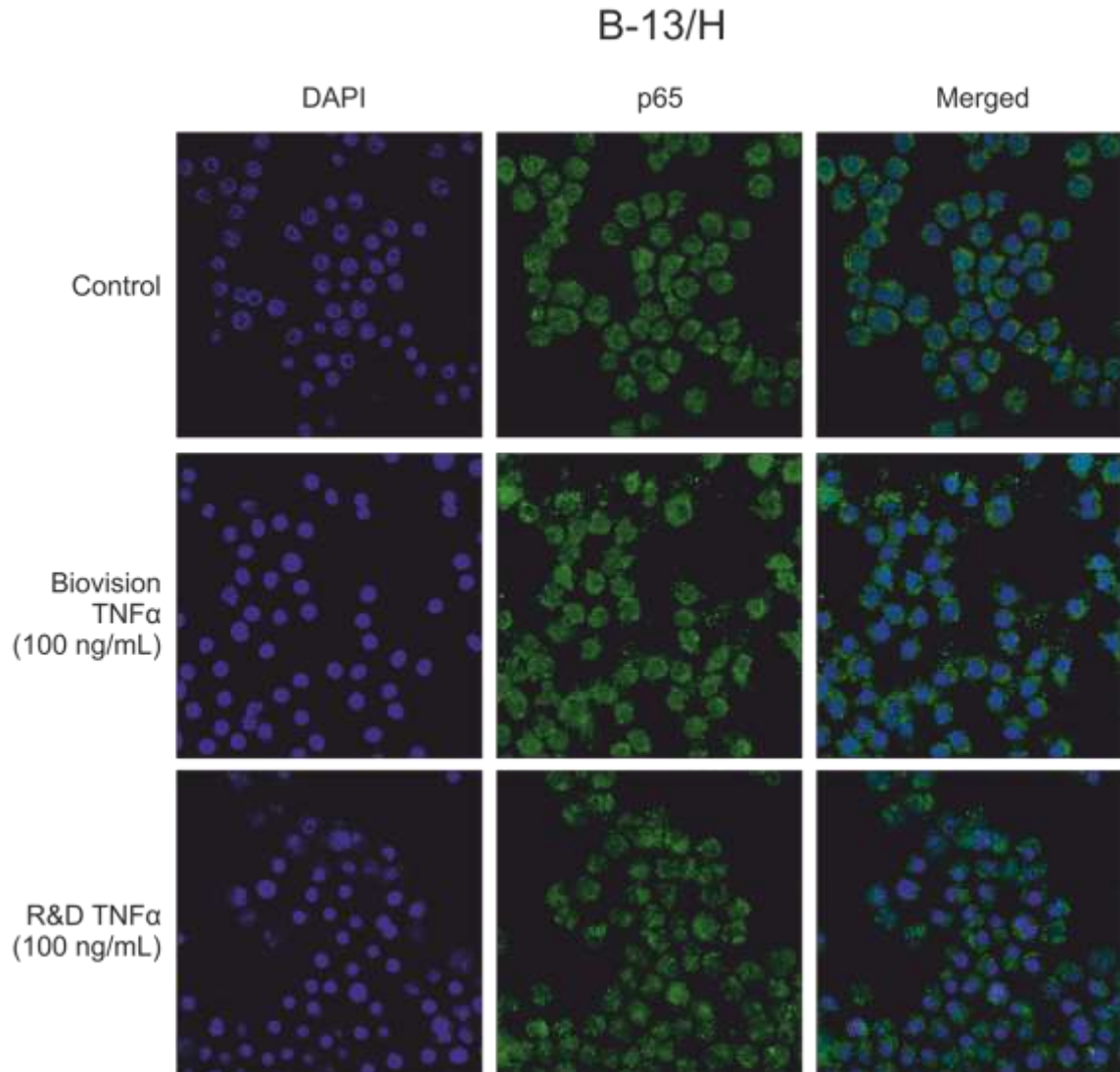


Figure 4.19 | B-13/H cells do not undergo TNFα-mediated p65 translocation. B-13/H cells were treated with two differently sourced rat TNFα proteins at a concentration of 100 ng/mL for 30 mins before being fixed. p65 nuclear translocation was visualised by confocal microscopy. Representative image of n=3.

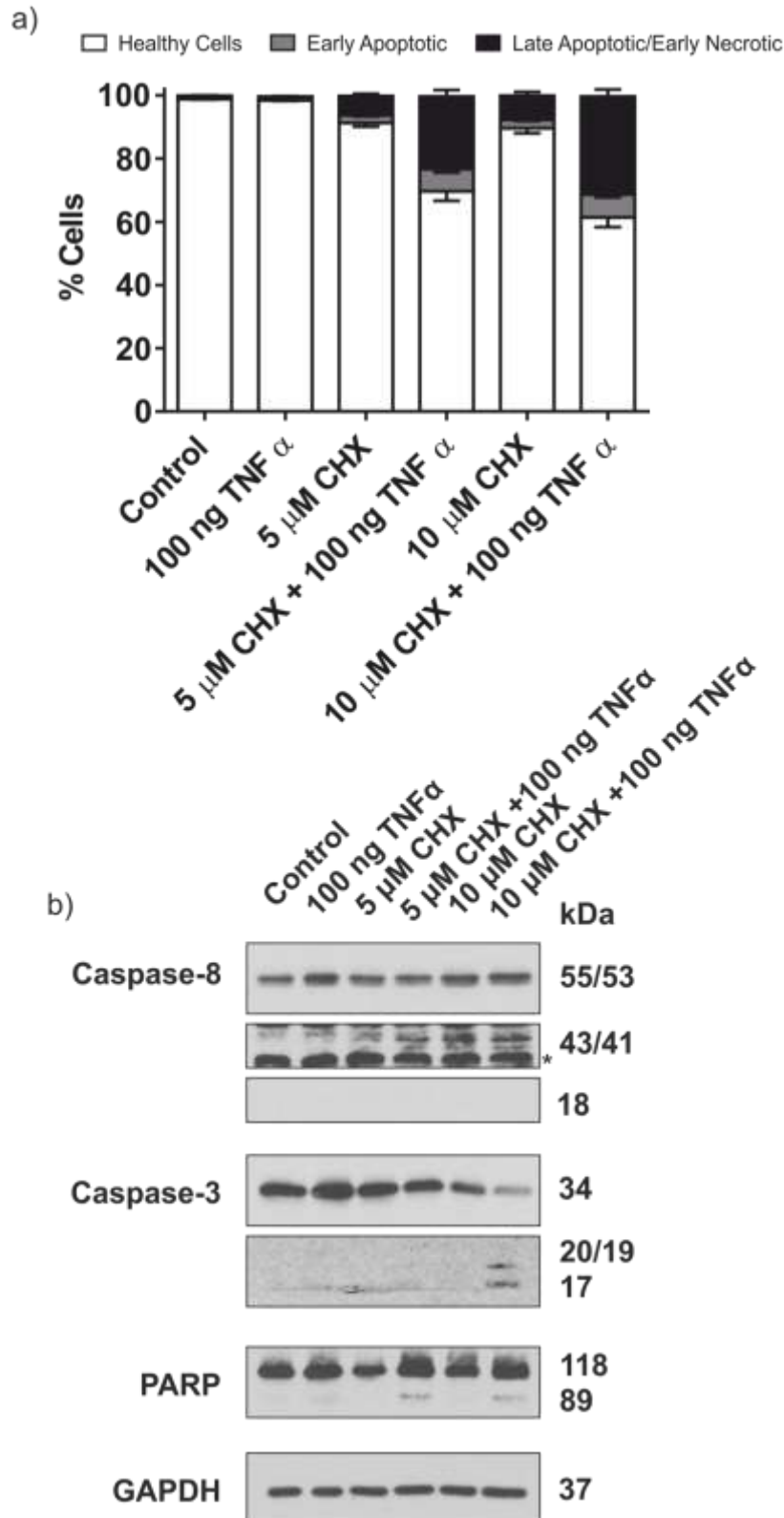
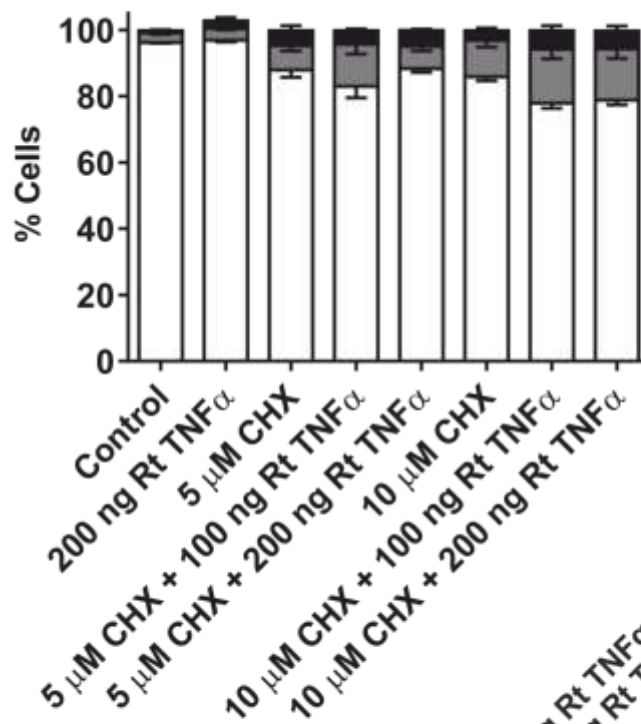


Figure 4.20 | MCF-10A cells have the ability to undergo Complex II-mediated cell death. MCF-10A cells were treated with CHX at 5 and 10 μ M and human TNF α at 100 ng/mL. **a)** Cell death was investigated by flow cytometry. **b)** MCF-10A cells were trypsinised, snap frozen and then lysed in RIPA buffer. Protein concentration was determined by Bradford Assay and SDS gels loaded based on equal protein amounts (20 μ g). Values represent mean \pm S.E.M, n=3. * = non-specific band.

a)



b)

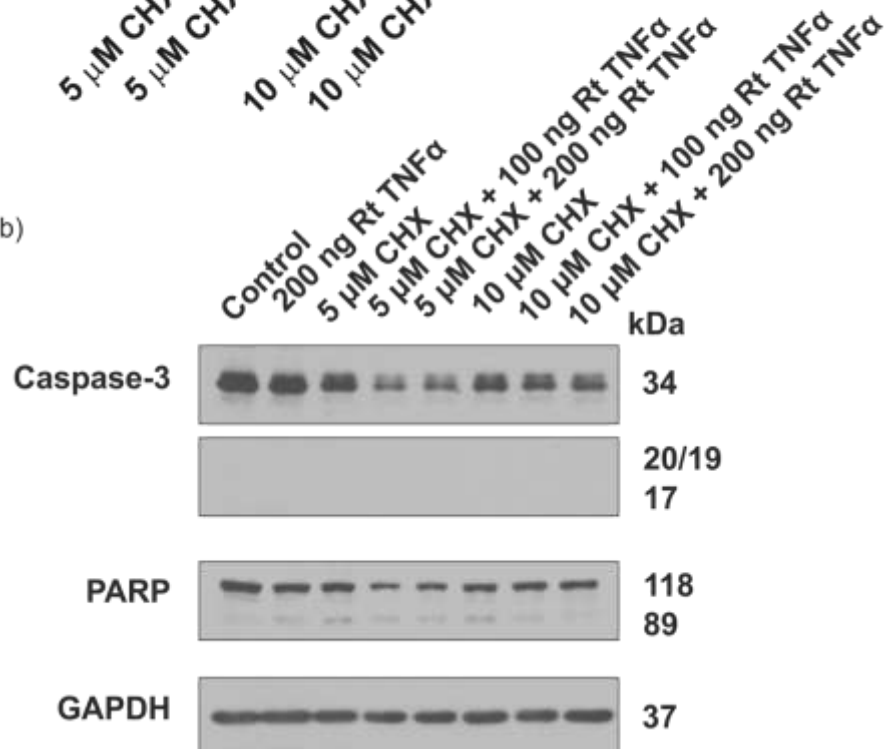


Figure 4.21| B-13 cells are unable to undergo TNF α -induced Complex II-mediated cell death. B-13 cells were treated with CHX at 5 and 10 μ M and Biovision Rat TNF α for 24 h. **a)** Cell death was analysed by flow cytometry. **b)** Whole cell pellets from B-13 cells were lysed and sonicated in 1x sample buffer and loaded according to cell number. Values represent mean \pm S.E.M, n=3.

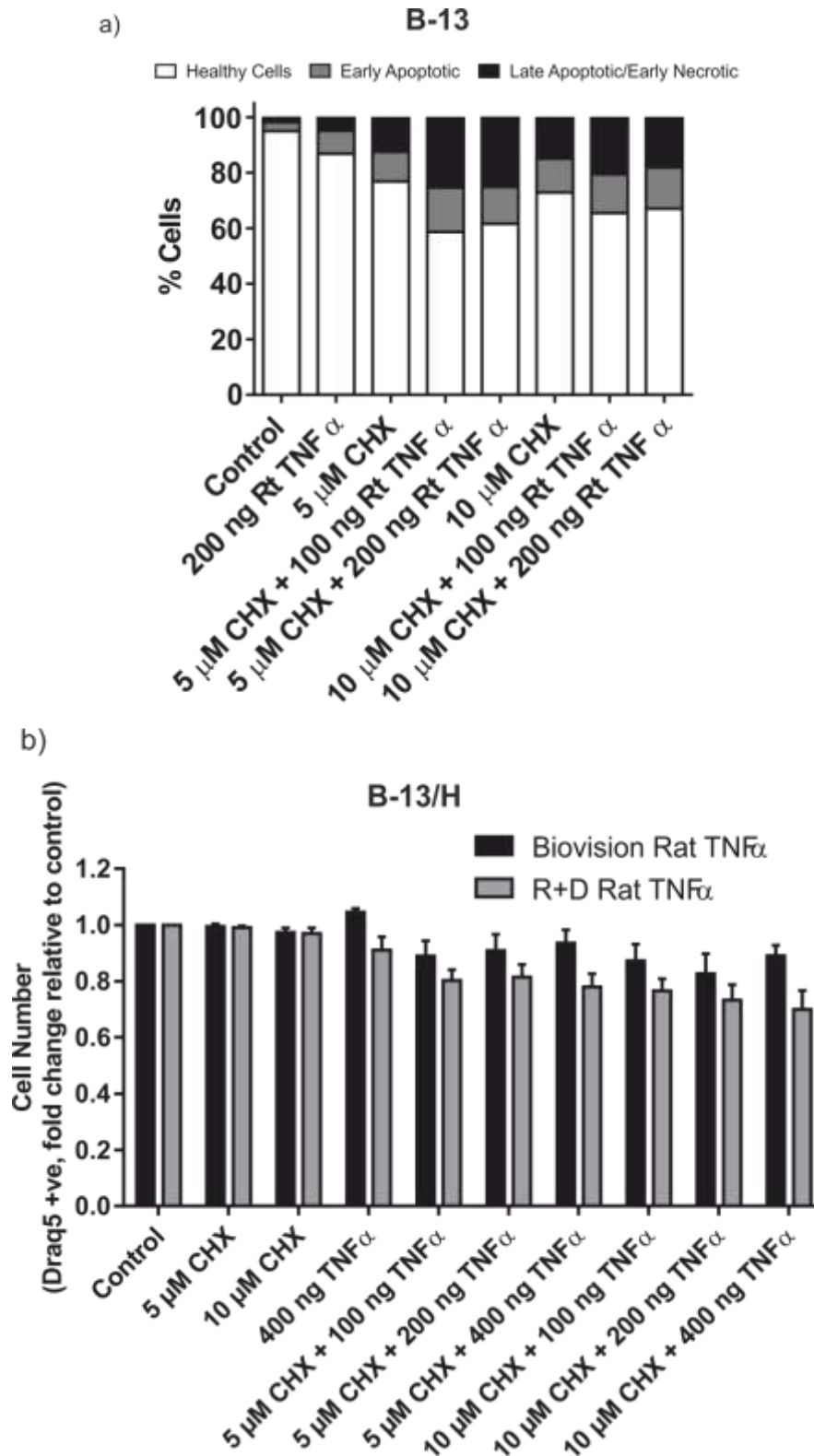


Figure 4.22 | B-13 and B-13/H cells are unable to undergo high levels of TNF α -induced Complex II-mediated cell death. a) B-13 cells were treated with CHX at 5 and 10 μ M and R&D Rat TNF α for 24 h. Cell death was analysed by flow cytometry. Values represent average, n=2. b) B-13/H cells were subjected to CHX at 5 and 10 μ M and two different rat TNF α s at a concentration of 100-400 ng/mL for 24 h. Cell death was investigated by counting nuclei stained with Draq5. Values represent mean \pm S.E.M, n=3.

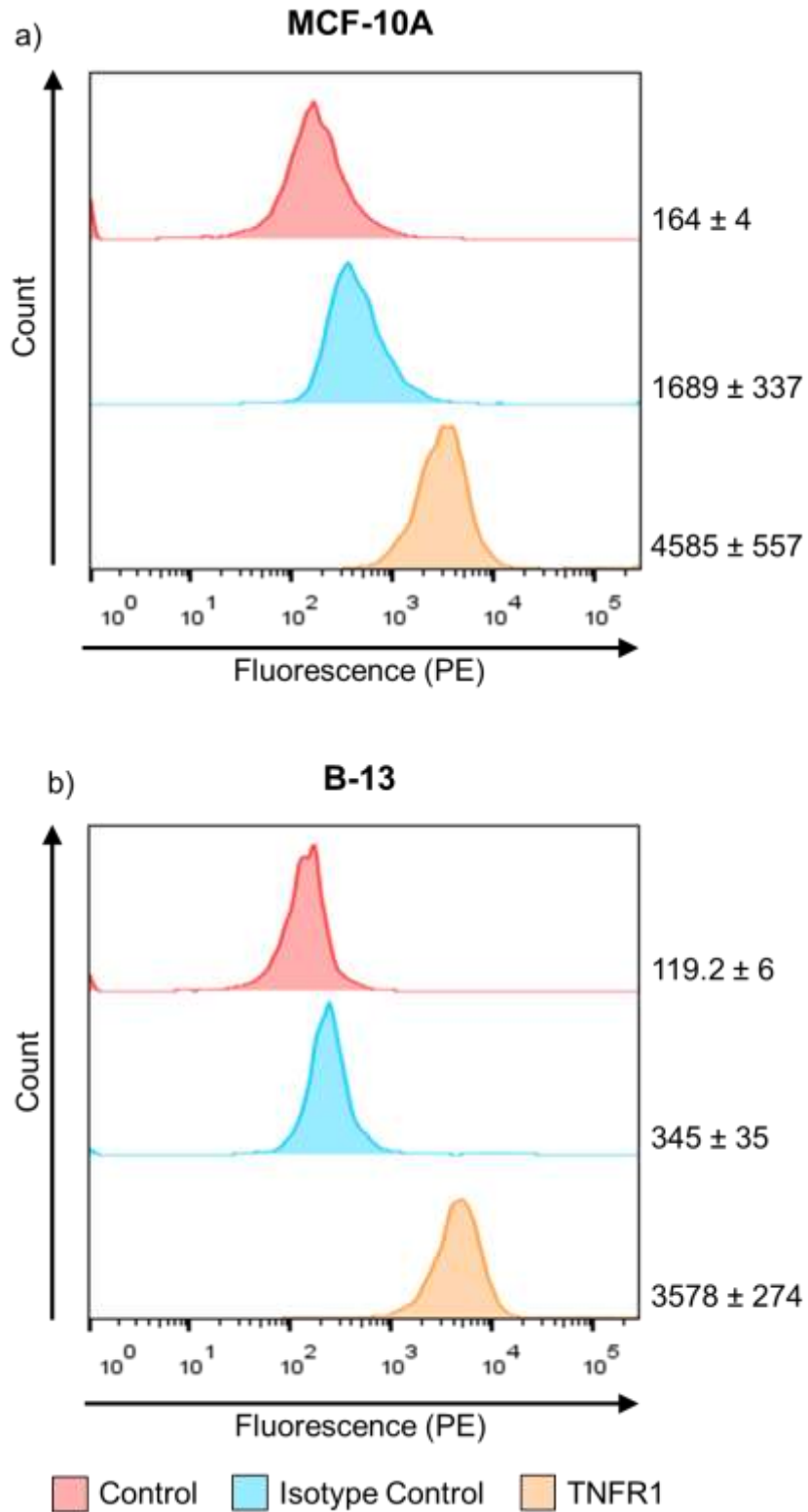


Figure 4.23 | MCF-10A and B-13 cells express TNFR1. For TNFR1 expression analysis, cells were harvested via trypsinisation and incubated with either goat serum (control), goat serum containing PE-conjugated isotype control or TNFR1 receptor specific antibody. After being washed with PBS, the fluorescence intensity was determined by flow cytometry. The values represent the mean fluorescence intensity (geometric mean) ± SEM (n=3).

As B-13 cells expressed high levels of TNFR1, I decided to determine whether either of the two commercial recombinant TNF α proteins was functionally active. To confirm this, I treated WT MEFs with 100 ng/mL of both commercial TNF α proteins for 30 mins. Using confocal microscopy to visualise p65 translocation, I found that only the R&D rat TNF α was functional and had the ability to induce p65 nuclear translocation (**Figure 4.24**). This suggests that B-13 and B-13/H cells may not have the appropriate molecular machinery for TNF α /NF- κ B-mediated p65 translocation.

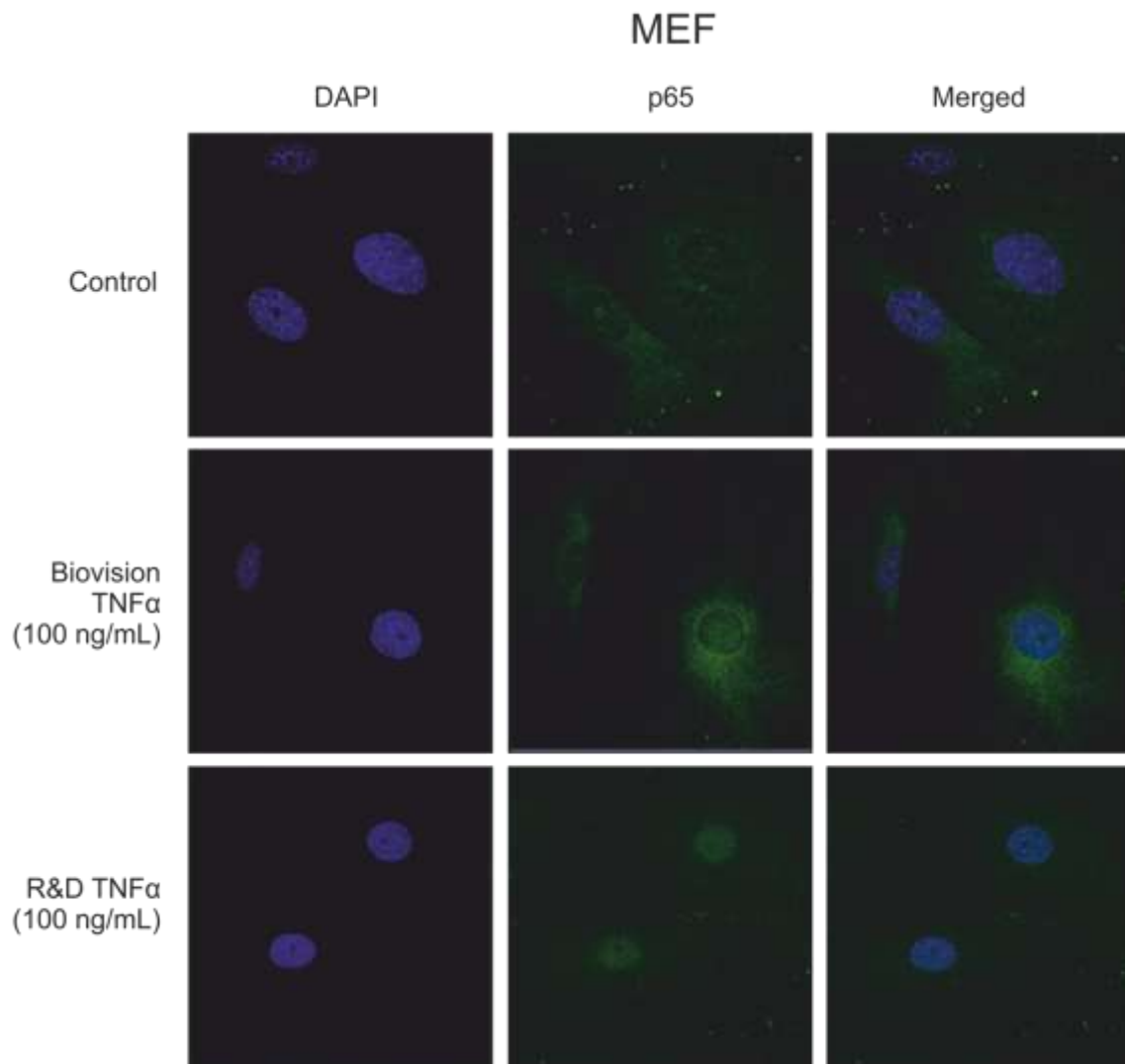


Figure 4.24 | The commercially available TNF α from R&D is functionally activate as evidenced by p65 translocation. MEF cells were treated with two different rat TNF α s at a concentration of 100 ng/mL for 30 mins before being fixed. p65 nuclear translocation was visualised by confocal microscopy. Representative image of n=1.

B-13 and B-13/H have a mutation in the *cflar* gene

As the entire genome of the B-13 cells was sequenced previously by the Newcastle group (Prof. Wright) who established the B-13 and B-13/H cells, I was able to ascertain whether there were any mutations in genes associated with TNF α -induced cell signalling. I chose a candidate list of 139 genes (**Appendix 1**) and found that there were three mutated proteins; *fos*, *map2k3* and *cflar*. *fos* is an proto-oncogene that encodes for transcription factor c-Fos, which forms a complex with c-Jun and AP-1 to stimulate transcription of AP-1 responsive genes²⁴⁶; *map2k3* which encodes for MAP2K3 and is involved in activation of the MAPK/p38 pathway²⁴⁷. Perhaps most interesting was the mutation in *cflar*, *cflar* transcribes for the protein cellular FLICE (FADD-like IL-1 β -converting enzyme)-inhibitory protein (cFLIP)²⁴⁸, and in B-13 cells showed a 2 nucleotide deletion in the 9th exon (**Figure 4.25**). Using the bioinformatics program, geneious, to determine the effect of the deletion on the genomic sequence, I found a stop codon resulting in either expression of cFLIP short (cFLIP_S), the inhibitory isoform of cFLIP, or no protein at all.

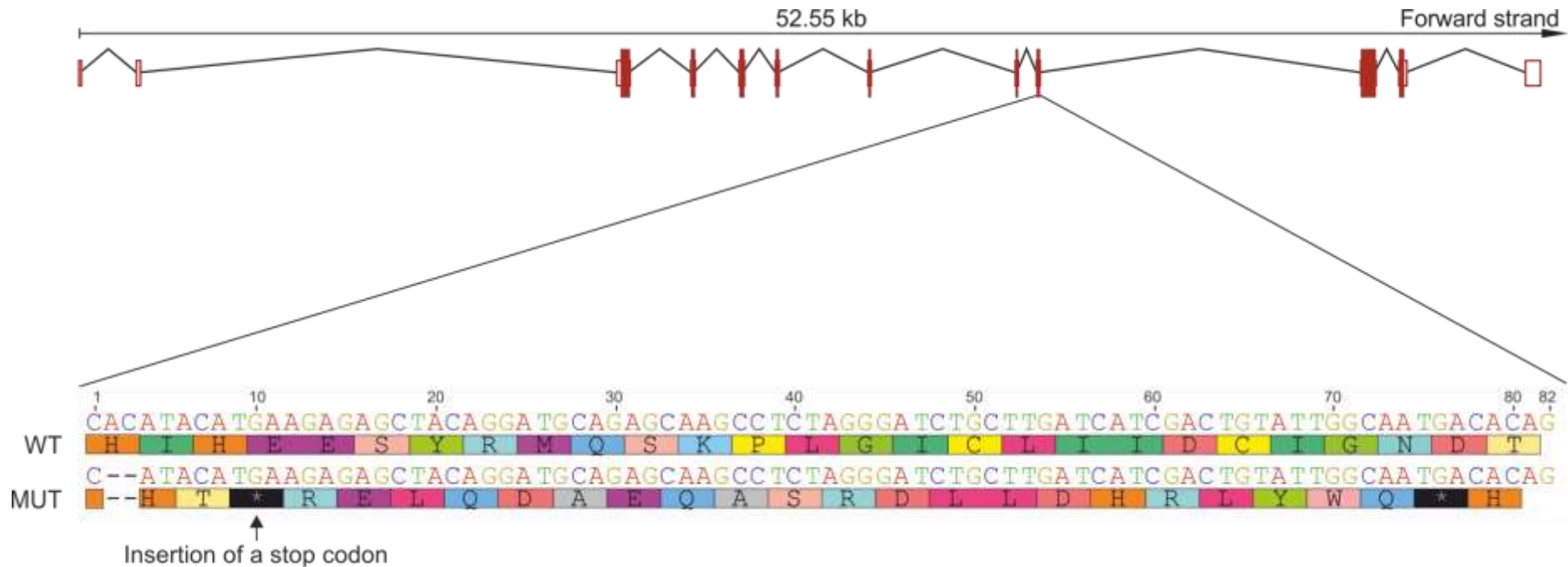


Figure 4.25 | The *cflar* gene is mutated in B-13 cells. The entire genome of the B-13 cells was sequenced by the group in Newcastle (Prof. Wright). Out of the 139 genes examined, the most relevant mutation was that found in the *cflar* gene which encodes for the protein cFLIP. The two nucleotide mutation in the 9th exon likely results in expression of the cFLIP_S isoform or no protein at all.

To test if this mutation affected cFLIP protein expression, I investigated cFLIP long (cFLIP_L) and cFLIP_S isoform expression at the protein level using western blotting. Firstly, I wanted to determine which species to use as a positive control. Using BLAST, I found there is only a 67% and 68% homology between humans compared to mice and rats in cFLIP, respectively. When the cFLIP gene is compared in mice against rats, there is an 84% homology. However, while not identical, the molecular weight between the three species is almost identical (480 amino acids in rats and humans compared to 481 for mice). I therefore used both human and mouse lysates as positive controls. The human sample was from an acute T-cell leukaemia, and the mouse samples were from untreated homogenised liver and from the neuroblastoma cell line N2a (a kind gift from Dr Panman's laboratory). I saw a band positive for cFLIP_L in the human control (55 kDa), but there was not a strong band for cFLIP_S (25 kDa) (**Figure 4.26**). In the rat and mouse samples, there was also a band around the weight of cFLIP_L, but this was slightly lower compared to the human band. As the band in the rat and mouse samples runs lower than the one observed in the human sample, I cannot confirm this band is in fact cFLIP_L. There was also a strong band at the correct molecular weight for cFLIP_S in the B-13/H cells, but as I did not detect a band in the human samples, I cannot say for sure whether this is indeed cFLIP_S (**Figure 4.26**). However, while this may be a putative mediator of their resistance to cell death, it does not explain why B-13 and B-13/H cells do not undergo p65 nuclear translocation when treated with TNF α .

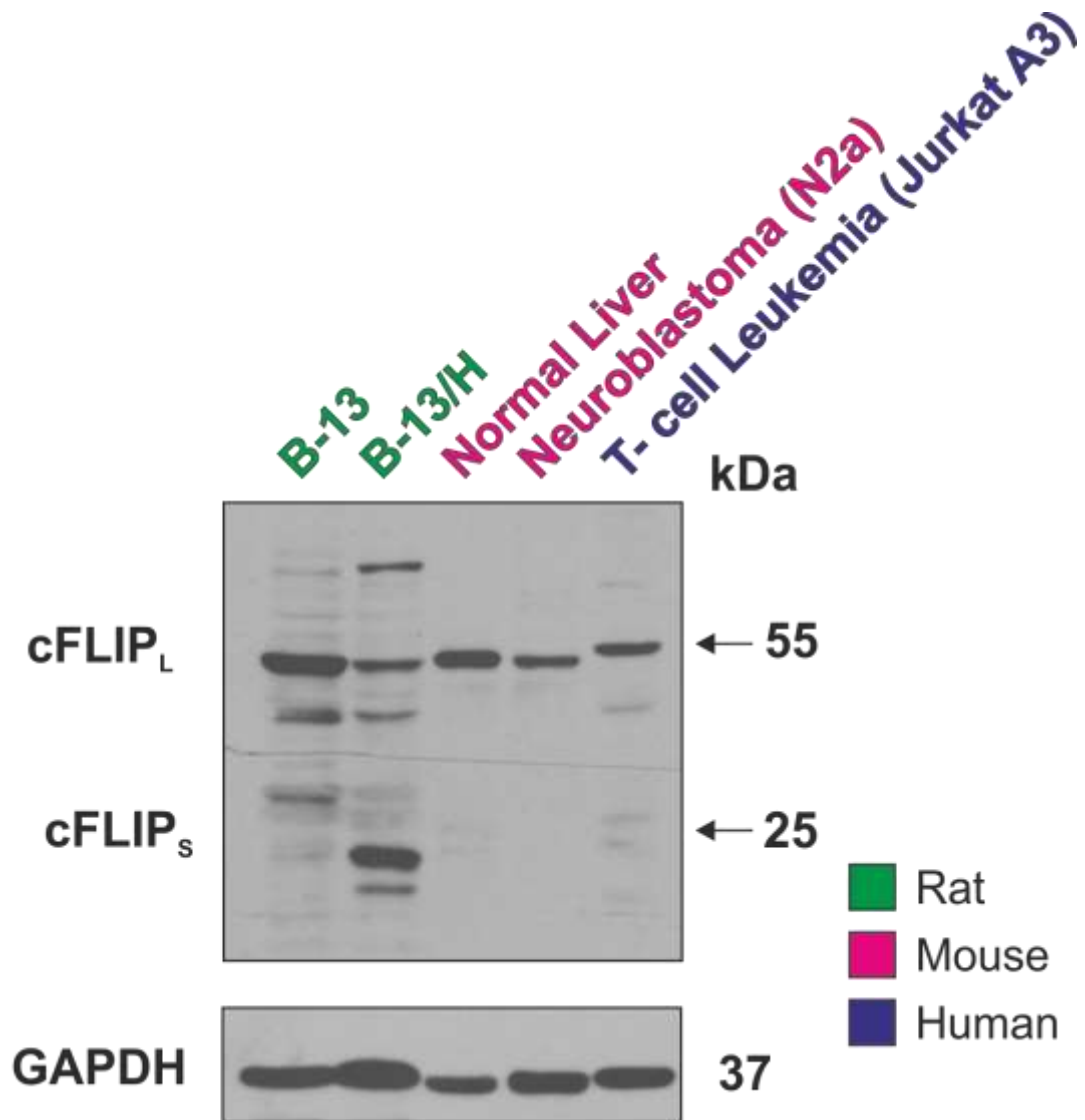


Figure 4.26 | B-13 and B-13/H cells do not express cFLIP_L or cFLIP_S. Protein expression of cFLIP_L and cFLIP_S were determined using western blotting. Lysates from mouse liver, and human and mouse cancer cell lines were used as a positive control.

Discussion

The purpose of this study was to determine the effect of SMs as a single agent, or in combination with the cytokine TNF α in non-tumour derived cells. I initially performed a wide range concentration-response curve to determine whether SMs deplete cIAP1, activate the non-canonical and induce cell death in non-tumour derived cells as single agents. To achieve this, I used human MCF-10A cells and two rat cell lines, B-13, a pancreatic progenitor cell line and B-13/H cells, a transdifferentiated hepatocyte-like cell. B-13/H cells have many hepatocyte characteristics, including expression of endogenous levels of CYP450 proteins, hepatocyte morphology and replicative quiescence^{240,241,243}. In all cells, SMs activated the non-canonical NF- κ B pathway, but this did not result in detectable TNF α secretion. In MCF-10A cells, SMs induced cIAP1 depletion and, while this could not be confirmed in the rat cells due to the lack of available antibodies, it is very likely this also occurred as cIAP1 depletion results in p100 processing²²², which was observed in these cell lines. It is not known why these non-tumour cells do not secrete TNF α despite activation of the NF- κ B pathway and cIAP1 depletion. As TNF α is such a potent cytokine, it is very heavily regulated by a variety of mechanisms, including transcription, message turnover, message splicing, translation, and protein cleavage from the cell surface. Furthermore, as TNF α is almost exclusively secreted by myeloid cells and T-cells in an homeostatic environment²⁴⁹, and as MCF-10A cells are a non-tumour derived epithelial cell line, it seems unsurprising that these cells do not secrete TNF α . While I did not investigate the precise regulation, it may be the result of pre-transcriptional regulation where p65 can enter the nucleus (as I have demonstrated) but cannot bind the TNF α promoter. There may even be epigenetic regulation. Indeed, there is some evidence demonstrating that TNF α protein stability can be perturbed by microRNA-124 and microRNA-187^{250,251}. Additionally, it is reported that the *tnf* locus is not acetylated in cell lineages that do not secrete TNF α and maturation of monocyte lineage cells was accompanied by increasing histone acetylation at the *tnf* locus²⁵². There is also evidence that TNF α is not secreted due to inhibition of matrix metalloproteinases, which are responsible for the cleavage of membrane-bound

TNF α . Therefore, it is likely these cells do not secrete TNF α as they are an epithelial, non-tumour cell line.

Interestingly, with AT-406, there actually appeared to an increase in the number of viable cells compared to control in both MCF-10A and B-13/H cells. While this is unlikely in B-13/H cells as they are replicatively quiescent, this was plausible in MCF-10A cells. Despite no TNF α secretion, the non-canonical NF- κ B pathway was clearly activated and this may have resulted in upregulation of a plethora of genes involved in promotion of proliferation²²⁹. In contrast to the MTT, I found that AT-406 did not induce proliferation in MCF-10A cells at any concentration when cells were analysed by the Cellomics platform. The discrepancy between this and the MTT data may be explained by the difference in approaches. Counting the cells is a more valid way of determining cell number compared to the MTT assay as the latter is actually a metabolic assay, from which cell number is inferred, rather than directly measured^{253,254}. MTT assays work on the principle that MTT, which is reduced to formazan, only occurs in viable cells with functional mitochondrial dehydrogenases^{253,255}. However, it has been shown that up to 50% of the dye entering the cell membrane can be reduced by non-mitochondrial, cytosolic, and microsomal enzymes^{254,256}. Furthermore, it was demonstrated that in the presence of compounds that alter intracellular levels of free radicals, MTT assays gave higher readings for cell viability compared to PI exclusion. However, while there is some evidence suggesting SMs can indirectly modulate intracellular free radical levels, this was only seen in combination with oleanolic acid¹³⁶. There is evidence that GDC-0152 can undergo metabolism to hippuric acid, which is excreted in urine²⁵⁷. However, as this metabolism was CYP450 dependent, it does not explain the increase in the MTT absorbance as MCF-10A cells do not have CYP450 enzymes. In summary, these data demonstrate that SMs do not induce proliferation in non-tumour derived cells.

To compare the kinetics of SMs in relatively insensitive MCF-10A cells with the sensitive MDA-MB-231 tumour cells, I performed a time course similar to that used in the tumour cells, but modified it to take into account the lack of cell death. I found that the kinetics of cIAP1 depletion and NF- κ B activation are

remarkably similar between the two cell types, as cIAP1 was depleted within minutes and non-canonical NF- κ B activated at within 2 h. Interestingly, the canonical NF- κ B pathway was also activated in MCF-10A cells, particularly with GDC-0152. This may be related to the structural activity relationship of this specific compound. Indeed, GDC-0152 is known to induce significant inflammation, resulting in induction of many NF- κ B-related genes, including TNF α ¹⁶¹. TL-32711, however is designed specifically not to activate the canonical NF- κ B pathway, which results in this inflammatory effect¹⁵¹. This lack of canonical NF- κ B activation was apparent in the MCF-10A cells in this study. These data demonstrate that SMs do not induce cell death or TNF α secretion, despite cIAP1 ablation and activation of both arms of the NF- κ B pathway. Moreover, the kinetics between this ablation or cIAP1 and non-canonical NF- κ B activation appear to be similar in between both tumour and non-tumour cells.

As SMs did not induce TNF α secretion in non-tumour derived cells, I sought to mimic the TNF α -rich, inflammatory microenvironment often present in tumours, through addition of exogenous TNF α . TNF α is important as its ligation of TNFR1 results in formation of Complex I which, upon cIAP1 depletion, results in cell death in certain tumour cells²²². As I have demonstrated that SMs target cIAP1 in non-tumour cells, the next question was do they induce cell death in the presence of TNF α in non-tumour cells? There is currently very limited research investigating this, with only one paper directly investigating this to my knowledge; incidentally, no cell death was reported³⁶. I therefore sought to look into this further, and hypothesised that there would be no induction of cell death in line with this previously published work³⁶. I used a range of physiologically relevant TNF α concentrations to mimic inflammation *in situ*. As BV6 has not advanced to clinical trials, I decided to continue this study with the clinically relevant SMs. Co-treatment of TNF α with AT-406, GDC-0152 and TL-32711 did not promote cell death in any of the non-tumour cells. It is currently unknown why there was no cell death. One hypothesis is that, as these cells are not reliant on the TNF α /NF- κ B pathway for survival, modulation of this pathway is not lethal.

However, another hypothesis may be that these non-tumour cells are not capable of undergoing Complex II-mediated cell death. As this is the primary mechanism by which SMs induce death, it would render these cells of no use as an *in vitro* model for SM-induced toxicity. To test this hypothesis, I treated MCF-10A, B-13 and B-13/H cells with species-specific TNF α to see if they had the capability to form a functional Complex I. Interestingly, while MCF-10A were able to form this complex, the B-13 and B-13/H cells were not as shown by a lack of p65 nuclear translocation, despite the B-13 cells expressing TNFR1. To investigate whether these cells could form the death-inducing Complex II, I treated non-tumour cells with TNF α and CHX which is the established way to induce Complex II-dependent cell death. MCF-10A cells were able to undergo Complex II-mediated cell death, whereas B-13 and B-13/H cells were not with the Biovision TNF α . To eliminate the possibility that the commercially sourced TNF α was not functional, I sourced another one from R&D. With this TNF α , I saw similar amounts of cell death induction in B-13 and B-13/H cells, compared to MCF-10A cells. It may be, therefore that B-13 and B-13/H cells require less TNFR1 engagement to activate TNF α /NF- κ B signalling. However, the distinct lack of p65 translocation with both commercial TNF α argues against this. Due to this, I decided to use MCF-10A cells as model for investigating the effects of SM in non-tumour cells *in vitro* as they can form both Complex I and II and undergo TNF α -signalling mediated cell death.

B-13 and B-13/H cells, however, do not appear to be able to form TNF α -mediated Complex I and II. It is currently unknown why these cells cannot undergo TNF α -mediated cell death. Furthermore, hepatocytes are well known to be sensitive to TNF α in combination with translation inhibitors, such as CHX²⁵⁸. To initiate effective extrinsic apoptosis, our laboratory has shown that caspase-8 forms a heterodimer with cFLIP_L, resulting in a FADD-caspase-8-cFLIP_L chain⁶. However, when there are higher levels of cFLIP_S, apoptosis is inhibited. Through collaboration with the group at Newcastle, I had access to the entire genome of B-13 cells. Interestingly, I found that *cflar*, which encodes for the protein cFLIP_L or cFLIP_S²⁵⁹, was mutated, possibly resulting in expression of either cFLIP_S or no protein at all. To test this, I probed for cFLIP_L and cFLIP_S, using human and mouse samples as positive controls. However,

the cFLIP_L band for the mouse and rat samples appeared to be of a lower molecular weight compared to the human sample, despite being predicted to be the same size. Furthermore, I could not detect a band where cFLIP_S is predicted to be in any of the samples. While these data need further investigation, it may mean that the mutation in *cflar* results in complete ablation of cFLIP expression in B-13 and B-13/H cells, thereby inhibiting cell death. This could explain why I did not see significant amounts of cell death in either of these cells with any of the treatments. However, this does not explain why these two cell lines were unable to undergo p65 nuclear translocation when challenged with TNF α . To investigate whether the inability of B-13 and B-13/H cells to undergo TNF α -mediated p65 translocation was a result of a mutation in genes associated with TNF α -mediated signalling, I analysed a repertoire of genes related to TNF α /NF- κ B signalling. Of the genes searched, there were no mutations in any of the genes that regulated TNF α -induced p65 translocation, suggesting the B-13 cells have all the appropriate machinery. One hypothesis was that both the recombinant TNF α proteins purchased were defective, therefore not promoting signalling through TNFR1. However, using MEFs as a positive control, I found that the commercially available R&D rat TNF α was indeed able to induce p65 nuclear translocation. The reason I used MEFs and not another rat cell line is that MEFs are widely available and, according to the datasheets for the TNF α sources, the companies used mouse cells lines to validate the recombinant TNF α proteins' activity. It may have been possible to perform an immunoprecipitation to determine if Complex I was being formed. However, due to the lack of available antibodies for rat proteins I was unable to investigate this further. As such, I do not know why B-13 and B-13/H cells do not have a functional TNF α /NF- κ B signalling axis. It may be there is some form of epigenetic regulation of the genes involved in TNF α signalling, such as promoter methylation, miRNA regulation or histone modifications, but without further investigation, this hypothesis cannot be confirmed or refuted.

However, it was still unknown why MCF-10A cells were resistant to TNF α in combination with SMs. To further investigate this, I optimised a knockdown of MIB2 which is also involved in the regulation of TNF α -mediated signalling through its E3 ligase activity²⁶⁰. However, due to time constraints I was unable

to pursue this line of investigation. As TNF α -regulated cell fate is well established to be dependent on the ubiquitination status of RIP1^{77,218,261–264}, another potential mechanism of resistance of the MCF-10A cells is expression of cIAP2. Indeed, there are many reports demonstrating that its expression status also determines TNF α -signalling outcome^{218,261,265}. A report from Petersen *et al*, found that in cancer cells previously resistant to SMs in combination with TNF α , cIAP2 depletion rendered these cells sensitive to this treatment⁴⁴. Additionally, there is evidence an E3 ubiquitin ligase, Pellino3, can target RIP1 for ubiquitination, thereby inhibiting TNF α -induced cell death. It would be interesting to see if knockdown of MIB2 either alone or in combination with IAP2 and/or Pellino3 knockdown would sensitise MCF-10A cells to SMs in combination with TNF α .

In summary, while B-13 and B-13/H cells express high levels of TNFR1 on the surface, they were unable to form TNF α -induced Complex I as inferred by a lack of p65 nuclear translocation. As Complex II proceeds Complex I, it follows that these cells cannot also undergo Complex II-mediated cell death. As such, it was decided not to proceed with B-13 and B-13/H cells as an *in vitro* model for investigating SM-mediated hepatotoxicity. Conversely, MCF-10A cells exhibit the ability to form Complex I, as shown by translocation of p65 from the cytosol to the nucleus; they can also undergo Complex II-dependent cell death. This is important as it is the primary cell death pathway for SMs. This makes MCF-10A cells a valid model for investigating the adverse effects of SMs in non-tumour cells.

4.1.4. Future work

As this is one of the first projects directly investigating the resistance mechanisms of non-tumour cells to SMs, there are still many questions to be answered. Firstly, I have still not determined the lowest concentration at which SMs induce cIAP1 depletion in non-tumour cells. This would easily be answered by an expanded concentration range similar to the one in Chapter 3. Secondly, I found that MCF-10A cells did not secrete TNF α at levels detectable by ELISA. There are many steps which may regulate this, and trying to determine which

process is behind this would be of interest. Thirdly, the flow cytometry data suggested that it was mainly apoptotic cell death induced by BV6 in MCF-10A cells. However, it would be useful to confirm this by treating these cells with zVAD and NSA alone and in combination with BV6. Fourthly, I found that B-13 and B-13/H cells do not have a functional Complex I or II. Trying to determine the mechanisms would be very important as it be there are unsuitable for use as an *in vitro* model for hepatotoxicity. Lastly, I had optimised a knockdown of the E3 ligase, MIB2, reported to sensitise both tumour and non-tumour cells to TNF α and SM-induced cell death²⁶⁰. I would like to confirm whether this phenotype would be replicated in MCF-10A cells. If not, then there are two other targets which are reported to sensitise cell to TNF α -mediated cell death, cIAP2 and Pellino 3^{44,266}. Knockdown of these proteins, either singularly or together, could elucidate the resistance mechanisms of the MCF-10A cells to TNF α and SM-induced cell death.

Chapter 5

Investigating the potential hepatotoxicity induced by TL-32711 *in vivo*

5. INVESTIGATING THE POTENTIAL HEPATOTOXICITY INDUCED BY TL-32711 *IN VIVO*

Introduction

In vitro models of toxicity have many limitations, one significant aspect being that there is currently a lack of physiologically-relevant models for hepatotoxicity. There are several reasons for this; there is a mixed cell population in the liver, there is a highly regulated microenvironment, and there are a very limited number of models in which cells express *in situ* levels of the xenobiotic metabolising enzymes. As such, the most representative model for studying human hepatotoxicity is the use of animals, most commonly rats and mice. Liver injury results in activation of the NF- κ B pathway and secretion of TNF α in an effort to simulate liver regeneration²⁶⁷. A group from Norway developed a strain of mice using luciferase as a reporter gene for NF- κ B activation, which allowed for real-time, live, *in vivo* imaging of the NF- κ B pathway through-out the whole mouse²¹³. This is a powerful model as it allows for spatial and temporal analysis of the NF- κ B pathway without having to cull the mouse, allowing for a significant reduction in the number of animals used. As SMs convert the TNF α /NF- κ B pathway from pro-survival to pro-death, it may be that, if SMs were to be administered in a situation of liver damage, this may result in significant liver toxicity. While SMs have undergone significant *in vivo* pre-clinical testing, there is currently no research directly investigating hepatotoxicity. As such, I sought to determine the effect of the most advanced SM compound, TL-32711, under conditions of acute liver injury induced by ANIT (α -Naphthylisothiocyanate) or CCl₄ (Carbon Tetrachloride). I hypothesised that TL-32711 would exacerbate liver damage induced by these two classic hepatotoxins known to induce TNF α secretion.

***In vivo* pilot to determine optimum TL-32711 dose**

Before I undertook the main study, I sought to determine at what concentration TL-32711 could be used *in vivo* without significant systemic toxicity and

hepatotoxicity. To maintain the clinical relevance of this study, Prof. Wright dosed mice^{WT} from the C57BL/6J background in a classic chemotherapy regime, i.e. daily for five days. Mice^{WT} were therefore dosed once a day for five days with either VC (vehicle control) or 5, 10, 20 or 30 mg/kg TL-32711 with three mice per group. The study was then terminated on day five and blood was extracted for determination of serum markers of liver damage. The liver was also collected fixed in formaldehyde or snap frozen for examination via histology and western blotting, respectively. Mice^{WT} showed no overt systemic toxicity or hepatotoxicity induced by TL-32711, although a slight drop in body weight was seen at 30 mg/kg TL-32711 compared to VC (**Figure 5.1**). To determine the effect of TL-32711 as single agent on liver function and cholestasis, alanine aminotransferase (ALT) and alkaline phosphatase (ALP) levels were measured, respectively. While there was a mean increase in ALT levels at 20 mg/kg (0.9-fold) and 30 mg/kg TL-32711 (0.8-fold), this was not statistically significant. ALP levels were also unchanged, further demonstrating a lack of hepatocellular injury (**Figure 5.1**).

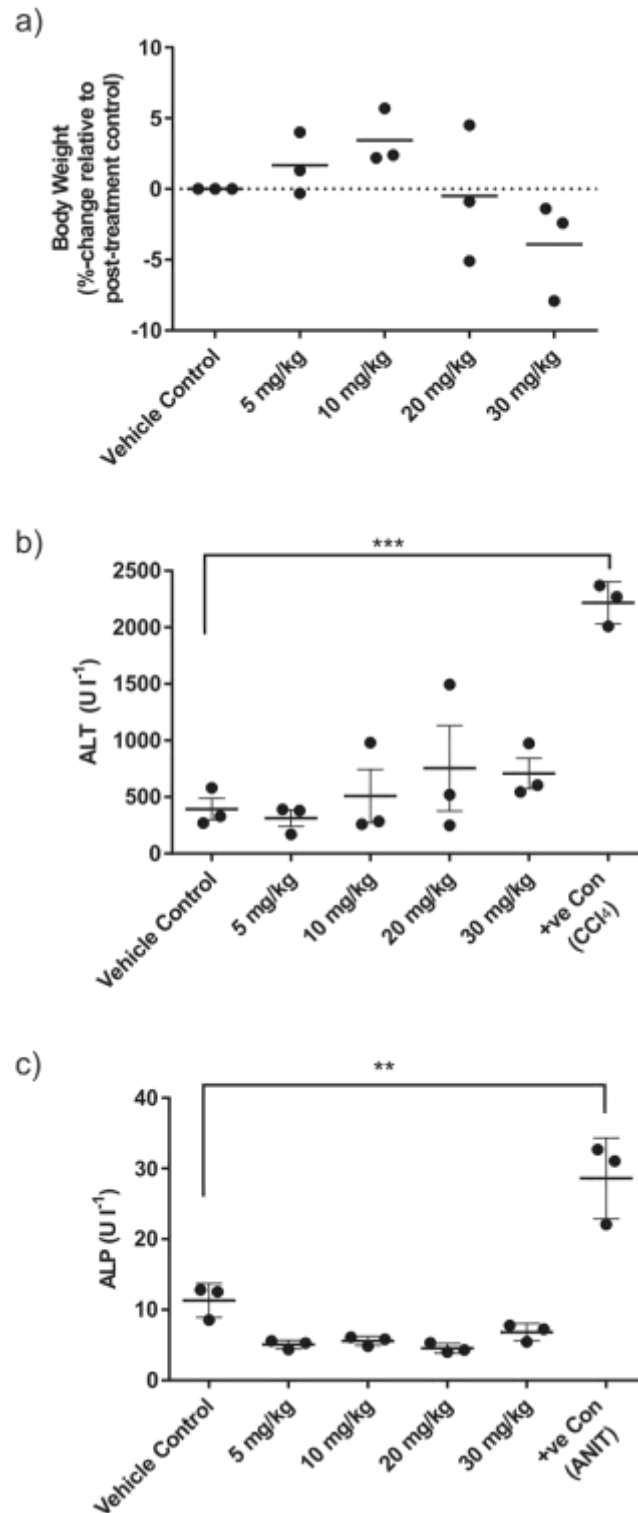


Figure 5.1 | TL-32711 does not induce increases in ALT or ALP. **a)** Body weights were measured pre-and post-treatment and shown by % change in each animal; **b)** ALT and **c)** ALP were determined using colorimetric assays from Abcam in Newcastle. Bars represent mean. ANOVAs were used for statistical analysis; significance values, ** <0.01, *** <0.005.

H&E staining and the pathology report provided by colleagues in Newcastle and the LRI demonstrated sinusoidal enlargement and scattered apoptosis at higher doses, and, at 30 mg/kg, limited focal and zonal necrosis were evident (**Figure 5.2**). To determine whether cells were undergoing apoptosis, I stained sections with cleaved caspase-3 (cC3) and cleaved PARP (cPARP). An increase in cC3 and cPARP in mice^{WT} dosed with TL-32711 at 20 and 30 mg/kg was observed, demonstrating TL-32711 induces scattered apoptosis as a single agent (**Figure 5.6, 5.7, 5.8 and 5.9**). H&E staining also demonstrated a dose-dependent increase in the number of small, interstitial cells following TL-32711 treatment and occasional small focal aggregates of these cells (**Figure 5.2**). The cells appeared to be infiltrating inflammatory cells, or fibrogenic hepatic stellate cells (HSCs) which negatively regulate hepatocyte regeneration²⁶⁸. To determine the nature of these cells, I stained for a variety of cells known to reside in the liver, including HSCs, lymphocytes, macrophages and neutrophils (data not shown), and found the cell population to be primarily made up of Kupffer cells, the resident liver macrophages (**Figure 5.4 and 5.5**).

These data demonstrate that at doses of up to 20 mg/kg, the bivalent SM, TL-32711, was tolerated, with limited apoptosis, minimal focal cell aggregates and only one mouse demonstrating prominent liver mitosis. However, at 30 mg/kg there was necrosis, inflammation, minimal focal round cell aggregates and prominent mitosis in the liver. I therefore chose 20 mg/kg as the optimal dose for the remaining experiments.

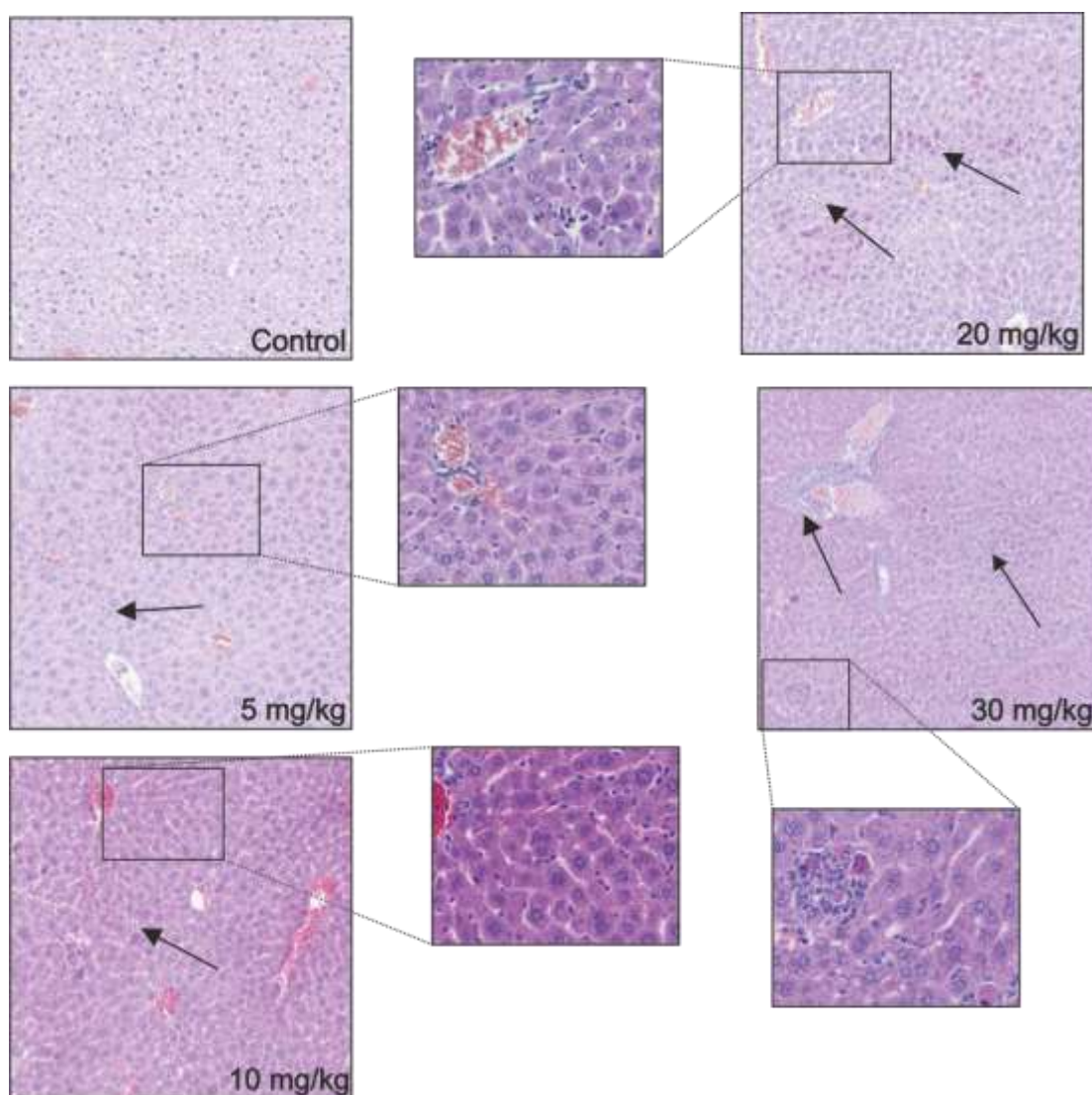


Figure 5.2 | TL-32711 induces sinusoidal enlargement, scattered apoptosis and proliferation. Sections were stained with haematoxylin and eosin using standard procedures. Arrows represent areas of interest, i.e. sinusoidal enlargement, interstitial cell aggregation. Representative image from each group.

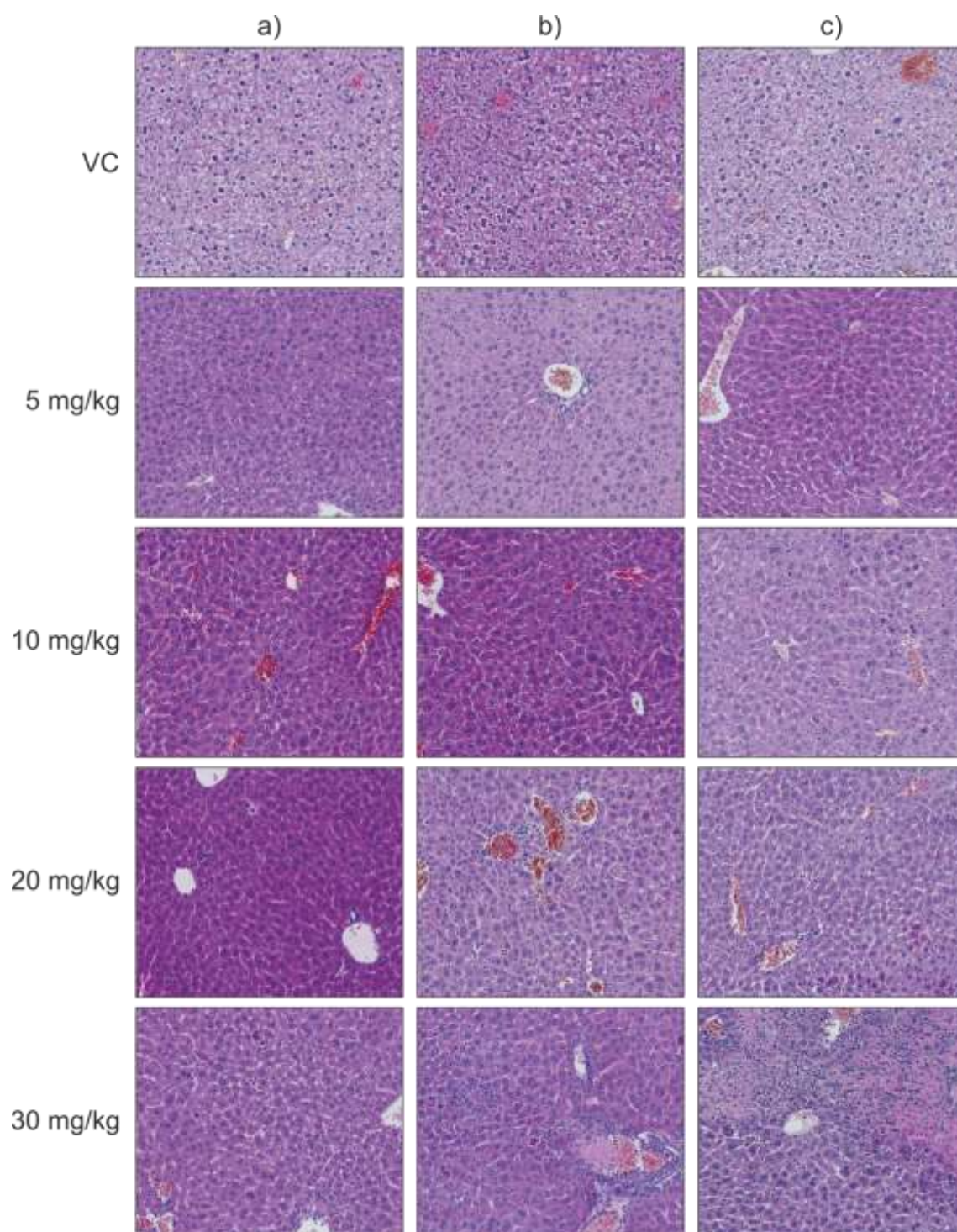


Figure 5.3 | TL-32711 induces sinusoidal enlargement, scattered apoptosis and proliferation. Sections were stained with haematoxylin and eosin using standard procedures. Images represent a liver section from each mouse.

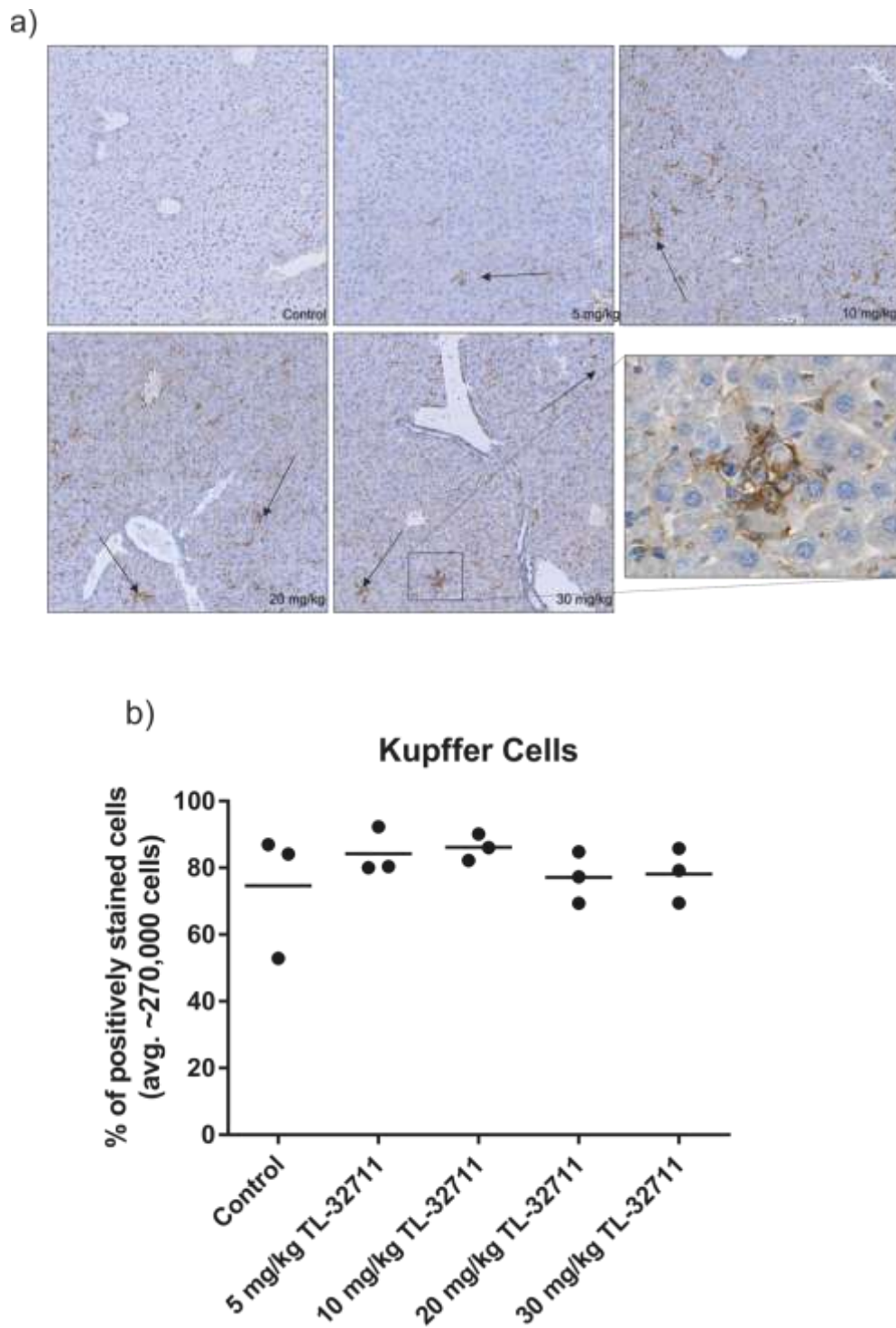


Figure 5.4 | TL-32711 induces infiltration of Kupffer Cells. a) Kupffer cells were stained with F4/80. b) The number of positively stained cells was quantified using Visiopharm software. Arrows represent areas of positive staining with F4/80. Bars represent mean. Representative image from each group.

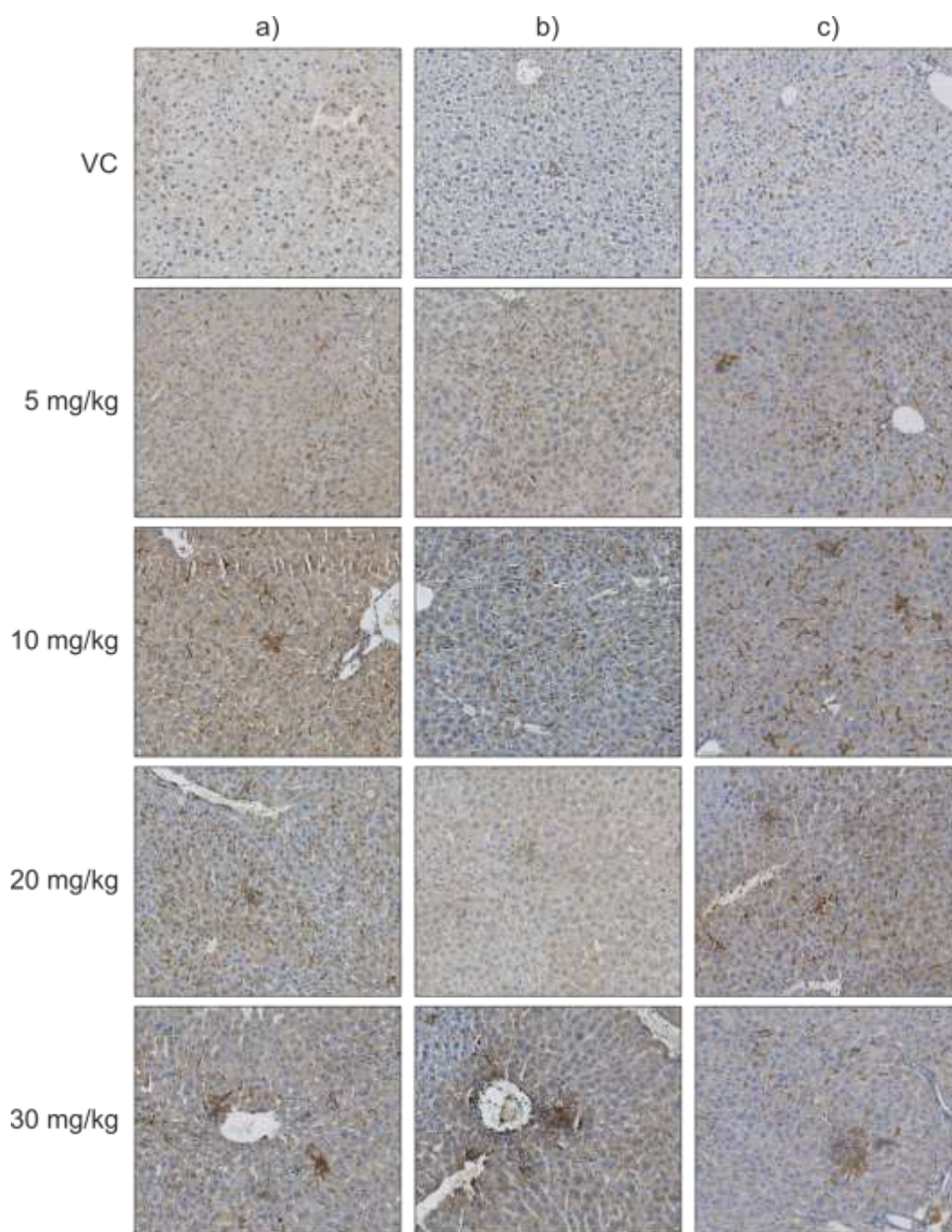


Figure 5.5 | TL-32711 induces infiltration of Kupffer Cells. Kupffer cells were stained with F4/80. Images represent a liver section from each mouse.

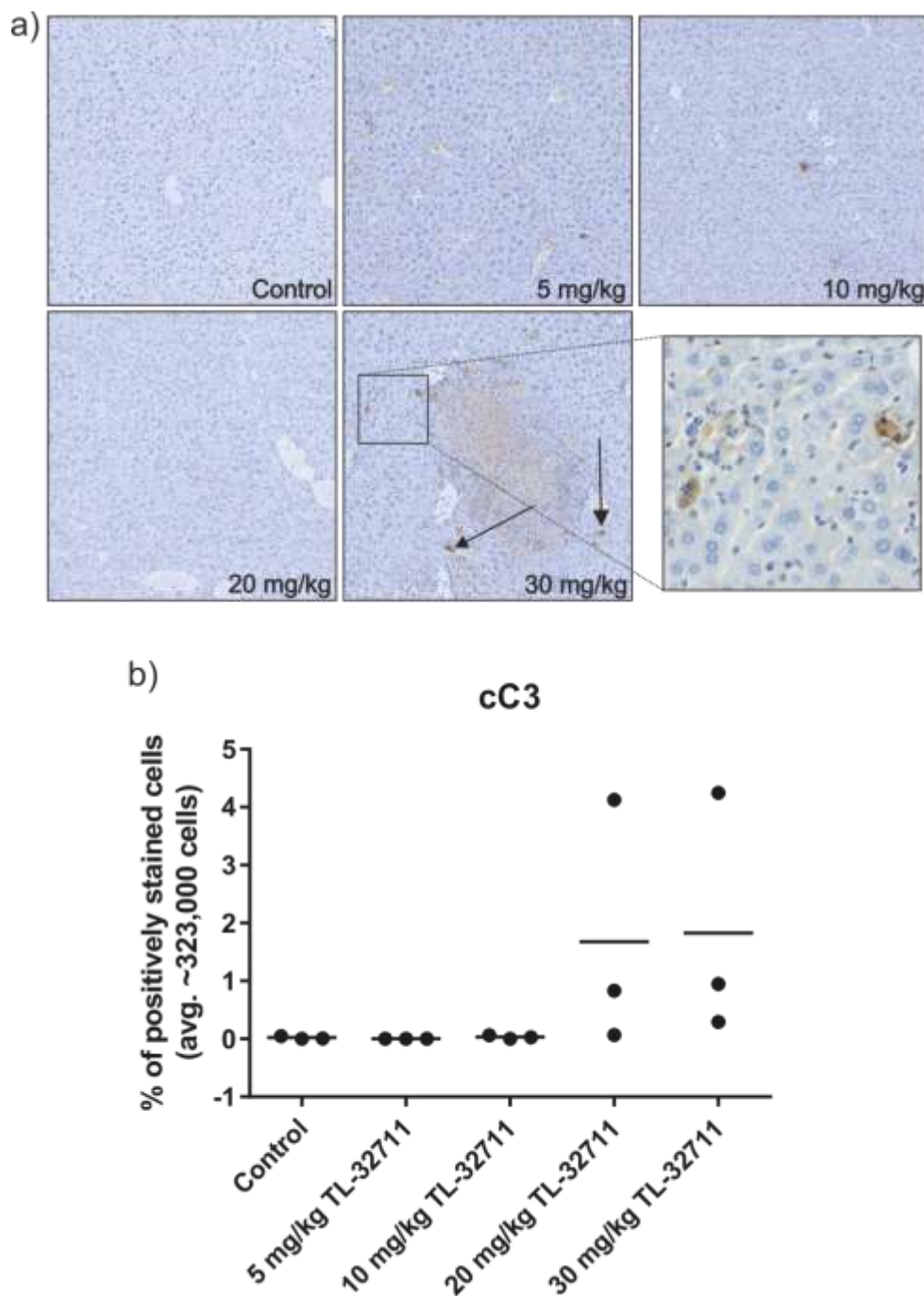


Figure 5.6 | TL-32711 induces scattered staining of cleaved C3, indicative of apoptosis. **a)** Sections were stained for cleaved C3 (cC3) using the Novolink Polymer kit. **b)** The number of positively stained cells was quantified using Visiopharm software. Arrows represent areas of positive staining with cC3. Bars represent mean. Representative image from each group.

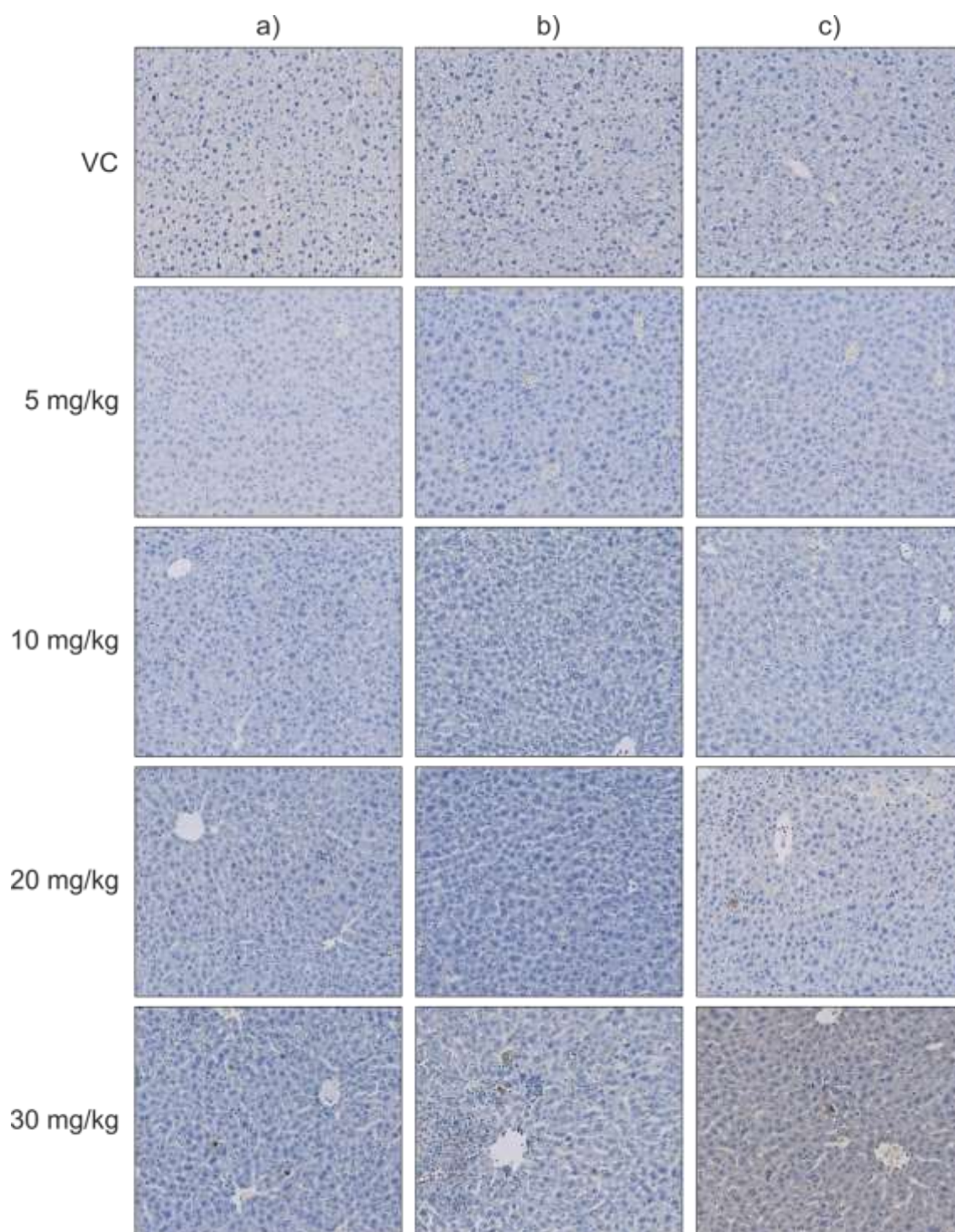


Figure 5.7 | TL-32711 induces scattered staining of cleaved C3, indicative of apoptosis. a) Sections were stained for cleaved C3 using the Novolink Polymer kit. Images represent a liver section from each mouse.

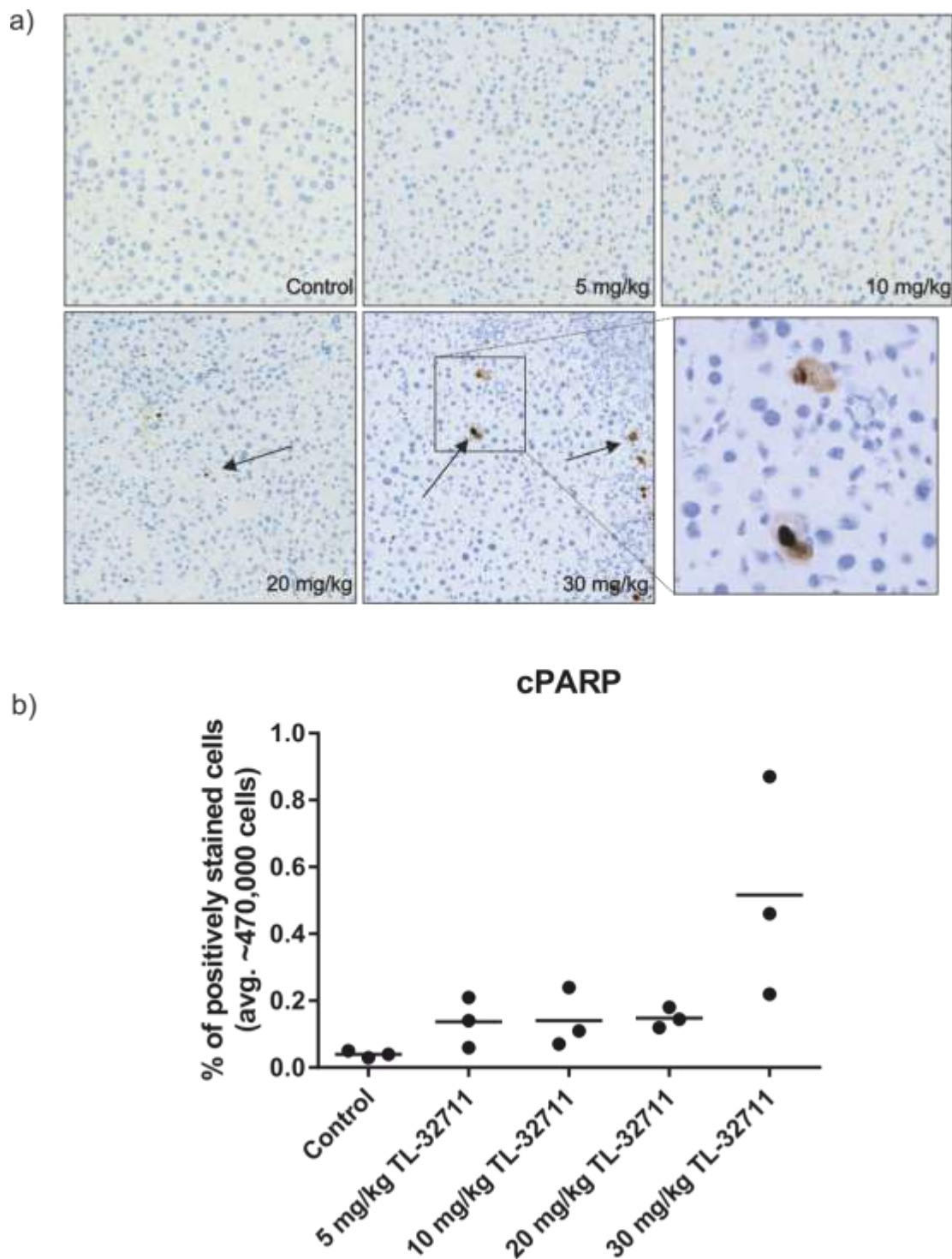


Figure 5.8 | TL-32711 induces an increase in cleaved PARP. a) Sections were stained using the DAKO Flex+ Automatic Stainer. b) The number of cleaved PARP (cPARP) positive cells was quantified using Visiopharm software. Arrows represent areas of positive staining with cPARP. Bars represent mean. Representative image from each group.

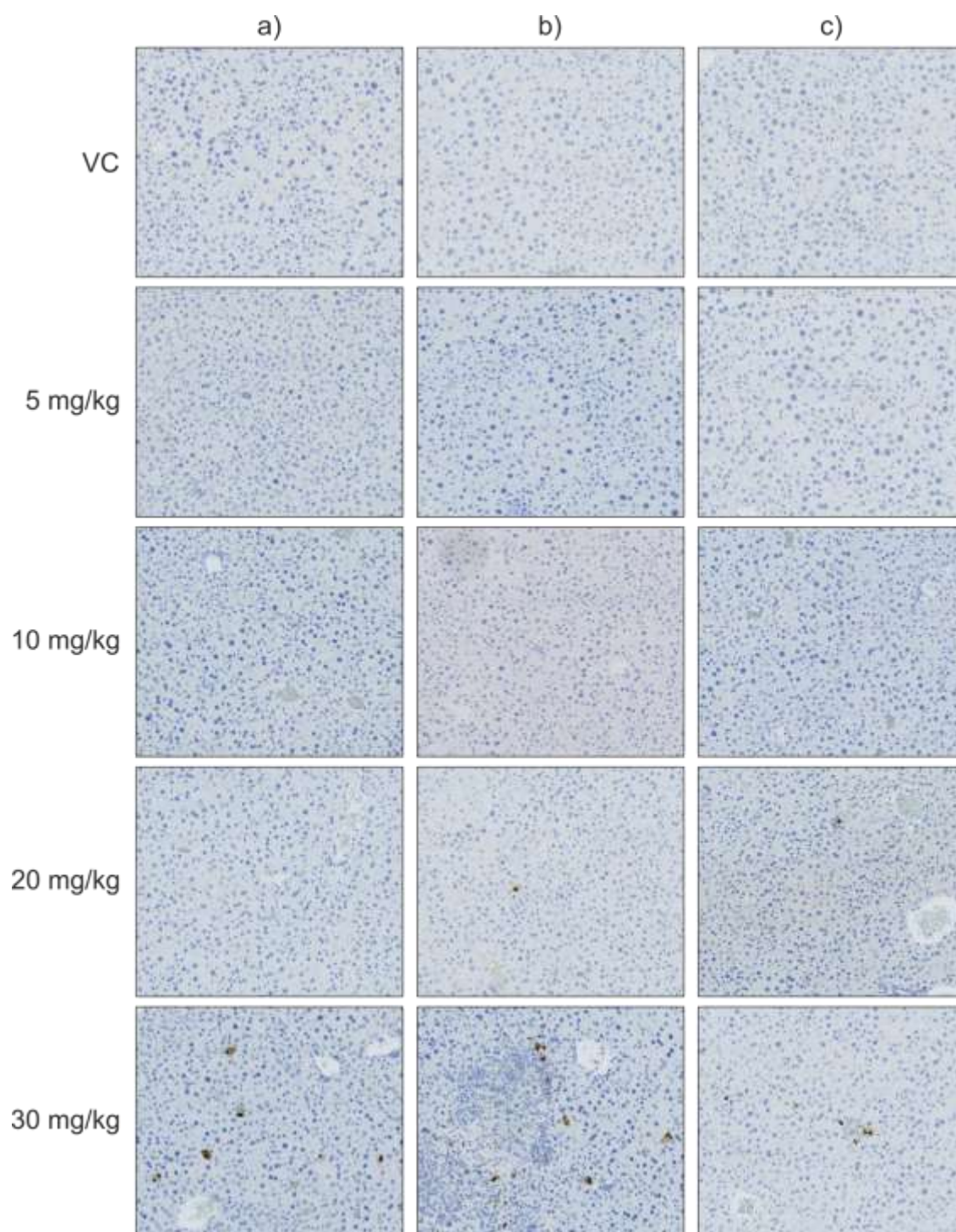


Figure 5.9 | TL-32711 induces an increase in cleaved PARP. a) Sections were stained for cleaved PARP using the DAKO Flex+ Automatic Stainer. Images represent a liver section from each mouse.

TL-32711 ameliorates liver damage induced by two classic hepatotoxins

As the liver is the main organ in first and second pass metabolism, it is unsurprising that DILI is a significant problem and one of the biggest reasons many drugs fail to make it to the market. As mentioned previously, SMs regulate the outcome of TNF α signalling, which is known to be essential in liver regeneration²⁶⁷. It is surprising therefore that there are no reports in the literature on the effect of SMs on this process. As such, I used two classic hepatotoxins ANIT and CCl₄, known to induce hepatocellular necrosis in the centrilobular and periportal regions of the lobule, respectively. To determine NF- κ B activation *in vivo*, I used mice from the C57BL/6J background expressing 3x- κ B-*luc* gene (mice^{*luc*}), which allowed for live, *in situ*, quantification of NF- κ B activity²¹³. Prof. Wright dosed mice either alone with ANIT (50 mg/kg), CCl₄ (0.5 mL [1:1 v/v with olive oil]/kg) or with one of the hepatotoxins in combination with TL-32711 (20 mg/kg) to investigate whether TL-32711 would regulate the outcome of liver injury.

5.1.1. TL-32711 prevents ANIT and CCL₄ induced hepatotoxicity

As with the pilot study, mice^{*luc*} were dosed daily for five days with TL-32711, and then on days three and four were dosed with ANIT or CCl₄, respectively. The rationale behind this dosing regime was that, as many chemotherapeutics are also hepatotoxins, I wanted to determine if TL-32711 would exacerbate liver injury caused by these hepatotoxic compounds. Body weight was reduced in all groups except VC and TL-32711 alone, with ANIT inducing the largest reduction (**Figure 5.10**). ANIT and CCl₄ demonstrated significant increases in the liver damage marker ALT, but only ANIT showed increases in ALP, a marker of bile duct insult. Remarkably however, TL-32711 in combination with either ANIT or CCl₄ resulted in decreases in the extent of ALT release to levels similar to those seen in the control. Similarly, ALP levels were reduced with TL-32711 and ANIT compared to ANIT alone (**Figure 5.10**). It should be noted that due to haemolysis, ALT and ALP were not able to be recorded for certain animals. These data are striking as it suggests that TL-32711 actually inhibits the hepatotoxicity mediated by ANIT and CCl₄.

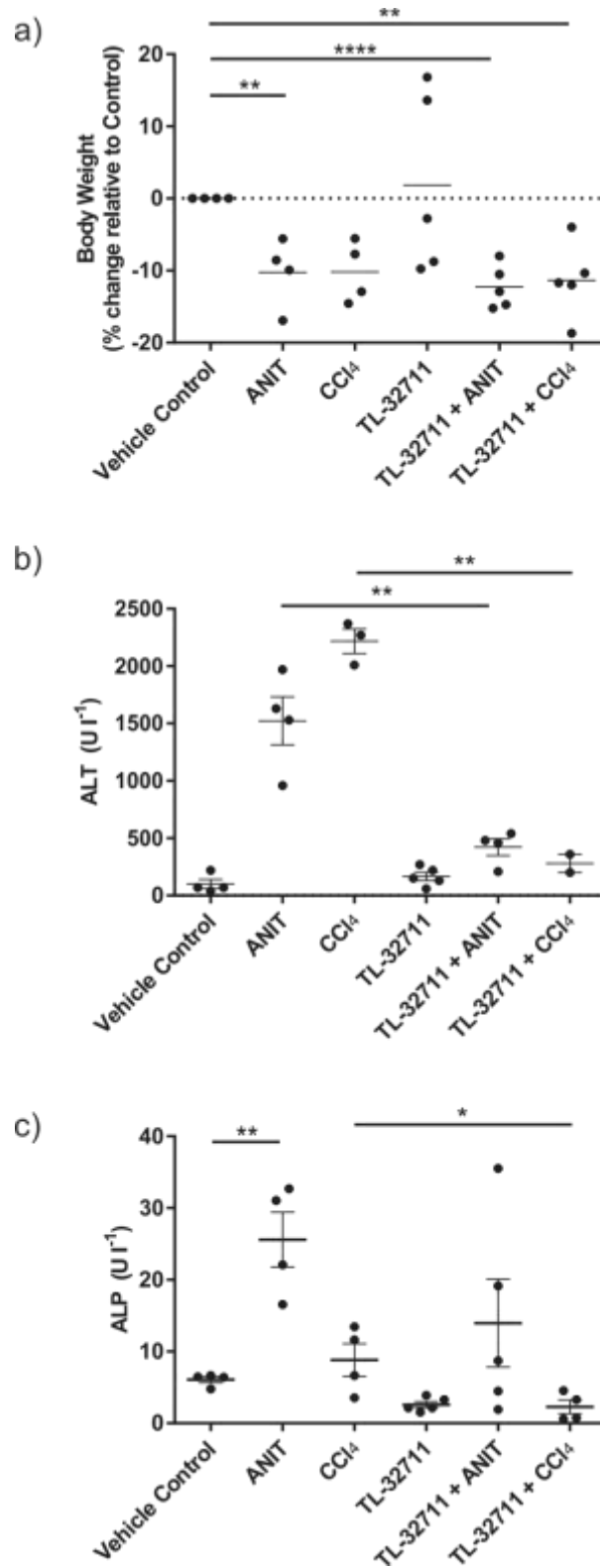


Figure 5.10 | TL-32711 protects against ANIT and CCl₄ induced hepatotoxicity. **a)** Body weights were measured pre-and post treatment and shown by % change in each animal; **b)** ALT and **c)** ALP were determined using colorimetric assays from Abcam in Newcastle. Bars represent mean. ANOVAs were used for statistical analysis; significance values, * <0.05 , ** <0.01 , **** <0.001

To further investigate this, Jenny Edwards performed H&E staining on the liver tissue. H&E analysis revealed no overt pathology with the VC or TL-32711 above that previously reported in the pilot study (**Figure 5.11 and 5.12**). ANIT and CCl₄, however, induced significant hepatotoxicity. ANIT induced mid-zonal focal necrosis and limited portal tract inflammation, and CCl₄ induced marked centrilobular necrosis. However, when these hepatotoxins were administered in mice^{luc} pre-treated with TL-32711, the amount of necrosis was markedly reduced. TL-32711 reduced ANIT-induced necrosis, which was localised to the portal zones. CCl₄-mediated necrosis was also reduced by TL-32711 with the pattern becoming more cellular and the centrilobular zones being infiltrated by inflammatory cells, indicating centrilobular degeneration (**Figure 5.11 and 5.12**).

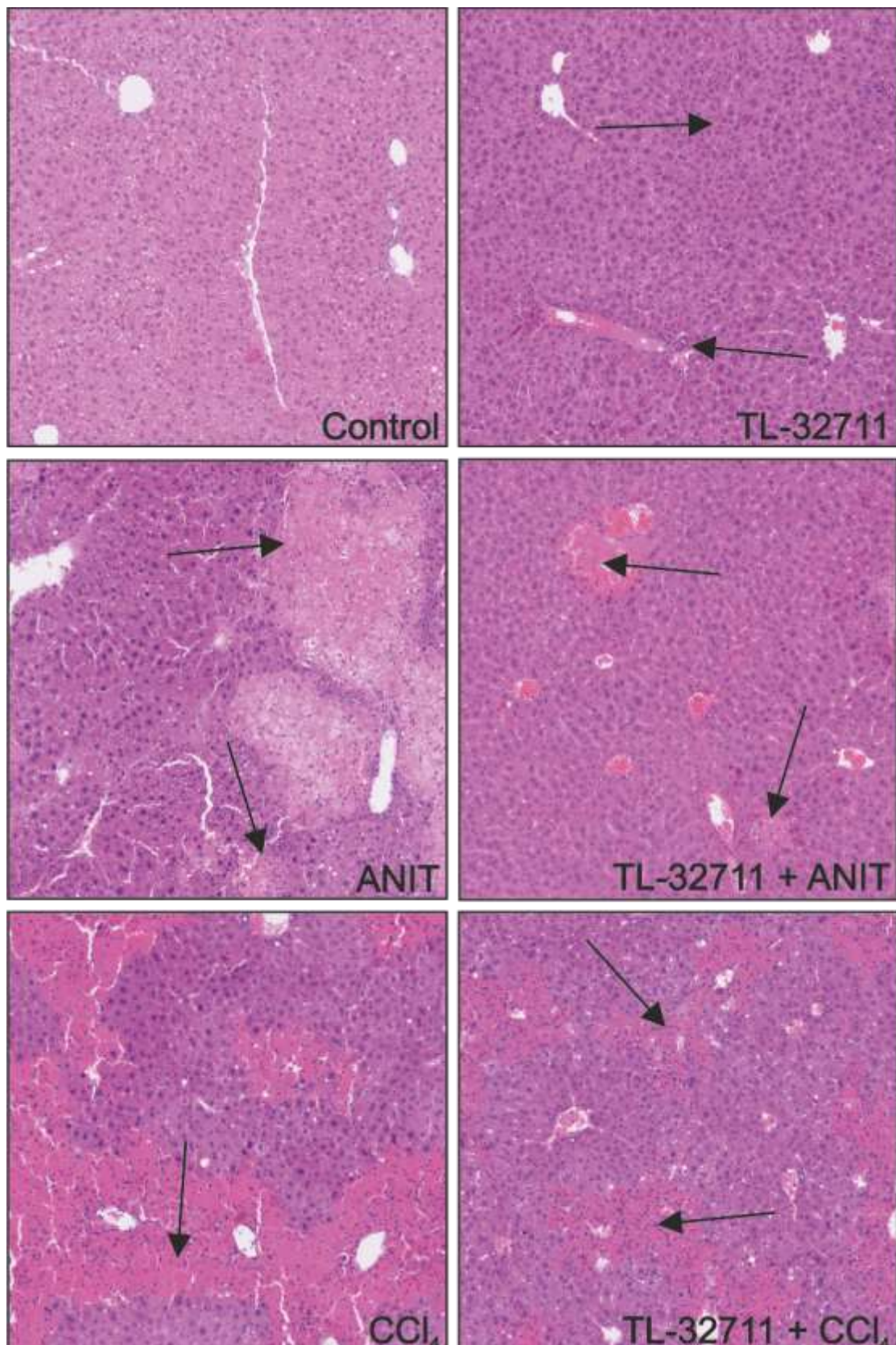


Figure 5.11 | TL-32711 ameliorates ANIT- and CCl₄-induced injury. Sections were stained with haematoxylin and eosin using standard procedures. Arrows represent areas of interest, i.e. necrosis, interstitial cell aggregation. Representative image from each group.

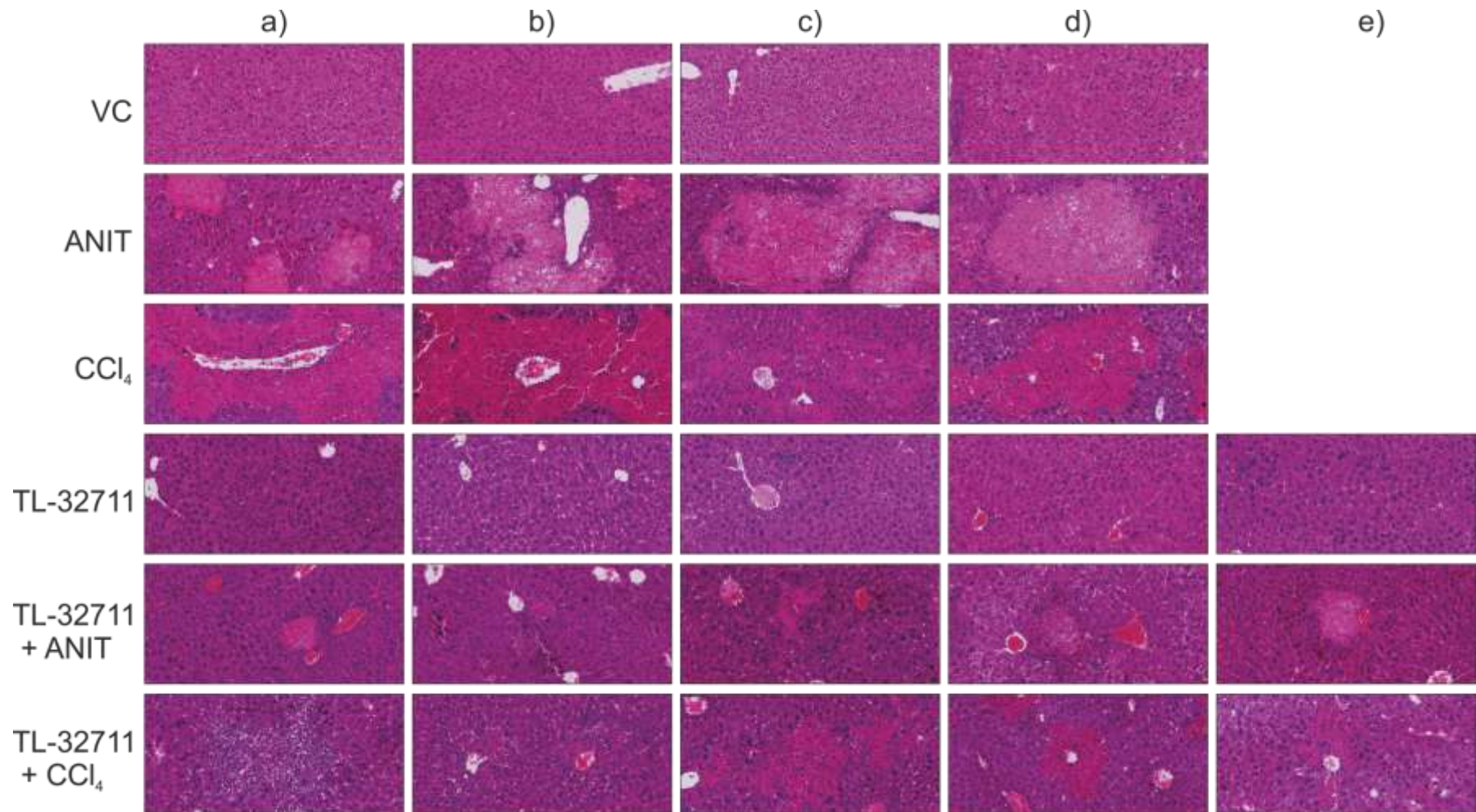


Figure 5.12 | TL-32711 ameliorates ANIT- and CCl₄-induced injury. Sections were stained with haematoxylin and eosin using standard procedures. Images represent a liver section from each mouse.

5.1.2. TL-32711 promotes NF- κ B activity and Kupffer cell recruitment

Using the In Vivo Imaging System (IVIS), Dr Probert and I were able to quantify NF- κ B activation induced by TL-32711 and the known hepatotoxins. Control mice^{luc} displayed minimal NF- κ B activation, and CCl₄ also induced minimal NF- κ B activity, with just a 5-fold increase. ANIT induced a 32-fold increase in NF- κ B activation, whereas TL-32711 induced an 83-fold increase compared to the control (**Figure 5.13**). In the TL-32711 in combination with ANIT, one mouse had to undergo early Schedule 1 as it was moribund. Interestingly, this activation appeared to be almost exclusively localised to the upper abdominal region. However, perhaps even more significantly, ANIT appeared to actually reduce TL-32711-induced NF- κ B activity by 37% compared to TL-32711 alone. CCl₄, however, had no effect on TL-32711-induced NF- κ B activation, despite there being a reduction in liver injury (**Figure 5.13**). Importantly, the NF- κ B activity induced by TL-32711 on day three, prior to mice^{luc} being dosed with ANIT or CCl₄, revealed no difference in NF- κ B activity to day five in TL-32711 only conditions, suggesting NF- κ B activity plateaus before this time point. Therefore, to further investigate the temporal and spatial activation of the NF- κ B signal, a single mouse^{luc} was dosed with 20 mg/kg TL-32711 and the NF- κ B signal was measured at 0.5 h, 1, 2, 4, 8, 12 and 24 h. The mouse was then culled and the organs removed to determine in which tissue NF- κ B was activated. While limited conclusions can be drawn from a single mouse, it appeared that NF- κ B activity began at 4-8 h and, fascinatingly, was localised almost exclusively to the liver (**Figure 5.14**).

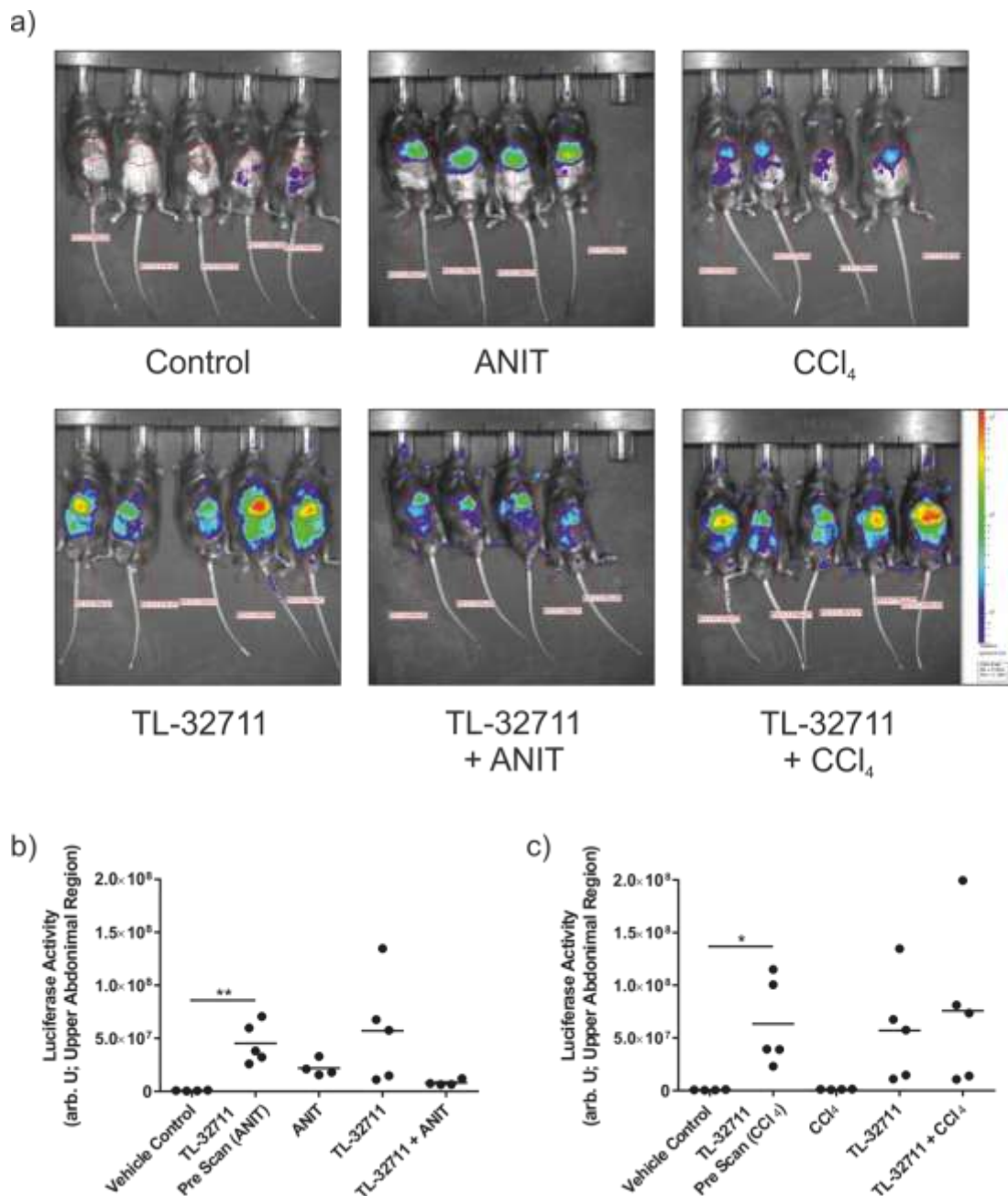


Figure 5.13 | TL-32711-induced NF- κ B activation differentially correlates with its hepatoprotective properties. a) Mice^{luc} were injected with β -Luciferin, anaesthetised and placed in a light-sealed chamber, where luciferase activity was quantified, and were then culled at a later time on the same day. b+c) Mice^{luc} were also scanned before being dosed with ANIT or CCl₄ (pre-scan). Bars represent mean. Paired t-tests were used for statistical analysis; significance values, * <0.05 , ** <0.01 .

Investigating the potential hepatotoxicity induced by TL-32711 *in vivo*

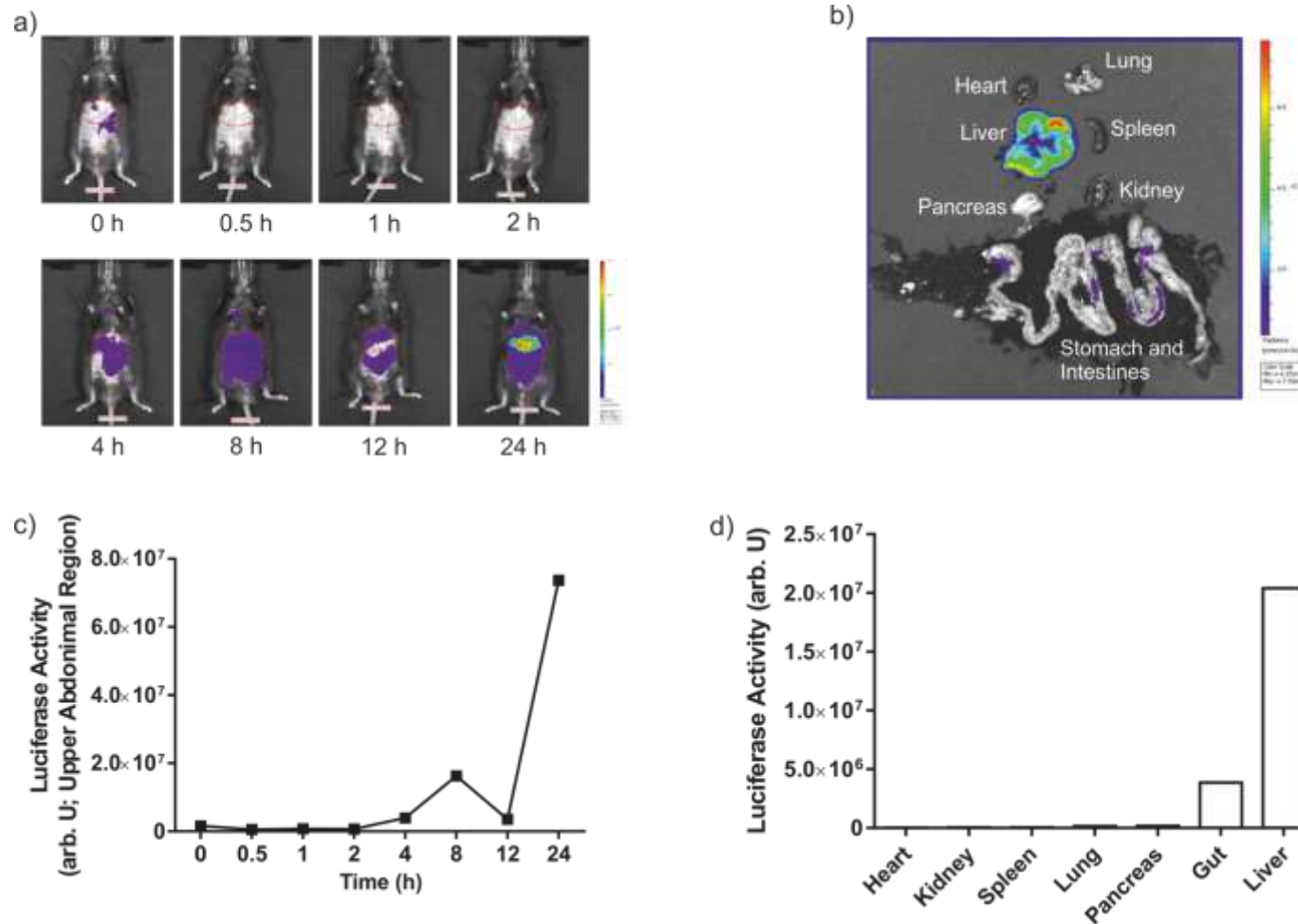


Figure 5.14 | TL-32711 activates the NF-κB pathway within 4-8 h, which is localised predominantly to the liver. a) A single mouse^{luc} was dosed with 20 mg/kg TL-32711 and NF-κB activity measured at the indicated time points using the In Vivo Imaging System, **b)** after culling the mouse^{luc}, the organs were then excised and scanned at 24 h.

While the ability to quantify NF- κ B activity is indeed useful as an insight into TL-32711's activity *in situ*, it should be noted that this only gives an indication of NF- κ B activity and not inflammation *per se*. To investigate inflammation, I stained liver sections with F4/80 to measure Kupffer cells, as with the pilot study, and with NIMP, a neutrophil marker. As neutrophils are known to drive ANIT-mediated hepatotoxicity¹⁹⁵, I sought to determine if TL-32711 prevented ANIT driven hepatotoxicity by a reduction in neutrophil recruitment. There was a marked increase in F4/80 positive cells in TL-32711 only and TL-32711 in combination with CCl₄ (**Figure 5.15 and 5.16**). Interestingly, this appeared to be closely correlated to NF- κ B activation as determined by the IVIS, further suggesting that it is indeed the Kupffer cells that mediate the NF- κ B signal seen in mice^{luc} dosed with TL-32711. In ANIT and CCl₄, with or without TL-32711 pre-treatment, the Kupffer cells appeared to be localised to the areas of damage. Although it was interesting to note there was significantly more Kupffer cells in the TL-32711 with CCl₄ dosed mice^{luc} compared to ANIT with TL-32711 (**Figure 5.15 and 5.16**). As expected there was a significant increase in the number of neutrophils with ANIT treated mice^{luc}. However, there was also a smaller, but still significant, increase in these cells in CCl₄ treated mice. When ANIT was co-treated with TL-32711, there was a reduction in neutrophils infiltration compared to ANIT alone, but no change in neutrophil numbers was seen in mice^{luc} treated with CCl₄ vs. TL-32711 in combination with CCl₄ (**Figure 5.17 and 5.18**). One mouse in the TL-32711 only group was removed due to high background.

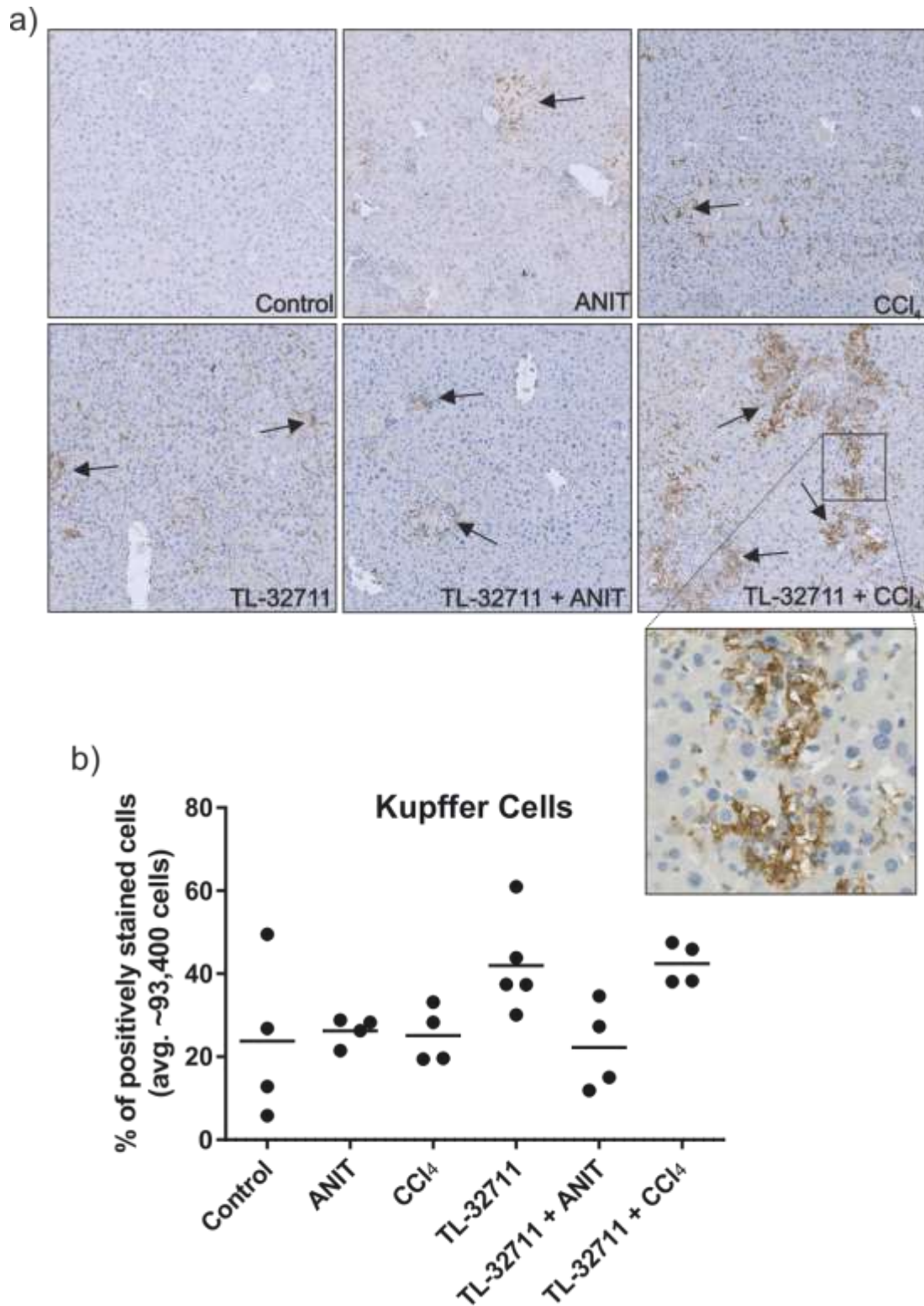


Figure 5.15 | TL-32711 results in increases in Kupffer cell number. a) Sections were kindly stained with F4/80 to detect Kupffer cells by Stephanie Meyer from Newcastle University, using the Vector ABC kit. b) The number of F4/80 positive cells was quantified using Visiopharm software. Arrows represent areas of positive staining. Bars represent mean. Representative image from each group.

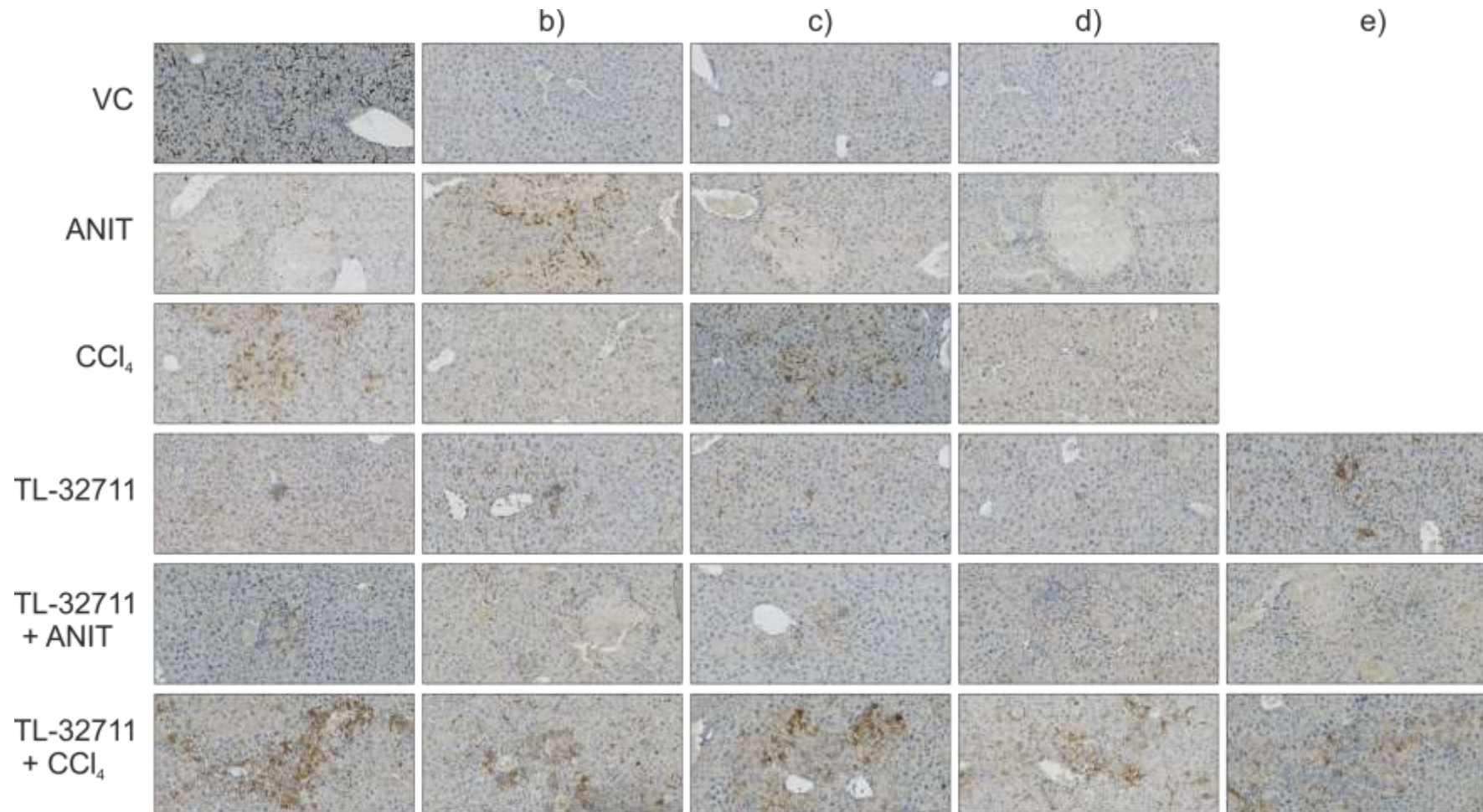


Figure 5.16 | TL-32711 results in increases in Kupffer cell number. a) Sections were kindly stained with F4/80 to detect Kupffer cells by Stephanie Meyer from Newcastle University, using the Vector ABC kit. Images represent a liver section from each mouse.

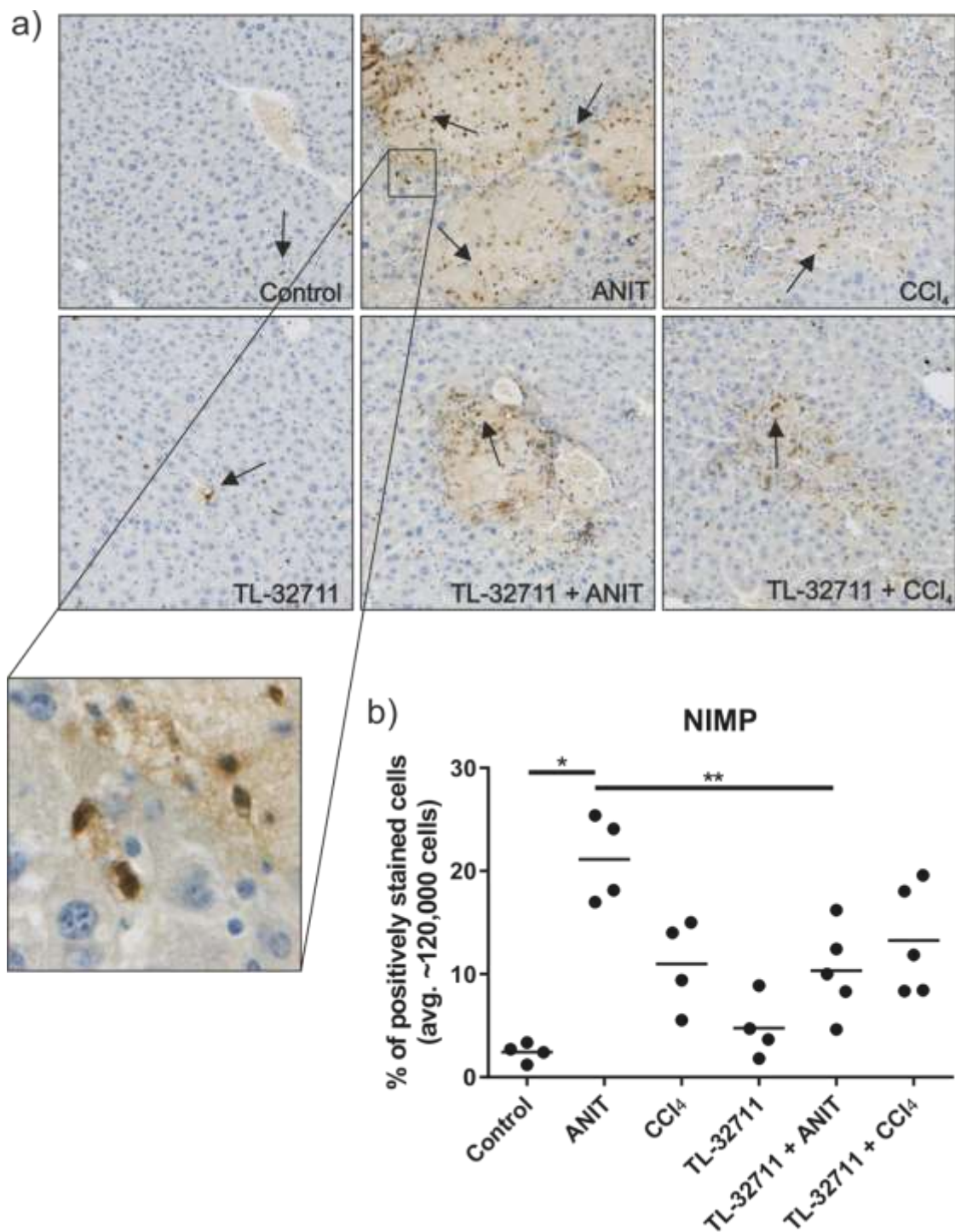


Figure 5.17 | TL-32711 reduces ANIT-induced Neutrophil infiltration. a) Sections were stained using the Vector ABC kit. b) Quantification of the number of neutrophils was performed using Visiopharm. Paired t-tests were used for statistical analysis; significance values, * <0.05 , ** <0.01 . Arrows represent areas of positive staining. Bars represent mean. Representative image from each group.

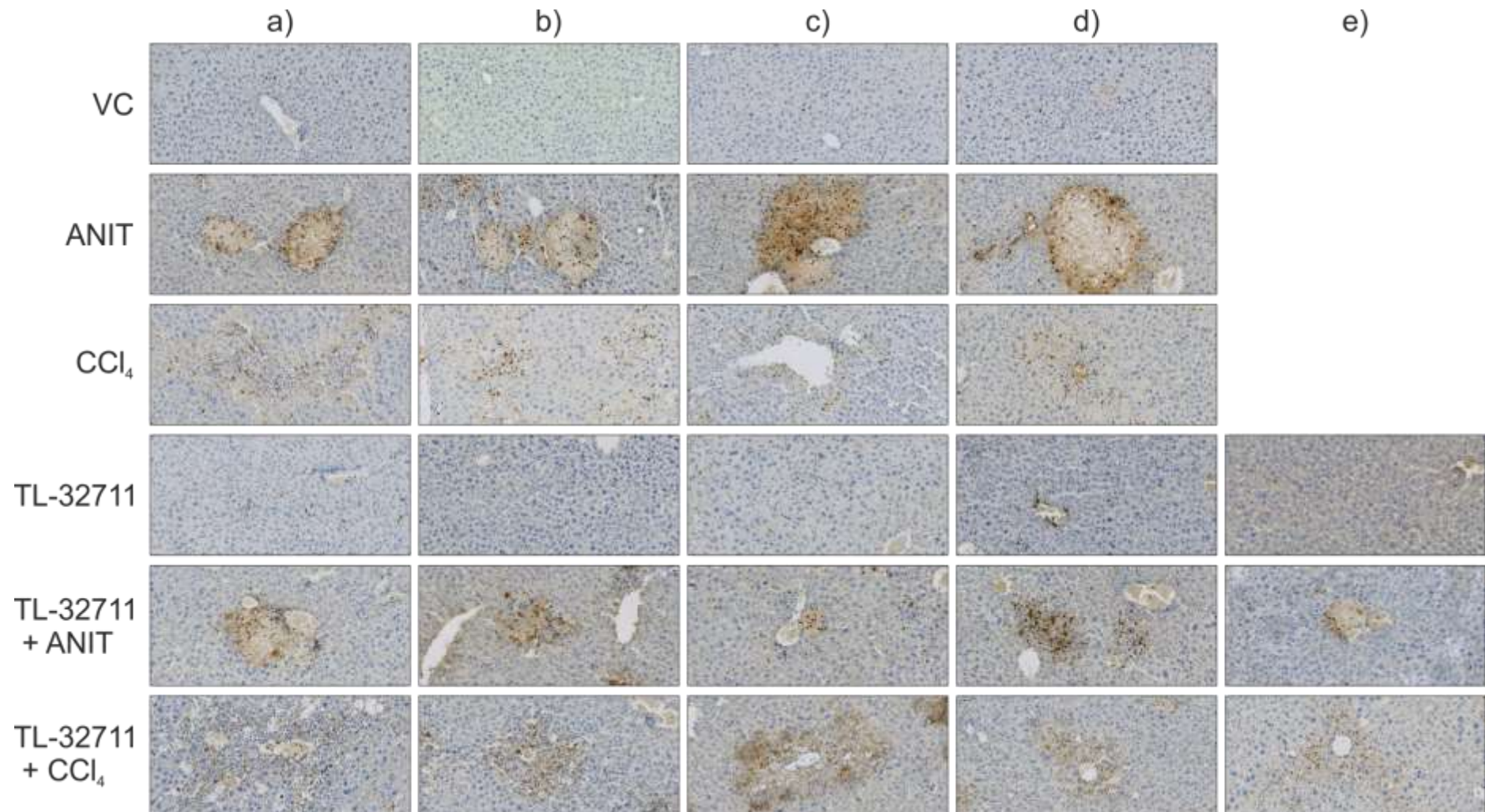


Figure 5.18 | TL-32711 reduces ANIT-induced Neutrophil infiltration. Sections were stained using the Vector ABC kit. Images represent a liver section from each mouse.

5.1.3. TL-32711 promotes proliferation and apoptosis simultaneously

As TNF α signalling regulates many genes associated with proliferation, I sought to determine if TL-32711 promoted hepatocyte proliferation, something observed in the histopathology report provided by colleagues at the Leicester Royal Infirmary. To confirm this, I stained liver sections with Ki-67, a marker of proliferation. Only sections dosed with TL-32711 as a single agent showed an increase in proliferation above control mice^{luc} (**Figure 5.19 and 5.20**). Interestingly, there also appeared to be a number of interstitial cells, likely Kupffer cells, which were Ki-67 positive present in the combination treatments. It may be, therefore, that TL-32711 promotes Kupffer cell proliferation as a protective mechanism. In the pilot study, TL-32711 induced scattered apoptosis. As such, I sought to determine whether TL-32711 exerted its protective effects by priming cells for apoptosis. Liver sections were stained from all groups with cPARP. Interestingly, I found that in all groups treated with TL-32711, there was a significant increase in cPARP (**Figure 5.21 and 5.22**).

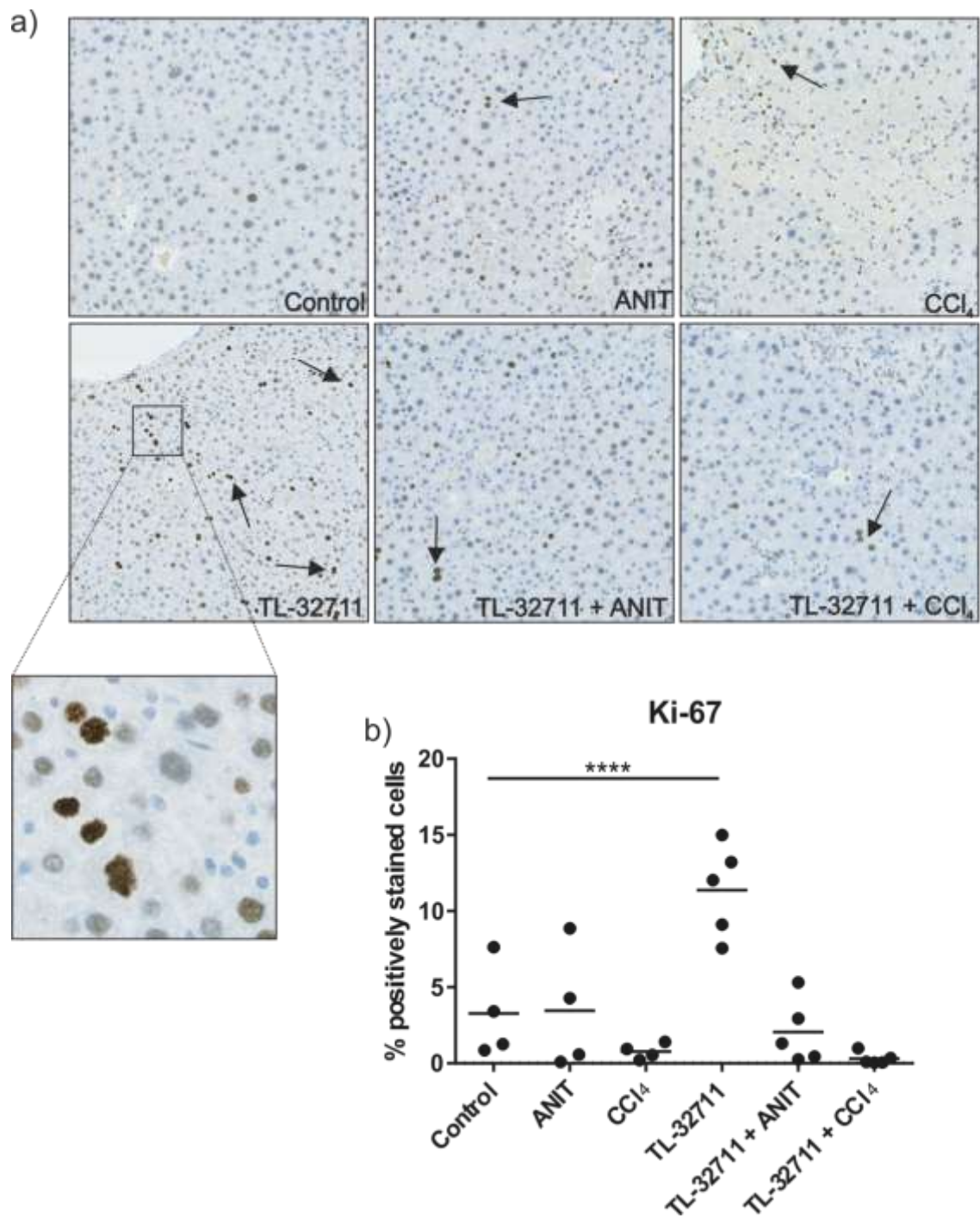


Figure 5.19 | TL-32711 induces proliferation as a single agent. **a)** Sections were stained for Ki-67 using the DAKO FLEX+ Autostainer. **b)** Quantification of the number of proliferating cells was performed using Visiopharm. Paired t-tests were used for statistical analysis; significance values, ****<0.001. Arrows represent areas of positive staining for Ki-67. Bars represent mean.

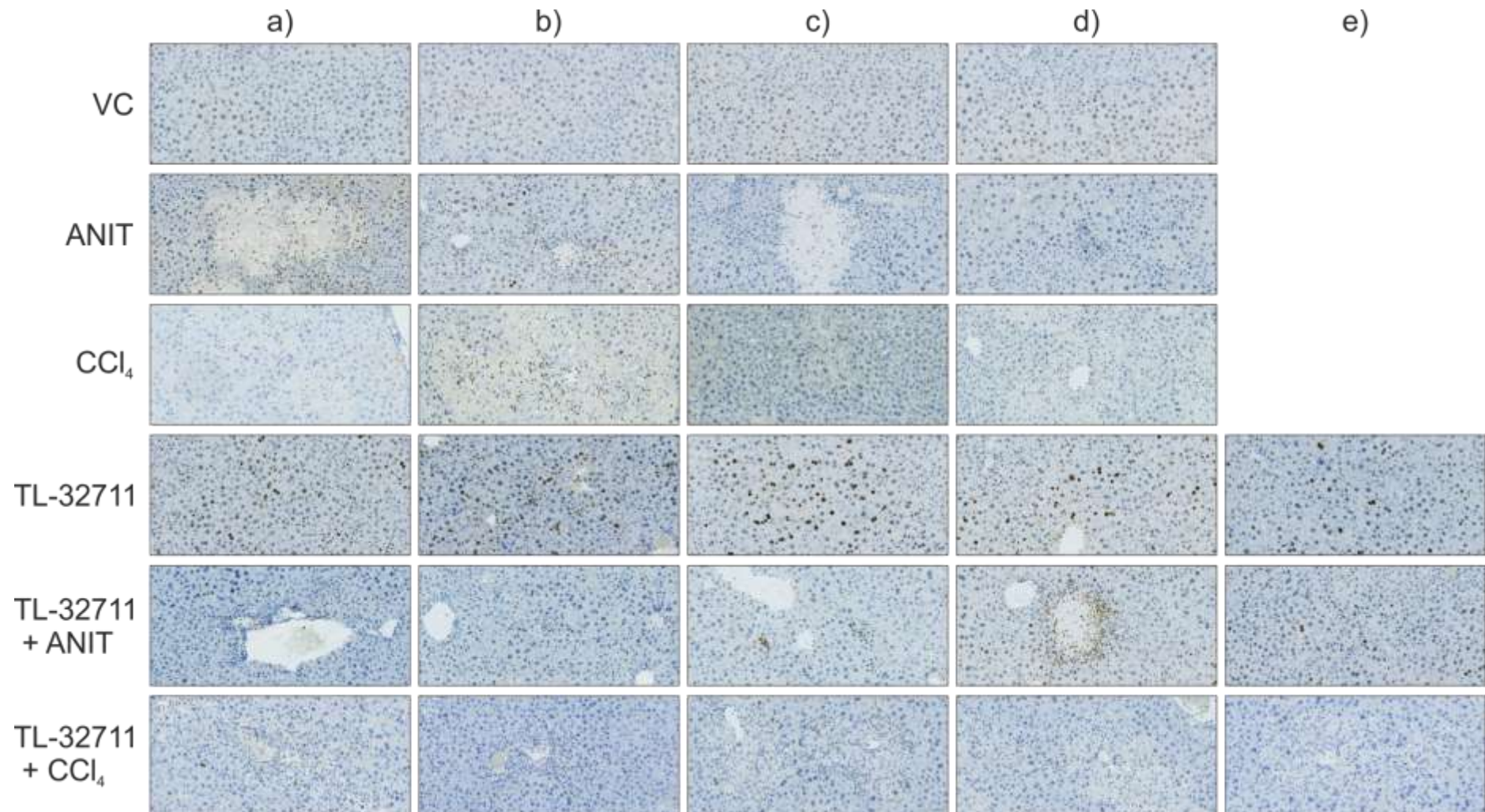


Figure 5.20 | TL-32711 induces proliferation as a single agent. a) Sections were stained for Ki-67 using the DAKO FLEX+ Autostainer. Images represent a liver section from each mouse.

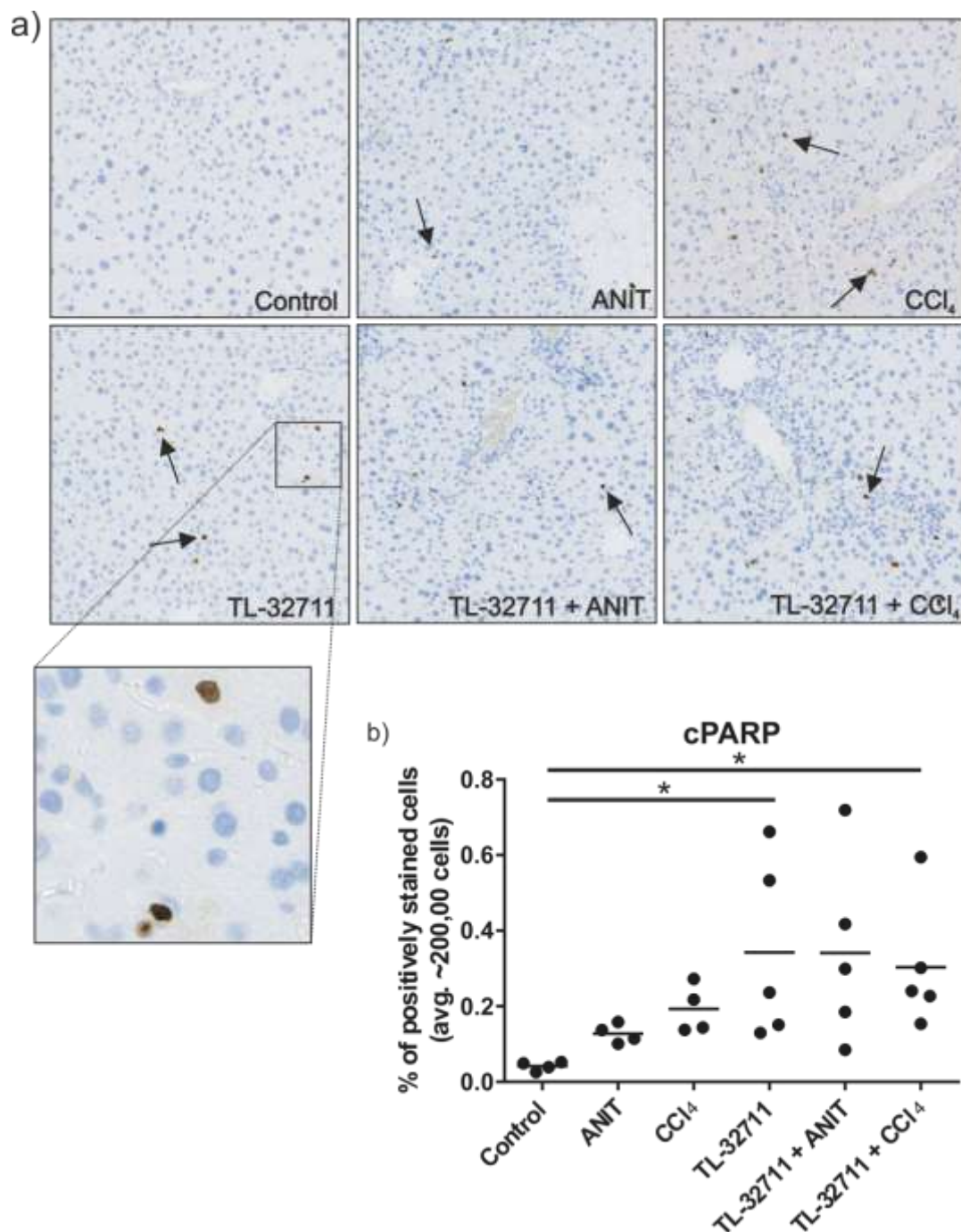


Figure 5.21 | TL-32711 ameliorates hepatotoxicity by promoting apoptosis. a) Sections were stained for cleaved PARP using the DAKO FLEX+ Autostainer. b) Quantification of the number of cleaved PARP (cPARP) positive cells was performed using Visiopharm. Paired t-tests were used for statistical analysis; significance values, $* < 0.05$. Arrows represent areas of positive staining for cPARP. Bars represent mean.

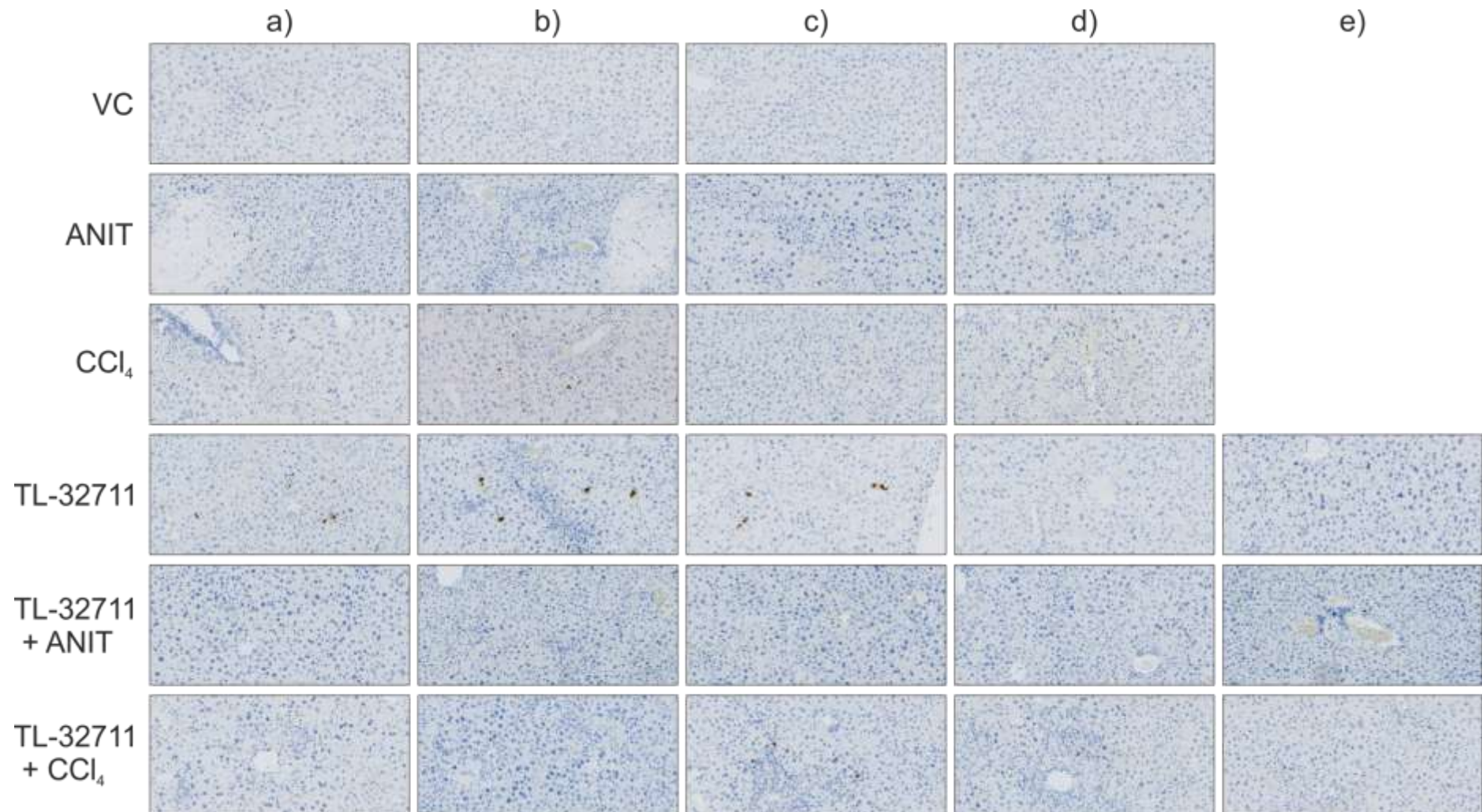


Figure 5.22 | TL-32711 ameliorates hepatotoxicity by promoting apoptosis. a) Sections were stained for cleaved PARP using the DAKO FLEX+ Autostainer. Images represent a liver section from each mouse.

TL-32711-induced NF- κ B activation and the resulting TNF α up-regulation is mediated by Kupffer cells

The IVIS data from the single mouse^{luc} demonstrated the NF- κ B signal induced by TL-32711 was localised to the liver. However, it was unknown whether this NF- κ B activation resulted in TNF α secretion. TNF α is a target gene of NF- κ B and is the key cytokine in mediating SM-induced cell death. Furthermore, I found that the NF- κ B signal was localised to the liver. Therefore, I isolated RNA from the liver samples from the dose-escalation pilot study and performed an RT-qPCR to determine whether there was any increase in TNF α mRNA. In the livers of mice^{WT} dosed with TL-32711, I found that there was a 3 to 4-fold increase in TNF α mRNA compared to VC (**Figure 5.23**). To investigate whether this resulted in TNF α secretion, I subjected mouse blood samples to mouse specific TNF α ELISAs; however, no signal was detected (data not shown).

To further dissect the hepatoprotective mechanism of TL-32711, I sought to determine which cell lineage resulted in TNF α secretion upon exposure to TL-32711. Unpublished data from Prof. Wright in Newcastle demonstrated that, in human livers, TNF α secretion is mediated only by Kupffer cells, and not quiescent HSC, myofibroblasts or hepatocytes. This hypothesis was appealing as I saw a significant increase in Kupffer cells in the livers of mice treated with TL-32711 as a single agent. To test this, I extracted Kupffer cells and HSCs from mice^{WT} and treated them with TL-32711 *ex vivo* at varying concentrations, using LPS as a positive control. TL-32711 induced TNF α mRNA up-regulation at comparable levels to LPS in Kupffer cells, but not HSCs (**Figure 5.23**). Using IL-6, which is also an established target of NF- κ B activation²⁶⁹, as a control, Dr Chernova and I found TL-32711 also induced transcription of this gene in Kupffer cells, but not HSCs. Interestingly, as the concentration of TL-32711 increased, the levels of TNF α mRNA actually decreased (**Figure 5.23**). It is currently unknown why this occurred. To determine whether the mRNA up-regulation resulted in TNF α secretion, I measured TNF α levels from both cell types by ELISA. Despite increases in the TNF α mRNA, due to the limited number of Kupffer cells extracted, only the LPS treated cells showed an increase in TNF α secretion of ~3-fold compared to VC (**Figure 5.23**). However, in line with the mRNA data, HSCs showed an increase in TNF α secretion in LPS treated cells only. These data indicate that it is likely Kupffer cells which mediated the increase in TNF α mRNA seen in the whole liver samples.

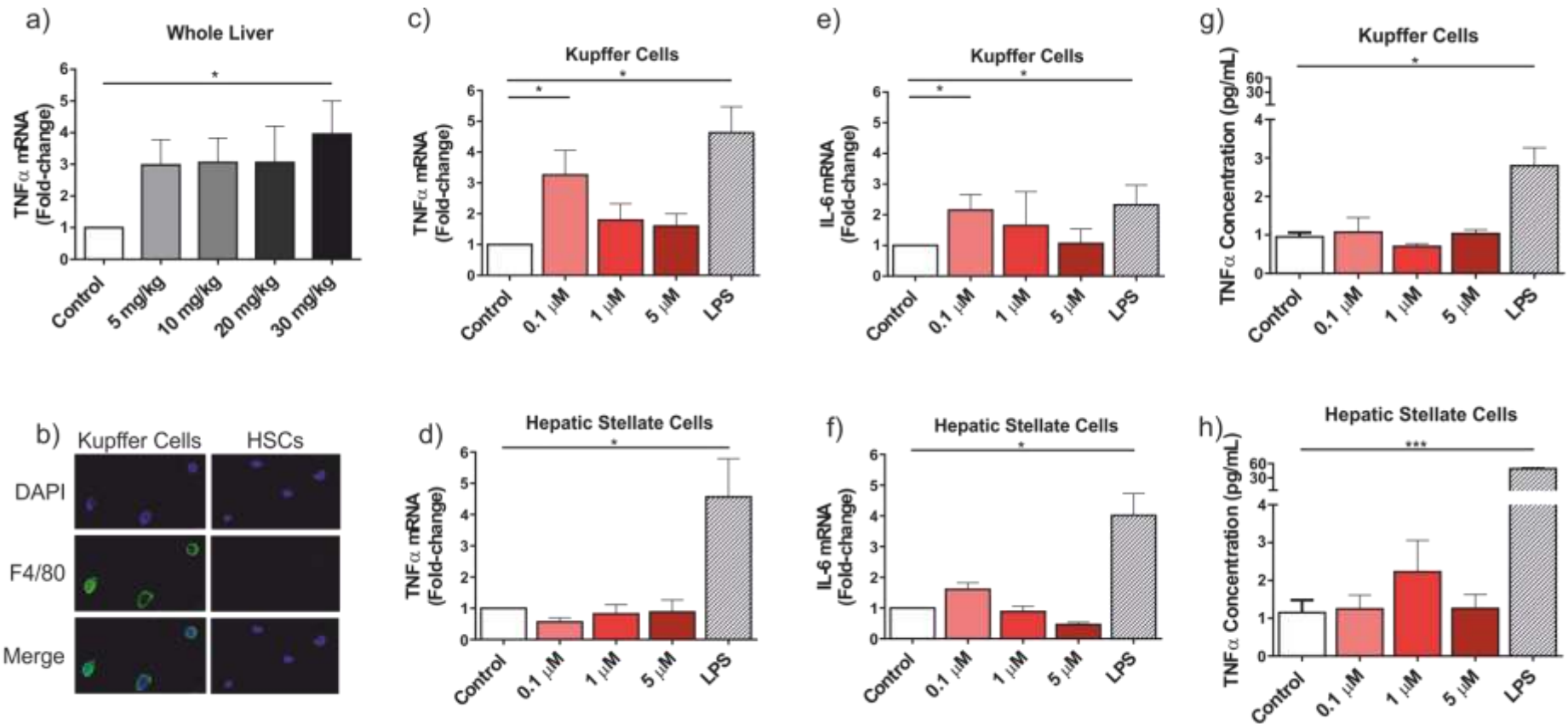


Figure 5.23 | Kupffer cells mediate TL-32711-induced TNF α mRNA up-regulation and secretion. **a)** TNF α mRNA concentration was determined by RT-qPCR using whole liver tissue. **b)** Kupffer cells were identified using F4/80 by confocal microscopy. Inactive HSCs do not have a marker and so were characterised by the absence of F4/80 staining. **c+e)** Kupffer cells and **d+f)** HSCs were subjected to RT-qPCR for up-regulation of the TNF α and IL-6 genes by Dr Chernova. **g+h)** Conditioned media was collected and subjected to a TNF α ELISA. Bars represent mean \pm SEM. Paired t-tests were used for statistical analysis; significance values, * <0.05 , *** <0.05 .

Conclusions

TNF α is essential for liver regeneration upon injury, as mice lacking the *tnf* gene are unable to recover after liver injury²⁶⁷. Furthermore, many hepatotoxins, including the two used in this study (ANIT and CCl₄), induce TNF α up-regulation upon liver injury^{206,270}, exacerbating hepatotoxicity. Whether TNF α initiates signals for cell death or cell survival is dependent on the presence of cIAP1/2^{36,37,271}. I have shown in Chapter 3 and 4 that SMs induce cIAP1/2 depletion. I therefore hypothesised that pre-treatment with TL-32711, an advanced, clinically relevant SM, would promote extensive cell death, thereby exacerbating hepatotoxicity. However, I have shown for the first time, to my knowledge, that TL-32711 actually ameliorates toxicity induced by ANIT and CCl₄. The applications of this research are almost instantly clinically relevant. Many drugs in the market are withdrawn or given a black box warning, i.e. the strictest warning label from the FDA about the potential side-effects, due to hepatotoxicity. My data suggest that TL-32711 could be used in combination with these hepatotoxins to reduce DILI. To ensure effective cytotoxicity, many chemotherapeutics must be used at high doses which often results hepatotoxicity. As SMs have the capacity to sensitise tumours to other chemotherapeutics, it may be the SMs could play a dual role by allowing current drugs to be used at a lower dose whilst simultaneously protecting against hepatotoxicity. This may result in more effective patient outcomes and a reduced toxicity profile.

Often, chemotherapeutics doses are limited due to DLT, i.e. dose limiting toxicity. The term maximum tolerated dose (MTD), is used to denote the dose below the DLT and is the highest dose used in the clinical setting. While this was applicable to many of the early cytotoxic drugs that targeted rapidly proliferating cells, many recent drugs are more targeted agents, including small molecule mimetics that bind to a target protein. As such, the traditional MTD could be replaced by a dose at which the protein of interest is still modulated. Indeed, the efficacy of SM can be shown by cIAP1 depletion in PBMC¹⁵⁵, removing the need for more invasive biomarkers. I have shown this effect in my

dose-escalation study, where I saw infiltration of Kupffer cells and TNF α mRNA up-regulation with the lowest dose. It was only when Prof. Wright treated mice with the highest dose of 30 mg/kg TL-32711 that I saw adverse effects, such as prominent mitosis, scattered apoptosis and limited amounts of focal necrosis. While the automated quantification of the Kupffer cells did not appear to correlate with the numbers observed in the sections, this issue was not seen in the combination study (see below). This discrepancy is due to the use of different staining protocols. In the dose-escalation study, I used a broad-spectrum secondary antibody that reacts with mouse tissue, which resulted in slight background staining, which the machine counted as cells. However, in the combination study, the reactivity of the secondary antibody on the mouse tissue was extensive, meaning I had to use a different staining protocol. As such, I used a staining protocol with a rat secondary antibody, which eliminated the background staining, allowing for more accurate quantification. The induction of apoptosis seen with cPARP and cC3 is likely due to the depletion of cIAP1 resulting in a switch of TNF α signalling from pro-survival, to pro-death.

As TL-32711 induced TNF α mRNA upregulation, the hypothesis that TL-32711 in combination with ANIT and CCl₄ would markedly exacerbate hepatotoxicity was based on two lines of evidence; 1) pro-survival TNF α signalling is dependent on the presence of cIAPs, and 2) previously published work has shown that degradation of cIAPs results in increased susceptibility to liver injury *in vitro*^{161,272}. To my surprise, however, I found that TL-32711 in combination with ANIT or CCl₄ actually resulted in reduced levels of ALT and ALP. This finding was confirmed upon H&E staining of livers where there was a marked reduction in necrosis upon treatment with ANIT or CCl₄ in the presence of TL-32711. As with the pilot study, there was a significant infiltration of Kupffer cells into the livers of mice treated with TL-32711. This infiltration is likely due to TL-32711-induced up-regulation of MCP-1, a chemoattractant. Indeed, TNF α signalling regulates expression of this protein and there is some evidence demonstrating SMs can increase its expression^{135,231}.

The role of Kupffer cells is under much debate as to whether they exacerbate or ameliorate liver injury^{180,181,183–186,273–276}. Kupffer cells are reported to

exacerbate both chronic and acute liver injury through secretion of pro-inflammatory cytokines (discussed in Chapter 1). In this study, my data show that Kupffer cells promote a protective effect, likely through TL-32711-induced secretion of TNF α . From my pilot study, I found the observed increase in interstitial cells was due primarily to infiltration of Kupffer cells. To investigate whether Kupffer cells were preventing liver damage, I stained for F4/80 and found a significant number of F4/80 positive cells in the TL-32711 only and TL-32711 in combination with CCl₄. It is interesting to note that there appeared to be a correlation between the number of Kupffer cells identified by F4/80 staining and the intensity of the NF- κ B signal detected by IVIS. There also appears to be no correlation between intensity of the NF- κ B signal and the ability for TL-32711 to protect against liver damage. While this may propose that Kupffer cells do not play a hepato-protective role, it may be explained by the fact that ANIT was dosed 48 h before termination of the study, whereas CCl₄ was only administered 24 h before. This may advocate the idea that Kupffer cells have a rapid mode of action occurring within 48 h and that I had caught Kupffer cells 'in the act' of preventing liver injury. This also has interesting clinical implications as to when TL-32711 could be administered. I found that NF- κ B activity began at 4-8 h, suggesting this is when the Kupffer cells begin to infiltrate the liver, my data also imply that TL-32711 acts within a period of 24-48 h. This, therefore, may provide a clinical window into when these drugs could be administered to a patient presenting with symptoms of liver damage, or reduce the duration of pre-administering of TL-32711 to prevent DILI.

To confirm whether it was the Kupffer cells that induced TNF α mRNA up-regulation and not an alternative cell population, I extracted Kupffer cells and HSCs. I chose HSCs as they are reported to play a critical role in negatively regulating liver regeneration²⁷⁷. My data confirm that it was indeed Kupffer cells that up-regulate TNF α and not HSCs. A caveat of the method I have used is that, *in vitro*, the HSCs were their inactive state. However, as the dose of ANIT and CCl₄ was acute, it is very unlikely that the HSC population would have been activated within 48 h²⁷⁸. Interestingly, TNF α mRNA up-regulation actually decreased with increasing concentrations of TL-32711. While an increase in cell death may explain this, it is unlikely as there was no apoptotic phenotype

observable in the Kupffer cells. Furthermore, previous work has shown that macrophages do not undergo cell death when challenged with TL-32711¹⁴⁹. Indeed, the authors found that when XIAP and cIAP1/2 are antagonised or deleted, bone-marrow derived macrophages (BMDMs) undergo cell death, but when only cIAP1/2 are targeted, i.e. in the case of TL-32711, do not undergo cell death. While in the current study I investigated the response of Kupffer cells rather than BMDM, as they are both macrophages, it is likely they will have a similar response²⁷⁹. It may be that using lower concentrations of TL-32711 would have produced a bell curve shape, and the concentrations used in this project were on the right hand, downward slope.

As ANIT-mediated hepatotoxicity is dependent on neutrophils, I questioned whether TL-32711 ameliorated ANIT-induced liver injury through a reduction in neutrophil invasion. I found a significant reduction in neutrophils in mice treated with ANIT alone compared to TL-32711 with ANIT. This has two potential explanations, either TL-32711 is impeding neutrophil invasion upon ANIT treatment or is it acting to reduce necrosis before neutrophils are recruited. Currently, there is no data to suggest that TL-32711 can perturb neutrophil migration. As such, this suggests that, upon liver injury, TL-32711 acts rapidly to prevent damage, meaning there is a reduced neutrophil invasion profile as a result of less damage and inflammation.

I had found that TL-32711 protects against hepatotoxicity and this is likely mediated by Kupffer cell-induced TNF α up-regulation. However, the precise mechanisms were still unknown. Due to the outcomes of TNF α signalling, I hypothesised two putative mediators; 1) TL-32711 was promoting survival through up-regulation of a plethora of pro-survival and proliferative genes, or 2) TL-32711 was priming cells for apoptosis and that, upon treatment of ANIT or CCl₄, cells underwent apoptosis instead of pro-inflammatory necrosis. To investigate whether TL-32711 induced proliferation, I stained sections with Ki-67, a marker of proliferation. I found the only treatment which induced significant proliferation was TL-32711 as a single agent, demonstrating TL-32711 induces proliferation in both hepatocytes and, interestingly, interstitial cells. This suggested that ANIT and CCl₄ somehow impeded TL-32711 induced

proliferation. To determine whether this was due to a switch in TNF α signalling from cell survival to cell death, I stained sections with cPARP. I found that in all groups treated with TL-32711 there was positive staining above that seen in the controls, suggesting TL-32711 has a two-step function in ameliorating liver injury. Firstly, there is, along with TNF α , likely an up-regulation of genes involved in proliferation and pro-survival signalling. This drives mitosis, increasing the pool of hepatocytes in anticipation for toxic insult. It also up-regulates signalling that strongly promote survival, so that any hepatotoxin does not signal as intensely for cell death. Secondly, as there is up-regulation of TNF α mRNA, this can also prime cells for induction of apoptosis upon cIAP1 depletion, which is a preferential form of cell death over necrosis due to its limited inflammatory signature. Curiously, there was also apoptosis present in TL-32711 only livers, which was not seen in the pilot study. However, it is important to note that I used a different strain of mice in the second study, i.e. mice^{luc}, which may account for this. Yet, that there was both proliferation and apoptosis with TL-32711 as a single agent, it may be there is an equilibrium between cells proliferating and undergoing apoptosis.

In conclusion, I present the exciting finding that the bivalent SM, TL-32711, prevented liver injury caused by the hepatotoxins, ANIT and CCl₄ (**Figure 5.24**). I also report that TL-32711 induced massive NF- κ B activation in the abdominal region, which appeared to be localised to the liver. This protective effect is likely due to the infiltration of Kupffer cells which promote proliferation and, upon injury, apoptosis.

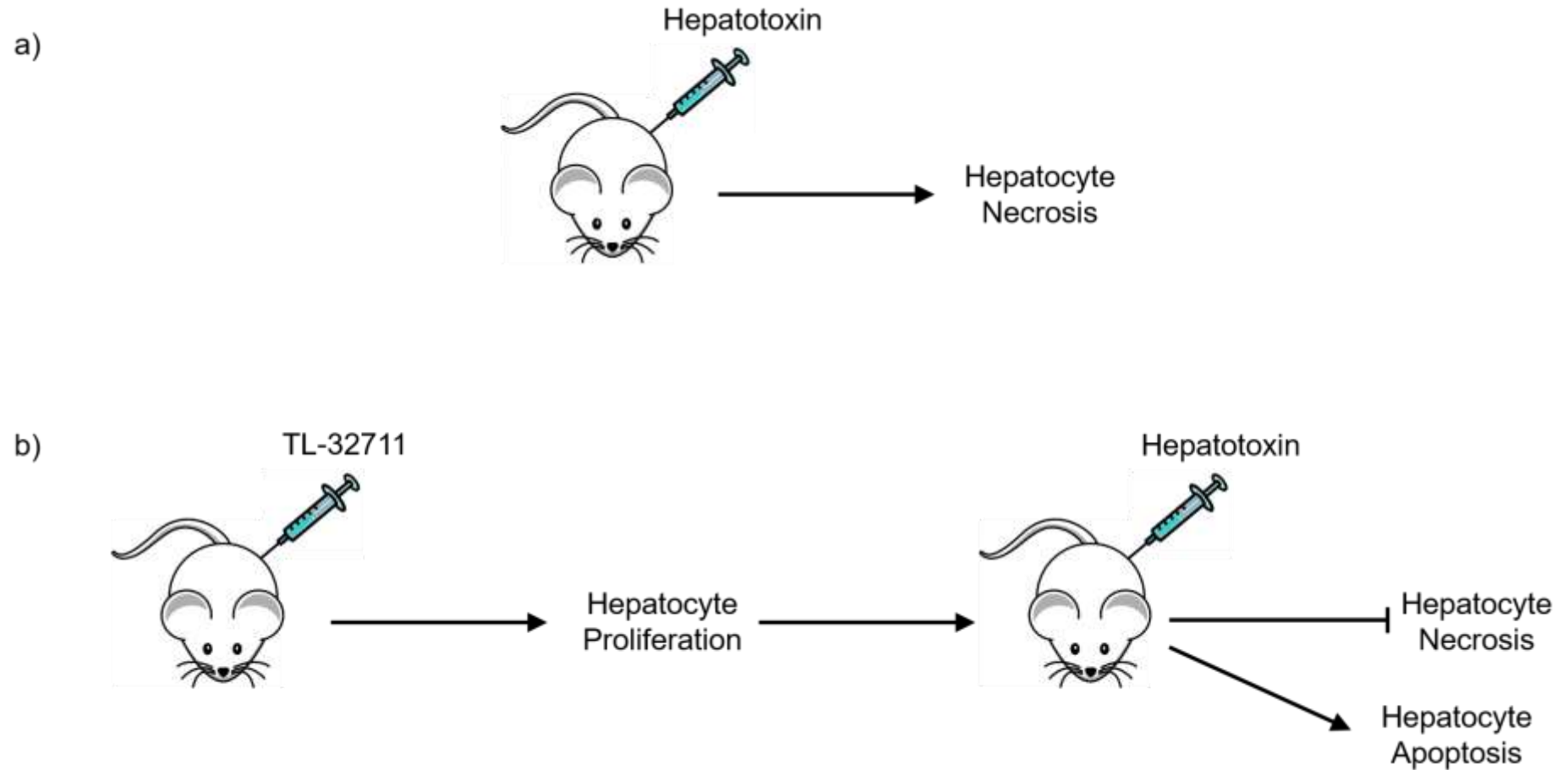


Figure 5.24 | Schematic representation of the major finding of the *in vivo* combination study. a) Mice treated with two common hepatotoxins in the absence of TL-32711, results in liver necrosis. **b)** Pre-treatment of mice with TL-32711 resulted in proliferation and, upon liver injury, apoptosis rather than necrosis.

5.1.4. Future Work

Due to the exciting findings of this Chapter, there are many future avenues of research to be conducted. Firstly, it would be interesting to determine what are the cell signalling processes that promoted Kupffer cell infiltration. This may allow for a 'personalised medicine' approach where patients with perturbed Kupffer cell function could benefit from an increase in Kupffer cell numbers mediated by SMS. Additionally, it would be useful to further confirm the vital role of Kupffer cells in the prevention of DILI in my model. Using the same protocol, but in Kupffer cell-deficient mice or in a model of Kupffer cell inhibition, would answer this. Secondly, while my protocol investigated the effect of TL-32711 on 'anticipated' DILI, many patients arrive in hospital already presenting with symptoms of liver injury. I would be fascinated to see if treatment of TL-32711 could prevent further DILI if administered after liver injury. Also, using more clinically relevant hepatotoxins, such as acetaminophen would also increase the clinical relevance of this research. Lastly, due to time constraints, I was unable to process any of the liver samples for western blotting. This would be vital to further determine the signalling processes behind my findings. While I was able to extract RNA from the pilot dose-escalation study, this was not possible for the combination study due to a lack of time. I want to perform RNA extraction from the latter study and subject it to a customised RT-qPCR array. This will further allow us to elucidate the cellular signalling process behind the hepatoprotective effect I report.

Chapter 6

Final Discussion

6. FINAL DISCUSSION

Key findings

Chemotherapeutic drugs are known to have dose-limiting side-effects. SMs are a class of small molecule inhibitors that have been reported to have limited side-effects in non-tumour cells. The purpose of this research was to investigate any potential adverse effects of SMs in non-tumour cells. I achieved this through the use of cancer cell lines for robust method development, non-tumour cell lines to elucidate mechanisms of sensitivity/resistance, and *in vivo* models to determine the effect of SMs in a model of drug-induced liver injury (DILI).

6.1.1. Results Chapter 3 - SM structure predicts efficacy in tumour cells

The key findings of Chapter 3 are that SMs that do not target XIAP have significantly reduced toxicity compared to those SMs that do. This is why many SMs in clinical trials are monovalent, as they do not target XIAP as strongly. However, bivalent SMs have much greater efficacy due to their ability to dimerise IAP proteins, which more closely mimics the role of SMAC *in situ*. Indeed, TL-32711, a cIAP1-specific bivalent SM, induced cell death at concentrations as low as 10 nM; significantly lower than doses used in the clinic. Interestingly, cIAP1 depletion did not correlate with induction of cell death in the resistant, MDA-MB-468, cells. These data suggest that in resistant cells there is a difference between target modulation and induction of cell death, which is important in a clinical setting. However, despite promising *in vitro* studies, the small number of published clinical trials have shown limited efficacy of SMs in patients^{121,122,155}. This argues that the dose of SMs should be related to modulation of cIAP1, rather than tumour killing. Indeed, in a recent study of AT-406, cIAP1 depletion at the lowest reported dose of 120 mg was not different to that of the highest dose of 900 mg¹²¹. Similarly, no additional increase in TL-32711-induced cIAP1 depletion was observed between doses of 5.67 mg and 63 mg¹⁵⁵. Importantly, there was also no difference in anti-tumour activity between the low and high doses in either of these studies. Interestingly, when AT-406 was administered in combination with daunorubicin and

Final Discussion

cytarabine there were patients that underwent either complete or partial remission. Moreover, this response was primarily observed in patients with increases in serum TNF α . These clinical data are similar to the effects that I observed in tumour cells lines; an increase in TNF α upon treatment with SMs resulted in increased sensitivity to SMs. These results, therefore, suggest that SMs should be used synergistically to sensitise tumours to other chemotherapeutics thereby reducing their toxicity through the application of lower doses.

When BV6 was used at high concentrations, necrosis was induced at 30 μ M, likely due its ability to inhibit both cIAP1/2 and XIAP. However, most interestingly, I saw that the pan-caspase inhibitor, zVAD, actually inhibited TNF α secretion when administered in combination with BV6. The mechanisms behind this are not known, but would be a very interesting avenue to investigate this further. This has important implications as SMs work primarily through modulation of TNFR1 signalling from cell survival to cell death. However, there are also reports showing that when apoptosis is inhibited, SMs can induce necroptosis^{113,137,232,280}. It is unclear why, in my model, caspase inhibition did not result in necroptosis, however, it is likely due to use of different cell lines. It also may be that I employed pharmacological inhibition of caspases, rather than genetic deletion of caspases. This could have clinical relevance to patients who have deficient apoptotic machinery; my data suggest that SMs may not induce TNF α secretion in these cohorts, thus reducing their efficacy as anti-cancer agents.

This chapter highlights an important point when establishing doses of targeted small molecule compounds. Should the dose be prescribed by the modulation of the target protein, or overall cell killing? By using target modulation, this would significantly limit toxicity. Indeed, I have shown this, as BV6 induced necrosis at higher concentrations, compared to apoptosis at lower concentrations. Despite this, overall cell killing is still the preferred dose determinant used in the clinic. However, this exposes patients to increased toxicity and side-effects which could potentially be minimised if target modulation was used instead.

I therefore wanted to further investigate the therapeutic window of these agents by determining their effects on non-tumour derived cells. As such, I used the same methodology developed in the tumour cells in Chapter 3 and applied them to non-tumour cells *in vitro*.

6.1.2. Results Chapter 4 - SMs exhibit limited toxicity in non-tumour cells

Many dose-limiting toxicities (DLTs) and side-effects arise due to the effects of the compound on non-tumour cells. In Chapter 4, I investigated the effects of SMs in this cell type. The use of tumour cells allowed us to 'range-find' concentrations of SM that could be applied to non-tumour derived cells *in vitro*. As I was interested in potential hepatotoxicity, I utilised a rat pancreatic progenitor cell line, B-13 (gift from Prof. Wright), which, upon treatment with dexamethasone, transdifferentiated into B-13/H hepatocyte-like cells. Initially I studied these rat cells and the human non-tumour cells, MCF-10A, in terms of their response to SMs as single agents. I found that all cells were resistant to the clinically relevant SMs at clinically relevant doses, but with a small amount of cell death at supra-clinical doses. These data demonstrate there is a large therapeutic window for SM treatment in cells that are not in an inflammatory microenvironment.

However, using SMs as single agents did not faithfully represent the hyper-inflammatory milieu in which non-tumour cells co-reside with tumour cells. This raises an important point regarding *in vitro* models, as often these models use cells in isolation. However, particularly in the case of SMs, the microenvironment created by tumour cells can play significant roles in not only the efficacy of drugs, but also their effect on non-tumour cells. In light of this, I sought to determine the role that the tumour cell-induced microenvironment plays through the addition of exogenous TNF α in an effort to activate TNFR1 signalling. Even with the addition of TNF α , I still saw no cell death in any of the non-tumour cells tested using physiologically relevant concentrations of TNF α and clinically relevant doses of SMs. Using a variety of techniques, I found that the rat-derived cell lines were unable to undergo TNFR1 signalling. This

highlights the importance of having robust models which reflect the signalling activity of non-tumour hepatic cells *in situ*. Without it, it is not possible to determine any compound-induced toxicity that agents may have in non-tumour tissues. Indeed, as previously discussed, hepatocytes are well known to be sensitive to TNF α and CHX-induced cell death, suggesting B-13/H cells do not faithfully reflect the TNF α /NF- κ B hepatocyte signalling model *in vitro*.

Using the human non-tumour, MCF-10A cells, I found these cells had similar kinetics of cIAP1 depletion and non-canonical NF- κ B activation compared to the tumour cells tested in Chapter 3. As these cells did not die in the presence of TNF α and SMs, I wanted to investigate whether there were additional E3 ligases that could prevent these cells undergoing cell death. Indeed, published and unpublished data has shown that additional E3 ligases can prevent tumour cells and non-tumour cells undergoing TNF α -mediated cell death^{44,260}. I had optimised the knockdown of other E3 ligases potentially involved in TNF α signalling (e.g. MIB2), but was unable to pursue these further due to time constraints. As such, non-tumour cells with functional E3 ligases other than cIAP1 are likely to be resistant to SM-induced cell death. This raises another issue of isolated *in vitro* studies. Due to the heterogeneity of tumour and non-tumour cells in patients, removal of a single protein, which may induce killing in an isolated cell line, may not have similar effects *in vivo*. Another caveat of *in vitro* studies is that cell signalling is often influenced in an endocrine and paracrine manner. This is very hard to replicate *in vitro*, sometimes leading to discordance between cell line data and *in vivo* data.

6.1.3. Results Chapter 5 - The SM, TL-32711, prevents liver injury *in vivo*

While *in vitro* models are useful for high throughput work and detailed mechanistic experiments, they do not accurately reflect the microenvironment in which both tumour and non-tumour cells co-reside. Indeed, one of the SM-mediated DLTs commonly reported in the literature is the induction of a 'cytokine storm'. It is incredibly technically challenging to replicate this *in vitro*. Furthermore, as I was interested in hepatotoxicity, I therefore needed a model that faithfully replicated the complex interplay of the various cell lineages and

Final Discussion

their functions *in vivo*, something not easily replicated *in vitro*. I had found limited SM-induced toxicity in non-tumour MCF-10A cells, I had investigated in Chapter 4, despite activation of the NF- κ B pathway. Additionally, liver regeneration is dependent on the TNF α /NF- κ B signalling axis to recover after injury. Therefore, I sought to determine the effect of the clinically relevant SM, TL-32711, in a situation of liver damage in which both TNF α and NF- κ B activity would be enhanced. Chapter 5 demonstrated that SMs have the ability to prevent DILI *in vivo* caused by two well established hepatotoxins, ANIT and CCl₄. Firstly, to determine at which dose TL-32711 could be administered without significant toxicity, I performed a dose-escalation study. I found that there was a large infiltration of Kupffer cells at all concentrations, but at 30 mg/kg TL-32711 there were adverse effects such as limited necrosis and extensive mitosis. As such I decided to use the preceding dose of 20 mg/kg.

I have shown that TL-32711 activates the NF- κ B pathway and previously published papers demonstrate activation of this pathway results in cell death in tumour cells. Fascinatingly, rather than exaggerating hepatotoxicity as I hypothesised, TL-32711 significantly ameliorated hepatotoxicity induced by ANIT and CCl₄. This finding was indeed surprising, but also very exciting due to its clinical applications. It may be that SMs could be used in combination with other chemotherapeutics to both sensitise tumours to cell death and reduce the compound hepatotoxicity profile. Using reporter mice, I also found that NF- κ B was activated within 4-8 h, suggesting that the clinical pre-dosing regimen could be shortened significantly. This again demonstrates the power of using reporter mice. Without them, it would not have been possible to define the spatial and temporal activation of specific pathways unless multiple mice are used. Furthermore, while cIAP1 is depleted in PBMCs in the clinic¹⁵⁵, I only observed significant amounts of NF- κ B activity in the liver. This presents a potential problem; is cIAP1 depletion in PBMCs a valid surrogate marker? As I saw the highest levels of NF- κ B in the liver, it may be that PBMC cIAP1-depletion underestimates SM target modulation in other organs. Conversely, this may just demonstrate that Kupffer cells have extensive NF- κ B activity, whereas the NF- κ B pathway in PBMCs is not activated to the same extent.

Final Discussion

These exciting findings have only come to light due to the use of animal models, in which I was able to accurately replicate the inflammatory milieu induced by TL-32711. Furthermore, this work further highlights the importance of the interplay between various cell types only found *in vivo*, namely Kupffer cells and their effect on hepatocytes, which is currently very challenging to model *in vitro*.

However, post-thesis submission, I reanalysed the liver sections stained with cPARP from TL-32711 in combination with ANIT or CCl₄; it appeared the initial quantification by Visiopharm (**Figure 5.22**) was not reflective of what was observed by eye. The Visiopharm software appeared to be identifying a number of non-specific background staining areas as positive cells. As such, I adjusted the protocol and reanalysed the same sections. Firstly, I excluded the areas that contained the background from analysis; secondly, I adjusted the Visiopharm protocol by increasing the average nucleus size to exclude any debris that the software was categorising as positive nuclei. Upon reanalysis, I found there were a reduced number of nuclei positive for cPARP in the groups TL-32711 in combination with ANIT or CCl₄. This resulted in a significant increase in cPARP positive cells in the TL-73211 only group (**Appendix Figure 2.1**). The hypothesis of the protective mechanisms of TL-32771 in preventing liver injury was therefore updated. Rather than TL-32711 switching the mode of cell death from necrosis to apoptosis in the presence of hepatotoxins, I now hypothesise that TL-32711 protects against hepatocyte cell death *in vivo* (**Figure 6.1**).

6.1.4. Concluding remarks

In conclusion, I have shown that SMs which strongly inhibit cIAP1/2 and XIAP have the greatest potential to induce toxicity in non-tumour cells. I also report that SMs induce NF- κ B activity and cIAP1 depletion with similar kinetics in non-tumour cells compared to the tumour cells used in this project. Lastly, I show that SMs have the ability to prevent liver injury caused by two well characterised hepatotoxins. This effect was likely mediated through TNF α secretion from Kupffer cells, which promoted proliferation and, upon liver injury, survival instead of necrosis. SMs are already in clinical trials, and, to date, the protocols with the best efficacy are where SMs are treated in combination with other chemotherapeutic drugs^{122,150,155}.

Future work

There are many exciting avenues for future work from the data presented here in this thesis. A few of the most important are:

1. To delineate the underlying mechanisms behind the zVAD-mediated reduction of TNF α secretion in BV6-treated MDA-MB-231 cells. This could be achieved using time course experiments and alternative caspase inhibitors, such as QVD.
2. Investigate why B-13 and B-13/H cells do not have the ability to undergo TNF α -mediated signalling. This could be performed by immunoprecipitation for key proteins in TNF Complex I and II. Further work characterising the extent to which the mutant *cflar* gene could affect cell death would also be very interesting.
3. Knockdown of the key E3 ligases associated with TNF α signalling in the non-tumour MCF-10A cells would further elucidate the role these proteins play in protection from SM-mediated cell death. These targets include cIAP2, MIB2 and Pellino 3.
4. Work further exploring the hepatoprotective effects of SMs *in vivo* would allow further characterisation of their potential clinical benefits. Of particular interest is whether SMs would still have a protective effect if they were administered after treatment with a hepatotoxin, rather than before. Also, clinically relevant compounds known to induce liver injury could be tested in this model, such as acetaminophen.

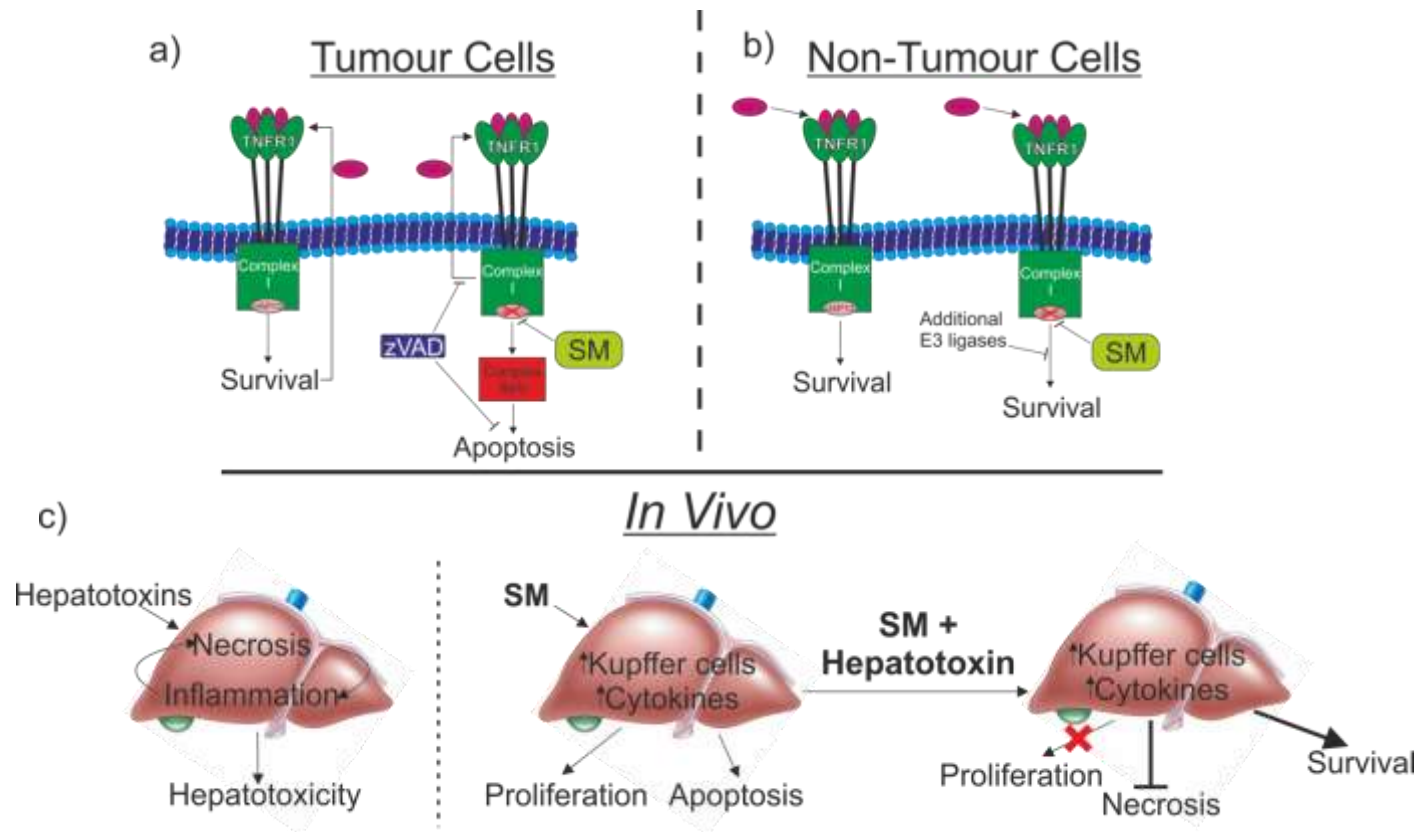


Figure 6.1 | Schematic representation of the major findings from this project. **a)** Tumour cells with a TNF α autocrine loop are sensitive to SMs as a single agent. However, zVAD inhibits SM-induced cell death at lower concentrations and, unexpectedly, inhibits TNF α secretion. **b)** Non-tumour derived cells are resistant to SMs as single agents and in combination with TNF α . While the mechanisms are unknown, this is likely due to other E3 ligases which can function in place of cIAP1. **c)** In the presence of cIAP1, hepatotoxins induce necrosis and inflammation. When cIAP1 is depleted with SMs there is an increase in Kupffer cell number, induction of cytokines and extensive proliferation in hepatocytes. In this situation, when hepatotoxins are administered, hepatocytes are protected from liver injury.

Appendix

APPENDIX

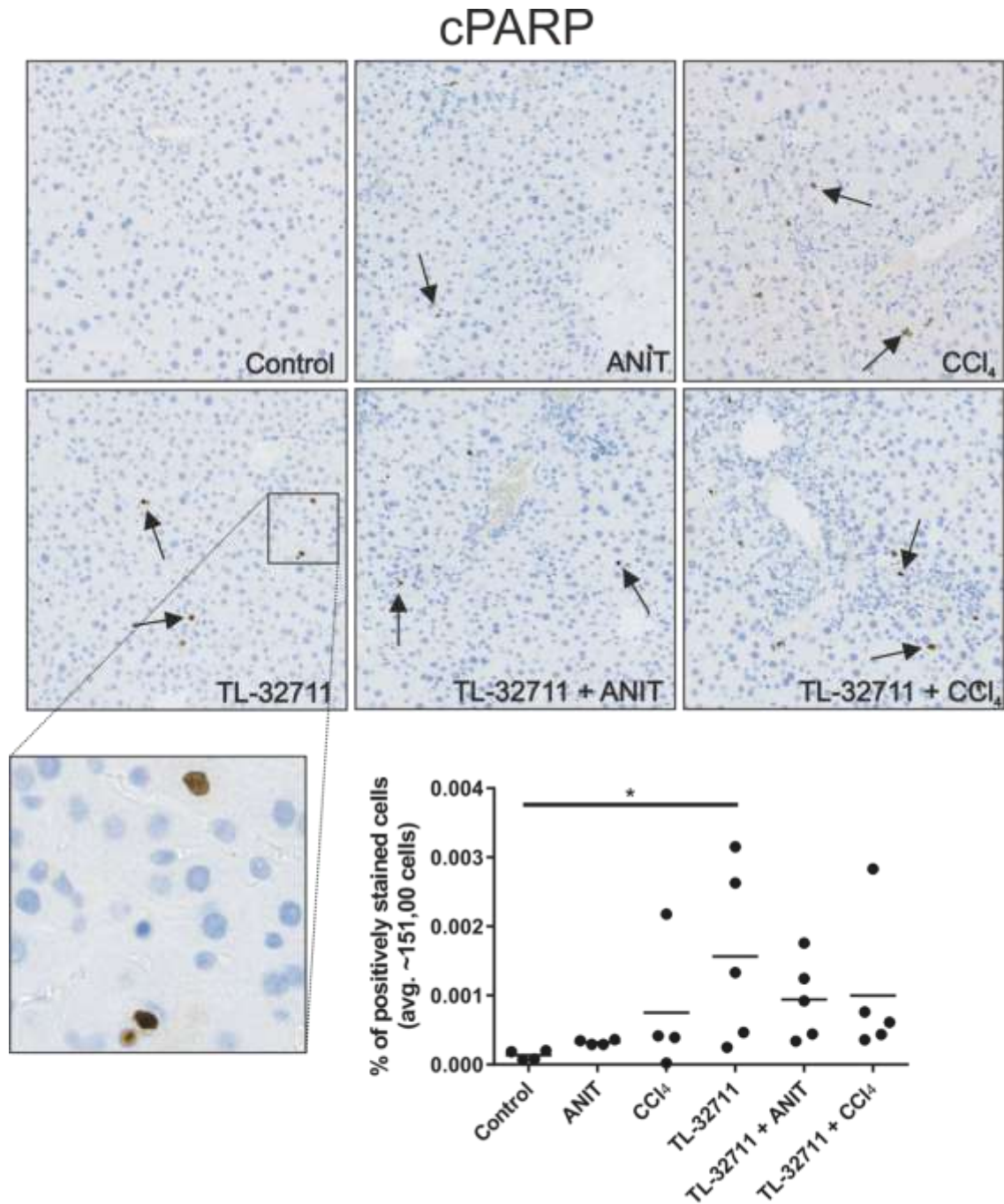
Appendix 1: List of genes relevant to TNF α signalling in B-13 genome (as detailed in Chapter 4)

AGFG1 (HRB),	DFFA,	LTB,
AGT,	EGFR,	LTBR,
AKT1,	EGR1,	MADD,
ARHGDIB,	EIF2AK2,	MAP2K3 ,
ATF1,	F2R,	MAP2K4 (JNKK1),
ATF2,	FAF1,	MAP3K1 (MEKK1),
BAG4,	FAS (TNFRSF6),	MAP3K7 (TAK1),
BCL10,	FASLG (TNFSF6),	MAPK3,
BCL2A1,	FOS ,	MAPK8 (JNK1),
BCL2L1,	HMOX1,	MYD88,
BCL3,	ICAM1,	NGFR,
CAD,	IFNA1,	NGFRAP1,
CARD10,	IFNG,	NSFL1C,
CASP1,	IFNG,	OPTN,
CASP2,	IKBKE,	OTUD7B,
CCL2 (MCP-1),	IL10,	OTULIN,
CCL5 (RANTES),	IL1A,	PAK1,
CD27 (TNFRSF7),	IL1B,	PAK2,
CD40LG	IL1R1,	PARP1 (ADPRT1),
(TNFSF5),	IRAK1,	PGLYRP1,
CD70 (TNFSF7),	IRAK2,	PPM1A,
CFLAR ,	IRAK4 (TRAF1),	PPM1B,
CHUK (IKKA),	IRF1,	PPM1D,
CREBBP,	ITCH,	PPP1CA,
CSF1 (MCSF),	JUN,	PPP2CA,
CSF2 (GM-CSF),	LMNA,	PPP2CB,
CSF2 (GM-CSF),	LMNB1,	PRKDC,
CSF3 (GCSF),	LTA (TNFB),	PSIP1,

Appendix 1 Data

PSMG2	TNFRSF12,
(TNFSF5IP1),	TNFRSF13,
RAF1,	TNFRSF14,
RB1,	TNFRSF15,
RELT	TNFRSF17,
(TNFRSF19L),	TNFRSF1A,
RIPK2,	TNFRSF1B,
SMAD4	TNFRSF21,
SPTAN1	TNFRSF25 (DR3),
STAT1,	TNFRSF4,
TBK1,	TNFRSF8,
TIMP1,	TNFRSF9,
TLR1,	TOLLIP,
TLR2,	TRAF6,
TLR3,	USP11,
TLR4,	USP15,
TLR6,	USP21,
TLR9,	USP31,
TNF,	USP4,
TNFRSF10	ZAP70.
(TRAIL),	
TNFRSF11,	

Appendix 2: Reanalysed data from Chapter 5



Appendix Figure 2.1 | TL-32711 does not ameliorate hepatotoxicity by promoting apoptosis. **a)** Sections were stained for cleaved PARP using the DAKO FLEX+ Autostainer. **b)** Quantification of the number of cleaved PARP (cPARP) positive cells was performed using Visiopharm. Paired t-tests were used for statistical analysis; significance values, * <0.05 . Arrows represent areas of positive staining for cPARP. Bars represent mean.

References

REFERENCES

1. Dickens, L. S., Powley, I. R., Hughes, M. A. & MacFarlane, M. The 'complexities' of life and death: Death receptor signalling platforms. *Exp. Cell Res.* **318**, 1269–1277 (2012).
2. Youle, R. J. & Strasser, A. The BCL-2 protein family: opposing activities that mediate cell death. *Nat. Rev. Mol. Cell Biol.* **9**, 47–59 (2008).
3. Chinnaiyan, A. M. The apoptosome: heart and soul of the cell death machine. *Neoplasia* **1**, 5–15 (1999).
4. Llambi, F. *et al.* A Unified Model of Mammalian BCL-2 Protein Family Interactions at the Mitochondria. *Mol. Cell* **44**, 517–531 (2011).
5. Dickens, L. S. *et al.* A Death Effector Domain Chain DISC Model Reveals a Crucial Role for Caspase-8 Chain Assembly in Mediating Apoptotic Cell Death. *Mol. Cell* **47**, 291–305 (2012).
6. Hughes, M. A. *et al.* Co-operative and Hierarchical Binding of c-FLIP and Caspase-8: A Unified Model Defines How c-FLIP Isoforms Differentially Control Cell Fate. *Mol. Cell* **61**, 834–849 (2016).
7. Hughes, M. A. *et al.* Reconstitution of the Death-Inducing Signaling Complex Reveals a Substrate Switch that Determines CD95-Mediated Death or Survival. *Mol. Cell* **35**, 265–279 (2009).
8. Li, H., Zhu, H., Xu, C.-J. & Yuan, J. Cleavage of BID by Caspase 8 Mediates the Mitochondrial Damage in the Fas Pathway of Apoptosis. *Cell* **94**, 491–501 (1998).
9. Moriwaki, K. & Chan, F. K. M. RIP3: A molecular switch for necrosis and inflammation. *Genes Dev.* **27**, 1640–1649 (2013).
10. Li, J. *et al.* The RIP1/RIP3 necrosome forms a functional amyloid signaling complex required for programmed necrosis. *Cell* **150**, 339–350 (2012).
11. Sun, L. *et al.* Mixed lineage kinase domain-like protein mediates necrosis signaling downstream of RIP3 kinase. *Cell* **148**, 213–227 (2012).
12. Dondelinger, Y. *et al.* MLKL Compromises Plasma Membrane Integrity by Binding to Phosphatidylinositol Phosphates. *Cell Rep.* **7**, 971–981 (2014).

References

13. Wang, H. *et al.* Mixed Lineage Kinase Domain-like Protein MLKL Causes Necrotic Membrane Disruption upon Phosphorylation by RIP3. *Mol. Cell* **54**, 133–146 (2014).
14. Kaczmarek, A., Vandenabeele, P. & Krysko, D. V. Necroptosis: The Release of Damage-Associated Molecular Patterns and Its Physiological Relevance. *Immunity* **38**, 209–223 (2013).
15. Kono, H., Karmarkar, D., Iwakura, Y. & Rock, K. L. Identification of the cellular sensor that stimulates the inflammatory response to sterile cell death. *J. Immunol.* **184**, 4470–8 (2010).
16. Oppenheim, J. J. & Yang, D. Alarmins: Chemotactic activators of immune responses. *Curr. Opin. Immunol.* **17**, 359–365 (2005).
17. Pop, C. & Salvesen, G. S. Human caspases: Activation, specificity, and regulation. *J. Biol. Chem.* **284**, 21777–21781 (2009).
18. Bredesen, D. E. Programmed cell death mechanisms in neurological disease. *Curr Mol Med* **8**, 173–186 (2008).
19. Fuentes-Prior, P. & Salvesen, G. S. The protein structures that shape caspase activity, specificity, activation and inhibition. *Biochem. J.* **384**, 201–232 (2004).
20. Dix, M. M., Simon, G. M. & Cravatt, B. F. Global Mapping of the Topography and Magnitude of Proteolytic Events in Apoptosis. *Cell* **134**, 679–691 (2008).
21. Mahrus, S. *et al.* Global sequencing of proteolytic cleavage sites in apoptosis by specific labeling of protein N termini. *Cell* **134**, 866–876 (2008).
22. Timmer, J. C. & Salvesen, G. S. Caspase substrates. *Cell Death Differ.* **14**, 66–72 (2007).
23. Tewari, M. *et al.* Yama/CPP32B, a mammalian homolog of CED-3, is a CrmA-inhibitable protease that cleaves the death substrate poly(ADP-ribose) polymerase. *Cell* **81**, 801–809 (1995).
24. Woo, E. J. *et al.* Structural mechanism for inactivation and activation of CAD/DFF40 in the apoptotic pathway. *Mol. Cell* **14**, 531–539 (2004).
25. Tinel, A. & Tschopp, J. The PIDDosome, a protein complex implicated in activation of caspase-2 in response to genotoxic stress. *Science* **304**, 843–6

References

- (2004).
26. Crook, N. E., Clem, R. J. & Miller, L. K. An apoptosis-inhibiting baculovirus gene with a zinc finger-like motif. *J. Virol.* **67**, 2168–2174 (1993).
 27. Uren, a G. *et al.* Role for yeast inhibitor of apoptosis (IAP)-like proteins in cell division. *Proc. Natl. Acad. Sci. U. S. A.* **96**, 10170–10175 (1999).
 28. Roy, N. *et al.* The gene for neuronal apoptosis inhibitory protein is partially deleted in individuals with spinal muscular atrophy. *Cell* **80**, 167–178 (1995).
 29. Duckett, C. S. *et al.* A conserved family of cellular genes related to the baculovirus iap gene and encoding apoptosis inhibitors. *EMBO J.* **15**, 2685–94 (1996).
 30. Uren, A. G., Coulson, E. J. & Vaux, D. L. Conservation of baculovirus inhibitor of apoptosis repeat proteins (BIRPs) in viruses, nematodes, vertebrates and yeasts. *Trends Biochem. Sci.* **23**, 159–162 (1998).
 31. Vaux, D. L. & Silke, J. Mammalian mitochondrial IAP binding proteins. *Biochem. Biophys. Res. Commun.* **304**, 499–504 (2003).
 32. Dynek, J. N. *et al.* c-IAP1 and Ubch5 promote K11-linked polyubiquitination of RIP1 in TNF signalling. *EMBO J.* **29**, 4198–4209 (2010).
 33. Gyrd-Hansen, M. *et al.* IAPs contain an evolutionarily conserved ubiquitin-binding domain that regulates NF-kappaB as well as cell survival and oncogenesis. *Nat. Cell Biol.* **10**, 1309–1317 (2008).
 34. Blankenship, J. W. *et al.* Ubiquitin binding modulates IAP antagonist-stimulated proteasomal degradation of c-IAP1 and c-IAP2 1. *Biochem. J* **417**, 149–160 (2009).
 35. Salvesen, G. S. & Duckett, C. S. IAP proteins: blocking the road to death's door. *Nat. Rev. Mol. Cell Biol.* **3**, 401–10 (2002).
 36. Vince, J. E. *et al.* IAP Antagonists Target cIAP1 to Induce TNFa-Dependent Apoptosis. *Cell* **131**, 682–693 (2007).
 37. Petersen, S. L. *et al.* Autocrine TNFa Signaling Renders Human Cancer Cells Susceptible to Smac-Mimetic-Induced Apoptosis. *Cancer Cell* **12**, 445–456 (2007).
 38. Varfolomeev, E. *et al.* IAP Antagonists Induce Autoubiquitination of c-IAPs,

References

- NF- κ B Activation, and TNF α -Dependent Apoptosis. *Cell* **131**, 669–681 (2007).
39. Eckelman, B. P., Salvesen, G. S. & Scott, F. L. Human inhibitor of apoptosis proteins: why XIAP is the black sheep of the family. *EMBO Rep.* **7**, 988–94 (2006).
40. Fulda, S. & Vucic, D. Targeting IAP proteins for therapeutic intervention in cancer. *Nat. Rev. Drug Discov.* **11**, 109–24 (2012).
41. Santoro, M. M., Samuel, T., Mitchell, T., Reed, J. C. & Stainier, D. Y. R. Birc2 (clap1) regulates endothelial cell integrity and blood vessel homeostasis. *Nat. Genet.* **39**, 1397–402 (2007).
42. Graber, T. E. & Holcik, M. Distinct roles for the cellular inhibitors of apoptosis proteins 1 and 2. *Cell Death Dis.* **2**, e135 (2011).
43. Darding, M. *et al.* Molecular determinants of Smac mimetic induced degradation of cIAP1 and cIAP2. *Cell Death Differ.* **18**, 1376–1386 (2011).
44. Petersen, S. L., Peyton, M., Minna, J. D. & Wang, X. Overcoming cancer cell resistance to Smac mimetic induced apoptosis by modulating cIAP-2 expression. *Proc Natl Acad Sci* 11936–41 **107**, 11936–41 (2010).
45. Hu, S. *et al.* cIAP2 is a ubiquitin protein ligase for BCL10 and is dysregulated in mucosa-associated lymphoid tissue lymphomas. *J. Clin. Invest.* **116**, 174–181 (2006).
46. Conte, D. *et al.* Inhibitor of apoptosis protein cIAP2 is essential for lipopolysaccharide-induced macrophage survival. *Mol. Cell. Biol.* **26**, 699–708 (2006).
47. Lopez, J. & Meier, P. To fight or die-inhibitor of apoptosis proteins at the crossroad of innate immunity and death. *Curr. Opin. Cell Biol.* **22**, 872–881 (2010).
48. Deveraux, Q. L. *et al.* Cleavage of human inhibitor of apoptosis protein XIAP results in fragments with distinct specificities for caspases. *EMBO J.* **18**, 5242–5251 (1999).
49. Srinivasula, S. *et al.* A conserved XIAP-interaction motif in caspase-9 and Smac/DIABLO regulates caspase activity and apoptosis. *Nature* **410**, 112–

References

- 116 (2001).
50. Chai, J. *et al.* Structural basis of caspase-7 inhibition by XIAP. *Cell* **104**, 769–780 (2001).
 51. Riedl, S. J. *et al.* Structural basis for the inhibition of caspase-3 by XIAP. *Cell* **104**, 791–800 (2001).
 52. Lee, T. J., Lee, J. T., Park, J. W. & Kwon, T. K. Acquired TRAIL resistance in human breast cancer cells are caused by the sustained cFLIPL and XIAP protein levels and ERK activation. *Biochem. Biophys. Res. Commun.* **351**, 1024–1030 (2006).
 53. Jost, P. J. *et al.* XIAP discriminates between type I and type II FAS-induced apoptosis. *Nature* **460**, 1035–9 (2009).
 54. Franke, T. F. *et al.* The protein kinase encoded by the Akt proto-oncogene is a target of the PDGF-activated phosphatidylinositol 3-kinase. *Cell* **81**, 727–736 (1995).
 55. Stambolic, V. *et al.* Negative regulation of PKB/Akt-dependent cell survival by the tumor suppressor PTEN. *Cell* **95**, 29–39 (1998).
 56. Van Themsche, C., Leblanc, V., Parent, S. & Asselin, E. X-linked inhibitor of apoptosis protein (XIAP) regulates PTEN ubiquitination, content, and compartmentalization. *J. Biol. Chem.* **284**, 20462–20466 (2009).
 57. Birkey Reffey, S., Wurthner, J. U., Parks, W. T., Roberts, a B. & Duckett, C. S. X-linked inhibitor of apoptosis protein functions as a cofactor in transforming growth factor-beta signaling. *J. Biol. Chem.* **276**, 26542–9 (2001).
 58. Yamaguchi, K. *et al.* XIAP, a cellular member of the inhibitor of apoptosis protein family, links the receptors to TAB1-TAK1 in the BMP signaling pathway. *EMBO J.* **18**, 179–187 (1999).
 59. Suzuki, Y., Nakabayashi, Y. & Takahashi, R. Ubiquitin-protein ligase activity of X-linked inhibitor of apoptosis protein promotes proteasomal degradation of caspase-3 and enhances its anti-apoptotic effect in Fas-induced cell death. *Proc. Natl. Acad. Sci. U. S. A.* **98**, 8662–7 (2001).
 60. Krieg, A. *et al.* XIAP mediates NOD signaling via interaction with RIP2. *Proc.*

References

- Natl. Acad. Sci. U. S. A.* **106**, 14524–14529 (2009).
61. Du, C., Fang, M., Li, Y., Li, L. & Wang, X. Smac, a mitochondrial protein that promotes cytochrome c-dependent caspase activation by eliminating IAP inhibition. *Cell* **102**, 33–42 (2000).
 62. Diez, E., Yaraghi, Z., MacKenzie, a & Gros, P. The neuronal apoptosis inhibitory protein (Naip) is expressed in macrophages and is modulated after phagocytosis and during intracellular infection with *Legionella pneumophila*. *J. Immunol.* **164**, 1470–1477 (2000).
 63. Diez, E. *et al.* Birc1e is the gene within the Lgn1 locus associated with resistance to *Legionella pneumophila*. *Nat. Genet.* **33**, 55–60 (2003).
 64. Maier, J. K. X. *et al.* The neuronal apoptosis inhibitory protein is a direct inhibitor of caspases 3 and 7. *J. Neurosci.* **22**, 2035–2043 (2002).
 65. Liston, P. *et al.* Suppression of apoptosis in mammalian cells by NAIP and a related family of IAP genes. *Nature* **379**, 349–353 (1996).
 66. Ambrosini, G., Adida, C. & Altieri, D. C. A novel anti-apoptosis gene, survivin, expressed in cancer and lymphoma. *Nat. Med.* **3**, 917–921 (1997).
 67. Tamm, I. *et al.* IAP-family protein Survivin inhibits caspase activity and apoptosis induced by Fas (CD95), bax, caspases, and anticancer drugs. *Cancer Res.* **58**, 5315–5320 (1998).
 68. Uren, A. G. *et al.* Survivin and the inner centromere protein INCENP show similar cell-cycle localization and gene knockout phenotype. *Curr. Biol.* **10**, 1319–1328 (2000).
 69. Hagemann, S. *et al.* Loss of Survivin influences liver regeneration and is associated with impaired Aurora B function. *Cell Death Differ.* **20**, 834–44 (2013).
 70. Pennati, M., Folini, M. & Zaffaroni, N. Targeting survivin in cancer therapy: Fulfilled promises and open questions. *Carcinogenesis* **28**, 1133–1139 (2007).
 71. Hauser, H. P., Bardroff, M., Pyrowolakis, G. & Jentsch, S. A giant ubiquitin-conjugating enzyme related to IAP apoptosis inhibitors. *J. Cell Biol.* **141**, 1415–1422 (1998).

References

72. Pennati, M., Millo, E., Gandellini, P., Folini, M. & Zaffaroni, N. RNA Interference-Mediated Validation of Survivin and Apollon/BRUCE as New Therapeutic Targets for Cancer Therapy. *Curr. Top. Med. Chem.* **12**, 69–78 (2012).
73. Hao, Y. *et al.* Apollon ubiquitinates SMAC and caspase-9, and has an essential cytoprotection function. *Nat. Cell Biol.* **6**, 849–860 (2004).
74. Vucic, D., Stennicke, H. R., Pisabarro, M. T., Salvesen, G. S. & Dixit, V. M. ML-IAP, a novel inhibitor of apoptosis that is preferentially expressed in human melanomas. *Curr. Biol.* **10**, 1359–1366 (2000).
75. Varfolomeev, E. *et al.* Characterization of ML-IAP protein stability and physiological role in vivo. *Biochem. J.* **447**, 427–436 (2012).
76. Richter, B. W. *et al.* Molecular cloning of ILP-2, a novel member of the inhibitor of apoptosis protein family. *Mol Cell Biol* **21**, 4292–4301 (2001).
77. Vucic, D., Dixit, V. M. & Wertz, I. E. Ubiquitylation in apoptosis: a post-translational modification at the edge of life and death. *Nat. Rev Mol Cell Biol* **12**, 439–452 (2011).
78. Deshaies, R. J. & Joazeiro, C. A. RING domain E3 ubiquitin ligases. *Annu Rev Biochem* **78**, 399–434 (2009).
79. Kulathu, Y. & Komander, D. Atypical ubiquitylation — the unexplored world of polyubiquitin beyond Lys48 and Lys63 linkages. *Nat. Rev. Mol. Cell Biol.* **13**, 508–523 (2012).
80. Emmerich, C. H. *et al.* Activation of the canonical IKK complex by K63/M1-linked hybrid ubiquitin chains. *Proc. Natl. Acad. Sci. U. S. A.* **110**, 15247–52 (2013).
81. Chai, J. *et al.* Structural and biochemical basis of apoptotic activation by Smac/DIABLO. *Nature* **406**, 855–862 (2000).
82. Wu, G. *et al.* Structural basis of IAP recognition by Smac/DIABLO. *Nature* **408**, 1008–1012 (2000).
83. Dubrez, L., Berthelet, J. & Glorian, V. IAP proteins as targets for drug development in oncology. *Onco. Targets. Ther.* **6**, 1285–1304 (2013).
84. Ashkenazi, A. & Dixit, V. M. Death receptors: signaling and modulation.

References

- Science* **281**, 1305–1308 (1998).
85. Baud, V. & Karin, M. Signal transduction by tumor necrosis factor and its relatives. *Trends Cell Biol.* **11**, 372–377 (2001).
 86. Park, Y. C. *et al.* A Novel Mechanism of TRAF Signaling Revealed by Structural and Functional Analyses of the TRADD–TRAF2 Interaction. *Cell* **101**, 777–787 (2000).
 87. Lee, T. H., Shank, J., Cusson, N. & Kelliher, M. A. The kinase activity of Rip1 is not required for tumor necrosis factor- α -induced I κ B kinase or p38 MAP kinase activation or for the ubiquitination of Rip1 by Traf2. *J. Biol. Chem.* **279**, 33185–33191 (2004).
 88. O'Donnell, M. A., Legarda-Addison, D., Skountzos, P., Yeh, W. C. & Ting, A. T. Ubiquitination of RIP1 Regulates an NF- κ B-Independent Cell-Death Switch in TNF Signaling. *Curr. Biol.* **17**, 418–424 (2007).
 89. Micheau, O. & Tschopp, J. Induction of TNF receptor I-mediated apoptosis via two sequential signaling complexes. *Cell* **114**, 181–190 (2003).
 90. Zhang, D. W. *et al.* RIP3, an energy metabolism regulator that switches TNF-induced cell death from apoptosis to necrosis. *Science* (80-.). **325**, 332–336 (2009).
 91. He, S. *et al.* Receptor Interacting Protein Kinase-3 Determines Cellular Necrotic Response to TNF- α . *Cell* **137**, 1100–1111 (2009).
 92. Oeckinghaus, A. & Ghosh, S. The NF- κ B family of transcription factors and its regulation. *Cold Spring Harb. Perspect. Biol.* **1**, a000034 (2009).
 93. Sun, S.-C. Non-canonical NF- κ B signaling pathway. *Cell Res.* **21**, 71–85 (2011).
 94. Hayden, M. S. & Ghosh, S. Shared Principles in NF- κ B Signaling. *Cell* **132**, 344–362 (2008).
 95. Pahl, H. L. Activators and target genes of Rel/NF- κ B transcription factors. *Oncogene* **18**, 6853–6866 (1999).
 96. Ghosh, S. & Karin, M. Missing pieces in the NF- κ B puzzle. *Cell* **109**, 81–96 (2002).
 97. Hacker, H. & Karin, M. Regulation and Function of IKK and IKK-Related

References

- Kinases. *Sci. STKE* **2006**, re13- (2006).
98. Perkins, N. Post-translational modifications regulating the activity and function of the nuclear factor kappa B pathway. *Oncogene* **25**, 6717–6730 (2006).
 99. Hoffmann, A., Natoli, G. & Ghosh, G. Transcriptional regulation via the NF-kappaB signaling module. *Oncogene* **25**, 6706–16 (2006).
 100. Vince, J. E. *et al.* TWEAK-FN14 signaling induces lysosomal degradation of a cIAP1-TRAF2 complex to sensitize tumor cells to TNFa. *J. Cell Biol.* **182**, 171 (2008).
 101. Hanahan, D. & Weinberg, R. A. The hallmarks of cancer. *Cell* **100**, 57–70 (2000).
 102. Cheung-Ong, K., Giaever, G. & Nislow, C. DNA-Damaging Agents in Cancer Chemotherapy: Serendipity and Chemical Biology. *Chem. Biol.* **20**, 648–659 (2013).
 103. Choices, N. Chemotherapy - Side effects - NHS Choices.
 104. O'Brien, S. G. *et al.* Imatinib Compared with Interferon and Low-Dose Cytarabine for Newly Diagnosed Chronic-Phase Chronic Myeloid Leukemia. *N. Engl. J. Med.* **348**, 994–1004 (2003).
 105. Hoelder, S., Clarke, P. A. & Workman, P. Discovery of small molecule cancer drugs: Successes, challenges and opportunities. *Mol. Oncol.* **6**, 155–176 (2012).
 106. Imai, K. & Takaoka, A. Comparing antibody and small-molecule therapies for cancer. *Nat. Rev. Cancer* **6**, 714–27 (2006).
 107. Kasper, B. *et al.* Favorable therapeutic index of a p210(BCR-ABL)-specific tyrosine kinase inhibitor; activity on lineage-committed and primitive chronic myelogenous leukemia progenitors. *Cancer Chemother. Pharmacol.* **44**, 433–438 (1999).
 108. Gathmann, I. *et al.* Five-Year Follow-up of Patients Receiving Imatinib for Chronic Myeloid Leukemia. *Methods* **355**, 2408–2417 (2006).
 109. Abe, O. *et al.* Tamoxifen for early breast cancer: An overview of the randomised trials. *Lancet* **351**, 1451–1467 (1998).

References

110. Li, L. *et al.* A Small Molecule Smac Mimic Potentiates TRAIL- and TNF α -Mediated Cell Death. *Science* (80-.). **305**, 1471–1474 (2004).
111. Sun, H., Lu, J., Liu, L., Yang, C. Y. & Wang, S. Potent and selective small-molecule inhibitors of cIAP1/2 proteins reveal that the binding of smac mimetics to XIAP BIR3 is not required for their effective induction of cell death in tumor cells. *ACS Chem. Biol.* **9**, 994–1002 (2014).
112. Dueber, E. C. *et al.* Antagonists induce a conformational change in cIAP1 that promotes autoubiquitination. *Science* **334**, 376–80 (2011).
113. Gerges, S., Rohde, K. & Fulda, S. Cotreatment with Smac mimetics and demethylating agents induces both apoptotic and necroptotic cell death pathways in acute lymphoblastic leukemia cells. *Cancer Lett.* **375**, 127–132 (2016).
114. Shekhar, T. M. *et al.* Inhibition of Bcl-2 or IAP proteins does not provoke mutations in surviving cells. *Mutat. Res. - Fundam. Mol. Mech. Mutagen.* **777**, 23–32 (2015).
115. Cai, Q. *et al.* A potent and orally active antagonist (SM-406/AT-406) of multiple inhibitor of apoptosis proteins (IAPs) in clinical development for cancer treatment. *J. Med. Chem.* **54**, 2714–2726 (2011).
116. Matzinger, O. *et al.* The radiosensitizing activity of the SMAC-mimetic, Debio 1143, is TNF α -mediated in head and neck squamous cell carcinoma. *Radiother. Oncol.* **116**, 495–503 (2015).
117. Duvefelt, C. F. *et al.* Increased resistance to proteasome inhibitors in multiple myeloma mediated by cIAP2--implications for a combinatorial treatment. *Oncotarget* **6**, 20621–35 (2015).
118. Langdon, C. *et al.* SMAC mimetic Debio 1143 synergizes with taxanes, topoisomerase inhibitors and bromodomain inhibitors to impede growth of lung adenocarcinoma cells. *Oncotarget* **6**, 37410–25 (2015).
119. Liu, N. *et al.* Debio 1143, an antagonist of multiple inhibitor-of-apoptosis proteins, activates apoptosis and enhances radiosensitization of non-small cell lung cancer cells in vitro. *Am. J. Cancer Res.* **4**, 943–51 (2014).
120. Ahmad, A. M. Recent advances in pharmacokinetic modeling. *Biopharm.*

References

- Drug Dispos.* **28**, 135–143 (2007).
121. Hurwitz, H. I. *et al.* Safety, pharmacokinetics, and pharmacodynamic properties of oral DEBIO1143 (AT-406) in patients with advanced cancer: Results of a first-in-man study. *Cancer Chemother. Pharmacol.* **75**, 851–859 (2015).
 122. Dipersio, J. F. *et al.* Oral Debio1143 (AT406), an antagonist of inhibitor of apoptosis proteins, combined with daunorubicin and cytarabine in patients with poor-risk acute myeloid leukemia - Results of a phase i dose-escalation study. *Clin. Lymphoma, Myeloma Leuk.* **15**, 443–449 (2015).
 123. Cohen, F. *et al.* Orally bioavailable antagonists of inhibitor of apoptosis proteins based on an azabicyclooctane scaffold. *J. Med. Chem.* **52**, 1723–1730 (2009).
 124. Flygare, J. A. *et al.* Discovery of a potent small-molecule antagonist of inhibitor of apoptosis (IAP) proteins and clinical candidate for the treatment of cancer (GDC-0152). *J. Med. Chem.* **55**, 4101–4113 (2012).
 125. Yang, L. *et al.* GDC-0152 attenuates the malignant progression of osteosarcoma promoted by ANGPTL2 via PI3K/AKT but not p38MAPK signaling pathway. *Int. J. Oncol.* **46**, 1651–1658 (2015).
 126. Hu, R., Li, J., Liu, Z., Miao, M. & Yao, K. GDC-0152 induces apoptosis through down-regulation of IAPs in human leukemia cells and inhibition of PI3K/Akt signaling pathway. *Tumor Biol.* **36**, 577–584 (2015).
 127. Tchoghandjian, A. *et al.* Inhibitor of apoptosis protein expression in glioblastomas and their in vitro and in vivo targeting by SMAC mimetic GDC-0152. *Cell Death Dis.* **7**, e2325 (2016).
 128. Shekhar, T. M. *et al.* IAP antagonists sensitize murine osteosarcoma cells to killing by TNF α . *Oncotarget* **7**, 33866–86 (2015).
 129. GDC 0152 - AdisInsight. Available at: <http://adisinsight.springer.com/drugs/800022402>.
 130. Shin, Y. G. *et al.* Validation and application of a liquid chromatography-tandem mass spectrometric method for the determination of GDC-0152 in human plasma using solid-phase extraction. *Biomed. Chromatogr.* **27**, 102–

References

- 110 (2013).
131. Sun, L. *et al.* Mixed lineage kinase domain-like protein mediates necrosis signaling downstream of RIP3 kinase. *Cell* **148**, 213–227 (2012).
132. Uegaki, T. *et al.* Inhibitor of apoptosis proteins (IAPs) may be effective therapeutic targets for treating endometriosis. *Hum. Reprod.* **30**, 149–158 (2015).
133. Lueck, S. C. *et al.* Smac mimetic induces cell death in a large proportion of primary acute myeloid leukemia samples, which correlates with defined molecular markers. *Oncotarget* **5**, 40–50 (2016).
134. Liese, J., Abhari, B. A. & Fulda, S. Smac mimetic and oleanolic acid synergize to induce cell death in human hepatocellular carcinoma cells. *Cancer Lett.* **365**, 47–56 (2015).
135. Lindemann, C., Marschall, V., Weigert, A., Klingebiel, T. & Fulda, S. Smac mimetic-induced upregulation of CCL2/MCP-1 triggers migration and invasion of glioblastoma cells and influences the tumor microenvironment in a paracrine manner. *Neoplasia* **17**, 481–489 (2015).
136. Liese, J., Abhari, B. A. & Fulda, S. Smac mimetic and oleanolic acid synergize to induce cell death in human hepatocellular carcinoma cells. *Cancer Lett.* **365**, 47–56 (2015).
137. Schenk, B. & Fulda, S. Reactive oxygen species regulate Smac mimetic/TNF α -induced necroptotic signaling and cell death. *Oncogene* **34**, 1–11 (2015).
138. Stadel, D. *et al.* Requirement of nuclear factor κ B for Smac mimetic-mediated sensitization of pancreatic carcinoma cells for gemcitabine-induced apoptosis. *Neoplasia* **13**, 1162–70 (2011).
139. Berger, R. *et al.* NF- κ B Is Required for Smac Mimetic-Mediated Sensitization of Glioblastoma Cells for γ -Irradiation-Induced Apoptosis. *Mol. Cancer Ther.* **10**, 1867–1875 (2011).
140. Vandenabeele, P. & Bertrand, M. J. M. The role of the IAP E3 ubiquitin ligases in regulating pattern-recognition receptor signalling. *Nat. Rev. Immunol.* **12**, 833–844 (2012).

References

141. Eckhardt, I., Roesler, S. & Fulda, S. Identification of DR5 as a critical, NF- κ B-regulated mediator of Smac-induced apoptosis. *Cell Death Dis.* **4**, e936 (2013).
142. Moriwaki, K., Bertin, J., Gough, P. J., Orlowski, G. M. & Chan, F. K. M. Differential roles of RIPK1 and RIPK3 in TNF-induced necroptosis and chemotherapeutic agent-induced cell death. *Cell Death Dis.* **6**, e1636 (2015).
143. Allensworth, J. L., Sauer, S. J., Lyster, H. K., Morse, M. A. & Devi, G. R. Smac mimetic Birinapant induces apoptosis and enhances TRAIL potency in inflammatory breast cancer cells in an IAP-dependent and TNF- α -independent mechanism. *Breast Cancer Res. Treat.* **137**, 359–371 (2013).
144. Lalaoui, N. *et al.* Correction: Targeting p38 or MK2 Enhances the Anti-Leukemic Activity of Smac-Mimetics (Cancer Cell (2016) 30(3) (499–500) (S1535610816000350) (10.1016/j.ccell.2016.01.006)). *Cancer Cell* **30**, 499–500 (2016).
145. Rettinger, E. *et al.* SMAC Mimetic BV6 Enables Sensitization of Resistant Tumor Cells but also Affects Cytokine-Induced Killer (CIK) Cells: A Potential Challenge for Combination Therapy. *Front. Pediatr.* **2**, 75 (2014).
146. Müller-Sienerth, N. *et al.* SMAC Mimetic BV6 induces cell death in monocytes and maturation of monocyte-derived dendritic cells. *PLoS One* **6**, e21556 (2011).
147. Tchoghandjian, a, Jennewein, C., Eckhardt, I., Rajalingam, K. & Fulda, S. Identification of non-canonical NF- κ B signaling as a critical mediator of Smac mimetic-stimulated migration and invasion of glioblastoma cells. *Cell Death Dis.* **4**, e564 (2013).
148. Yang, C. *et al.* Antagonism of inhibitor of apoptosis proteins increases bone metastasis via unexpected osteoclast activation. *Cancer Discov.* **3**, 212–223 (2013).
149. Wong, W. W. L. *et al.* cIAPs and XIAP regulate myelopoiesis through cytokine production in an RIPK1- And RIPK3-dependent manner. *Blood* **123**, 2562–2572 (2014).

References

150. Senzer, N. *et al.* Clinical Activity and Tolerability of the SMAC-Mimetic Birinapant (TL32711) plus Irinotecan in Irinotecan-Relapsed / Refractory Metastatic Colorectal Cancer. 32711 (2013).
151. Condon, S. M. *et al.* Birinapant, a smac-mimetic with improved tolerability for the treatment of solid tumors and hematological malignancies. *J. Med. Chem.* **57**, 3666–3677 (2014).
152. Krepler, C. *et al.* The novel SMAC mimetic birinapant exhibits potent activity against human melanoma cells. *Clin. Cancer Res.* **19**, 1784–1794 (2013).
153. Min, D. J., He, S. & Green, J. E. Birinapant (TL32711) improves responses to GEM/AZD7762 combination therapy in triple-negative breast cancer cell lines. *Anticancer Res.* **36**, 2649–2657 (2016).
154. Eytan, D. F. *et al.* Combination effects of SMAC mimetic birinapant with TNF α , TRAIL, and docetaxel in preclinical models of HNSCC. *Laryngoscope* **125**, E118–E124 (2015).
155. Amaravadi, R. K. *et al.* A Phase 1 Study of the SMAC-Mimetic Birinapant in Adults with Refractory Solid Tumors or Lymphoma. *Mol. Cancer Ther.* **14**, 1535-7163.MCT-15-0475- (2015).
156. Benetatos, C. a *et al.* Birinapant (TL32711), a bivalent SMAC mimetic, targets TRAF2-associated cIAPs, abrogates TNF-induced NF- κ B activation, and is active in patient-derived xenograft models. *Mol. Cancer Ther.* **13**, 867–79 (2014).
157. Srivastava, A. K. *et al.* Effect of a smac mimetic (TL32711, birinapant) on the apoptotic program and apoptosis biomarkers examined with validated multiplex immunoassays fit for clinical use. *Clin. Cancer Res.* **22**, 1000–1010 (2016).
158. Lalaoui, N. *et al.* Correction: Targeting p38 or MK2 Enhances the Anti-Leukemic Activity of Smac-Mimetics (Cancer Cell (2016) 30(3) (499–500) (S1535610816000350) (10.1016/j.ccell.2016.01.006)). *Cancer Cell* **30**, 499–500 (2016).
159. Condon, S. M. The Discovery and Development of Smac Mimetics-Small-Molecule Antagonists of the Inhibitor of Apoptosis Proteins. *Annu. Rep. Med.*

References

- Chem.* **46**, 211–226 (2011).
160. Rudmann, D. G. On-target and off-target-based toxicologic effects. *Toxicol. Pathol.* **41**, 310–4 (2013).
 161. Erickson, R. I. *et al.* Toxicity profile of small-molecule IAP antagonist GDC-0152 is linked to TNF- α pharmacology. *Toxicol. Sci.* **131**, 247–258 (2013).
 162. West, A. C. *et al.* The SMAC mimetic, LCL-161, reduces survival in aggressive MYC-driven lymphoma while promoting susceptibility to endotoxic shock. *Oncogenesis* **5**, e216 (2016).
 163. Fulda, S. Regulation of cell migration, invasion and metastasis by IAP proteins and their antagonists. *Oncogene* **33**, 671–676 (2013).
 164. Liu, J. *et al.* X-linked Inhibitor of Apoptosis Protein (XIAP) mediates cancer cell motility via Rho GDP Dissociation Inhibitor (RhoGDI)-dependent regulation of the cytoskeleton. *J. Biol. Chem.* **286**, 15630–15640 (2011).
 165. Oberoi, T. K. *et al.* IAPs regulate the plasticity of cell migration by directly targeting Rac1 for degradation. *EMBO J.* **31**, 14–28 (2011).
 166. Novack, D. V. *et al.* The I κ B function of NF- κ B2 p100 controls stimulated osteoclastogenesis. *J. Exp. Med.* **198**, 771–81 (2003).
 167. Edwards, I. R. & Aronson, J. K. Adverse drug reactions: definitions, diagnosis, and management. *Lancet* **356**, 1255–1259 (2000).
 168. Davies, E. C. *et al.* Adverse drug reactions in hospital in-patients: A prospective analysis of 3695 patient-episodes. *PLoS One* **4**, e4439 (2009).
 169. Lazarou, J., Pomeranz, B. H. & Corey, P. N. Incidence of adverse drug reactions in hospitalized patients: a meta-analysis of prospective studies. *Jama* **279**, 1200–1205 (1998).
 170. Watkins, P. B., Seligman, P. J., Pears, J. S., Avigan, M. I. & Senior, J. R. Using controlled clinical trials to learn more about acute drug-induced liver injury. *Hepatology* **48**, 1680–1689 (2008).
 171. Meier, Y. *et al.* Incidence of drug-induced liver injury in medical inpatients. *Eur. J. Clin. Pharmacol.* **61**, 135–143 (2005).
 172. Kaplowitz, N. Idiosyncratic drug hepatotoxicity. *Nat. Rev. Drug Discov.* **4**, 489–99 (2005).

References

173. Lasser, K. E. *et al.* Timing of new black box warnings and withdrawals for prescription medications. *Jama* **287**, 2215–20 (2002).
174. Dahlin, D. C., Miwa, G. T., Lu, A. Y. H. & Nelson, S. D. N-acetyl-p-benzoquinone imine: A cytochrome P-450-mediated oxidation product of acetaminophen. *Proc. Natl. Acad. Sci. U. S. A.* **81**, 1327–1331 (1984).
175. Mitchell, J, R. *et al.* Acetaminophen-induced hepatic necrosis. *J. Pharm. Exp. Ther.* **187**, 211–217 (1973).
176. Luster, M. I. *et al.* Role of inflammation in chemical-induced hepatotoxicity. *Toxicol. Lett.* **120**, 317–321 (2001).
177. Parker, G. a & Picut, C. a. Liver immunobiology. *Toxicol. Pathol.* **33**, 52–62 (2005).
178. Ding, H., Peng, R., Reed, E. & Li, Q. Q. Effects of Kupffer cell inhibition on liver function and hepatocellular activity in mice. *Int. J. Mol. Med.* **12**, 549–557 (2003).
179. Bilzer, M., Roggel, F. & Gerbes, A. L. Role of Kupffer cells in host defense and liver disease. *Liver Int.* **26**, 1175–1186 (2006).
180. Cullen, J. M. *et al.* Effects of Kupffer cell depletion on acute alpha-naphthylisothiocyanate-induced liver toxicity in male mice. *Toxicol. Pathol.* **41**, 7–17 (2013).
181. TAKEISHI, T. *et al.* The Role of Kupffer Cells in Liver Regeneration. *Arch. Histol. Cytol.* **62**, 413–422 (1999).
182. Ebe, Y. *et al.* The role of Kupffer cells and regulation of neutrophil migration into the liver by macrophage inflammatory protein-2 in primary listeriosis in mice. *Pathol. Int.* **49**, 519–532 (1999).
183. Mosher, B. *et al.* Inhibition of Kupffer cells reduced CXC chemokine production and liver injury. *J. Surg. Res.* **99**, 201–10 (2001).
184. Muriel, P., Alba, N., Pérez-Alvarez, V. M., Shibayama, M. & Tsutsumi, V. K. Kupffer cells inhibition prevents hepatic lipid peroxidation and damage induced by carbon tetrachloride. *Comp. Biochem. Physiol. C. Toxicol. Pharmacol.* **130**, 219–26 (2001).
185. Muriel, P. & Escobar, Y. Kupffer cells are responsible for liver cirrhosis

References

- induced by carbon tetrachloride. *J. Appl. Toxicol.* **23**, 103–108 (2003).
186. Tsutsui, H. & Nishiguchi, S. Importance of kupffer cells in the development of acute liver injuries in mice. *Int. J. Mol. Sci.* **15**, 7711–7730 (2014).
187. van Furth, R. Origin and Kinetics of Mononuclear Phagocytes. *Ann. N. Y. Acad. Sci.* **278**, 161–175 (1976).
188. Schulz, C. *et al.* A lineage of myeloid cells independent of Myb and hematopoietic stem cells. *Science* **336**, 86–90 (2012).
189. Jenkins, S. J. *et al.* Local macrophage proliferation, rather than recruitment from the blood, is a signature of TH2 inflammation. *Science* **332**, 1284–8 (2011).
190. Hoeffel, G. *et al.* Adult Langerhans cells derive predominantly from embryonic fetal liver monocytes with a minor contribution of yolk sac-derived macrophages. *J. Exp. Med.* **209**, 1167–81 (2012).
191. Balzola, F., Cullen, G., Ho, G. T. & Russell, R. K. Inflammatory monocytes regulate pathologic responses to commensals during acute gastrointestinal infection. *Inflamm. Bowel Dis. Monit.* **14**, 30 (2013).
192. Davies, L. C., Jenkins, S. J., Allen, J. E. & Taylor, P. R. Tissue-resident macrophages. *Nat. Immunol.* **14**, 986–995 (2013).
193. Zigmond, E. *et al.* Ly6Chi Monocytes in the Inflamed Colon Give Rise to Proinflammatory Effector Cells and Migratory Antigen-Presenting Cells. *Immunity* **37**, 1076–1090 (2012).
194. Zigmond, E. *et al.* Infiltrating Monocyte-Derived Macrophages and Resident Kupffer Cells Display Different Ontogeny and Functions in Acute Liver Injury. *J. Immunol.* **193**, 1400574 (2014).
195. Kodali, P., Wu, P., Lahiji, P. a, Brown, E. J. & Maher, J. J. ANIT toxicity toward mouse hepatocytes in vivo is mediated primarily by neutrophils via CD18. *Am. J. Physiol. Gastrointest. Liver Physiol.* **291**, G355–G363 (2006).
196. Tanaka, Y., Aleksunes, L. M., Cui, Y. J. & Klaassen, C. D. ANIT-induced intrahepatic cholestasis alters hepatobiliary transporter expression via Nrf2-dependent and independent signaling. *Toxicol. Sci.* **108**, 247–257 (2009).
197. Roth, R. A. & Dahm, L. J. Neutrophil- and Glutathione-Mediated

References

- Hepatotoxicity of α -Naphthylisothiocyanate. *Drug Metab. Rev.* **29**, 153–165 (1997).
198. Desmet, V. J., Krstulović, B. & Van Damme, B. Histochemical study of rat liver in alpha-naphthyl isothiocyanate (ANIT) induced cholestasis. *Am. J. Pathol.* **52**, 401–21 (1968).
199. Dietrich, C. G., Ottenhoff, R., De Waart, D. R. & Oude Elferink, R. P. J. Role of MRP2 and GSH in intrahepatic cycling of toxins. *Toxicology* **167**, 73–81 (2001).
200. Hill, D. A., Jean, P. A. & Roth, R. A. Bile duct epithelial cells exposed to alpha-naphthylisothiocyanate produce a factor that causes neutrophil-dependent hepatocellular injury in vitro. *Toxicol. Sci.* **47**, 118–125 (1999).
201. Nathan, C. *et al.* Cytokine-Induced Respiratory Burst of Human-Neutrophils - Dependence on Extracellular-Matrix Proteins and Cd11/Cd18 Integrins. *J. Cell Biol.* **109**, 1341–1349 (1989).
202. Liu, P. *et al.* Activation of Kupffer cells and neutrophils for reactive oxygen formation is responsible for endotoxin-enhanced liver injury after hepatic ischemia. *Shock* **3**, 56–62 (1995).
203. Gruebele, A., Zawaski, K., Kaplan, D. & Novak, R. F. Cytochrome P450E1- and cytochrome P450B1/2B2-catalyzed carbon tetrachloride metabolism: Effects on signal transduction as demonstrated by altered immediate-early (c-Fos and c-Jun) gene expression and nuclear AP-1 and NF-kB transcription factor levels. *Drug Metab. Dispos.* **24**, 15–22 (1996).
204. Castro, J. A. in *IUPHAR 9th International Congress of Pharmacology* 243–250 (Macmillan Education UK, 1984). doi:10.1007/978-1-349-86029-6_34
205. Castro, J. A. in *IUPHAR 9th International Congress of Pharmacology* 243–250 (Macmillan Education UK, 1984). doi:10.1007/978-1-349-86029-6_34
206. Weber, L. W. D., Boll, M. & Stampfl, A. Hepatotoxicity and mechanism of action of haloalkanes: carbon tetrachloride as a toxicological model. *Crit. Rev. Toxicol.* **33**, 105–136 (2003).
207. Thiers, R. E., Reynolds, E. S. & Vallee, B. L. The effect of carbon tetrachloride poisoning on subcellular metal distribution in rat liver. *J. Biol.*

References

- Chem.* **235**, 2130–2133 (1960).
208. Clawson, G. A., MacDonald, J. R. & Woo, C. H. Early hypomethylation of 2'-O-ribose moieties in hepatocyte cytoplasmic ribosomal RNA underlies the protein synthetic defect produced by CCl₄. *J. Cell Biol.* **105**, 705–711 (1987).
209. Nishimaki-Mogami, T., Suzuki, K. & Takahashi, A. The role of phosphatidylethanolamine methylation in the secretion of very low density lipoproteins by cultured rat hepatocytes: Rapid inhibition of phosphatidylethanolamine methylation by bezafibrate increases the density of apolipoprotein B48-containing . *Biochim. Biophys. Acta - Lipids Lipid Metab.* **1304**, 21–31 (1996).
210. Luckey, S. W. & Petersen, D. R. Activation of Kupffer cells during the course of carbon tetrachloride-induced liver injury and fibrosis in rats. *Exp. Mol. Pathol.* **71**, 226–240 (2001).
211. Czaja, M. J., Xu, J. & Alt, E. Prevention of carbon tetrachloride-induced rat liver injury by soluble tumor necrosis factor receptor. *Gastroenterology* **108**, 1849–54 (1995).
212. Shi, J., Aisaki, K., Ikawa, Y. & Wake, K. Evidence of Hepatocyte Apoptosis in Rat Liver after the Administration of Carbon Tetrachloride. *Am. J. Pathol.* **153**, 515–525 (1998).
213. Carlsen, H., Moskaug, J. O., Fromm, S. H. & Blomhoff, R. In Vivo Imaging of NF- κ B Activity. *J. Immunol.* **168**, 1441–1446 (2002).
214. Gaither, A. *et al.* A Smac mimetic rescue screen reveals roles for inhibitor of apoptosis proteins in tumor necrosis factor- α signaling. *Cancer Res.* **67**, 11493–11498 (2007).
215. Chauhan, D. *et al.* Targeting mitochondrial factor Smac/DIABLO as therapy for multiple myeloma (MM). *Blood* **109**, 1220–1227 (2007).
216. Ziegler, D. & Wright, R. Resistance of human glioblastoma multiforme cells to growth factor inhibitors is overcome by blockade of inhibitor of apoptosis proteins. *J. Clin. Invest.* **118**, 3109–22 (2008).
217. Naik, S. Characterisation of TRAIL receptor signalling to apoptosis in pre-

References

- clinical models of breast cancer. (2011).
218. Bertrand, M. J. M. *et al.* cIAP1 and cIAP2 Facilitate Cancer Cell Survival by Functioning as E3 Ligases that Promote RIP1 Ubiquitination. *Mol. Cell* **30**, 689–700 (2008).
 219. LaCasse, E. C. *et al.* IAP-targeted therapies for cancer. *Oncogene* **27**, 6252–6275 (2008).
 220. Lu, J. *et al.* SM-164: A novel, bivalent smac mimetic that induces apoptosis and tumor regression by concurrent removal of the blockade of cIAP-1/2 and XIAP. *Cancer Res.* **68**, 9384–9393 (2008).
 221. Petrucci, E. *et al.* A Small Molecule SMAC Mimic LBW242 Potentiates TRAIL- and Anticancer Drug-Mediated Cell Death of Ovarian Cancer Cells. *PLoS One* **7**, e35073 (2012).
 222. Wu, H., Tschopp, J. & Lin, S. C. Smac Mimetics and TNF α : A Dangerous Liaison? *Cell* **131**, 655–658 (2007).
 223. Cossu, F. *et al.* Structural Basis for Bivalent Smac-Mimetics Recognition in the IAP Protein Family. *J. Mol. Biol.* **392**, 630–644 (2009).
 224. Sun, H. *et al.* Design, synthesis, and characterization of a potent, nonpeptide, cell-permeable, bivalent smac mimetic that concurrently targets both the BIR2 and BIR3 domains in XIAP. *J. Am. Chem. Soc.* **129**, 15279–15294 (2007).
 225. Suzuki, Y., Nakabayashi, Y., Nakata, K., Reed, J. C. & Takahashi, R. X-linked Inhibitor of Apoptosis Protein (XIAP) Inhibits Caspase-3 and -7 in Distinct Modes. *J. Biol. Chem.* **276**, 27058–27063 (2001).
 226. Silke, J. No Title. *Personal Communication* (2014).
 227. Zhang, Y. *et al.* X-linked inhibitor of apoptosis positive nuclear labeling: a new independent prognostic biomarker of breast invasive ductal carcinoma. *Diagn Pathol* **6**, 49 (2011).
 228. Xu, Y.-C. *et al.* Tissue microarray analysis of X-linked inhibitor of apoptosis (XIAP) expression in breast cancer patients. *Med. Oncol.* **31**, 764 (2014).
 229. Liu, Z. G. Molecular mechanism of TNF signaling and beyond. *Cell Res.* **15**, 24–27 (2005).

References

230. Oeckinghaus, A., Hayden, M. S. & Ghosh, S. Crosstalk in NF- κ B signaling pathways. *Nat Immunol* **12**, 695–708 (2011).
231. Wajant, H., Pfizenmaier, K. & Scheurich, P. Tumor necrosis factor signaling. *Cell Death.Differ.* **10**, 45–65 (2003).
232. Laukens, B. *et al.* Smac mimetic bypasses apoptosis resistance in FADD- or caspase-8-deficient cells by priming for tumor necrosis factor α -induced necroptosis. *Neoplasia* **13**, 971–9 (2011).
233. Lecis, D. *et al.* Smac mimetics induce inflammation and necrotic tumour cell death by modulating macrophage activity. *Cell Death Dis.* **4**, e920 (2013).
234. Moulin, M. *et al.* IAPs limit activation of RIP kinases by TNF receptor 1 during development. *EMBO J.* **31**, 1679–1691 (2012).
235. Lu, J. *et al.* Therapeutic potential and molecular mechanism of a novel, potent, nonpeptide, Smac mimetic SM-164 in combination with TRAIL for cancer treatment. *Mol. Cancer Ther.* **10**, 902–914 (2011).
236. Kushner, B. H. *et al.* Desmoplastic small round-cell tumor: Prolonged progression-free survival with aggressive multimodality therapy. *J. Clin. Oncol.* **14**, 1526–1531 (1996).
237. Chen, K. F. *et al.* Inhibition of Bcl-2 improves effect of LCL161, a SMAC mimetic, in hepatocellular carcinoma cells. *Biochem. Pharmacol.* **84**, 268–277 (2012).
238. Tosh, D., Shen, C.-N. & Slack, J. M. W. Molecular basis of transdifferentiation of pancreas to liver. *Nat. Cell Biol.* **2**, 879–887 (2000).
239. Marek, C. J., Cameron, G. A., Elrick, L. J., Hawksworth, G. M. & Wright, M. C. Generation of hepatocytes expressing functional cytochromes P450 from a pancreatic progenitor cell line in vitro. *Biochem. J.* **370**, 763–769 (2003).
240. Probert, P. M. E. *et al.* Utility of B-13 progenitor-derived hepatocytes in hepatotoxicity and genotoxicity studies. *Toxicol. Sci.* **137**, 350–370 (2014).
241. Wallace, K., Fairhall, E. A., Charlton, K. A. & Wright, M. C. AR42J-B-13 cell: An expandable progenitor to generate an unlimited supply of functional hepatocytes. *Toxicology* **278**, 277–287 (2010).
242. Wallace, K., Long, Q., Fairhall, E. a, Charlton, K. a & Wright, M. C.

References

- Serine/threonine protein kinase SGK1 in glucocorticoid-dependent transdifferentiation of pancreatic acinar cells to hepatocytes. *J. Cell Sci.* **124**, 405–13 (2011).
243. Wallace, K., Marek, C. J., Hoppler, S. & Wright, M. C. Glucocorticoid-dependent transdifferentiation of pancreatic progenitor cells into hepatocytes is dependent on transient suppression of WNT signalling. *J. Cell Sci.* **123**, 2103–2110 (2010).
244. Fairhall, E. A. *et al.* Pancreatic B-13 Cell trans-differentiation to hepatocytes is dependent on epigenetic-regulated changes in gene expression. *PLoS One* **11**, e0150959 (2016).
245. Crawford, N. *et al.* SAHA overcomes FLIP-mediated inhibition of SMAC mimetic-induced apoptosis in mesothelioma. *Cell Death Dis.* **4**, e733 (2013).
246. Chiu, R. *et al.* The c-fos protein interacts with c-Jun AP-1 to stimulate transcription of AP-1 responsive genes. *Cell* **54**, 541–552 (1988).
247. Dérijard, B. *et al.* Independent human MAP-kinase signal transduction pathways defined by MEK and MKK isoforms. *Science* **267**, 682–5 (1995).
248. Irmeler, M. *et al.* Inhibition of death receptor signals by cellular FLIP. *Nature* **388**, 190–195 (1997).
249. Beutler, B. & Brown, T. A CAT reporter construct allows ultrasensitive estimation of TNF synthesis, and suggests that the TNF gene has been silenced in non-macrophage cell lines. *J. Clin. Invest.* **87**, 1336–1344 (1991).
250. Sun, Y. *et al.* MicroRNA-124 negatively regulates LPS-induced TNF- α production in mouse macrophages by decreasing protein stability. *Acta Pharmacol. Sin.* **37**, 889–897 (2016).
251. Rossato, M. *et al.* IL-10-induced microRNA-187 negatively regulates TNF- α , IL-6, and IL-12p40 production in TLR4-stimulated monocytes. *Proc. Natl. Acad. Sci. U. S. A.* **109**, E3101–E3110 (2012).
252. Lee, J. Y., Kim, N. a, Sanford, A. & Sullivan, K. E. Histone acetylation and chromatin conformation are regulated separately at the TNF- α promoter in monocytes and macrophages. *J. Leukoc. Biol.* **73**, 862–871 (2003).
253. Mosmann, T. Rapid colorimetric assay for cellular growth and survival:

References

- Application to proliferation and cytotoxicity assays. *J. Immunol. Methods* **65**, 55–63 (1983).
254. Gonzalez, R. J. & Tarloff, J. B. Evaluation of hepatic subcellular fractions for Alamar blue and MTT reductase activity. *Toxicol. Vitro*. **15**, 257–259 (2001).
255. Denizot, F. & Lang, R. Rapid colorimetric assay for cell growth and survival. Modifications to the tetrazolium dye procedure giving improved sensitivity and reliability. *J. Immunol. Methods* **89**, 271–277 (1986).
256. Collier, A. C. & Pritsos, C. A. The mitochondrial uncoupler dicumarol disrupts the MTT assay. *Biochem. Pharmacol.* **66**, 281–287 (2003).
257. Yue, Q. *et al.* Evaluation of metabolism and disposition of GDC-0152 in rats using ¹⁴C labeling strategy at two different positions: A novel formation of hippuric acid from 4-phenyl-5-amino-1,2,3-thiadiazoles. *Drug Metab. Dispos.* **41**, 508–517 (2013).
258. Leist, M. *et al.* Murine hepatocyte apoptosis induced in vitro and in vivo by TNF- α requires transcriptional arrest. *J. Immunol.* **153**, 1778–1788 (1994).
259. Irmeler, M. *et al.* Inhibition of death receptor signals by cellular FLIP. *Nature* **388**, 190–195 (1997).
260. Feltham, R. A novel role for Mind Bomb-2 (MIB2) in cell death and inflammation | Walter and Eliza Hall Institute of Medical Research. Available at: <http://www.wehi.edu.au/student-research-project/novel-role-mind-bomb-2-mib2-cell-death-and-inflammation>.
261. Dynek, J. N. & Vucic, D. Antagonists of IAP proteins as cancer therapeutics. *Cancer Lett.* **332**, 206–214 (2013).
262. O'Donnell, M. A. & Ting, A. T. RIP1 comes back to life as a cell death regulator in TNFR1 signaling. *FEBS J.* **278**, 877–887 (2011).
263. O'Donnell, M. A., Legarda-Addison, D., Skountzos, P., Yeh, W. C. & Ting, A. T. Ubiquitination of RIP1 Regulates an NF- κ B-Independent Cell-Death Switch in TNF Signaling. *Curr. Biol.* **17**, 418–424 (2007).
264. Ofengeim, D. & Yuan, J. Regulation of RIP1 kinase signalling at the crossroads of inflammation and cell death. *Nat. Rev. Mol. Cell Biol.* **14**, 727–

References

- 36 (2013).
265. Jeon, Y. K. *et al.* Pellino-1 confers chemoresistance in lung cancer cells by upregulating cIAP2 through Lys63-mediated polyubiquitination. *Oncotarget* **5**, (2016).
 266. Yang, S. *et al.* Pellino3 targets RIP1 and regulates the pro-apoptotic effects of TNF- α . *Nat. Commun.* **4**, 2583 (2013).
 267. Yamada, Y., Kirillova, I., Peschon, J. J. & Fausto, N. Initiation of liver growth by tumor necrosis factor: deficient liver regeneration in mice lacking type I tumor necrosis factor receptor. *Proc. Natl. Acad. Sci. U. S. A.* **94**, 1441–1446 (1997).
 268. Bataller, R. & Brenner, D. A. Liver fibrosis. *J Clin Invest* **115**, 209–218 (2005).
 269. Libermann, T. a & Baltimore, D. Activation of interleukin-6 gene expression through the NF-kappa B transcription factor. *Mol. Cell. Biol.* **10**, 2327–2334 (1990).
 270. Wang, T. *et al.* Resveratrol effectively attenuates α -naphthyl-isothiocyanate-induced acute cholestasis and liver injury through choleretic and anti-inflammatory mechanisms. *Acta Pharmacol. Sin.* **35**, 1527–36 (2014).
 271. Varfolomeev, E. *et al.* c-IAP1 and c-IAP2 are critical mediators of tumor necrosis factor α (TNF α)-induced NF-kB activation. *J. Biol. Chem.* **283**, 24295–24299 (2008).
 272. Akazawa, Y. *et al.* Degradation of cIAPs contributes to hepatocyte lipoapoptosis. *AJP Gastrointest. Liver Physiol.* **305**, G611–G619 (2013).
 273. Kolios, G., Valatas, V. & Kouroumalis, E. Role of Kupffer cells in the pathogenesis of liver disease. *World J. Gastroenterol.* **12**, 7413–7420 (2006).
 274. Roberts, R. A. *et al.* Role of the Kupffer cell in mediating hepatic toxicity and carcinogenesis. *Toxicol. Sci.* **96**, 2–15 (2007).
 275. Kiso, K. *et al.* The role of Kupffer cells in carbon tetrachloride intoxication in mice. *Biol. Pharm. Bull.* **35**, 980–3 (2012).
 276. Selzner, N. *et al.* ICAM-1 triggers liver regeneration through leukocyte

References

- recruitment and Kupffer cell-dependent release of TNF- α /IL-6 in mice. *Gastroenterology* **124**, 692–700 (2003).
277. Ebrahimkhani, M. R. *et al.* Stimulating healthy tissue regeneration by targeting the 5-HT_{2B} receptor in chronic liver disease. *Nat. Med.* **17**, 1668–1673 (2011).
278. Martín-Vílchez, S. *et al.* Inhibition of Tyrosine Kinase Receptor Tie2 Reverts HCV-Induced Hepatic Stellate Cell Activation. *PLoS One* **9**, e106958 (2014).
279. Kitani, H. *et al.* Establishment of c-myc-immortalized Kupffer cell line from a C57BL/6 mouse strain. *Results Immunol.* **4**, 68–74 (2014).
280. Feoktistova, M. *et al.* CIAPs Block Ripoptosome Formation, a RIP1/Caspase-8 Containing Intracellular Cell Death Complex Differentially Regulated by cFLIP Isoforms. *Mol. Cell* **43**, 449–463 (2011).
281. Gordon, S. *et al.* in *Current topics in microbiology and immunology* **181**, 1–37 (1992).
282. Wang, J. & Kubes, P. A Reservoir of Mature Cavity Macrophages that Can Rapidly Invade Visceral Organs to Affect Tissue Repair. *Cell* **165**, 668–678 (2016).
283. Schmukle, A. C. & Walczak, H. No one can whistle a symphony alone – how different ubiquitin linkages cooperate to orchestrate NF- κ B activity. *J Cell Sci* **125**, 549–559 (2012).